ABSTRACT

WEI, MIN. FABRICATION OF POLYMER MATERIALS FROM THEIR CYCLODEXTRIN INCLUSION COMPLEXES. (Under the direction of Prof. Alan E. Tonelli.)

Inclusion complexed (IC) and coalesced biodegradable poly(ε-caprolactone) (PCL), poly(*l*-lactic acid) (PLLA), and their diblock copolymer (PCL-*b*-PLLA) were achieved by forming ICs between host α-cyclodextrin(α-CD) and guest PCL, PLLA, and PCL-*b*-PLLA, followed by removing the α-CD host with an amylase enzyme. The melting and crystallization behavior of these CD-IC treated polymers are investigated. Both isothermal and nonisothermal crystallization studies demonstrate that the PCL and PLLA blocks in the IC-coalesced samples are more readily and homogeneously crystallized than those in the as-synthesized samples or their physical blend, even though the level of crystallinity in the IC-coalesced diblock copolymer is significantly lower. Moreover, unlike the as-synthesized diblock copolymer, the crystallization of PCL and PLLA blocks in the IC-coalesced diblock copolymer are not influenced by their covalent connection.

Poly(ethylene terephthalate) (PET) and bisphenol A polycarbonate (PC) samples have been produced by the coalescence of their segregated, extended chains from the narrow channels of the crystalline inclusion complexes formed between the γ-cyclodextrin (γ-CD) host and PET and PC guests. Experimental observations of PET and PC samples coalesced from their crystalline ICs suggest structures and morphologies that are different from those of samples obtained by ordinary solution and melt processing techniques. PC

crystals formed upon the coalescence of highly extended and segregated PC chains from the narrow channels in the CD host lattice are possibly more chain-extended and certainly more stable than chain-folded PC crystals. The coalesced PET melt rapidly recrystallizes during the attempted quench, and so upon reheating, it displays neither a glass transitions temperature (*T*g) nor a crystallization exotherm but simply remelts at the as-coalesced melting temperature (*T*m). An inclusion complex between nylon-6 and α-cyclodextrin was obtained and we attempted to use the formation and subsequent disassociation of the nylon-6/α-CD inclusion complex to manipulate the properties of nylon-6. Examination of as-received and IC coalesced nylon-6 samples shows that dominated α-form crystalline phase of nylon-6 and a great increase in crystallinity are in the coalesced sample.

When inherently immiscible polymers are included as guests in the narrow channels of their common inclusion complexes formed with host cyclodextrins and then these polymer-1/polymer-2-CD-IC crystals are coalesced, an intimately mixed blend of the polymers is obtained. Polycarbonate (PC)/poly(methyl methacrylate) (PMMA) blends coalesced from their common γ-CD-ICs are amorphous and generally exhibit single glass transitions at temperature (*T*g) between those of pure PC and PMMA. FTIR spectroscopy suggests an intimate mixing of and possible specific interactions between PC and PMMA chains in the coalesced blends. An attempt to achieve an intimate blend between nylon 6 and nylon 66 by forming and dissociating their common α-CD-IC was also made. Experimental results demonstrate that α-cyclodextrin can only host single nylon polymer chains in the IC channels. Spectroscopic results illustrate that there is intimate mixing existing in the IC coalesced blend, but not in their solution cast physical blend.

FABRICATION OF POLYMER MATERIALS FROM THEIR CYCLODEXTRIN INCLUSION COMPLEXES

By

MIN WEI

A dissertation submitted to the Graduate Faculty of
North Carolina State University
in partial fulfillment of the
requirements for the Degree
of Doctor of Philosophy

FIBER AND POLYMER SCIENCE
MATERIALS SCIENCE AND ENGINEERING

Raleigh

2003

APPROVED BY

_____	_____
_____	_____
_____	_____
Chair of Advisory Committee	Co-Chair of Advisory Committee

TO MY DEEPLY LOVED FATHER

BIOGRAPHY

The author was born in Baoding, Hebei Province, China. Before coming to US, he obtained Bachelor and Master degrees in Science in China. He went to North Carolina State University working towards a Doctor of Philosophy Degree co-majoring in Fiber & Polymer Science and Materials Science & Engineering in 2000. Along with his Ph.D study, he obtained Master of Materials Science & Engineering and Master of Computer Science.

He is married to Miss Yanqiu Song. They have one son, Xuchen Wei and one daughter, Yanni Wei.

ACKNOWLEDGEMENTS

I would like to take this opportunity to express my sincere thanks to all who love me and help me.

The first one I want to thank is my advisor, Dr. Alan E. Tonelli, Chair of my advisory committee, for his guidance, support, consideration, caring and encouragement in the course of my studies and my life. My gratitude to the other members of the advisory committee : Profs. C. Balik, R. Spontak, J. White, S. Hudson and the Graduate School Representative : Prof. H. Ade for their advising, teaching and endless help. Special thank goes to Dr. B. Gupta for his kindly help.

Gratitude is extended to the following people: Drs. X. Shuai, F. Porbeni, X. Wang, C. Rusa, T. Bullions and J. Lu. Many thanks to my colleagues and friends : B. Urban, W. Davis, C. Jenkins, Mark and Tamer. Lab manager Ms. Shim and Ms. Anderson are appreciated for their technical help.

Finally, I would like to express my very deep gratitude to my parents and numerous family members for always standing by me. Their love has been the major spiritual support in my life.

TABLE OF CONTENTS

LIST OF FIGURES

LIST OF TABLES

1 Literature review

1.1 Introduction

1.1.1 General chemical and physical properties of cyclodextrin

Cyclodextrins (CDs) are cyclic oligosaccharides that encapsulate various small organic molecules, forming inclusion complexes. The glucose ring is a "rigid" unit. The overall shapes and conformations of individual glucose units in all cyclodextrins so far investigated are comparable. α-CD has an interior diameter of about 5Å and a channel length of 7-8Å. In the chair form, the C3 and C5 CH groups of each glucose unit and the glucosidic oxygen point to the interior, whereas in the boat form only the CH groups of C1 and C4 point inward. The lowest layer of the chair form consists of the secondary hydroxyls on C2 and C3; that of the boat form is made up of the secondary hydroxyls on C3 and CH of C2, leading to a more hydrophobic lining than the chair form.[1] In no case has a glucose conformation other than the classical C1 chair been observed, no matter what guest is included within the cavity. Moreover, the endocyclic torsion angles in the glucose rings are rather rigidly confined to plus or minus gauche values within a narrow range, suggesting that the glucose ring can be considered to be a fairly rigid building block. Cyclodextrins have doughnut shapes, with all the glucose units in substantially undistorted C1 (D) (chair) conformations. Figures 1 and 2 show schematic diagrams, as well as the configuration when complexed with C60, for CDs.

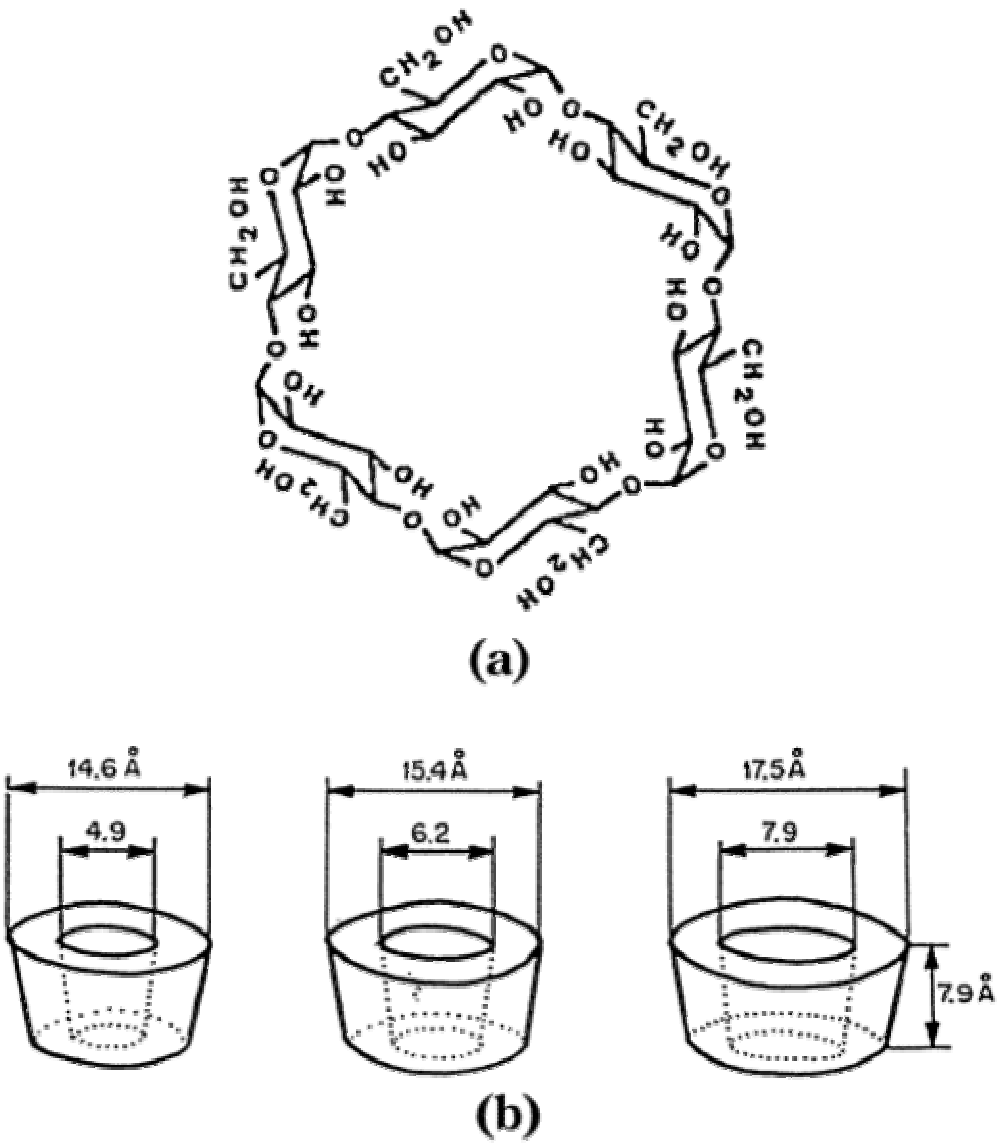

Figure 1. Chemical structure of (a) α-cyclodextrin and (b)molecular dimensions of (left to right) α-, β-, and γ-cyclodextrins (following reference 1)

These structures produce a special arrangement of the functional groups in CD molecules, resulting in a variety of interesting features. The secondary hydroxyl groups (on the C2 and C3 atoms of the glucose units) are located on the opposite side of the torus. The interior of the torus consists only of a ring of C—H groups. Therefore, they

contain no polar functional groups, so the interior of the torus of CDs is relatively apolar compared to water.

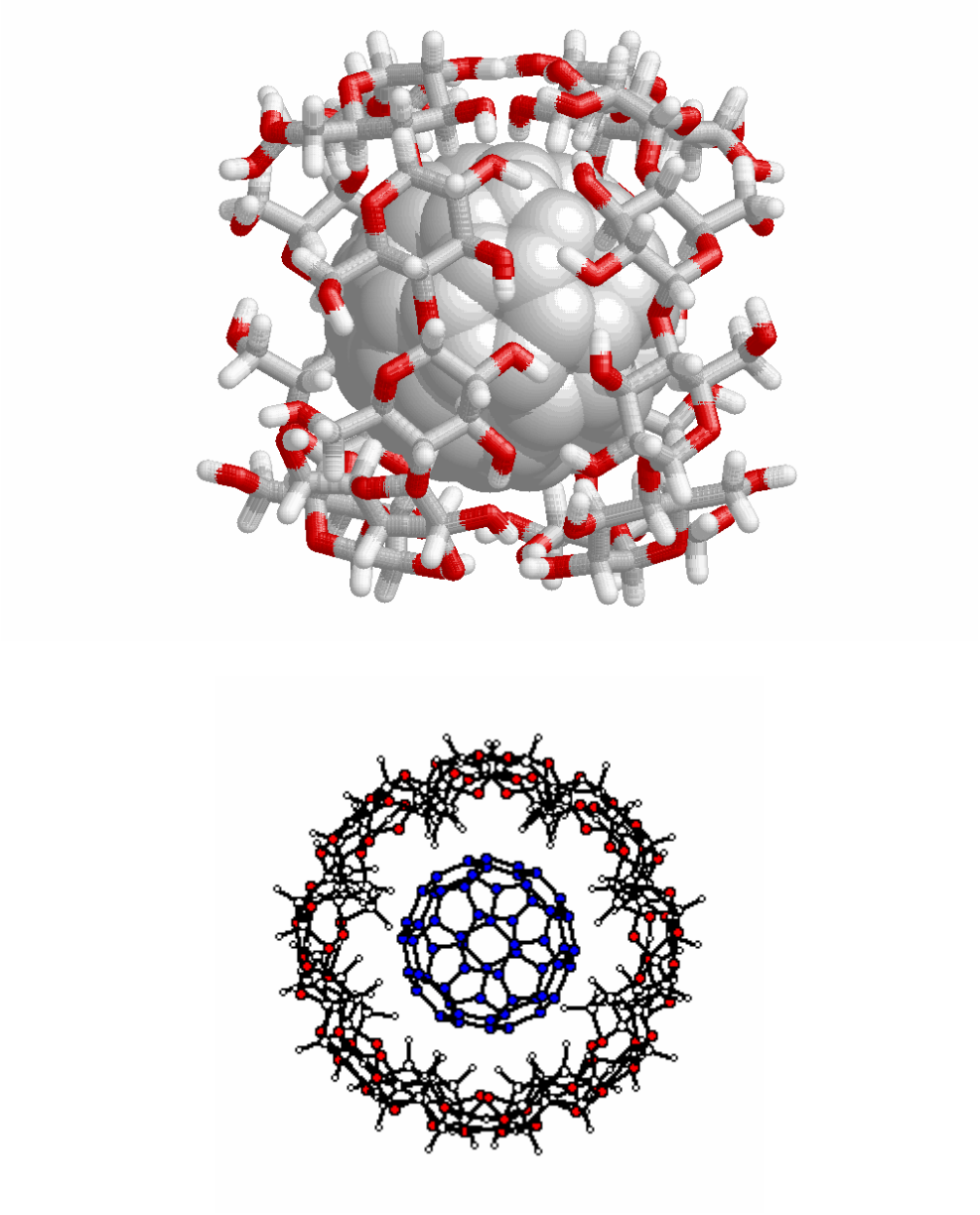

Figure 2. C60 is trapped inside a nearly spherical cavity consisting of two half-cycles of γ-cyclodextrin held together by hydrogen bonds (following reference 36)

As a consequence of these structural features, CDs have some unique physical and chemical properties. Table 1 lists the dimensional sizes of CDs, as well as some of their important physical properties.

Table 1. General properties of cyclodextrins

Cylcodextrin	α	β	γ
Number of Glucose Unites	6	7	8
Molecular Weight	972	1135	1297
Solubility in H_2O (g/ml)	14.5	1.85	23.2
Pka	12.33	12.2	12.08
Inner Diameter (nm)	0.45-0.57	0.62-0.78	0.79-0.95
Outer Diameter (nm)	1.37	1.53	1.69
Height (nm)	0.79	0.79	0.79
Cavity Volume (nm^3)	0.174	0.262	0.472

Cyclodextrins are stable in alkaline solutions. However, they are susceptible to acid hydrolysis. Partial acid hydrolysis of CDs produces glucose and a series of acylic maltosaccharides.[2] The stability of CDs toward acid hydrolysis depends on the temperature and acidity. Under normal experimental conditions (pH higher than 3.5 and temperature below 60 °C), CDs are fairly stable. Although cleavage of the 1,4-glycosidic bonds can occur in γ-cyclodextrins, they are fairly resistant to light within the ultraviolet-visible spectrum (UV-visible) and infared (IR) ranges. Cyclodextrin properties also include the following:

1. Cyclodextrins are nonreducing;

2. Glucose is the only product of acid hydrolysis of CDs
3. Molecular weights are integral multiples of the value [162.1] for a glucose residue.
4. Periodate oxidation does not produce formic acid or formaldehyde.

1.1.2 Hydration

The cyclodextrins can crystallize from water as hydrates of variable composition. α-CD is usually encountered as the hexahydrate, α-CD·6H_2O, which can exist in crystal forms I and II,[3-6] but a third form III, α-CD·7.57 H_2O, has been crystallized from aqueous $BaCl_2$.[7] β-CD exists as the undecahydrate, β-CD·11H_2O, and as the dodecahydrate, β-CD·12H_2O;[8,9] but these integral ratios are idealizations, the actual composition depending upon the relative humidity.[10,11] γ-CD is sometimes described as an octahydrate, but it can crystallize with from 7 to 18 molecules of water.[12-15]

α-CD·6H_2O (Form I) has two water molecules in the CD cavity and four molecules outside the cavity; the positions of the two included molecules are fixed by hydrogen bonding to each other and to O(6) hydroxy groups. Form II of α–CD·6H_2O has one water molecule inside the cavity. In Form III, 2.57 molecules of water are found in the cavity, distributed statistically over four sites, with an occupancy of 0.64 per site. The fixed location of cavity-bound water in α-CD·6H_2O is unusual. The other CD hydrates have their included water statistically distributed among alternate sites. Thus β–CD·12H_2O has 6.5 included water molecules distributed among eight sites, and γ-CD·13.3H_2O has 5.3 included waters distributed among 13 sites. As a consequence of the hydrogen-bonding

arrangement in α-CD·6H_2O, the α-CD ring does not possess 6-fold symmetry, but is "puckered", and therefore has a higher conformational strain energy than the hexagonally symmetrical conformation. The "relief of strain energy" accompanying the process of guest inclusion has been proposed as a driving force for complex formation. Form III is nearly symmetrical, so it is considered not to possess excess conformational strain energy. The β-CD and γ-CD molecules are also close to symmetrical in their hydrated forms.

NMR studies on hydrates of β-CD and γ-CD show that the ^2H exchange rates of water molecules and hydroxy groups are greater than $10^6 s^{-1}$ (the NMR time scale). A neutron scattering study of β-CD·11H2O revealed two jump distances for H atom reorientation;[16] one of these describes jumps of hydroxy groups and water molecules over distances of about 1.5A, the other constitutes diffusive motion of water within the cavity over distances of about 3.0A. At room temperature both motions have rates of 2×10^{10} to 2×10^{11} s^{-1}.

1.1.3 Polarity of the Cyclodextrin Cavity

In 1967 van Etten et al.[17] showed that the ultraviolet absorption spectrum of 4-tert-butylphenol in an aqueous solution of α-CD closely matches its spectrum in dioxane. These authors did not explicitly conclude that the polarity of the α-CD cavity is similar to that of dioxane; rather they took the spectral coincidence as evidence that the aromatic chromophore was included in the ether-like cavity of the α-CD. Uno et al.[18] concluded, on the basis of blue shifts in the spectra of amine N-oxides in the presence of CDs, that

the cavity environment is like methanol or ethanol, depending upon the probe. A series of 1,4-disubstituted benzenes gave no consistent spectral shifts in α-CD solutions compared with spectra of these guest molecules in pure solvents, and it was decided that UV spectral probes cannot provide unambiguous evidence of the cavity polarity.[19] The spectrum of 1,4-dimethoxybenzene in 0.1 M aqueous α-CD exhibits fine structure closely mimicking its spectrum in cyclohexane, which is quite different from the nearly featureless bands observed in water or in dioxane.

Fluorescence spectroscopy is another method used to explore the polarity of cyclodextrin cavities and is relied on to study CD complexing, because fluorescence quantum yields are sensitive to the polarity of the probe's environment[23-25]. Cramer et al.,[20] in an important paper in the CD field, showed an enhancement in the fluorescence intensity of 1-anilino-8-naphthalenesulfonate in solutions of CDs, with β-CD and γ-CD having more profound effects than α-CD. This difference was attributed to the relative sizes of the guest and the CD cavities and was consistent with inclusion of the probe molecule. Later authors have related fluorescent probe behavior in the presence of CDs to cavity polarity,[21,22] in some cases comparing the cavity environment with that of a pure organic solvent, and in other cases attempting to attach a quantitative measure of polarity to the CD cavity. Heredia et al.[26] developed correlations between diphenylamine fluorescence energy and ET(30) and with Kosower's Z value used for polarity.[27] They assigned a Z value of 88 (similar to ethanol) to the cavity of β-CD. Street and Acree[28] related the emission wavelength of pyrene-3-carboxaldehyde to solvent dielectric constant, concluding that ε= 55 for α-CD and ε = 48 for β-CD. (The dielectric constant of dimethyl sulfoxide acid is 49; that of formic acid is 58.) Fluorescence enhancement

studies are not unambiguous routes to estimating effective CD polarity, because the fluorescence quantum yield is subject not just to the polarity of the environment, but also to restrictions placed on the motional freedom or collisional probability of the fluorescent probe.[29-31] The effect of a CD on fluorescence efficiency may be a consequence of both factors, as discussed by several authors.[29-34]

Some calculational studies have led to inferences about the environment within the cavity. Lichtenthaler and Immel[35] concluded that the β-CD cavity is hydrophobic, but that the α-CD cavity cannot clearly be placed in this category. They developed "lipophilicity patterns" based on solid-state complex structures, concluding that the three CD's are quite similar, with the wider (secondary hydroxyl) ends of the cavity being hydrophilic and the narrower ends hydrophobic.

1.1.4 Industrial Applications

Pharmaceutical

A drug substance has to have a certain level of water solubility to be readily delivered to the cellular membrane, but it needs to be hydrophobic enough to cross the membrane. The majority of pharmaceutically active agents do not have sufficient solubility in water, and traditional formulation systems for insoluble drugs involve a combination of organic solvents and surfactants, leading to extreme pH conditions, which often cause irritation or other adverse reactions. Cyclodextrins are not irritants and offer distinct advantages, such as the stabilization of active complexes, reduction in volatility of drug molecules, and masking of malodors and bitter tastes.

Agricultural and Chemical

Cyclodextrins form complexes with a wide variety of agricultural chemicals including herbicides, insecticides, fungicides, repellents, pheromones, and growth regulators. Benefits include stabilization and increased solubility. In the chemical industry, cyclodextrins are widely used to separate isomers and enantiomers, to catalyse reactions, to aid in various processes, and to remove or detoxify waste materials.

Cosmetics, Personal Care and Toiletry

The major benefits of cyclodextrins in this sector are stabilization, odor control, and process improvement upon conversion of a liquid ingredient to a solid form. Applications include toothpaste, skin creams, liquid and solid fabric softeners, paper towels, tissues and underarm shields.

Foods and Flavors

Cyclodextrins are used in food formulations for flavor protection or flavor delivery. Most natural and artificial flavors are volatile oils or liquids, and complexation with cyclodextrins provides a promising alternative to the conventional encapsulation technologies used for flavor protection. Cyclodextrins are also used as process aids - for example, to remove cholesterol from products such as milk, butter and eggs.

Adhesives, Coatings, and other Polymers

Cyclodextrins increase the tackiness and adhesion of some hot melts and adhesives. They also make additives and blowing agents compatible with hot melt systems. The interaction between polymer molecules in associative thickening emulsion-type coatings,

such as paints, tends to increase viscosity, and cyclodextrins can be used to counteract this effect when undesirable.

1. 2 Cyclodextrin Inclusion Complexes

1.2.1 General concepts

Cyclodextrin cavities are slightly V-shaped, with the secondary hydroxyl side more open than the primary hydroxyl side. The primary hydroxyl groups can rotate to partially block the cavity, while the secondary hydroxyl groups attached directly to the relatively rigid glucose ring cannot.[36] Because of the chemical structure and overall molecular shapes of α-, β-, γ-CDs, one of the most important characteristics of CDs is the formation of ICs with various guests in which the guest molecules are included in the cavities of the CDs (host). Figure 3 schematically illustrates a polymer-cyclodextrin inclusion complex. Guest complexes range from polar reagents such as acids, amines, small ions, and halogen anions to highly apolar aliphatic and aromatic hydrocarbons and even rare gases. Recently, even polymers have been found to be included as guests in CDs. Inclusion complexes can be formed either in a solution or in the crystalline state. Water is usually used as the solvent, although IC formation may also take place in dimethyl sulfoxide and in dimethyl formamide. This particular feature distinguishes CDs from other host molecules, in which single molecules are unable to form ICs and require crystallization into a lattice in order to provide a matrix with suitable cavities for the included guests.

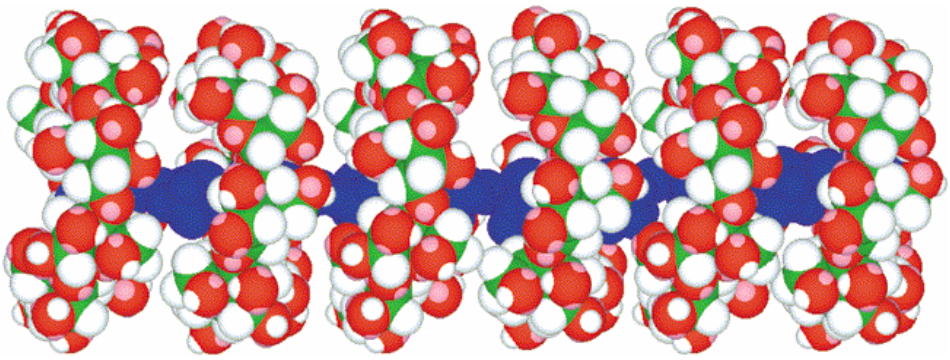

Figure 3. Schematic representation of a polymer cyclodextrin inclusion complex (following reference 70)

Cyclodextrin complexes have great stability when the guest molecule can adopt an orientation in the CDs that allows maximal interaction with groups lining the interior of the ring. γ-Cyclodextrin appears to be too large to form stable complexes with small molecules, but α-, β-cyclodextrins will complex them more readily and α-cyclodextrin excludes large molecules.

Cyclodextrins (CDs) are carbohydrates that can form ICs with a wide range of guest complexes. Unlike urea,[37,38] thiourea(TU),[39] and perhydrotriphenylene (PHTP),[40,41] with ICs that can only exist in the solid state and in which guest molecules are included in channels provided by the crystalline structure of the host, CDs can also form ICs that are soluble and stable in solutions because of their ring structures. In solution, a single CD molecule can provide the cavity in which a guest molecule is bound. Figure 4 shows the ICs formed with urea and PHTP hosts.

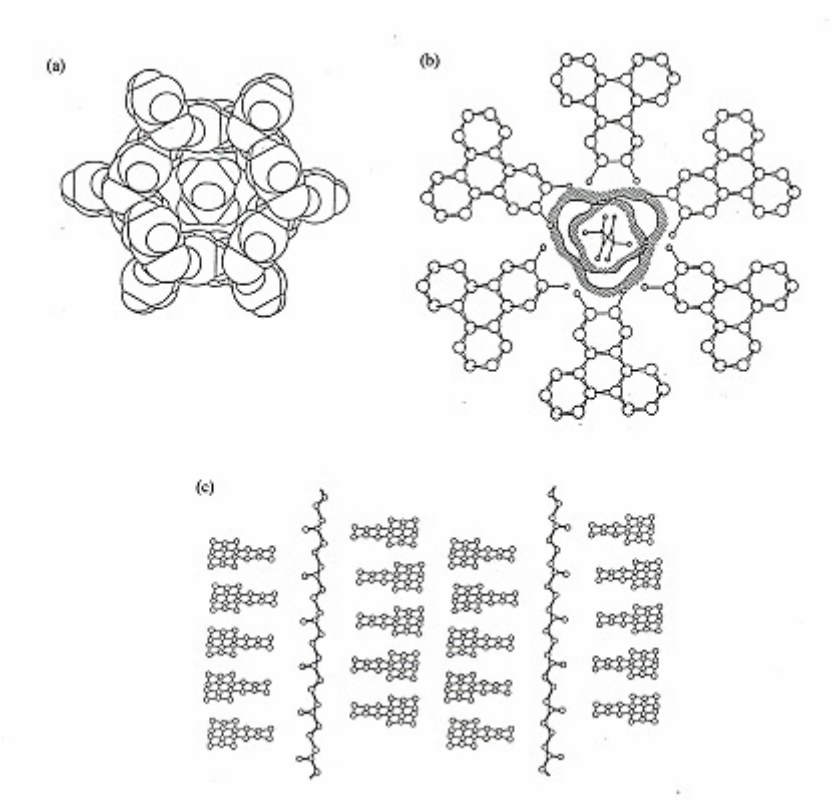

Figure 4. View down the channel of the (a) n-hexadecane-U-IC crystal (b) polybutadiene-PHTP-IC crystal, (c) view perpendicular to the channel of the polybutadiene-PHTP-IC crystal (following reference 1)

Two types of crystal structures have been observed for solid CD IC's. They are the channel and cage structures shown in Figure 5.[42] In channel-type complexes, CD molecules are stacked on top of each other like coins in a roll, producing linearly aligned, "endless" channels in which guest molecules are included. The stacks of CDs are stabilized by hydrogen bonds either between O_2H/O_3H and O_6H sides, producing a head-to-tail pattern, or between O_2H/O_3H on one side and between O_6H/ O_6H on the other, leading to a head-to-head/tail-to-tail arrangement. In crystal structures belonging to the

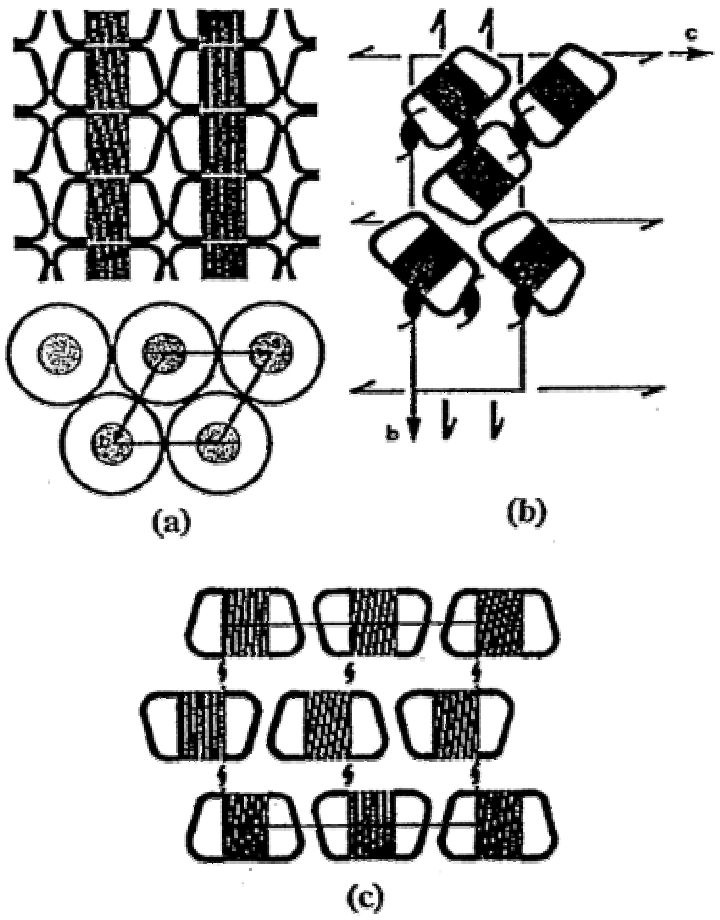

Figure 5. Schematic description of (a)channel type, (b)cage herringbone type, and (c)cage brick type crystal structures formed by crystalline cyclodextrin inclusion complexes. (following reference 2)

cage type, the cavity of each CD molecule is blocked off on both sides by adjacent CD's, thereby leading to isolated cavities. Depending on the packing of the CD molecules, two categories of cage complexes are encountered. In the first, CDs are packed crosswise in herringbone fashion, a pattern most common in pure α-, β-, and γ-CDs. In the other, thus far observed only for α-CD complexes with some para-substitued benzene derivatives or with a dimethylsulfoxide/methanol mixture, a motif reminiscent of bricks in a wall is

found. There, the α-CDs are arranged in sheets with all O_2H/O_3H hydroxyls on one side and all O_6H's on the other side. Adjacent sheets face each other with lateral displacements, so the α-CDs cavities are closed on both sides by adjacent molecules.

What are the conditions for channel- or cage-type CD-IC formation? We know the conditions only for α-CD. Small molecular guests reside in cages, whereas long and ionic guests prefer channels. This behavior is especially obvious with carboxylic acids. The α-CD complexes with acetic, propionic, and butyric acid cystallyize in cages, whereas valeric acid and higher analogues reside in channels- a clear and well-defined size selectivity. Since polymers are long chains, normally they will adopt channel-type crystal structures when they form ICs with CDs, as illustrated in Figure 3.

X-ray measurements have been compared with solid-state NMR data to describe the host-guest interaction. The neat guest structures are compared to the included guest. By studying the differences in these structures, it is hoped to increase our understanding of the interactions involved in molecular and chiral recognition. Cramer[43] reported unit cell dimensions for channel complexes of 1-hexanol, 1-octanol, and 1-dodecanol with α- and β-CDs that are the same as the pure CDs. For Cramer's α-CD complexes, the cell dimensions were reported as a=14.95 Å, b=3.11 Å, and c=9.5 Å for an orthorhombic crystal form system. These differ slightly from the cell dimensions reported by James, French, and Rundle, with a=14.78 Å, b=33.96 Å, and c=9.51 Å for α-CD cage complexes with iodine and lower alcohols and may be due to hydration and the overall difference in cage and channel structures.

1.2.2 Small Molecule Cyclodextrin Inclusion Complexes

A large number of ICs with low molecular weight complexes as guests have been prepared and characterized. The normal parameters found for the inclusion of small molecules are:

1. Stoichoimetry (guest : CD): 1:1, 1:2, 2:1, 2:2
2. Formation speed $T_{1/2} \sim 0.001$ - 1 ms
3. Complex stability constants
4. Complexes suitable for complexation >5 atoms (C,P,N,S)
5. Solubility in water <10 mg/mL

Several recently made small molecule inclusion complexes are introduced here to shed light on progress in this field. Because CD complexes are held together purely by noncovalent interactions, they function as excellent models for the study of chiral and molecular recognition mechanisms. Recently, room-temperature crystallographic studies of both the 2:2 N-acetyl-L-phenylalanine methyl ester/β-CD and 2:2 N-acetyl-L-phenylalanine amide/ β–CD complexes were reported. The effect of changes in carboxyl back-bone functional groups on molecular recognition by the host CD molecule was examined for the nearly isomorphous supramolecular complexes. A new perturbation of the system is now examined, specifically perturbation of the aromatic side chain. Clark reports a room-temperature crystal structure determination for the 2:2 N-acetylp-methoxy-L-phenylalanine methyl ester/ β-CD inclusion complex.[44] The complex crystallizes isomorphously with the two previously reported examples in space group PI; the asymmetric unit consists of a hydrated head-to-head host dimer with two included guest molecules. The crystal packing provides both a nonconstraining extended

hydrophobic pocket and an adjacent hydrophilic region, where hydrogen-bonding interactions can potentially occur between primary hydroxyl groups of neighboring CD molecules and waters of hydration. The rigid host molecules show no sign of conformational disorder, and water of hydration molecules exhibit the same type of disorder observed for the other two complexes, with a few significant differences in locations of water molecules in the hydrophilic region near guest molecules. There is evidence from the electron density map for modest disorder in the guest region. In comparing this system with the two previously reported complexes of phenylalanine derivatives, it is found that the packing of the guest molecules inside the torus of the CD changes upon substitution of a methoxy group at the para position of the aromatic phenyl ring. Backbone hydrogen-bonding interactions for the guest molecules with the CD primary hydroxyls and waters also change. This structure determination is a new and revealing addition to a small but growing data base of amino acid and peptidomimetic interactions with carbohydrates.

Naturally occurring CDs and their derivatives have been widely applied for improving the oral delivery of drugs, in particular for increasing the rate of absorption through an increase in the rate of dissolution, decreasing gastrointestinal irritancy, preparing ready-to-use solution formulations, and masking of objectionable tastes.

An additional approach has recently been claimed by Penkler et al[45]. They found that by using hydroxylamines, such as tromethamine, it is possible to increase the association constant between naproxen and CD at neutral (physiological) pH due to a combination of ionic, hydrogen bond, and van der Waals interactions, as opposed to the exclusive van der Waals interactions, in the binary system. In addition to increasing the solubility, the

higher association constant of the ternary complex retards dissociation of naproxen in the oral cavity and thereby better masks its taste.

Several studies concerning the structural features/thermodynamic properties of the complexes of the salts of arylpropionic nonsteroidal anti-inflammatory drugs with CD have also been carried out. Ketoprofen in the ionized form and CD form a 1:1 complex with an equilibrium constant of 190 M^{-1}. The reduced affinity for the CD cavity in comparison with the unionized form indicates that the site of interaction is not far from the carboxyl group[46]. Bettinetti et al.[47] studied the interaction of naproxen with CDs in solution on addition of NaOD by ^{13}C NMR. They found that α-CD forms a 1:2 complex, β-CD and derivatives form 1:1 adducts, and γ-CD forms both 1:1 and 1:2 complexes. The highest stability of the complex with γ-CD was explained in terms of a better fitting inclusion of the naphthalene ring. Salvadori et al.[48] reported that fenoprofen calcium salt forms a 1:1 complex with γ-CD with an association constant of 2010±20 M^{-1}. The inclusion occurs through penetration from the larger-diameter side of the γ-CD by the aromatic ring and is favored by the interaction of the protruding carboxylate group of fenoprofen with the hydrophilic external part of the cavity. Also the (+)- and (-)-enantiomers of flurbiprofen sodium salt form 1:1 complexes with γ-CD with association constants of 3500 and 5700 M^{-1}, respectively. Both enantiomers are similarly included into the cavity from the small-diameter side of γ-CD.

1.2.3 Polymer Cyclodextrin Inclusion Complexes

In recent years, published reports concerning polymer inclusion complexes formed with CD hosts have increased. Initially, there were only a few examples in which a

monomer was polymerized in situ within a CD complex. Ogata, Sanui, and Wada[49] prepared hexamethylenediamene complexed with β-CD. Polyamides were obtained by condensation of dibasic acid chlorides and the ICs of the diamine. Maciejewski[50] reported the polymerization and copolymerization of vinylidene chloride as adducts of β-CD. Some reports suggested interactions between CDs and some polymers in aqueous solutions. Kitano and Okubu[51] reported that CDs show some effects on the critical micelle concentrations of some micelle-forming surfactants. Iijima et al.[52] studied diffusion of CD in the presence of poly(styrenesulfonate) in aqueous solutions and reported that there are some interactions between CD and the polymer.

Table 2. Inclusion complexes formation between CD and PEG terminated with various small end groups[53]

$R(CH_2CH_2O)_nCH_2CH_2R'$			Yields (%)	
R	R'	M_n	α-CD	β-CD
-OH	-OH	1000	90	0
$-NH_2$	$-NH_2$	1450	94	0
		2000	96	0
$-OCH_3$	$-OCH_3$	500	88	0
		1000	93	0
		2000	98	0
$-OCH_3$	-OH	750	89	0

One Japanese research group, Harada et al[53]. reported that α-CD can form ICs with poly(ethylene glycol) (PEG) (monomer: CD=2:1) of various molecular weights to give

stiochiometric complexes in a crystalline state. When aqueous solutions of PEG were added to a saturated aqueous solution of α-CD at room temperature, the solution became turbid, and the complexes were obtained as precipitates when the average molecular weight of PEG was between 400 and 10,000. This was the first observation that CD forms a solid state complex with a polymer[53]. Table 2 lists the results of complex formation between α-CD and PEG with different end groups. PEG's with small end groups, such as methyl, dimethyl, and amino groups, form complexes. The yields are rather higher than unmodified PEG. These results indicate that interactions (hydrogen bonds) between the OH groups of PEG and OH groups of α-CD may not be the driving force for complex formation. PEG carrying bulky substituents, such as a 3,5-dinitrobenzol group and a 2,4-dinitophenyl group at the ends of the PEG, which do not fit or pass through the α-CD cavity, did not form any complex with α-CD.

As we discussed above, the structures of ICs and CDs can be roughly classed into two groups: cage and channel. The x-ray powder pattern of the α-CD-PEG complex shows that the complexes are crystalline, and the patterns are very similar to those of the complexes of α-CD with valeric acid or octanol, which have been reported to have the extended column structure and are totally different from those of the cage complexes formed with small molecules such as acetic acid, propanol, and propionic acid. These results indicate that the complex of α-CD and PEG is isomorphous with those of channel-type structure rather than the so-called cage-type structures.

Figure 6 shows a proposed structure of the complex of PEG with α-CD. The IC formation of PEG in the α-CD's channel is entropically unfavorable. However, formation of the complex is thought to be promoted by hydrogen bond formation

between α-CDs. Harada, Li, and Kamachi[53] proposed this head-to-head and tail-to-tail arrangement as the most probable structure.

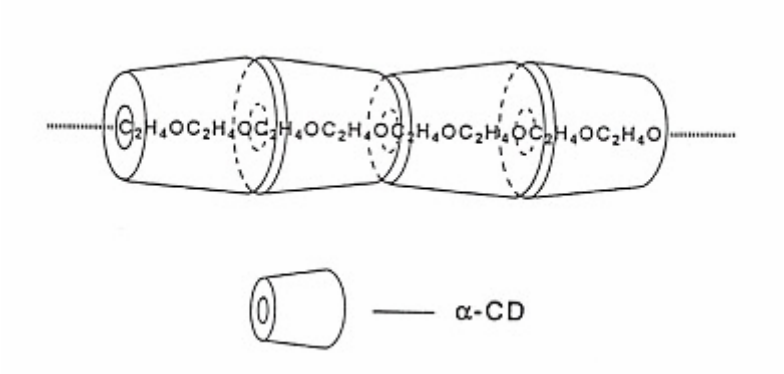

a

b

Figure 6. Inclusion complex of PEG and α-CD (a)scheme and (b)single crystal structure presented by X-ray (following reference 53)

Cyclodextrins thread onto polymer chains to form inclusion complexes, especially when the polymer is hydrophobic relative to the solvent. Selective threading might occur

when the polymer architecture contains both hydrophobic and hydrophilic segments. Olson et al.[54] report that α-CD formed crystalline inclusion complexes with (AB)(n) microblock copolymers, where the A block was a linear alkyl segment containing a single double bond and the B block was an exact length segment of poly(ethylene oxide). The complexes were isolated and characterized by solution and solid-state NMR, X-ray diffraction, differential scanning calorimetry, and thermogravimetric analysis. Each method confirmed complex formation and showed that the physical properties of the complexes were distinct from those of its individual components.

The X-ray data were consistent with known inclusion complexes having a channel or column crystal structure. The stoichiometry of the complex formation, 2.3 α-cyclodextrin rings per polymer repeat unit, was determined by NMR analysis of the complexes and from an analysis of the inclusion complex yields. The data suggest that the inclusion complex stoichiometry is defined by the increasing insolubility of the polymer-cyclodextrin complex. Solid-state NMR data were consistent with a preference for threading onto hydrophobic segments of the (AB)(n) polymer. The NMR spectroscopy of inclusion complexes of α-CD and (AB)(n) block copolymers is shown in Figure 7.

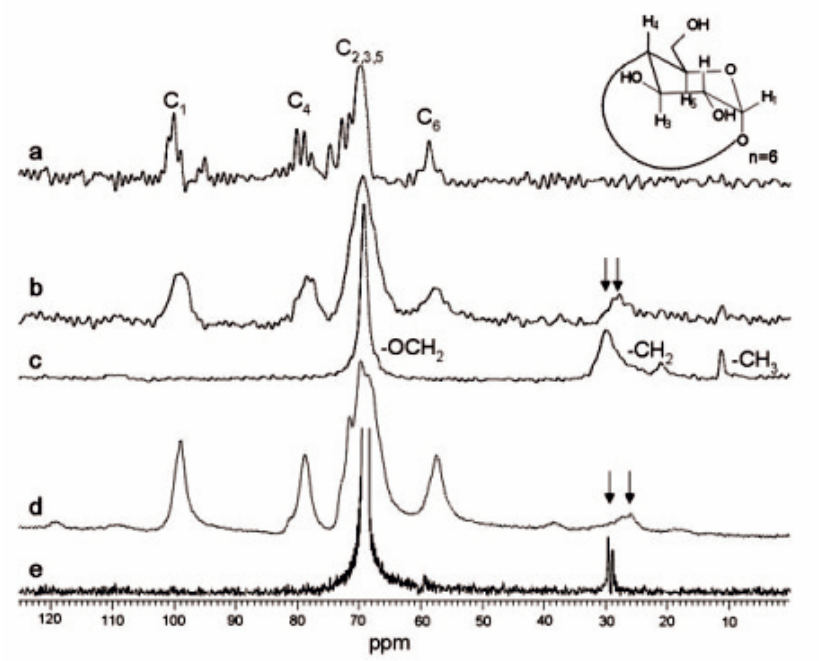

Figure 7. ^{13}C CP-MAS NMR spectra of (a) α-CD, (b) $C_{12}EO_{14}C_{12}$/α-CD, (c)$C_{12}EO_{14}C_{12}$, (d)[$C_3C_3EO_8$]n/α-CD, and (e)[$C_3C_3EO_8$]n. Arrows indicate ^{13}C resonances for the alkyl segments of [$C_3C_3EO_8$]n and the ABA oligomer that shift when complexed with α-CD. The resonances labeled in spectrum (a) follow the normal priority rules for naming carbohydrates (anomeric carbon = 1). Spectra were taken at a spinning rate of 4.0 kHz (following reference 54)

1.3 Parameters Characteristic of Polymers that form Cyclodextrin Inclusion Complexes

1.3.1 Chemical Structure

It is easy to imagine that the chemical structure of a polymer is important to the formation of polymer cyclodextrin inclusion complexes, since the interior diameter of cyclodextrins are somewhat rigid and fixed. Besides this steric effect, the intermolecular

interactions between guest and host may also be important to prevent guest polymers from sliding out of the host cyclodextrin rings[55].

Cyclodextrins form inclusion complexes with various low molecular weight compounds, ranging from nonpolar hydrocarbons to polar acids and amines. The Harada group have reported that CDs form inclusion complexes with some organic polymers to give crystalline complexes with high selectivity. For example, α-CD forms complexes with poly(ethylene glycol) and polyethylene (MW < 1000). β-CD formed complexes with poly(propylene glycol) and polypropylene (MW < 1000). γ-CD formed complexes with poly(methyl vinyl ether)[53]. Other groups also reported complex formation between CDs and polyesters. A polyrotaxane, in which many α-CDs were threaded onto a poly(ethylene glycol) chain, was also prepared. Wenz et al. reported α-CDs threaded on a polyamine[56].

Although PEG can form an IC with α-CD, PPG can form ICs with β-CD and γ-CD. PEG and OE (oligomeric polyethylene), which have the smallest cross-sectional areas, selectively form complexes with α-CD (D=5.0 Å), while PPG and squalane, which have larger cross-sectional areas, selectively form complexes with β-CD (D=7.0 Å) and γ-CD (D=8.5 Å). The complex formation is chain-length dependent and stoichiometric. The IC's were isolated and found to be 2:1 (monomer unit:CD) for PEG-CD IC and PPG-CD IC. Table 3 lists the formation of complexes between cyclodextrins and hydrophobic polymers/oligomers with various chain cross-sectional areas.

Results have been reported [57-59] of IC studies between CDs and low molecular weight PEO-PPO and PEO-PPO-PEO (diblock and triblock copolymers of ethylene oxide and propylene oxide, M_n varies from $2.0*10^3$ to $4.7*10^3$). The proposed model of the chain

copolymer ICs is that the main structural elements are the polymer guest chain, with a sequence of host ß-CD molecules threaded on the PPO block, with one molecule of CD per two units of propylene oxide.

Table 3. Formation of complexes between cyclodextrins and hydrophobic polymers/oligomers with various chain cross-sectional areas[53]

Polymer/Oligomer	Structure	Mw	Yield(%)		
			α-CD	β-CD	γ-CD
OE(20)	$-CH_2CH_2-$	563	63	0	0
Squalane	$-CH_2CH(CH_3)CH_2CH_2-$	423	0	62	24

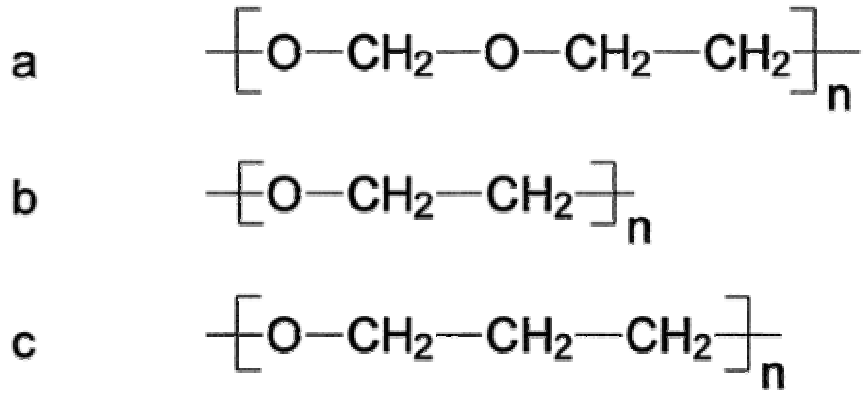

Figure 8. Molecular Structures of (a) Poly(1,3-dioxolane), (b) Poly(ethylene glycol), and (c) Poly(trimethylene oxide) (following reference 60)

Li et al.[60] reported that α-, β-, and γ-CDs are all able to form crystalline inclusion complexes with poly(1,3-dioxolane) (PDXL). Though it was reported that PEG only forms inclusion complexes with α-CD and γ-CD and PPG only forms an inclusion

complex with β-CD. Among the three polyethers, PDXL possesses the highest oxygen atom density (see Figure 8), and it seems intermolecular interactions predominate over the geometric incompatibility. Furthermore, the results of this article are important in probing the driving force in the formation of crystalline inclusion complex between cyclodextrins and polymer chains. These phenomena were attributed to the geometric compatibility or fit between hosts and polymeric guests. It seems the intermolecular interaction also plays an important role due to the high oxygen atom density in PDXL chains. Therefore, PDXL can form crystalline inclusion complexes with all three CDs. The results of X-ray diffraction study indicate that all the crystalline inclusion complexes have columnar structures.

Mayer[61] et al presented a computational study on the formation of a molecular necklace formed by specific threading of cyclodextrins (CDs) on block copolymers. Structural as well as energetic principles for the selective complexation of α-CD and β-CD with poly(ethylene oxide)-poly(propylene oxide) block copolymers (PEO-PPO) were elucidated by considering a diblock copolymer of equimolecular composition (PEO)(4)-(PPO)(4) as guest. A non-statistical distribution of CDs, i.e. α-CD primarily located on the PEO chain and β-CD on PPO blocks of the polymer, is based on a variety of structural features and energetic preferences considering both potential as well as solvation energies. This selectivity, is already evident when considering 1:1 complexes between PEO and PPO monomers and the two CDs, but becomes increasingly obvious when calculating higher order ensembles. Besides the host-guest interactions, docking between CDs themselves is an important, also non-statistical, prerequisite for the self-assembly of highly ordered tubes. The formation of intermolecular hydrogen bonds

between adjacent CDs in a tubular aggregate gives an important contribution to the overall stability of the molecular necklace. The net effect, based on the preferential interaction between host and guest, as well as that between the host molecules themselves, results in the formation of a stable, highly ordered macromolecular, multicomponent aggregate.

Some inclusion complexes between cyclodextrin and end-group modified polyethers have been investigated. Sandier[62] reported formation of inclusion complexes between a telechelic polymer and a second polymer containing appropriate receptor groups. The main focus of this paper describes such complexes between an adamantane end-capped poly(ethylene oxide) (PEO) (M_w = 10^4g/mol) with a polymer of β-cyclodextrin (M_w= $3.5*10^4$g/mol) as studied by light scattering. There is a pronounced broadening of the width of the particle size distribution with increasing concentration of end-capped polymer, accompanied by a strong increase in the average relaxation time. Viscosity enhancement in the system was measured on the same samples. Newtonian behavior was observed in the shear rate range 0.017-90 s^{-1}. Light scattering experiments (static and dynamic) were also made on the telechelic PEO itself. Light scattering shows the presence of a slowly relaxing component which dominates the scattering and this reflects large structures (radius 80 nm) created by interchain association to form a loose network, albeit at low concentration. Static and time-resolved fluorescence experiments show that there is no detectable tendency for "micellization" of the adamantane groups.

Popova[63] studied the complex formation in the ternary γ-cyclodextrin-PEO-nitroxyl radical and γ-cyclodextrin-(PPO-PEO-PPO)triblock copolymer-nitroxyl radical systems. It was shown that self-assembly processes in both systems result in the formation of a

mixture of two binary inclusion complexes: a γ-cyclodextrin-polymer molecular necklace and a γ-cyclodextrin-nitroxyl radical. None of the systems studied showed evidence of the formation of a ternary complex. In the case of the γ-cyclodextrin-triblock copolymer-nitroxyl radical system, the probe is localized in microphases formed by amorphous PEO blocks.

Amiel[64] reports associating systems which have been obtained by mixing hydrophobically end-capped polyethylene oxide and water soluble β-cyclodextrin polymers in aqueous solutions. The hydrophobic naphthyl and adamantyl end groups, were chosen in order to match the β-cyclodextrin cavities. Inclusion complex formation between the PEO terminal groups and β-cyclodextrin are responsible for the association of polymers. Complexation constants were determined by fluorescence methods, using the fluorescent probe 1-8 ANS as a competitor for complexation against the adamantyl groups or by directly checking the fluorescence of the naphthyl groups by fluorescence anisotropy measurements. The onsets of the polymolecular associations were also monitored by viscosimetry.

Harada[65] also described the complex formation between cyclodextrins (CDs) and poly(propylene glycol) (PPG) derivatives. β-CD and γ -CD formed complexes with PPG derivatives such as l-naphthyl (1NA), 2-naphthyl (2NA), 3,4-dinitrobenzoyl, and 2,4-dinitrophenyl PPG. α-CD did not form complexes with these PPG derivatives. Although γ-CD gave complexes with 9-anthryl PPG (PPG9An), β-CD did not efficiently form complexes with PPG9An. β-CD did not form complexes with trityl PPG, demonstrating that trityl groups were too bulky to thread a β-CD cavity. The emission spectra of the complexes showed that β-CD bound a single 2NA moiety in its cavity and that γ-CD

included two 2NA moieties. In contrast, γ-CD bound a single 1NA moiety in the cavity. X-ray diffraction studies and H^1 NMR analysis showed that the CD molecules were stacked along a PPG chain forming a channel structure.

Recently, some other classes of polymers were also found to be able to form ICs with cyclodextrins. Harada found that CDs form inclusion complexes with aliphatic polyesters $[-O(CH_2)_xOCO(CH_2)_4CO-]_n$ (where x = 2, 3, or 4) to give crystalline complexes[66]. α- and γ-CD formed complexes with these polyesters in high yields, although β-CD gave complexes in moderate yields. Although the yields of the complexes of α-CD with poly(trimethylene adipate) (PTA) (x = 3) and poly(1,4-butylene adipate) (PBA) (x = 4) decreased with increasing molecular weight, γ-CD formed complexes with poly(ethylene adipate) (PEA) (x = 2) in high yields even at higher molecular weights. The yields of the complexes of CD with these polyesters showed a maximum at a molecular weight of 1000.

Yui et al made the polymer IC between poly(ε-lysine) (PL)and α-CD by simple mixing of two aqueous solutions of PL and α-CD with initial stirring[67]. They also found that the β- and γ-CD could not form complexes with PL. Their cavity sizes are too large for tight steric fit with the polymer chain. In such cases, even if the polymeric guests form complexes with CDs for an instant, the complexes may dissociate easily.

Jiao et al. showed that poly(neopentyl glycol sebacate) (PNGS) is able to form inclusion complexes with three cyclodextrins (α-CD, β-CD, and γ-CD)[68]. The complexes possess a column structure wherein some structural change occurs when the "raw" γ-CD/PNGS complex is washed and dried. It was suggested that α-CD can "squeeze" over

the bulky dimethyl groups and settle on and complex the thinner part of the polymer chain. Figure 9 shows the chemical structure of the polymers investigated. Besides organic polymers, it was recently reported that β-CD and γ-CD form complexes with poly(dimethylsiloxane) (PDMS), a typical inorganic polymer and that the chain-length selectivities between β-CD and γ-CD are reversed[69,70].

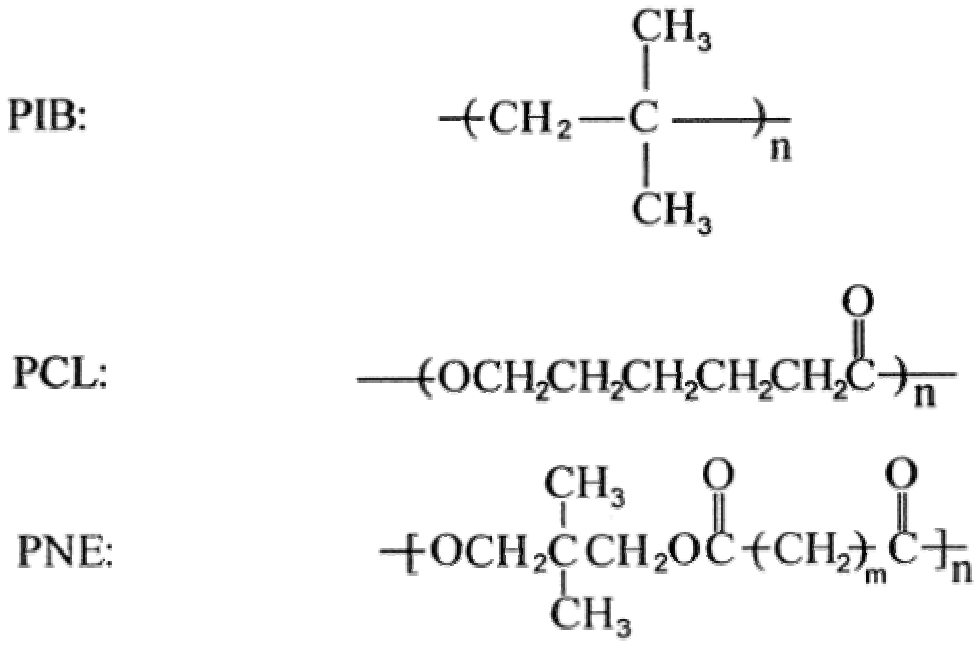

Figure 9. Structures of PIB, PCL, and PNE (m=10 for PNGS) (following reference 68)

1.3.2 Conformation and Configuration

To form an inclusion complex, the polymer chain must be able to adopt a conformation which can fit into the CD cannel. Inclusion complex formation between polyaniline with emeraldine base and β-cyclodextrin has been studied by frequency-domain electric

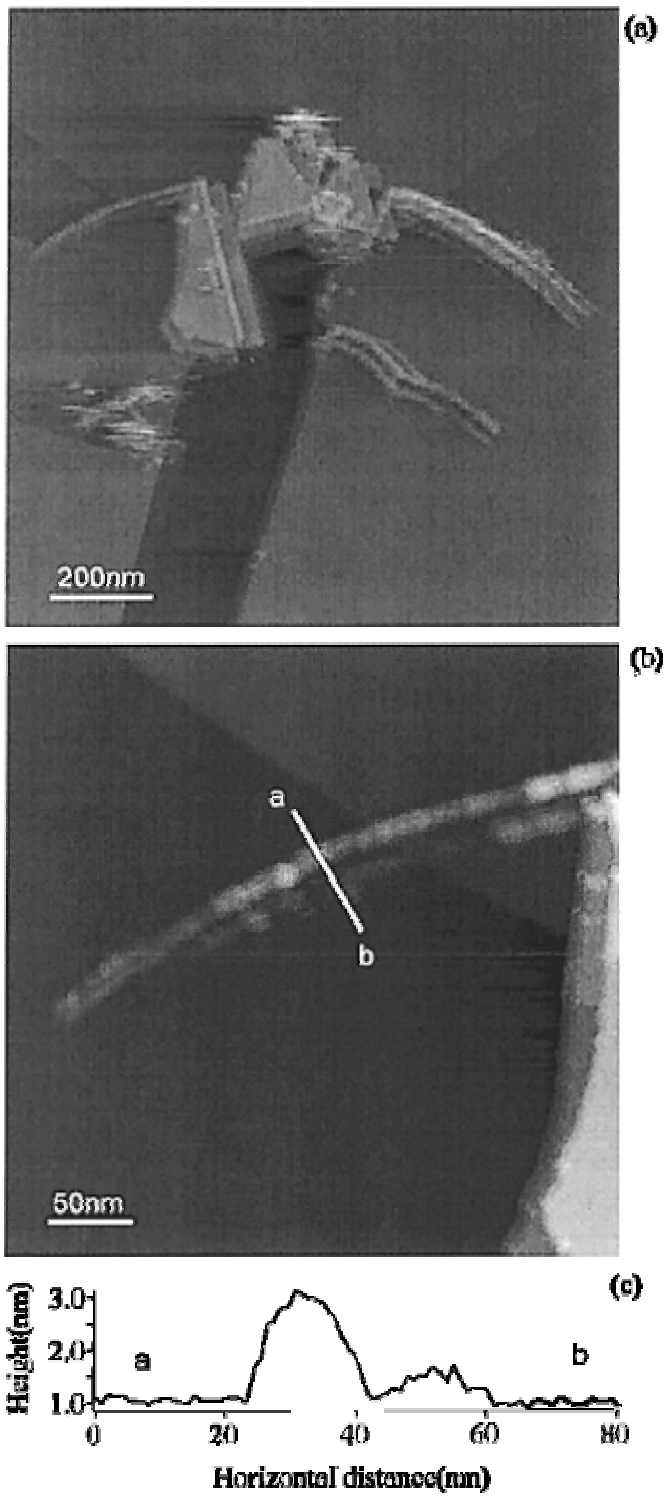

Figure 10. STM images where fields of view are (a) 1200 nm × 1200 nm and (b) 350 nm × 350 nm. (c) The height profile of the cross section (following reference 71)

birefringence (FEB) spectroscopy in a solution of N-methyl-2-pyrrolidone (NMP) and by scanning tunneling microscopy (STM). The FEB results show that polyaniline in the solution with cyclodextrin changes its conformation from coil to rod at low temperature (below 275 K), and some rodlike images are observed on a substrate by STM[71]. These results suggest that cyclodextrins are threaded onto polyaniline and confine and extend the conformation of the polymer chain to a rodlike one. Furthermore, it was found that the threaded cyclodextrins prevent chemical oxidation, i.e., doping of polyaniline by iodine. This indicates formation of a new inclusion complex, a conjugated conducting polymer covered by insulating cyclic molecules, namely, an "insulated molecular wire", which is shown in Figure 10.

The conformations of stereoregular poly(L-lactide) (PLLA, optically active) and regularly alternating poly(L,D-lactide) (PLDLA, optically inactive) confined to occupy cylinders of varying radii were determined in an effort to learn if either polylactide could be incorporated in the narrow channels of its inclusion complex (IC). Tonelli[72] reported that only PLLA chains in the extended, nearly planar zigzag, all-trans conformation fit in cylinders whose diameters D correspond closely to those observed in polymer-urea-IC's, namely, D approximately 5.5 Å. PLDLA chains were not able to fit in cylinders with D < 7.5 Å. Because in its IC the PLLA chains are nearly all-trans, while in bulk crystalline PLLA and in the 1:1 crystalline complex formed between PLLA and PDLA the chains adopt 10(3) and 3(1) helical conformations, respectively, significant differences were found between their high-resolution, solid-state CPMAS/DD ^{13}C NMR spectra.

Two different kinds of poly(3-hydroxybutyrate)s (PHB)s have attracted attention recently. One kind of PHB is the optically active poly(R-3- hydroxybutyrate) (i-PHB),

which has an isotactic stereosequence and is synthesized and accumulated by a variety of bateria as a reserve energy source. Another kind of PHB is man-made and usually atactic

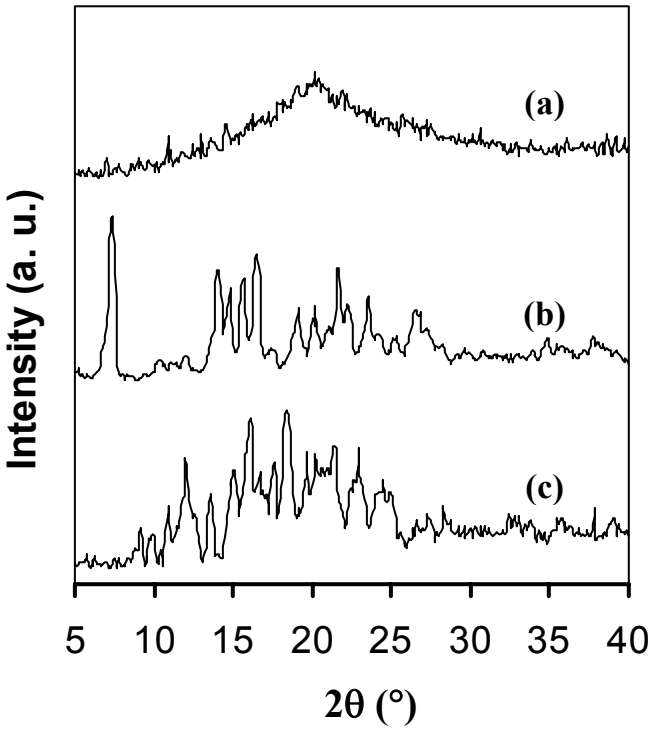

Figure 11. X-ray diffraction patterns of (a) a-PHB, (b) γ-CD-a-PHB IC, and (c) γ-CD

polymer(R,S-3-hydroxybutyrate)(a-PHB). i-PHB and a-PHB may have different cross-sectional sizes in their extended conformations. Therefore, it is anticipated that they will show different complex behavior with cyclodextrin. The NMR and WAXD results showed that a-PHB may form an IC with γ-CD, but does not form ICs with α-CD and β-CD. Figure 11 shows the X-pattern of γ-CD-a-PHB IC. Due to the side methyl groups and their atactic attachment, the cross sectional area of a-PHB is larger than, e.g., PCL and PLLA, which have been demonstrated to form ICs with α-CD. Therefore, α-CD and β-CD cavities might be too small to accommodate the a-PHB chain in low energy,

extended conformations necessary for inclusion. In contrast, i-PHB only forms IC with α-CD, while β- and γ-CD did not form complexes with i-PHB. Their cavity sized might be too large for a close steric fit with i-PHB chain that is required for inclusion[75].

Polybutadienes were found to form inclusion complexes with cyclodextrins in high selectivity to give crystalline complexes. α-Cyclodextrin and β-cyclodextrin form complexes only with polybutadienes of low molecular weight and high 1,4-addition content. Polybutadienes with high 1,2-content gave complexes with γ-cyclodextrin in low yield. The yields of the γ-cyclodextrin complexes decreased with increasing molecular weights of the polybutadienes of similar composition[76].

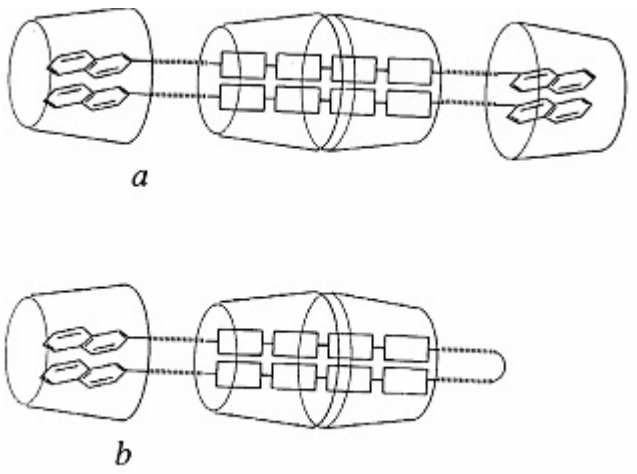

Figure 12. Probable structures of complexes of mononapthyl PEG: (a) an intermolecular double-chain complex; (b) an intramolecular single-chain complex (following reference 77)

Through consideration of both the size compatibility and stoichoimetry, it was found that only single PEO chains can be incorporated inside the narrow α-CD channels, while

two side-by-side PEO chains can be incorporated inside the γ-CD channels [77, 78]. In this case, the conformation of polymer chain should be more extended. Probable structures of complexes of double chains of mononapthyl PEG are shown in Figure 12.

1.3.3 Molecular Weight

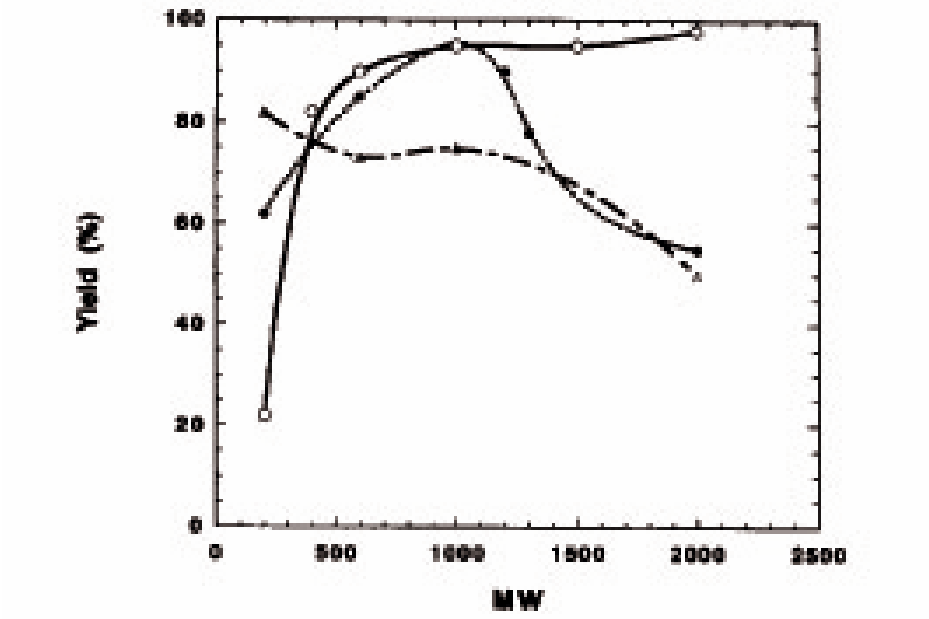

Figure 13. Yield of the complexes of α-CD with (o)poly(ethylene glycol)(PEG), (•)poly(trimethylene oxide)(PTO) and (Δ)poly(tetrahydrofunan)(PTHF) as a function of polymer molecular weight (following reference 79)

It has been found that the molecular weight of guest polymers has an influence on the formation of their cyclodextrin inclusion complexes. Figure 13 shows the effects of the molecular weight on the complex formation of PEG, PTO, and PTHF with α-CD.

The yields of the complex of PEG with α-CD increased with increase in the molecular weight of the polymer and reached saturation at about molecular weight of 1000. The yields are based on weight of isolated complex. However, in the case of PTO, the yields increased with increase in the molecular weight, reached a maximum at about molecular weight 1000, and then decreased with increased molecular weight[79,80]. In contrast, the yield of the complexes with PTHF decreased with increase in the molecular weight, with a slight increase in the yields at molecular weight 1000[81]. These results indicate that the stability of the complexes with hydrophilic polymers increase with increase in the molecular weight of polymer, and reached a maximum at about molecular weight 1000. However, as polymers become more hydrophobic, it becomes more difficult for cyclodextrin to include such polymer chains completely by dissolving both CDs and polymer in water.

It has also been reported that α-cyclodextrin hosts were used in order to separate a mixture of poly-(ethylene glycols) (PEGs) with two different molecular weights (Mw = 600 [PEG(600)] and Mw = 20000 [PEG(20000)]) by forming their respective inclusion complexes (ICs)[82]. The high melting point of the urea inclusion complex (PEG*-U IC), formed from the solution containing both polymers, was the first evidence that urea preferentially included poly(ethylene glycol) with the higher molecular weight. The PEG*-U IC and PEG(20000)-U IC X-ray diffraction patterns and FTIR spectra were very similar to each other, confirming that urea preferentially complexes PEG(20000) in their mutual solution. Since the same techniques were not as useful in the case of α-CD ICs, viscosity measurements were made in order to demonstrate the molecular weight selectivity of α-CD host. The efflux time of PEG*-α-CD IC solution was much closer to

that of a PEG(20000)-α-CD IC solution, which suggested that α-CD also preferentially included poly(ethylene glycol) having a high molecular weight rather than the low molecular weight PEG(600). The efflux time of PEG*-U IC solution was almost identical with that of the PEG(20000)-U IC solution indicating that urea has better molecular weight selective properties than α-CD.

In the case of hydrophobic polymers as guests in CD-ICs, β-CD and γ-CD formed inclusion complexes with poly(isobutylene) (PIB) of various molecular weights to give stoichiometric complexes in crystalline states. α-CD did not form complexes with PIB of any molecular weight. The yields of the complexes with β-CD decreased with an increase in the molecular weight of PIB. In contrast, the yields of the complexes with γ-CD increased with an increase in the molecular weight and the complexes were obtained almost quantitatively with PIB of molecular weight 1350. The chain-length selectivity is

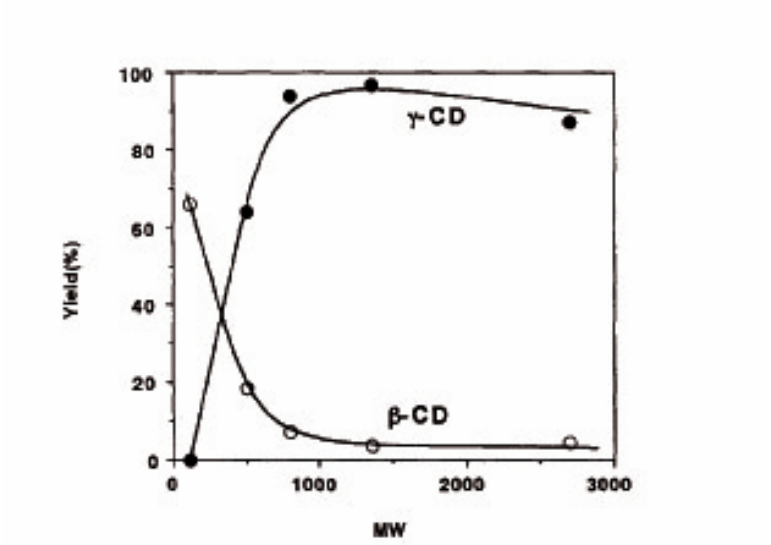

Figure 14. Yields of the complexes between PIB and cyclodextrins as a function of the molecular weight of PIB (o)β-CD-PIB (•)γ-CD-PIB complexes (following reference 83, 84)

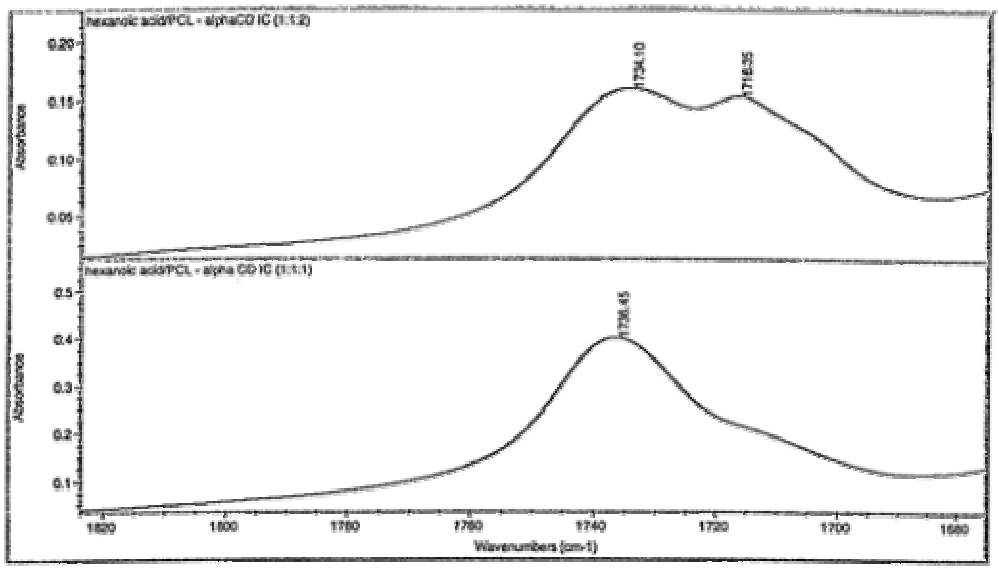

Figure 15. Expansions of the carbonyl stretching regions of the FTIR spectra (a) HA/PCL-α-CD IC (1:1:1) and (b) HA/PCL-α-CD IC (1:1:2) (following reference 85)

reversed between β-CD and γ-CD. The inclusion complexes were isolated and found to be 3:1 (monomer unit : CD)[83,84]. Figure 14 shows the yields of the complexes between PIB and cyclodextrins as a function of the molecular weight of PIB.

α-CD inclusion complexes were prepared in the presence of a polymer and a small molecule model for the polymer repeat unit. By means of this technique, it is possible to demonstrate that α-cyclodextrin prefers the inclusion of the longer molecular chain guest. Comparison of the cyclodextrin inclusion complexes formed with PCL and hexanoic acid, separately and from solution containing both PCL and hexanoic acid in varying amounts, enables certain conclusions concerning both the thermodynamic and kinetic aspects of PCL-α-CD IC formation[85]. Figure 15 presents an expansion of the carbonyl

stretching region of these FTIR spectra, which clearly establish the preference for PCL inclusion compared with its repeat unit model complex HA. Comparison of the intensities of PCL and HA carbonyl bands at 1734 and 1714 cm^{-1}, respectively, illustrates that the amounts of both components in the common α-CD IC can be controlled by the stoichiometry of the starting guest and host solutions. In the α-CD IC formed with a 1:1:1 molar ratio of PCL:HA: α-CD, the included guest is found to be predominantly PCL, while for a 1:1:2 ratio with sufficient α-CD to include both guests, we do in fact see comparable amounts of PCL and HA included (Figure 7d).

As another example, it is well known that α-CD forms IC with PEG. However, α-CD does not form complexes with the low molecular weight analogues ethylene, di(ethylene glycol), and tri(ethylene glycol). The rate of the complex formation depends on the molecular weight of PEG. PEG of molecular weight 1000 forms complexes most rapidly.

1.4 Coalescence of Polymers from Their CD-ICs

1.4.1 Concept of Coalescence

Crystallization of polymers in confined microdomains could exhibit different features, including crystalline structure, morphology and novel dynamic processes. An important impetus for polymer IC studies resides in the unique environments provided for the included polymer chains by the narrow channels, which are molecular nanotubes[86-88] (Figure 16), formed in the crystalline matrices of the host. Through the use of ICs, it is possible to create an environment in which individual polymer chain behavior can be distinguished from cooperative interchain interactions in ordered, bulk polymer phases.

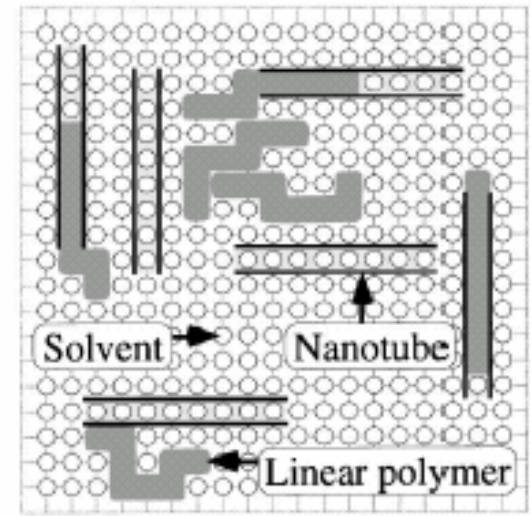

Figure 16. A lattice model for the system consisting of molecular nanotubes, polymer chains and solvent molecules (following reference 87)

When these polymer-IC crystals are disrupted by dissolving or breaking the hosts by means which can not have the same influence on the polymer, the guest polymer chains are forced to reorganize into a bulk solid. This process is called "coalescence" of polymers from their inclusion complexes. Figure 17 schematizes the coalescence of guest

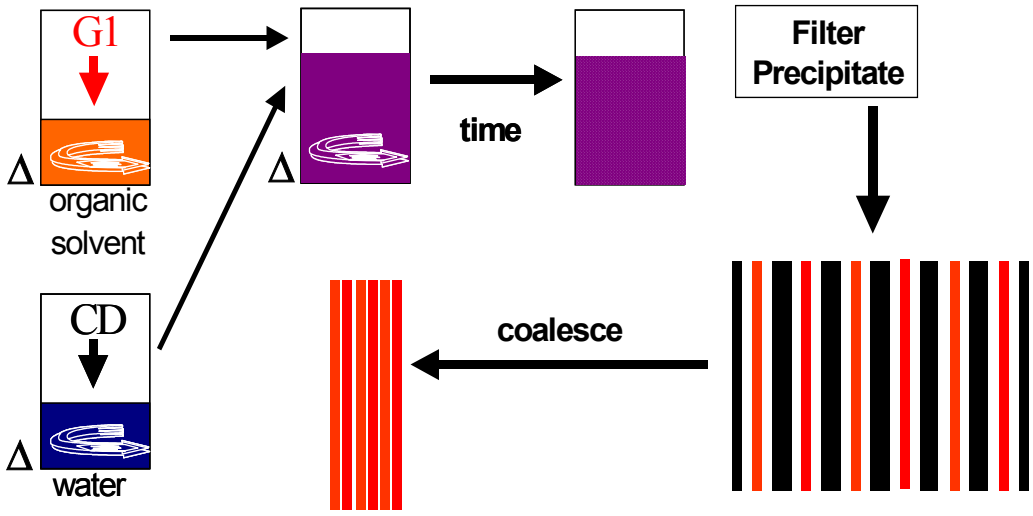

Figure 17. Scheme of cyclodextrin IC fabrication and coalescence molecules (G) from the CD host.

1.4.2 Homopolymers

Based on theoretical calculations, the polymer chains in IC channels should maintain very extended conformations. Figure 18 shows schematically a polymer chain in the randomly coiling state, in the bulk crystal lattice and in the channel of its IC. From this figure, it is easy to imagine that homopolymer chains coalesced from their ICs will retain more extended stretched conformations than normal bulk homopolymers. DSC and small-angle X-ray scattering (SAXS) observations[89-92] of crystallizable polymer samples coalesced from their ICs have often revealed melting temperatures that are elevated from those measured on samples crystallized from their completely disordered solutions and melts, and an absence of discrete reflections from the long spacing between chain-folded lamellae. These observations suggest an extended-chain crystalline morphology for the IC-coalesced polymer samples.

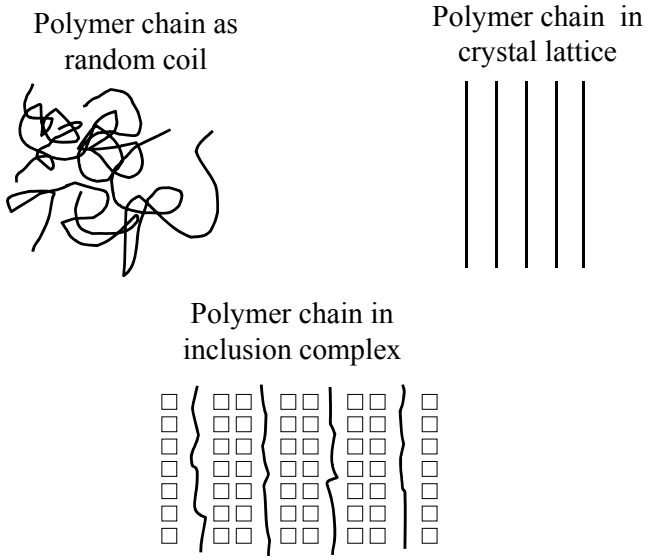

Figure 18. Scheme of polymer chains in random coil state, in crystal lattice and in channel of IC

Bulk poly(ethylene terephthalate) (PET) and bisphenol-A polycarbonate (PC) samples have been produced by the coalescence of their segregated, extended chains from the narrow channels of the crystalline inclusion complexes (ICs) formed between γ-cyclodextrin (γ-CD) host and PET and PC guests.[93] DSC, FTIR, and X-ray observations of PET and PC samples coalesced from their crystalline γ-CD-ICs suggest structures and morphologies that are different from samples obtained by ordinary solution and melt processing techniques. It appears that the polymer crystals formed upon coalescence of the highly extended and segregated polymer chains from the narrow channels in the γ-CD

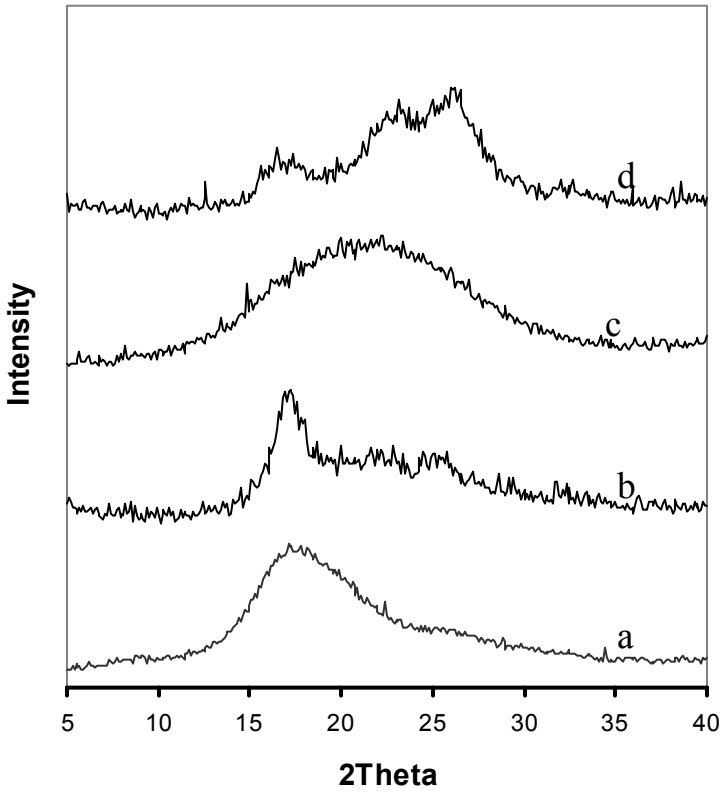

Figure 19. X-ray diffraction patterns of (a)as-received PC (b)coalesced PC (c)as-received PET and (d)coalesced PET

host lattice are possibly more chain extended and certainly more stable than the chain-folded PC crystals grown from solution. Figure 19 show the X-ray diffraction patterns of coalesced PET and PC compared to as-received samples. As-received PC and PET appear to be largely amorphous, while the coalesced PC and PET samples are clearly crystalline as seen in the diffractograms. A weak peak at $2\theta \sim 25^{\circ}$ is observed in the diffractogram of coalesced PC, and may be a result of an increase in the ordering along the PC chain axis[95] as retained from its highly extended conformation in the PC-γ-CD-IC channels. Diffraction peaks at $2\theta = 16.5$, 23.2, and 26.0º, which have been assigned[95] to the (010), $(1\bar{1}0)$, and (100) lattice planes, are evident in the diffractograms of coalesced PET. The (100) peak, which is commonly enhanced in oriented samples, such as uniaxially drawn PET fibers and films[96], is clearly more pronounced in the coalesced sample.

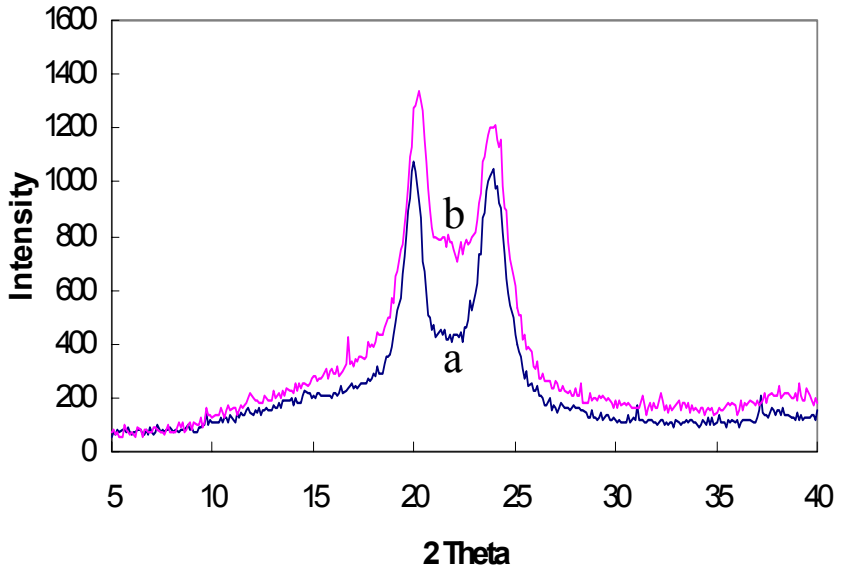

Figure 20. X-ray diffraction patterns of (a) IC coalesced nylon 6 (b)as-received nylon 6

Polycaprolactam, nylon-6, exhibits polymorphism with two types of stable crystal forms: monoclinic α-form and monoclinic (or pseudohexagonal) γ-form, The γ-form crystal of PA6 can be transformed into the α-form crystal by annealing PA6[97] or by drawing and then by annealing PA6[98] or by treating PA6 with a phenol aqueous solution.[99] Conversely, the α-form of PA6 can be transformed to the γ-form by treating PA6 with iodine. The principal structural difference between α and γ forms is that the amide-to-methylene dihedral angles are near trans (164-168°) in α and nearly perpendicular to the peptide plane (~126°) in γ. With axial tension the γ form can usually be converted to the α form[100]. To fit in the channel of CD, nylon-6 has to maintain an extended conformation. In this case, the α form crystalline conformation may be more favorable. Therefore, the γ -> α crystal transformation can be induced by coalescence from PA6-CD-IC.[101] Figure 20 shows the X-ray diffraction patterns of as-received PA6 and coalesced PA6. The large increase in the two crystalline peaks intensities confirms the crystal transformation.

1.4.3 Polymer Blends Coalesced From Their Common CD-ICs

Nucleation is the process of generating with in a metastable mother phase the initial fragments of a new and more stable phase[102]. This initial fragment is called a nucleus, which will grow and lead to phase separation (Figure 21). Nucleation is an activated process, which forms unstable intermediate embryos. A nucleus is different from an equal number of nearest neighbor molecules, because it possesses an excess of surface energy which produces the aggregate as a new phase. If we can intimately mix two kinds of

polymers, the possibility to form a nucleus will be decreased. Therefore, phase separation may not take place as easily in the well-mixed system. Moreover, if the mixing of the two polymers takes place at a temperature lower than Tg and without solvent, the growth of a nucleus to form a separate phase will be frustrated given the high viscosity of the polymer chains and their slow diffusion.

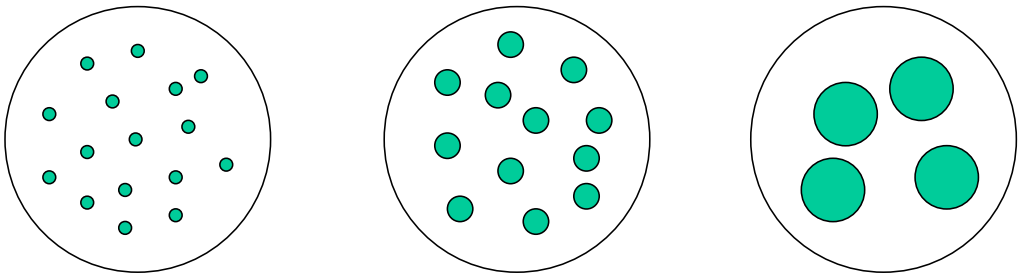

Figure 21. Phase separation nucleation and growth mechanism

Taking advantage of the ability of α-CD to form ICs with both PLLA and PCL, an intimately compatible blend was achieved when PLLA/PCL-α-CD IC was obtained and afterwards washed with a solvent (H_2O) for the α-CD host, which is a nonsolvent for the guest polymers. It was found that α-CD can form complexes with PLLA as well as simultaneously with PLLA and PCL[103]. The miscibility of the PLLA/PCL blend extracted from the α-CD IC channels has been investigated and compared to those of a PLLA/PCL blend cast from their common solution in dioxane.

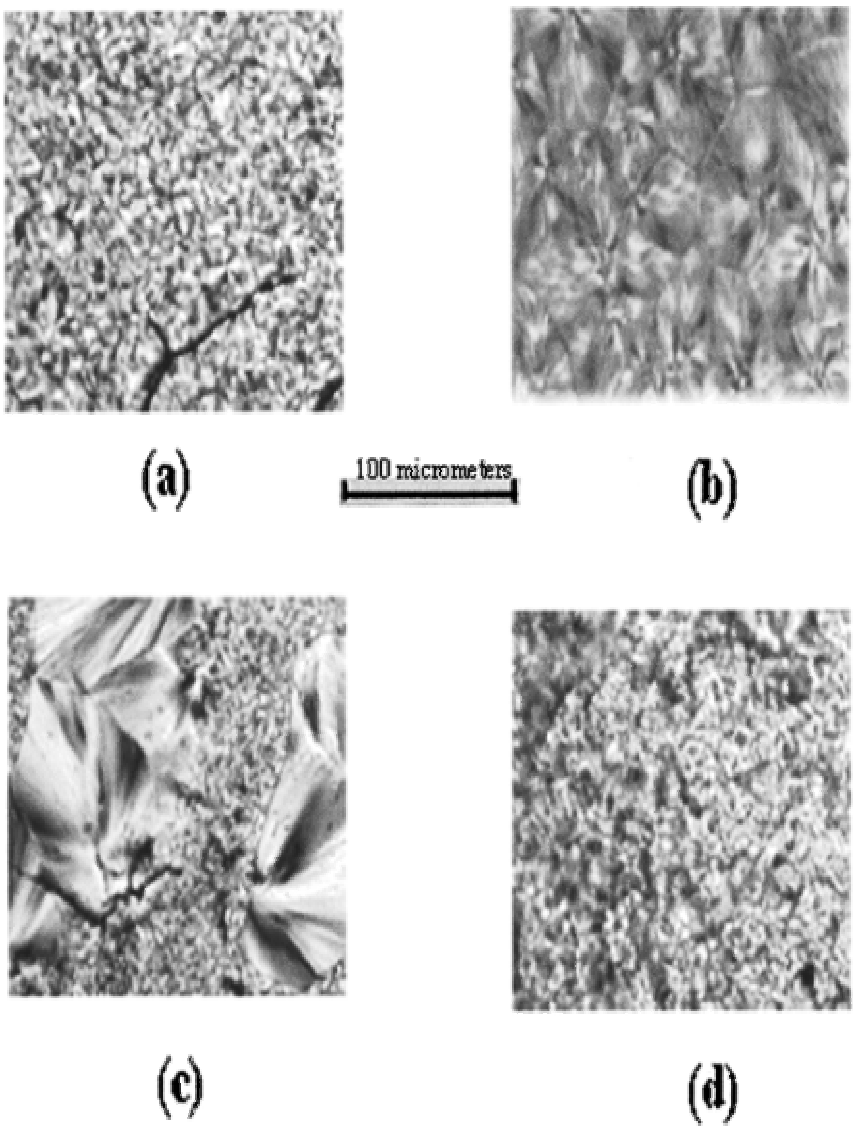

Figure 22. Polarized photomicrographs of (a) PLLA, (b) PCL, (c) solution-cast, and (d) coalesced PLLA/PCL blends

Figure 22 shows the polarized optical photomicrographs of PLLA (a), PCL (b), and their blends cast from dioxane (c), as well as coalesced from their common α-CD IC (d). It is apparent in the solution-cast blend that a phase-separated morphology was formed, indicating that PLLA and PCL were not fully miscible. The spherulites with a maximum radius of 100 μm are attributed to PCL, whereas the smaller spherulites with a radius of

about 20 μm are attributed to PLLA. On the contrary, the morphology observed for the coalesced PLLA/PCL blend strongly suggests that a homogeneous phase was formed.

The simultaneous complexing of both poly(ethylene 2,6-naphthalate) and poly(ethylene terephthalate) with γ-cyclodextrin is documented[104]. Coalescence of these simultaneously complexed molecules generates an intimate blend of the two polymers (HPB). Thermal analysis, via differential scanning calorimetry, reveals thermal behavior indicative of an intimate blend of PET and PEN. ^{1}H nuclear magnetic resonance confirms the blending is not due to transesterification during thermal analysis, and the NMR spectra are shown in Figure 23.

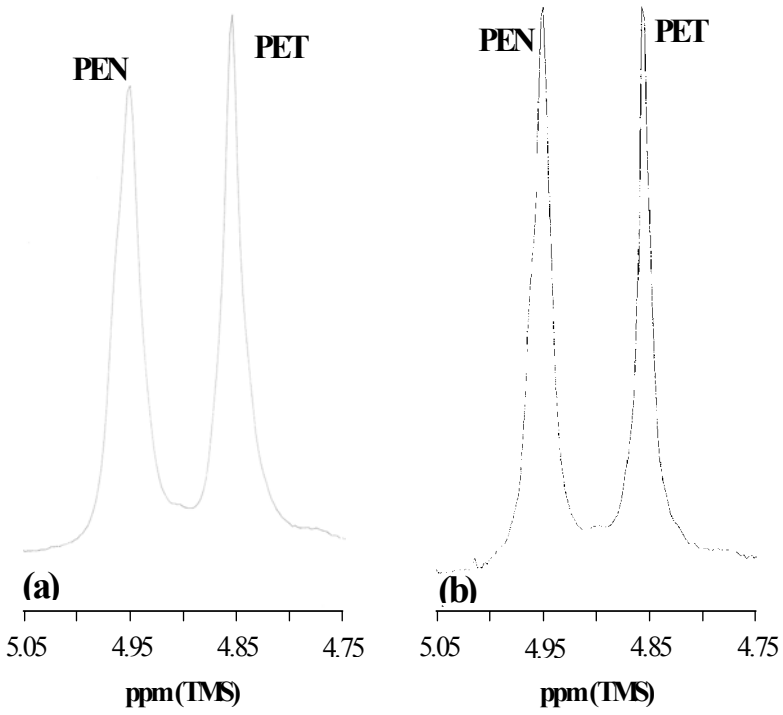

Figure 23. Solution ^{1}H NMR Spectra: (a) precipitated HPB and (b) coalesced HPB

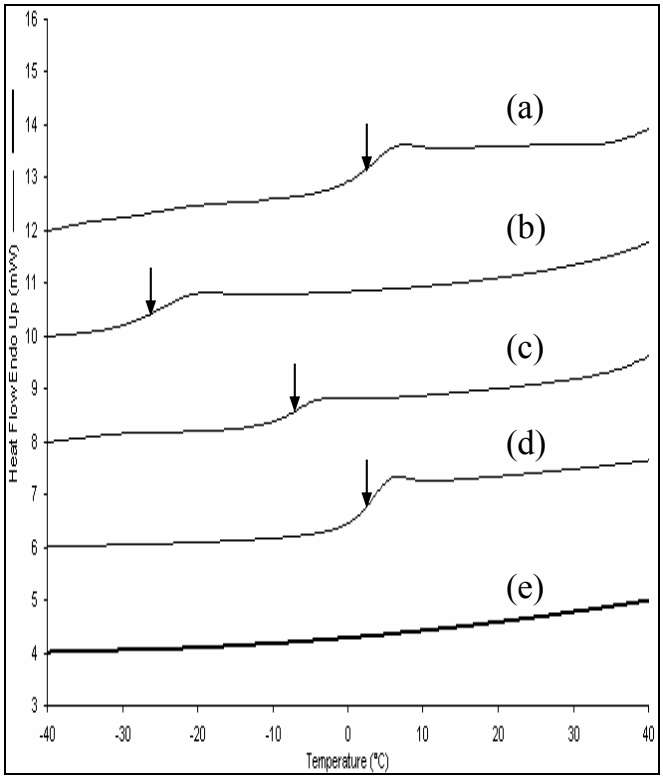

Figure 24. First heating run DSC thermograms of (a) physical a-PHB/PCL blend ($r_{a\text{-}PHB/PCL}$=1:1.76), (b) coalesced a-PHB/PCL blend ($r_{a\text{-}PHB/PCL}$= 1:1.76), (c) coalesced a-PHB/PCL blend ($r_{a\text{-}PHB/PCL}$= 1.48:1), (d) a-PHB, (e) γ-CD-PCL/a-PHB common IC

Washing the common IC of atactic poly(R,S-3-hydroxybutyrate) (a-PHB) and poly(ε-caprolactone) (PCL) with hot water removed the γ-CD, and the molecular chains of the two polymers were coalesced. A single glass transition temperature (T_g), dependent on the composition, was observed between the T_g's of a-PHB (~ 5 °C) and PCL (~ -60 °C) in the differential scanning calorimetry (DSC) measurements of the coalesced samples. To the contrary, T_g of a-PHB (~5 °C) was found to remain unchanged in the physical blend

with PCL. T_m's of coalesced blend samples are lower than that of pure PCL, while the T_m of the physical blend is almost the same as that of pure PCL. These results demonstrate that the miscibility of the inherently immiscible a-PHB/PCL pair has been improved in the coalesced blends[105]. Figure 24 shows the change in Tgs observed in the intimate a-PHB/PCL blends compared with other controlled samples.

Another pair of immiscible polymers, polycarbonate and polystyrene (PC/PS), which are generally substantially and totally amorphous, have been employed to demonstrate the feasibility of producing miscible polymer blends by coalescence from their common γ-CD-ICs. DSC results on PC and PS and their blend coalesced from their common γ-CD-ICs and cast from solution are presented in Table 4[106]. It is observed that there are only single Tg's in the coalesced blends, which are different from those observed in the neat polymers and their solution-cast blend.

Table 4. Tg in the intimate polymer blends of PC/PS as revealed by DSC

Sample	repeat unit molar ratio PC:PS	Tg (^{o}C)
PC	10:0	145
PC/PS blends coalesced	8:2	143
From common γ-CD	5:5	133
Inclusion Complexes	2:8	91
PS	0:10	100

1.4.4 Block Copolymers

Block copolymers have become one of the most widely studied fields in polymer science, because of their tendencies for self-assembling[107-112]. It is found that α-CD molecules may simultaneously thread onto both poly(ε-caprolactone) (PCL) and poly(L-lactide) (PLLA) blocks of PCL-b-PLLA to form an inclusion complex (IC). Washing the copolymer-α-CD IC with hot water removed the α-CD and the copolymer chains were coalesced. Very interestingly, the coalesced copolymer sample shows a great suppression in microphase separation, compared with the as-synthesized copolymer[113]. In contrast to the significant decrease in crystallinity of ca. 50 % and up to 79 % for PCL and PLLA blocks respectively, the melting points (T_m's) and the cold crystallization temperatures (T_{cc}'s) of both PCL and PLLA blocks of the coalesced sample increased in DSC measurements. These results may imply that only small amounts of more extended crystals, with less chain folding, were produced during the process of copolymer coalescence.

Expansion of the carbonyl regions of FTIR spectra, as shown in Figure 25, gives us very helpful information concerning the formation of IC and the phase structures of the coalesced and as-synthesized copolymer samples. Here, the carbonyl absorption of the PLLA block is not well resolved into amorphous and crystalline bands for all samples. Therefore we are not able to study the changes in phase structure of PLLA domains from the FTIR measurements. However, the PCL carbonyl absorption band of the as-synthesized copolymer are well resolved into a peak at 1726cm^{-1} and a prominent shoulder at 1736cm^{-1}, corresponding to the carbonyl absorption of the crystalline PCL phase and that of the amorphous PCL regions, respectively. As shown in Figure 24, the

C=O absorption of crystalline PCL regions completely disappears, and only the C=O absorption of noncrystalline PCL blocks is detected in the spectrum of the IC. This result indicates that no crystalline PCL phase exists in the inclusion complex, and all polymer chains have been involved in the inclusion process. Very interestingly, the absorption of crystalline PCL regions at 1726 cm^{-1} becomes weak and appears as a shoulder, while the absorption of the amorphous PCL regions at 1736 cm^{-1} is much stronger and becomes the main peak, in the spectrum of the coalesced sample. This result demonstrates that the crystallization of PCL blocks has been significantly suppressed in the coalesced sample.

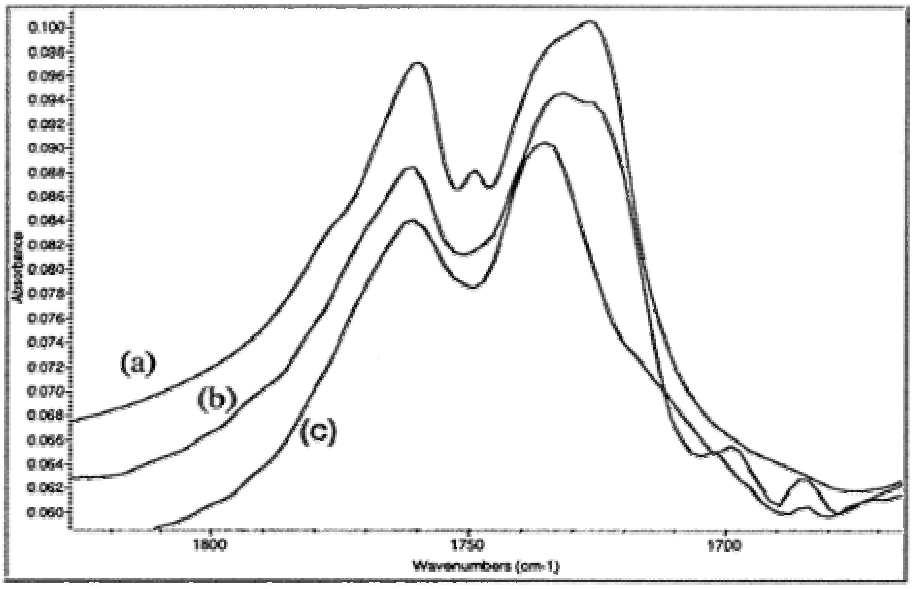

Figure 25. FTIR in the carbonyl region (s, $\nu_{C=O}$) for (a) as-synthesized PCL-b-PLLA, (b) coalesced sample, (c) and α-CD-block copolymer IC

Films of the as-synthesized and coalesced copolymer samples, PCL and PLLA homopolymers of approximately the same chain lengths as the corresponding blocks of PCL-b-PLLA, and a physical blend of PCL/PLLA homopolymers with the same molar

composition as PCL-b-PLLA were prepared by melt-compression molding. Subsequently, the *in-vitro* biodegradation behavior of these films was studied in phosphate buffer solution containing lipase from *Rhizopus arrhizus*. During the examinations, the coalesced copolymer sample led to a much faster enzymatic degradation than that of either as-synthesized copolymer or the PCL/PLLA physical blend sample, especially during the early stages of biodegradation[114]. Figure 26 shows the degradation process as monitored by UV spectrophotometry.

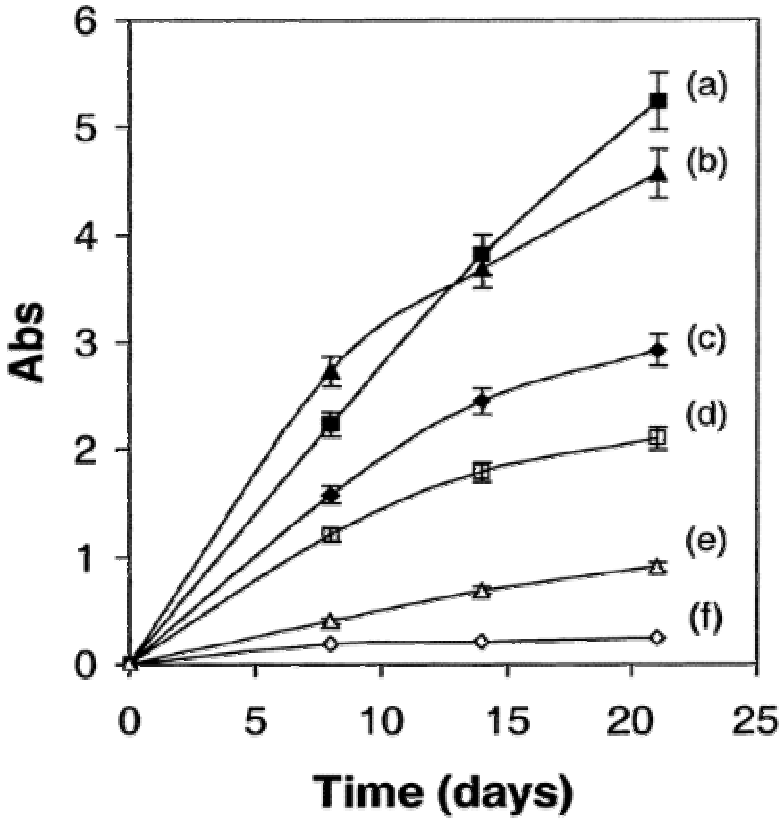

Figure 26. UV absorbance detected at 205 nm during the 3-week enzymatic degradation (37^{o} C, pH = 7.0) of (a) PCL, (b) coalesced PCL-b-PLLA, (c)as-synthesized PCL-b-PLLA, (d) PCL/PLLA blend, and (e) PLLA , in comparison with a (f) PCL control hydrolyzed in the absence of enzyme

In the ICs of the PCL-PPG-PCL triblock copolymer, only PCL blocks were included as guests in the IC formed with α-CD, while both PCL and PPG blocks were included in the IC formed with γ-CD. As a result, the copolymer coalesced from its IC crystals with α-CD showed an increased crystallinity, while to the contrary, the copolymer coalesced from its IC crystals with γ-CD exhibited a decreased crystallinity, when both were compared to the as synthesized triblock copolymer[115].

Table 5. Thermal properties and crystallinity of various PCL-PPG-PCL triblock copolymer samples as revealed by DSC

Identity	$T_{m\text{-}PCL}$ (°C)	ΔH_{PCL} ($J/g_{\text{-sample}}$)	$\chi_{c\text{-}PCL}$* (%)
As-synthesized copolymer	57.3	58.62	56.5
Sample coalesced from α-CD-copolymer IC	63.8	76.84	74.1
Sample coalesced from γ-CD-copolymer IC	63.0	51.33	49.5

*PCL fraction in the copolymer is 74.6 % (in wt%) according to the ^{1}H NMR results

In the DSC measurements of as-synthesized PCL-PPG-PCL, a strong melting peak for the PCL blocks was observed. Although the atactic PPG is completely amorphous, the glass transition of the PPG blocks is too weak to be detected, apparently because the PPG block is too short (DP=60). No fusion peak was observed for the two ICs in the heating run, which indicates again that PCL blocks have been included in both CD-ICs.

From the results discussed above, it is concluded that, in the γ-CD-copolymer IC, both PCL and PPG blocks have been included, while in the α-CD-copolymer IC only PCL blocks have been included. The crystallinities (χ_c) of PCL blocks in the samples coalesced from the γ-CD-copolymer IC and the α-CD-copolymer IC were investigated. DSC results shown in Table 5, however, indicate opposite changes in the PCL crystallinity for the two coalesced samples, compared to the as-synthesized PCL-PPG-PCL. The crystallinity of PCL blocks in the sample coalesced from γ-CD-copolymer IC decreased, while the crystallinity of PCL blocks in the sample coalesced from α-CD-copolymer IC showed an obvious increase. Melting temperatures of the PCL blocks (T_m) in both coalesced samples increased slightly, which are consistent with the results discovered in the coalesced sample from α-CD/PCL-b-PLLA IC.

Considering the structural differences between the two IC samples, the opposing changes in the PCL crystallinity of the two coalesced samples are not unexpected. Since only PCL blocks are included in the α-CD-copolymer IC, the neighboring IC channels should be filled only with extended PCL blocks. Therefore, PCL blocks will aggregate easily when the CD molecules are washed way. Although PPG may affect the crystallization of PCL blocks in the as-synthesized copolymer, the aggregation of neighboring PCL blocks should not be affected by the uncomplexed PPG blocks in the process of copolymer coalescence. Therefore, the observed increased crystallinity of PCL blocks in this coalesced sample is reasonable. In contrast, PCL and PPG blocks should have the opportunity to be included in neighboring channels of the γ-CD-copolymer IC, since both PCL and PPG blocks have been included. This means that the aggregation of some PCL blocks might be hindered by PPG blocks in the process of copolymer

coalescence, as occurred with PCL-b-PLLA. Therefore, a decrease in PCL crystallinity for this coalesced sample also seems reasonable. Because 2 PCL blocks may be included side-by-side in each γ-CD IC channel, inclusion of PCL and PPO blocks in neighboring channels may produce less intimate mixing than expected.

1.5 Recent Highlights of Polymer Cyclodextrin Inclusion Complexes

1.5.1 Visual Observations

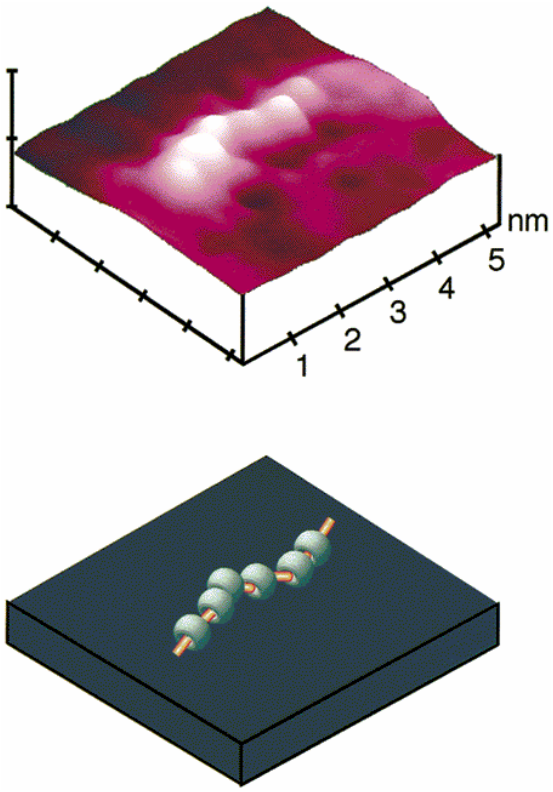

Figure 27. A typical STM image of the polymer cyclodextrin inclusion complex (PEG-α-CD) and its schematic structure (following reference 116)

The scanning tunneling microscope (STM) and atomic force microscope (AFM) have been recognized as two of the most powerful tools for the visualization of atoms and molecules[116-118]. Harada[119] et al. have used STM manipulation of a molecular necklace of cyclodextrin to develop a "molecular abacus". (See Figure 27). They demonstrated that the selected α-CD molecule(s) in a PEG/α-CD polyrotaxane could be reversibly shuttled using a STM. Since the α-CD molecules are noncovalently bound to poly(ethylene glycol) (PEG), all manipulations are carried out under ambient conditions.

Figure 27 shows a typical STM image of the molecular necklace on a MoS_2 substrate. Regularly aligned α-CDs are clearly observed. The main chain of PEG runs along the surface of the substrate, and the α-CDs lie with their longitudinal axis parallel to the surface. The rotaxane structure of the molecular necklace has been clearly visualized on an atomic scale. It is noteworthy that stable imaging was accomplished at room temperature in air. One of the α-CDs in the molecular necklace was mechanically pushed by the STM tip along the main chain of PEG. An example of the shuttling is shown in Figure 28. The images were acquired before and after each manipulation, respectively. As designed, the target α-CD moved by sweeping the tip from right to left. Since the PEG chain is oriented diagonally in this case, the target CD stably moved by 2.4 nm in the direction along the chain. All the other α-CDs retained their initial positions. Upon moving the tip in the reverse direction, the α-CD retraced its path and returned to its

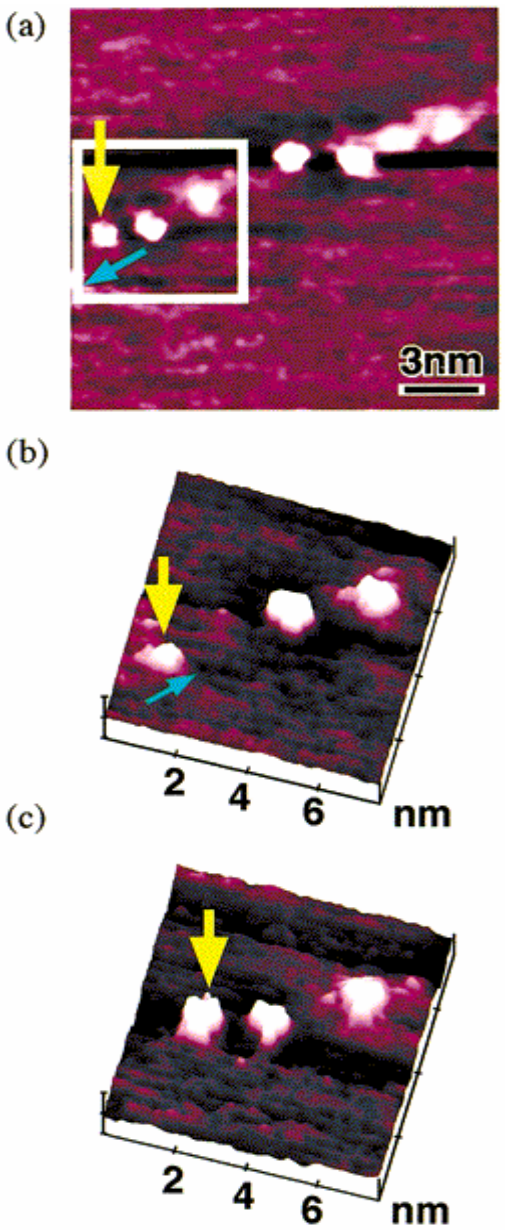

Figure 28. STM images of the simple-shuttling of α-CDs along the PEG chain (following reference 119)

original position. Thus, the shuttling of one α-CD could be stably repeated. There is no requirement for a specific surface structure on the substrate to guide the shuttle in a prescribed manner.

1.5.2 Water Soluble Polymer Cyclodextrin Inclusion Complexes

Although most pure polymer-cyclodextrin inclusion complexes are water insoluble, water soluble polymer CD-ICs can be obtained by modifiying the cyclodextrin. Simultaneous static and dynamic light experiments have been made on the inclusion complexes formed between different polyethylene oxide/polypropylene oxide triblock copolymers (PEO-PPO-PEO) (pluronics) and dimethyl-β-cyclodextrin (DIMEB). The inclusion complexes formed between DIMEB and pluronics are highly soluble, in contrast to the insoluble complexes formed between β-cyclodextrin and the same substances. The static light-scattering (LS) data show that approximately 11 DIMEB molecules thread onto the copolymer chains and are located on the PPO block[120]. With the inverse structure (PPO-PEO-PPO), about seven DIMEB molecules are present in the complex. NMR measurements are used to substantiate complex formation by means of characteristic changes in the proton signals. Hydrodynamic radii obtained from dynamic LS data at infinite dilution for the cyclodextrins correspond well with dimensions determined using X-ray methods. Inverse Laplace transformation (ILT) allowed resolution of the relaxational modes from the cyclodextrin/pluronic complex and the excess cyclodextrin. The complexes formed with the DIMEB are shown to be significantly larger than the copolymer unimers, which may be due to accentuation of steric hindrance to flexing in the PPO block. With the inverse pluronic structure, on the other hand, the complex is smaller in radius than the unimer. At temperatures above which the copolymer forms micelles, addition of DIMEB inhibits both cluster formation

and micellization of the pluronics and also prevents network formation with the inverse pluronic, whereas the trimethyl analogue (TRIMEB) does not have this effect.

1.5.3 Smart Gels

A polyrotaxane, in which many β-CDs are threaded onto a triblock copolymer of poly(ethylene glycol) (PEG)-poly(propylene glycol)(PPG)- poly(ethylene glycol) (PEG) capped with fluorescein-4-isothiocyanate (FITC), was synthesized as a model of stimuli-responsive molecular assemblies for nanoscale devices by the Yui group[121,122]. Coupling of FITC with the terminal amino groups in the polypseudorotaxane was performed in DMF at 5^{o} C. Under these conditions, a side reaction between the hydroxyl groups of β-CD and FITC was prevented. The interaction of the β-CDs with terminal FITC moieties in the polyrotaxane was significantly observed at low temperature. However, the interaction of the β-CDs with the PPG segment was observed with increasing temperature. On the basis of these results, it is concluded that the majority of the β-CDs move toward the PPG segment with increasing temperature although some β-CDs may reside on the PEG segments.

Supramolecular-structured hydrogels were prepared on the basis of the inclusion complexation between PEG grafted dextrans and α-CDs in aqueous media. The inclusion complexes from the PEG grafted dextrans showed a unique gel-sol phase transition which cannot be obtained from usual polymer inclusion complexes that form crystalline precipitates. The gel-sol transition was based on the supramolecular assembly and dissociation, and the transition was reversible with hysteresis. The transition temperature

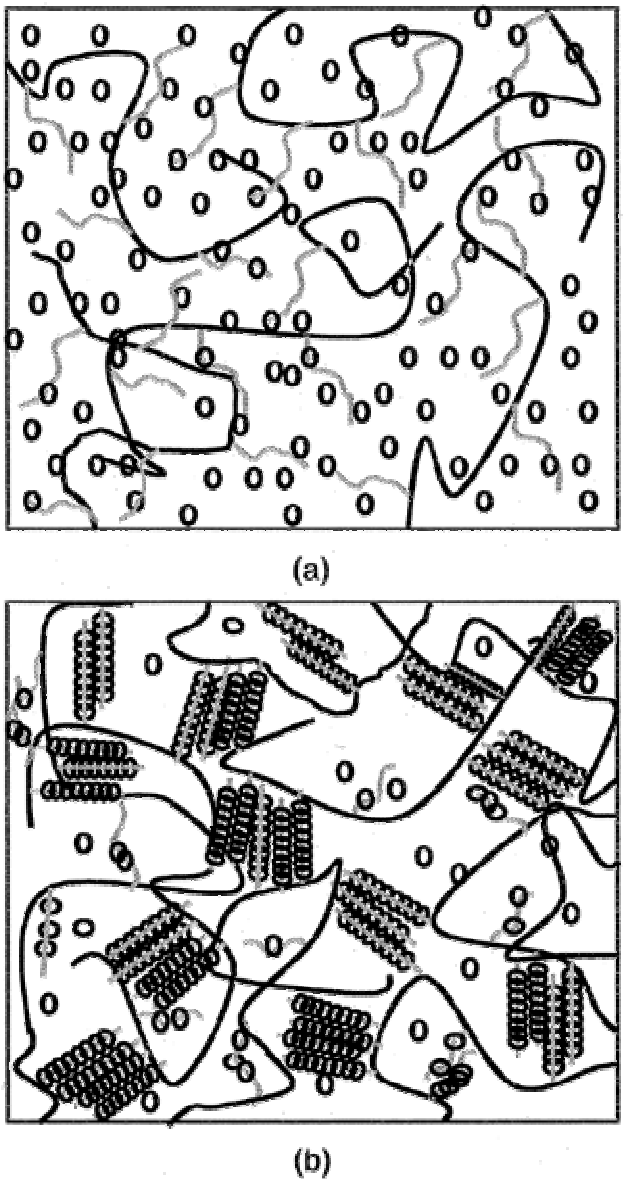

Figure 29. Schematic illustration of proposed structure of supramolecular-structured gel by inclusion complexation between PEG(gray line) grafted dextran(black line) and α-CD(black cycle): (a)uncomplexed or dissociated state corresponding to the initial stage before inclusion complexation between PEG grafts and α-CD molecules or above the gel-melting temperature (sol phase); (b) complexed state corresponding to the stage where inclusion complexation was partially or completely achieved or below the gelation temperature (gel phase) (following reference 121)

was controllable by variation in the polymer concentration and the PEG content in the graft copolymers, as well as the stoichiometric ratio between the guest and host molecules. It was confirmed from DSC and C^{13} CP/MAS NMR measurements that all the PEG grafts participate in the complexation. A phase-separated structure consisting of hydrophobic and channel-type crystalline PEG inclusion complex domains and hydrated dextran matrices was suggested as the internal structure, which comprises the supramolecular-structured hydrogel, as depicted in Figure 29.

1.5.4 Molecular Machines

Cyclodextrins have been used as a cyclic component in the construction of supramolecular architectures. Recently Harada has studied CDs as components in the construction of rotaxanes and catenanes. A cyclodextrin ring can translocate in some rotaxanes and catenane structures[123]. Therefore, much attention has been given to cyclodextrins as a component of molecular shuttles, motors, and machines. Attempts to design and synthesize molecular-level machines using cyclodextrins as a cyclic component are mentioned here.

Cyclodextrins form inclusion complexes with metallocenes such as ferrocene to form crystalline complexes. The structures of the complexes are dependent on the sizes of cyclodextrins . Although ferrocene and its derivatives are strongly bound in uncharged states, when they are oxidized, the complexes dissociate. Dendrimers containing ferrocene units at the ends of the molecule have been prepared (Figure 30). The

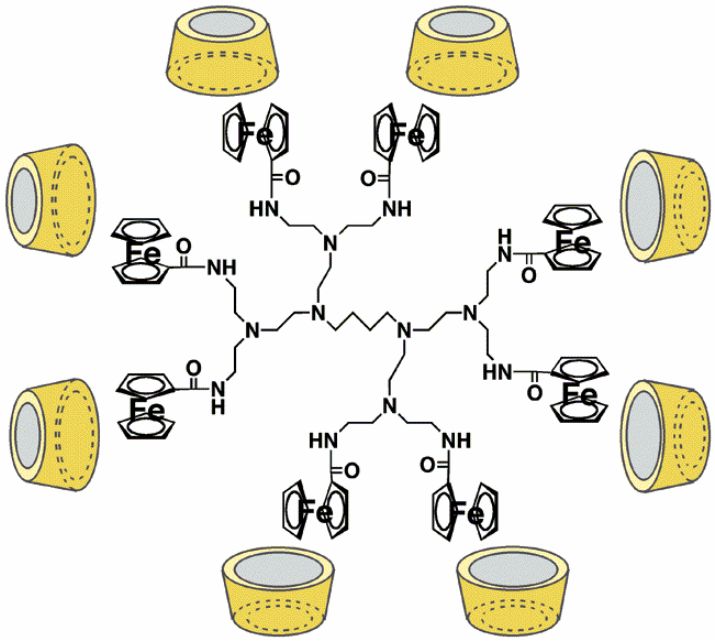

Figure 30. Dendrimer containing ferrocenes at the ends of the molecule and cyclodextrin (following reference 124)

dendrimers form large supramolecular structures that can be broken apart or assembled on oxidation of the ferrocene units[124] of electrochemically driven molecular complexes.

Catenanes containing cyclodextrins, which are illustrated as Figure 31, have been prepared by Stoddart et al.[125]. One or two cyclodextrins are incorporated in a catenane structure. These complexes are important as "a molecular train" in which a small ring can slide along a large circle as though they are trains on a molecular scale. Harada et al.[120] have prepared cyclodextrin-containing catenanes starting from the complexes of cyclodextrin with polymethylene derivatives using a poly(ethylene glycol) spacer. In this case, a cyclodextrin ring may move along the polymer chain if the solvents are changed from hydrophilic to hydrophobic ones.

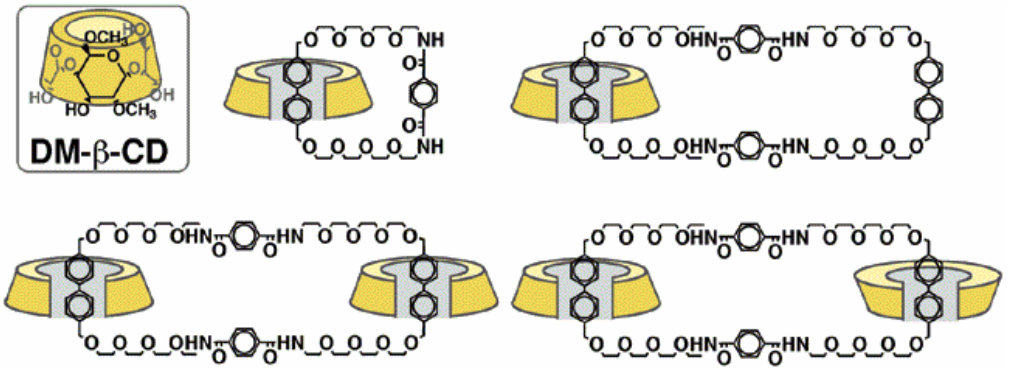

Figure 31. Catenanes containing cyclodextrin (following reference 125)

1.6 Proposed Research

As we know, the properties of polymers, such as glass transition temperatures, crystallinity, melting points and so on, are greatly influenced by their various conformations, as well as by the interactions and entanglements between polymer chains within ordered and disordered bulk polymer phases. In order to understand and modify the properties of bulk polymers, it is necessary to study both the intrinsic nature of individual polymer chains and the effects of polymer-polymer interactions. The impetus for inclusion complex study resides in the unique environments provided for the included polymer chains by the narrow channels formed in the crystalline matrices of the host clathrates. Through the use of inclusion complexes, it is possible to create an environment where individual polymer chain behavior can be different from that dominated by cooperative interactions in bulk polymers. The guest polymer chains are confined to narrow, cylindrical channels created by the host, small-molecule lattice, where the polymers are highly extended as a consequence of being squeezed, and are separated from neighboring polymer chains by the IC channel walls composed exclusively of the small-molecule lattice. Since the polymer chains in the IC channels are

expected to exist in more extended conformations than in their amorphous bulk and solution phases, we would hope that there is a way to retain this extended, unentangled conformation when removing the host molecules of the IC. By this method, we may obtain reorganized polymers with unique properties.

Nylon polymers consist of polyethylene segments (CH2)*n* separated by amide bonds (NH-CO), which are packed either parallel or antiparallel in their crystals[126]. The amide bonds provide hydrogen bonding between polymer chains, giving nylon some of its unique properties. In contrast to other highly crystalline polymers like polyethylene, nylon polymers can have their degree of crystallinity controlled over a wide range, leading to a unique combination of stiffness, toughness, lubricity, and resistance to abrasion, fatigue, and high temperatures that makes it one of the most versatile thermoplastics in use today. By changing the amide bond density, one can modify such properties as the melting temperature, modulus, low temperature impact strength, moisture absorption, and chemical resistance to metal salts and acids. The two largest volume nylon polymers are nylon-6 and nylon-6,6 which are widely used for carpets and garments. Nylon-11 and nylon-12 are mainly used in tubing extrusion, cable jacketing, injection molding, and coating of metal objects. Nylons have different crystal structures, because of different hydrogen bonding patterns. Since the unique structures and properties of nylon polymers are dominated by these hydrogen bonding patterns[127], we must pay careful attention to them. Forming nylon cyclodextrin inclusion complexes may provide a way to temporarily eliminate hydrogen bonding, allowing orientation to the desired degree, followed by reformation of the hydrogen bonds in the oriented state through coalescence. Moreover, it may be possible to manipulate the hydrogen bonding

in nylons by changing the conformations of the polymer chain within the IC channels, and therefore, to get different crystal structures, crystallinities and orientations. On the other hand, the hydrogen bonds in the nylon could be manipulated by making intimate blends of different nylons. It is easy to imagine that the hydrogen bonds formed between different kinds of nylon will be distinguished from those formed between the same nylon chains. Normal solution or melt blends are not able to be employed for this purpose, since different nylons are normally immiscible. However, miscible blends may possibly be achieved by coalescence from their common CD-IC as an additional method for controlling the hydrogen bond pattern in nylons.

Fabrication of polymer-cyclodextrin inclusion complexes may have application as drug delivery systems, because cyclodextrins have been widely used by pharmaceutical researchers as a drug delivery carrier and can form inclusion complexes with biodegrable polymers, which are also widely used as a matrix for the controlled-release of drugs. Cyclodextrins can be employed in nasal, ophthalmic, transdermal, and rectal applications, and for peptide and protein delivery[128-133]. Normally, drug release from cyclodextrin complexes is rapid and quantitative in most cases. In aqueous solution, drug/cyclodextrin complexes are continually forming and dissociating with lifetimes in the range of milliseconds or less. On the other hand, polymer based drug delivery systems often have a low release rate[134]. Therefore, we expect to associate the matrix polymer, the drug and cyclodextrin together in forming a drug delivery system. Ideally, we can simultaneously form CD ICs containing both the biodegradable polymer and drug as common guests. The polymer and drug can be consolidated from its IC during the coalescence process, resulting in a homogeneous polymer/drug blend that can control the drug release rate. In

addition, the properties of biodegradable polymers can also be modified during their coalescence from CD ICs.

The aim of this research is to demonstrate the formation of polymer-cyclodextrin inclusion complexes, and investigate the properties of polymers in and coalesced from the confined environment of the cyclodextrin channels. Based on this work, hopefully we can gain some new insight into the relative contributions made to the properties of ordered, bulk polymers by the inherent behavior of isolated polymer chains and the interactions between them, and modify the properties of polymers consolidated from their confined CD-IC channel environment. Furthermore, it is hoped to employ new experiential methods to investigate the polymer chain behaviors in or coalesced from CD-IC channels, such as selected area electron diffraction, to study the orientation and crystallization of polymers squeezed in or pulled out from the host cyclodextrin crystalline lattice.

2 Melting and Crystallization Behaviors of Biodegradable Polymers Enzymatically Coalesced from Their Cyclodextrin Inclusion Complexes

2.1 Introduction

Inclusion complexes (ICs) formed between host and guest molecules have been intensively studied for a long time. Among their important applications is their ability to act as drug delivery systems. One class of host molecules are the cyclodextrins (CDs), which can complex and include water insoluble drugs and form soluble inclusion complexes[135-138]. Because they are biologically safe solubilizers, cyclodextrins are being developed for new medical formulations. Solid crystalline polymer-CD ICs have also been widely studied during the past decade. In these ICs, the guest polymer chains occupy narrow cylindrical channels (diameter = D ~ 5-10Å) created by the crystalline CD host lattice. As a consequence, the included polymer chains are constrained to assume highly extended conformations and are generally segregated from neighboring included polymer chains by the channel walls of the host crystalline CD lattice. Therefore, polymer-CD ICs may provide a means to generate polymer samples with unique morphologies, resulting in samples with novel thermal, mechanical, and barrier properties that are specific to them[139].

Since both drug molecules and polymers can form inclusion complexes with cyclodextrin, it may be interesting to explore a new method for designing polymer-based drug delivery systems by simultaneous formation of CD-ICs with both the drug and the polymer included as common guests. A polymer/drug controlled release system involves the combination of a polymer with the active agent drug in such a way that the drug can be delivered in a controlled manner. The motivation for our research is to directly employ

the inclusion complex as a drug delivery system. The scheme of the invisioned system is illustrated in Figure 32. Previously we have imbedded small molecule additive-CD ICs into polymer matrices and then released the additives *in situ* by subsequent coalescence[140,141]. In this manner, the drug molecules could be somewhat dispersed in the polymer matrix, but the stable kinetic release of the drug may be thwarted by their segregation into large particles or crystals which could cause "bursts" during their release[142]. Thus, in our current work, we are trying to make common ICs containing both drug molecules and biodegradable polymers as guests with CDs as the host. After the common polymer/drug-CD IC is introduced into the body and the CD is enzymatically decomposed *in vivo*, the biodegradable drug delivery system will, *via* their simultaneous coalescence, form an intimate, well-mixed polymer/drug blend.

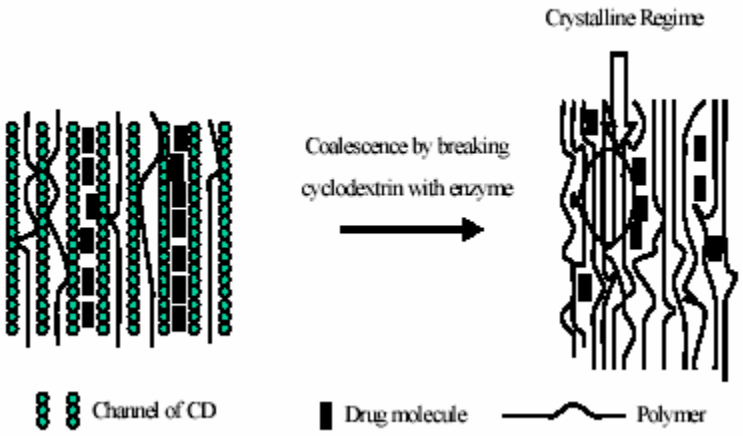

Figure 32. Scheme of a polymeric drug delivery system formed by the simultaneous coalescence of matrix polymer and drug molecules from their common inclusion complex.

The process of disrupting polymer-IC crystals by removing the host and consolidating the guest polymer chains, is called coalescence. DSC and small-angle X-ray scattering (SAXS) observations of crystallizable polymer samples coalesced from their ICs have often revealed melting temperatures that are elevated above those measured on samples crystallized from their completely disordered solutions and melts, and an absence of discrete reflections from the long spacing between chain folded lamellae. These observations suggest an extended-chain crystalline morphology for the IC-coalesced polymer samples.

To study the drug release behavior of polymer/drug-CD IC systems, we initially need to examine the melting and crystallization behaviors of polymers, used as matrices in controlled release systems, after they are coalesced from their ICs, because it is well known that the crystalline morphology of biodegradable polymers greatly affects their material performance, especially their biodegradation and permeability, which are of decisive importance in the controlled release of drugs. In this study, we achieved the coalescence of biodegrable polymers with an enzyme at moderate temperatures, and the melting and crystallization behaviors of these enzymatically coalesced polymers were investigated in detail. Among the most important polymers used for biomaterials, poly(ε-caprolactone) (PCL) and poly(L-lactide) (PLLA) have a growing presence in the field of biomedical applications, especially, as matrices for controlled drug delivery systems[143-145]. Therefore, PCL, PLLA and their diblock copolymer, PCL-b-PLLA, were selected for investigation in this work.

2.2 Experimental

Materials

Poly(ε-caprolactone) (PCL) and polyL-lactide (PLLA) and their diblock copolymer (PCL-b-PLLA) were synthesized by ring-opening polymerization, as shown in Figure 33. previously reported.

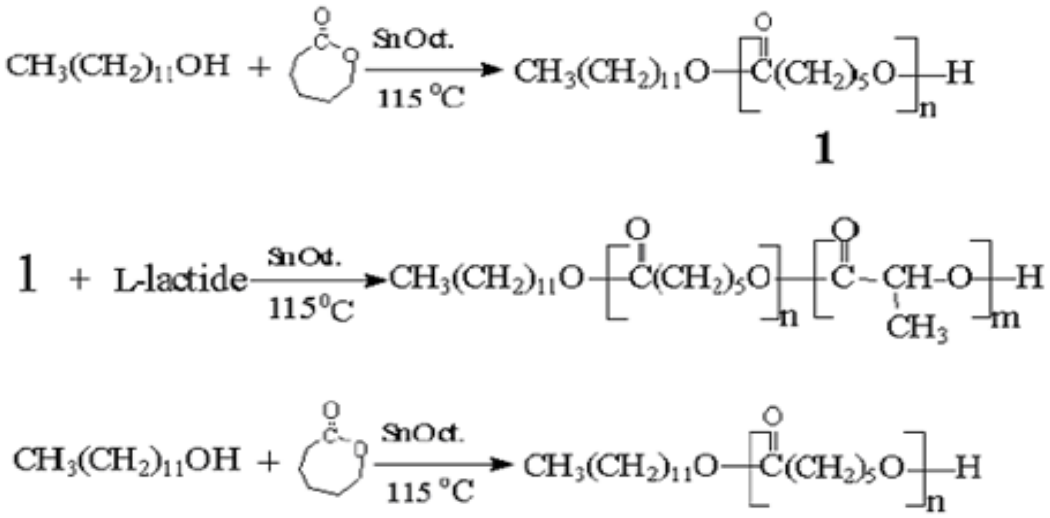

Figure 33. Scheme of the polymerization of PCL, PLLA and their block copolymer

In the case of the diblock copolymer, monohydroxyl PCL was first synthesized by polymerizing ε-caprolactone (Aldrich) with 1-dodecanol (Aldrich) as an initiator and Stannous (II) octoate (SnOct, from Aldrich) as catalyst. Then the monohydroxyl PCL was used as a macroinitiator for the polymerization of L-lactide to yield the diblock copolymer. The polymerizations of ε-caprolactone (to form PCL) and L-lactide (to form PLLA) were also carried out by initiating with 1-dodecanol under catalysis by SnOct.

All the polymerizations were performed at 115° C for 24 h in toluene solution. The physical blend of PCL and PLLA was prepared by casting from their common acetone solution. Molecular weights of as-synthesized polymers are shown in Table 6, and were determined by Gel permeation chromatography (GPC) and NMR. GPC analysis was carried out using a Waters Styragel HR4 10^4 Å WAT044225 column with THF as an eluent and PMMA standards (Waters and American Polymer Standards) for column calibration. The eluent was analyzed with a Differential Refractometer R401 (Waters), together with a Model 730 Data Module (Waters). ^{1}H NMR spectra were recorded on a Bruker 300MHz DPX spectrometer in $CDCl_3$ at room temperature.

Table 6. Molecular weights

	M_n[a] ($\times 10^{-3}$)	M_w/M_n[b]	Wt%(PCL)
PCL	10.1	1.18	100
PLLA	7.0	1.22	0
PCL/PLLA blend	-	-	60
PCL-*b*-PLLA	16.8[c]	1.37	64

[a]Calculated from the integration of characteristic signals in ^{1}H NMR spectra.
[b]Determined by SEC/GPC measurements.
[c]PCL and PLLA block lengths in the homopolymers and PCL-b-PLLA are essentially equal.

Preparation of Samples

To prepare the inclusion complexes, α-CD (15g) was dissolved in distilled water (60ml) and heated to 60 °C in a flask equipped with a condenser. Polymers (0.75g) were dissolved in acetone (150 ml) and heated to 50° C. Then the polymer solutions were added dropwise to the α-CD solution. After stirring for 3 hrs. at 60° C, the solutions were allowed to cool to room temperature while continuously stirring overnight. White

powders were collected by filtration and then washed repeatedly with dichloromethane and water to remove free polymer and uncomplexed α-CD, respectively. Finally, the ICs were dried in a vacuum oven at 30° C for 48 hrs. During the coalescence, 5g of polymer-α-CD IC were placed into a beaker containing 150 ml of a dilute aqueous solution (1:150, v/v) of the alpha-amylase enzyme from Bacillus licheniformis, with a declared activity of 360KNU/g, which was supplied by Novozymes (Franklinton, NC). The mixture was held at ~35° C under stirring for several hours, followed by filtration, washing and drying of the precipitate in a vacuum oven at ~25° C overnight.

Fourier Transform Infrared Spectroscopy (FTIR)

The FTIR spectral studies were carried out with a Nicolet 510P FTIR spectrometer in the frequency range between 4000 and 750 cm^{-1}, with a resolution of $2cm^{-1}$. All powder samples were pressed into KBr pellets for the FTIR measurements.

Differential Scanning Calorimetric (DSC) Analyses

DSC measurements were performed at heating rates of 20^{o} C/min. on a Perkin-Elmer differential scanning calorimeter (DSC-7) calibrated with indium. To carry out the isothermal crystallizations, the crystallization exotherms were obtained by heating the samples to 190^{o} C. After holding at this temperature for 10 min., the samples were rapidly cooled at a rate of 320^{o} C/min. to a specified crystallization temperature. For the non-isothermal crystallization studies, temperatures indicated by DSC are corrected due to the thermal lag originating either in the samples and/or in the instrument itself. During the measurements, the samples were rapidly heated to 200^{o} C and held there for 10 min. to remove the previous thermal history. Then the samples were cooled down at various

cooling rates from 5 to 80° C/min.. The exothermic crystallization peaks and crystallinity levels were recorded as a function of time (or temperature).

Polarized Optical Microscopy Observations

To provide clarification of a special case encountered during the isothermal crystallizations, isothermally crystallized samples were made by heating to 190° C, held there for 10 min, and then quickly quenched into a 30° C silicon oil bath. After the crystallization was over, the samples were placed on glass slides and observed with a Nikon Labophot2-pol polarizing optical microscope, and the images were captured by a CCD-IRIS/RGB color video camera made by Sony Co..

2.3 Results and Discussion

Figure 34 shows the FTIR spectra of α-CD, the as-synthesized polymers, and the polymers enzymatically coalesced from their α-CD ICs. The characteristic bands of α-CD, which are at 1158 cm^{-1} (antisymmetric ν_s of the C-O-C glycosidic bridge), 1079 and 1026 cm^{-1} (coupled $\nu_{s(C\text{-}C/C\text{-}O)}$)[146,147], cannot be found in the spectra of the IC coalesced polymers, and all bands characteristic for as-synthesized PCL, PLLA and PCL-*b*-PLLA are present in the corresponding IC coalesced polymers. This confirms that the host α-CD in their ICs was completely removed by the enzyme. Furthermore, the –COOH band (at ~1790 cm^{-1}, ν_s of C=O in aliphatic acids), which is expected if there were some

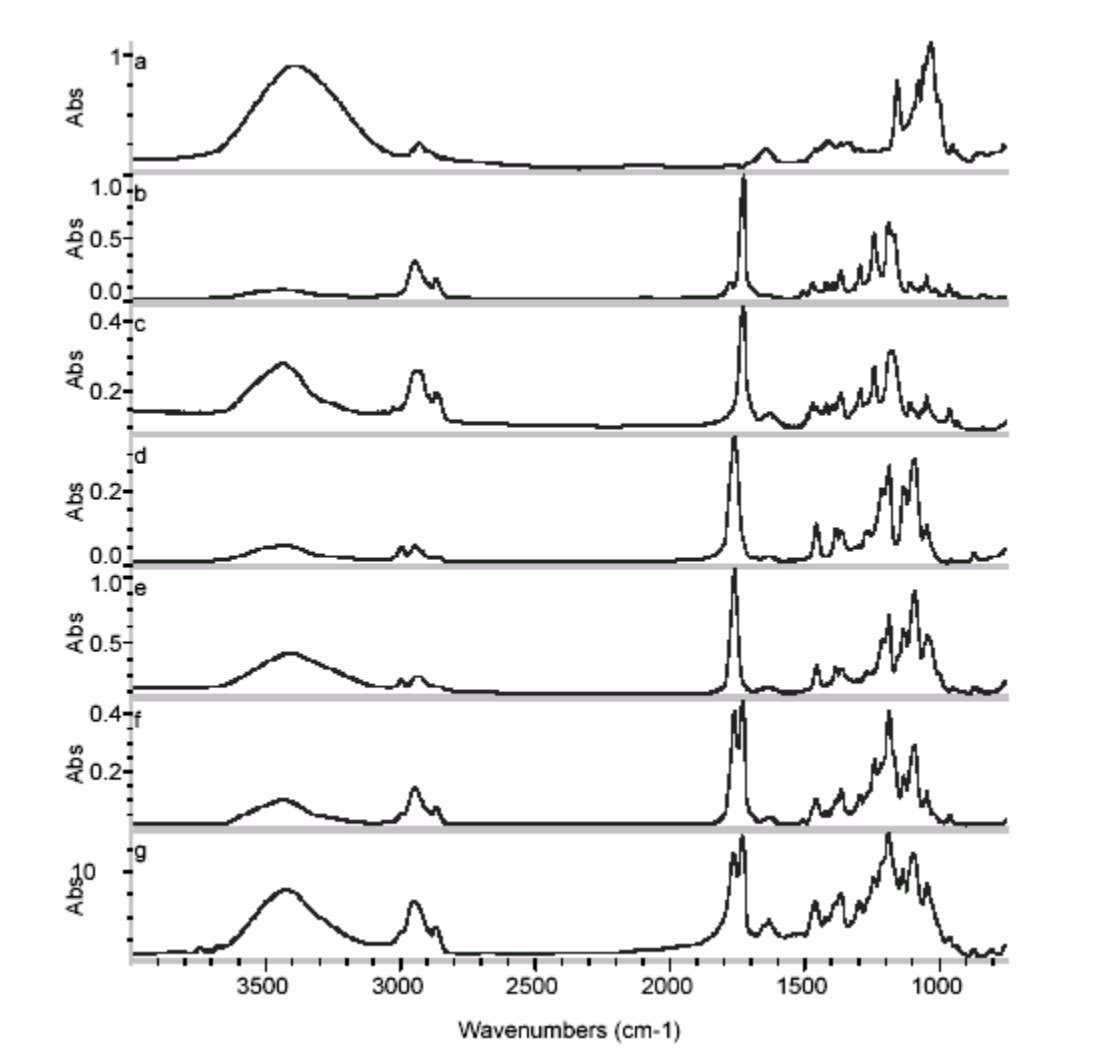

Figure 34. FTIR spectra of (a) α-CD, (b) as-synthesized PCL, (c) IC-coalesced PCL, (d) as-synthesized PLLA, (e) IC-coalesced PLLA, (f) as-synthesized , and (g) IC-coalesced PCL-b-PLLA diblock copolymer.

degradation of the two polyesters in either the as-synthesized or the enzymatically coalesced diblock copolymer samples, is absent in both diblock copolymer spectra. This shows that biodegradation of PCL and PLLA blocks did not take place during coalescence.

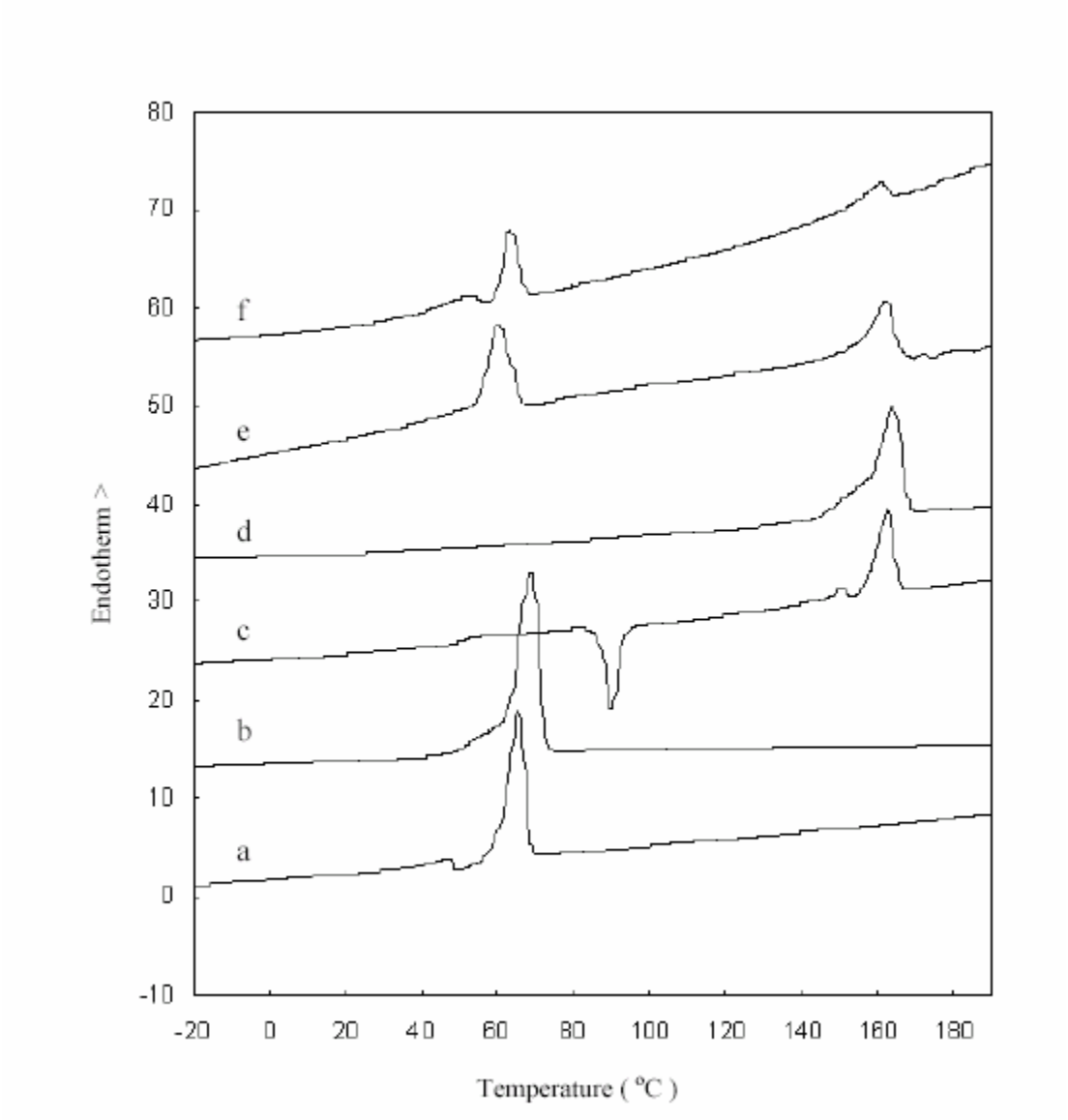

Figure 35. DSC scans of (a) as-synthesized PCL, (b) IC-coalesced PCL, (c) as-synthesized PLLA, (d) IC-coalesced PLLA, (e) as-synthesized, and (f) IC-coalesced PCL-b-PLLA diblock copolymer.

The DSC heating scans of as-synthesized and IC-coalesced polymers are presented in Figures 35, and their resultant thermal data are summarized in Table 7.

Table 7. Melting characteristics

Heating rate		Samples	T_m (^{o}C)	Crystallinity(%)
20(^{o}C/min.)	PCL	As-synthesized	65	74
		In as-synthesized diblock copolymer	60	62
		In IC-coalesced homopolymer	69	82
		In IC-coalesced diblock copolymer	63	25
	PLLA	As-synthesized	162	60
		In as-synthesized diblock copolymer	162	54
		In IC-coalesced homopolymer	164	69
		In IC-coalesced diblock copolymer	161	25

The crystallinity of samples was calculated from $\Delta H_f / \Delta H^o$, where ΔH^o is the enthalpy of melting expected for samples with 100% crystallinity, ie., 139 J/g for PCL[148] and 93 J/g for PLLA[149]. In the scan with a heating rate of 20^o C/min, both the melting temperature and crystallinity of PCL and PLLA have been elevated, and the IC coalesced PLLA did not show a T_g nor crystallization during the heating, although the as-synthesized PLLA did. As we reported before, homopolymers may form chain extended crystals after coalescence from ICs, with higher T_ms and crystallinties. In the as-synthesized diblock copolymer, T_m is lower than that of the as-synthesized homopolymer. The depression of T_m can be explained with the following equation:

$$T_m = T_m^0 (1 - \frac{2\gamma_e}{\Delta H_f L}) \quad (1)$$

where γ_e is the free energy of chain folding at the surface of the lamellae, ΔH_f the heat of fusion of the lamellae, L the thickness of the lamellae and T_m^0 the melting point of a 100% perfect polymer crystal[150]. As we can see, the reduction of the lamellar thickness can lead to a melting point depression. The covalent bond between the different blocks is expected to have a dominant effect on reducing L in the diblock copolymer. However, the

depression in T_m became much weaker in the IC coalesced diblock copolymer, suggesting that PCL and PLLA blocks crystallize independently in the IC coalesced diblock copolymer, despite their covalent connection.

Moreover, as we have already found in the diblock copolymer coalesced using hot water, the crystallinity of the enzymatically coalesced diblock copolymer shows a great reduction compared to the as-synthesized diblock copolymer. The reason could be that the coalesced polymer segments can only crystallize locally with segments that were proximal in the α-CD IC, and only if they have the same chemical structure. Since the coalescence is carried out in an environment and manner unfavorable to slow polymer crystallization, such as in solution at a temperature lower than T_m, the consolidation of polymer chains during coalescence is rapid and does not permit the formation of crystals with other block chains that were relatively far away in the IC. In the process of IC formation, both blocks have the opportunity to reside in neighboring IC channels, so they may remain proximal, unable to crystallize, and thus, form more well-mixed amorphous regions upon coalescence.

The kinetics of the isothermal crystallization of polymers can be analyzed using the Avrami treatment[151].

$$X_t = 1 - \exp[-K_n t^n] \quad (2)$$

where X_t is the fraction of material crystallized after time t, K_n the crystallization rate constant, which depends on the rates of nucleation and growth, and n the Avrami exponent, the value of which depends both on the nature of the primary nucleation and the growth geometry of the crystalline phase. The crystallization isotherms, obtained by plotting X_t against time are recorded in Figures 36, 38 and 40, which present the data

from isothermal crystallizations performed at 0, 30, and 90° C, respectively. Considering the melting and glass-transition temperatures of PCL and PLLA, crystallization at 0 and 30ºC should involve PCL only, while at 90° C only PLLA can crystallize. Even though we rapidly cool our samples from the melt (-320 ºC/min.), the isothermal crystallizations observed at low temperatures may not begin entirely from the completely amorphous state.

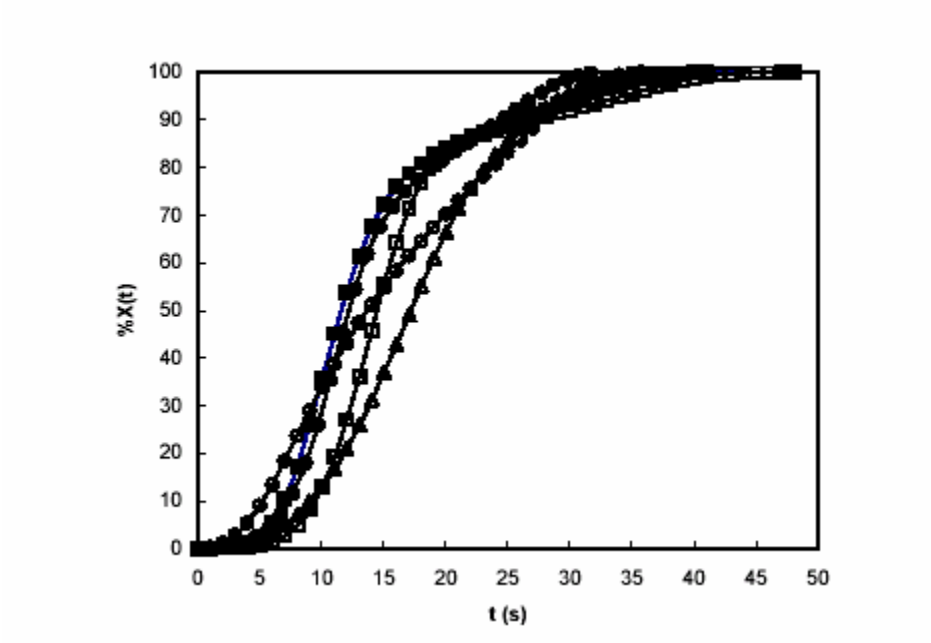

Figure 36. 0° C crystallization isotherms for (■) as-synthesized PCL, (Δ) PCL/PLLA physical blend, (●) as-synthesized PCL-b-PLLA diblock copolymer, (□) IC coalesced PCL, and (○) IC-coalesced PCL-b-PLLA diblock copolymer.

In Figure 36 crystallization isotherms measured at 0° C for the solution-cast blend of homopolymers, IC-coalesced PCL, and the as-synthesized and IC-coalesced PCL-b-PLLA diblock copolymer are compared with the typical exponential crystallization curve observed for pure as-synthesized PCL homopolymer. Note the disparity between the PCL

crystallization isotherms observed for the homopolymer blend and the as-synthesized and IC-coalesced diblock copolymer samples, on the one hand, and that observed for the pure as-synthesized and IC-coalesced PCL homopolymer. This may be caused by "sub-T_g nucleation" and crystallization of PLLA at low temperature, which can be observed in the fast DSC cooling scan shown in Figure 37.

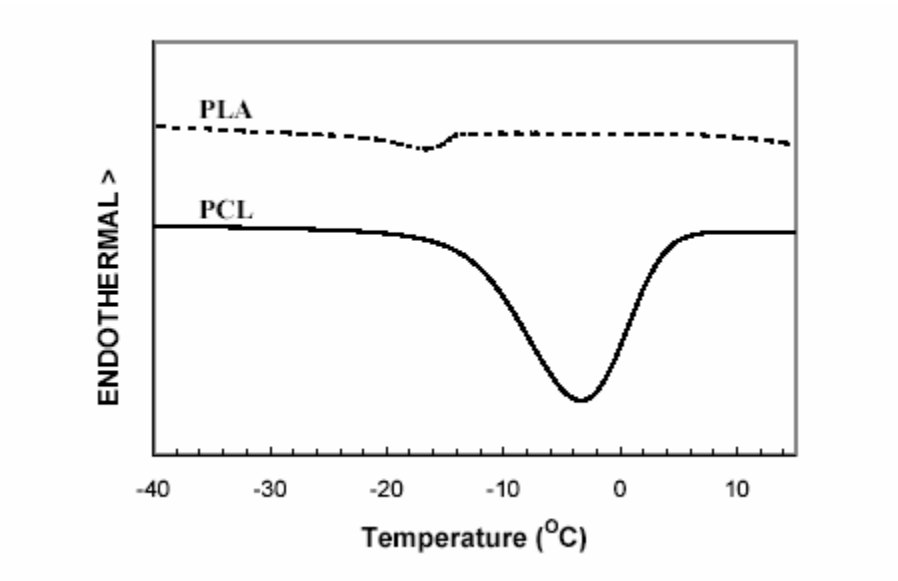

Figure 37. DSC scans observed with a cooling rate of 100° C/min for PLLA ($\Delta Hcc/\Delta H^o$ = 0.31%) and for PCL ($\Delta Hcc/\Delta H^o$ = 48.7%).

Figure 38 shows the isothermal crystallizations at 30° C, where it is interesting to see that the curve for the IC-coalesced diblock copolymer is almost the same as that of pure as-synthesized and IC-coalesced PCL, while the crystallizations of the as-synthesized diblock and the homopolymer physical blend are clearly different. This demonstrates that

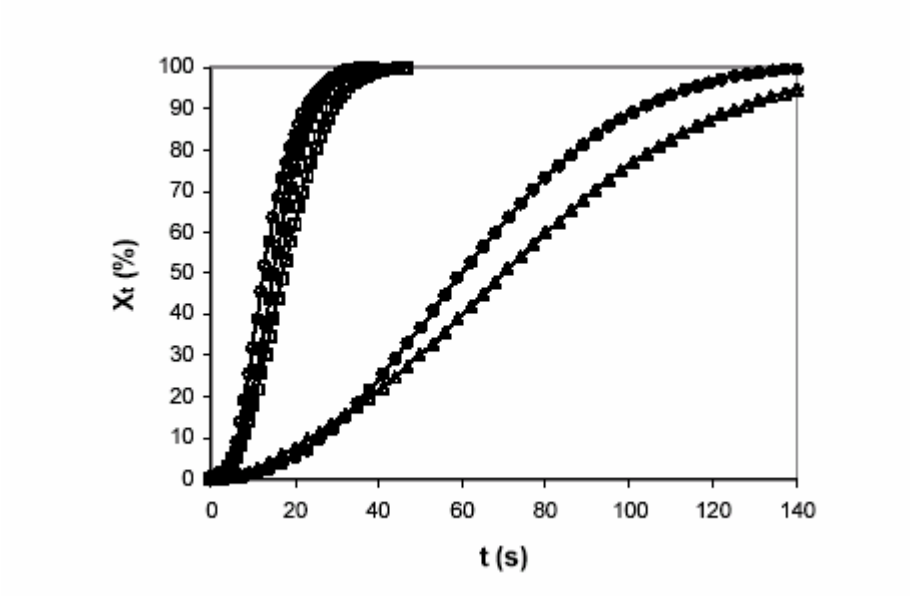

Figure 38. 30° C crystallization isotherms for (■) as-synthesized PCL, (Δ) PCL/PLLA physical blend, (●) as-synthesized PCL-b-PLLA diblock copolymer, (□) IC coalesced PCL, and (○) IC-coalesced PCL-b-PLLA diblock copolymer.

the crystallizable regions of PCL, although possibly small in the IC-coalesced diblock copolymer, are hardly influenced by the PLLA blocks. To illustrate the difference in crystallization of uninfluenced PCL and PCL in the binary blend, Figure 39 shows the polarized micrographs of as-synthesized PCL and the PCL/PLLA physical blend obtained by isothermal crystallization at 30° C. Compared to the spherulites of as-synthesized PCL, the ringed spherulite morphology in the blend reflects the influence of PLLA during the crystallization of PCL at this temperature[152]. This may be the explanation for the distinct crystallization behavior observed for the homopolymer blend sample at 30° C. The low T_g of PCL may be the reason for very minor differences in the isothermal crystallization kinetics exhibited by as-synthesized and IC-coalesced PCL at low

temperatures (0 and 30º C). Heating the IC coalesced PCL at 190º C for 10 min. before quenching to these low crystallization temperatures has likely disordered the as-coalesced morphology of extended, unentangled chains to that more typical of randomly-coiling, entangled chains expected in the as-synthesized PCL.

In Figure 40 the crystallization isotherms at 90^{o} C for PLLA in the IC-coalesced homopolymer and diblock copolymer are distinct from those of the other three samples. The coalesced samples undergo the fastest crystallizations, reflecting a superior ability to crystallize. An explanation for this behavior could be the presence of more extended, unentangled polymer chains in the IC-coalesced samples. When comparing the isotherms of as-synthesized PLLA, PCL/PLLA physical blend, and as-synthesized diblock copolymer, we can see an effect of the molten PCL chains on the crystallization of PLLA, which may be that of a diluent. Moreover, this "diluent" effect is greatest in the as-synthesized diblock copolymer as judged by its longer crystallization delay, which

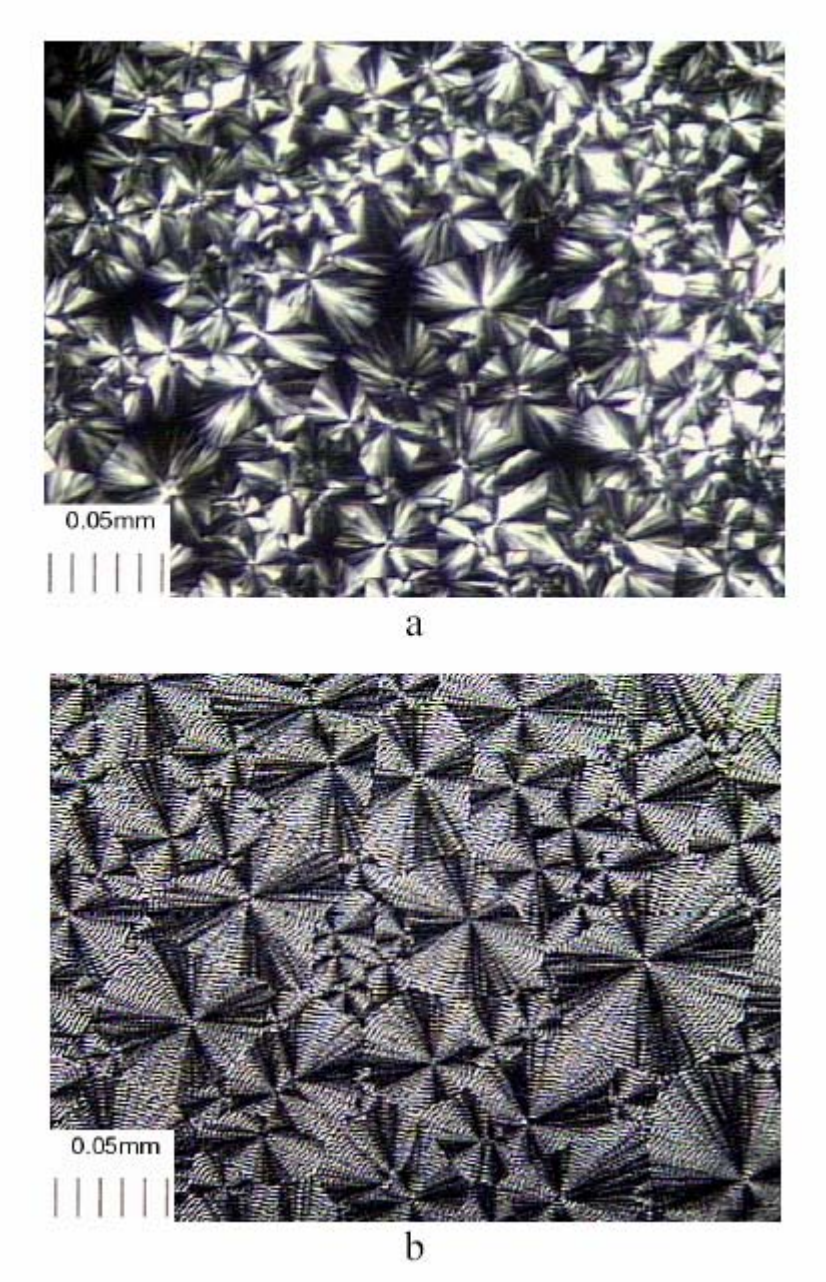

Figure 39. The crystalline morphologies of (a) as-synthesized PCL and (b) PCL/PLLA physical blend isothermally crystallized at 30º C, as observed by polarized microscopy.

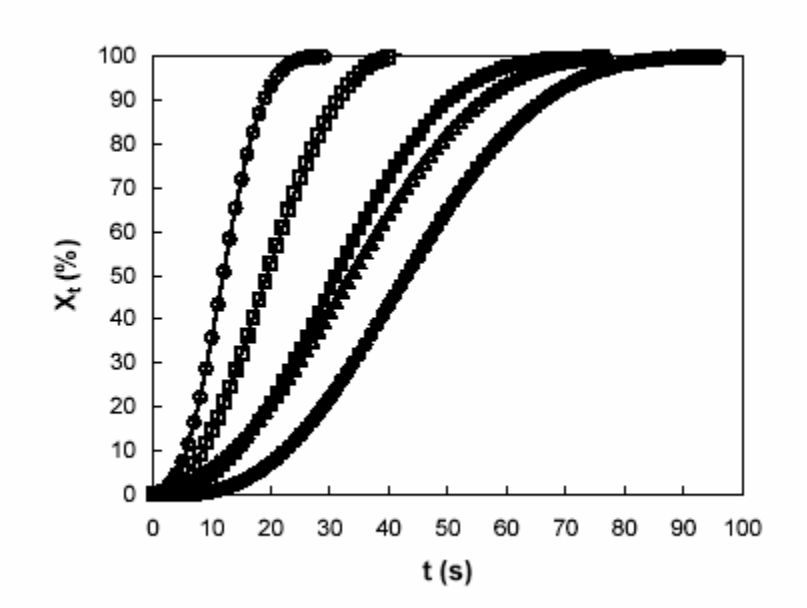

Figure 40. 90° C crystallization isotherms for (■) as-synthesized PLLA, (Δ) PCL/PLLA physical blend, (●) as-synthesized PCL-b-PLLA diblock copolymer, (□) IC coalesced PLLA, and (○) IC-coalesced PCL-b-PLLA diblock copolymer.

may be caused by the chemical connection between the two blocks of the copolymer rather than by simple physical contact. However, this possible dilution effect cannot be seen in the IC-coalesced diblock copolymer. It would appear that the crystallization of polymer chain blocks in the IC-coalesced sample is a much more localized process that reflects the distribution of neighboring, proximal blocks in the α-CD IC channels. The combination of lower crystallinity and a higher degree of perfection in the crystalline regions achieved by coalescence may also contribute to this behavior.

Table 8. The half-times of crystallization, $t_{1/2}$ (s), observed isothermally at different temperatures.

Temperature	0º C	30º C	90º C
PCL	11.7	15.1	-
PLLA	-	-	31.0
Physical blend	17.1	70.1	33.9
PCL-b-PLLA	11.0	59.9	82.4
IC-coalesced PCL	14.5	17.3	-
IC-coalesced PLLA	-	-	19.4
IC-coalesced PCL-b-PLLA	13.6	12.8	11.8

Table 8 lists the half-times of crystallization, $t_{1/2}$, which are used to represent the crystalization rate of crystals, in different samples at various temperatures. At 0^{o} C, the PCL crystallizations in the physical blend and as-synthesized diblock copolymer have significantly smaller $t_{1/2}$s and thus faster crystalization rates than those observed at 30^{o} C. This further confirms the possible sub-T_g nucleation and crystallization of PLLA. However, PLLA nucleation cannot be seen in the IC-coalesced diblock copolymer, because there is not much difference in the $t_{1/2}$s for crystallization at 0 and 30^{o} C. Consequently, there must not be sub-T_g crystallization of short PLLA segments in the coalesced sample at low temperature. In the case of isothermal crystallization at 90^{o} C, the as-synthesized diblock copolymer has the longest $t_{1/2,}$ which is significantly shortened after IC-coalescence. Also the IC-coalesced PLLA has a shorter $t_{1/2}$ than the as-synthesized PLLA. These results clearly demonstrate that the states of the polymer chains were likely more extended, less entangled, and so more readily able to form crystals in both IC-coalesced samples.

Transformation of eq. 2 to the double-logarithmic form leads to:

$$\ln[-\ln(1-X_t)] = \ln K_n + n \ln t \quad (3)$$

Thus, from a plot of $\ln[-\ln(1-X_t)]$ *vs* $n\ln t$, the Avrami exponent can be determined from the slope of the curve. As an example, Figures 41 illustrates the plots of $\ln[-\ln(1-X_t)]$ *vs* $n\ln t$ and the linear fitting of the data for the samples crystallized at 0° C. The Avrami exponents obtained in this way are summarized in Table 9. At 0° C, all the samples have values which are below 3. This indicates a crystallization process with heterogeneous nucleation and the presence of three dimensional growth. Some researchers have reported that pure PCL can crystallize with heterogeneous nucleation at certain temperatures[153]. The Avrami value of 3 observed at 0° C for pure as-synthesized PCL in our study also demonstrates that portions

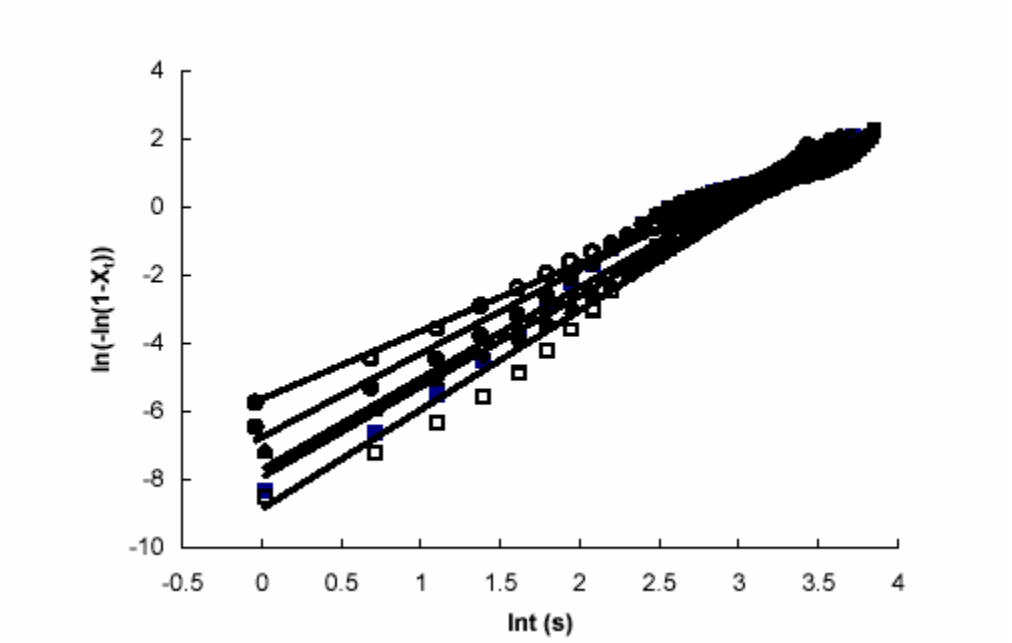

Figure 41. Avrami plots for the samples isothermally crystallized at 0° C: (■) as-synthesized PCL, (Δ) PCL/PLLA physical blend, (●) as-synthesized PCL-b-PLLA diblock copolymer, (□) IC-coalesced PCL, and (○) IC-coalesced PCL-b-PLLA diblock copolymer.

Table 9. The Avrami Index n observed in isothermal crystallizations at different temperatures.

Temperature	0º C	30º C	90º C
PCL	3.0	4.1	-
PLLA	-	-	4.0
Physical blend	2.1	3.8	3.2
PCL-b-PLLA	2.2	2.8	3.1
IC-coalesced PCL	2.7	4.1	-
IC-coalesced PLLA	-	-	3.7
IC-coalesced PCL-b-PLLA	2.4	4.2	4.2

of the PLC chains crystallize on the nuclei of other PCL crystals. As for the physical homopolymer blend and as-synthesized diblock copolymer, they have Avrami exponents ($n \sim 2.2$) that are significantly less than the pure as-synthesized PCL. This shows the contribution of the nucleation of PCL crystals by tiny PLLA crystals at low temperature. The IC-coalesced samples have Avrami exponents that are higher relative to the physical blend and the as-synthesized samples, which verify that the PLLA has less effect on the crystallization process of the IC-coalesced samples. Without heterogeneous nucleation, both of the bulk homopolymers, PCL and PLLA, show an Avrami exponent of about 4 at 30 and 90^{o} C, which reflect homogenous nucleation and three-dimensional crystallization. A very similar Avrami exponent is also observed for the IC-coalesced diblock copolymer at these two temperatures. However, the exponents for the as-synthesized diblock copolymer are close to 3. This clearly shows that the chemical connection between the two blocks has an influence on the crystallization of the two blocks in the largely phase-segregated, as-synthesized sample, but not on the more intimately mixed, IC-coalesced sample.

Although the process of non-isothermal crystallization in slowly crystallizing materials, such as polymers, is likely complex, it is very attractive to study, for both scientific and industrial reasons. Several methods have been employed to describe the non-isothermal crystallization process, and one of the most commonly used was proposed by Ozawa[154]. He assumed that the process of non-isothermal crystallization is governed by the same mechanism as that predicted by the KAE model (Kolmogorov, Avrami, and Evan)[155], for which

$$1 - X_{rel} = \exp\left(\frac{-\kappa(T)}{|dt/dt|^{n}}\right) \quad (4)$$

where X_{rel} is the relative crystallinity, $\kappa(T)$ is the so-called cooling function of non-isothermal crystallization, dT/dt = the constant rate of temperature change (V is used to represent the rate of temperature change, or cooling rate, in this study), and n is the Avrami exponent. In a non-isothermal process there is a shift in the dependence of crystallization rate from temperature to time. Taking the logarithm of eq. 4 twice yields

$$\ln[-\ln(1 - X_{rel})] = \ln[\kappa(T)] + n\ln\left(\frac{1}{|dT/dt|}\right) \quad (5)$$

If the Ozawa approach is valid for the crystallizing system, a plot of $\ln[-\ln(1 - X_{rel})]$ *vs* $\ln(dT/dt)^{-1}$ at constant temperature should be linear with n as the slope.

Figures 42 and 43 show the DSC thermograms of crystallization of the two homopolymers, their physical blend, and the as-synthesized and IC-coalesced diblock copolymers recorded at various cooling rates. In both figures, the crystallization process begins at higher temperatures for slower cooling rates. This likely results, because at slower cooling rates there is enough time to activate or form nuclei at higher

temperatures, while as the cooling rate is increased, nuclei are only activated at lower

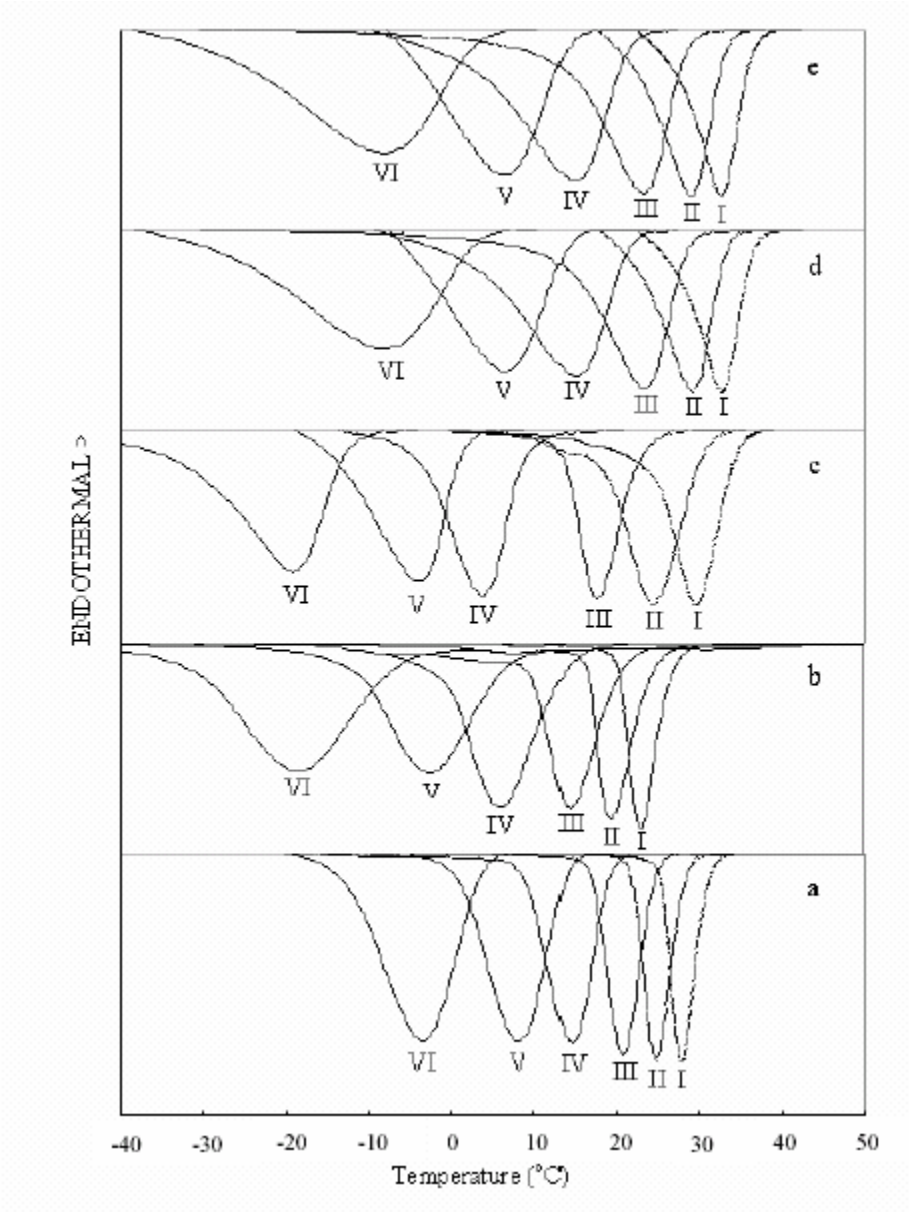

Figure 42. DSC crystallization thermograms for (a) as-synthesized PCL, (b) PCL in PCL/PLLLA physical blend , (c) PCL in as-synthesized PCL-b-PLLA diblock copolymer, (d) IC-coalesced PCL, and (e) PCL in IC-coalesced PCL-b-PLLA diblock copolymer. The cooling rates are (I) 5, (II) 10, (III) 20, (IV) 40, (V) 60, and (VI) 80^{o} C/min..

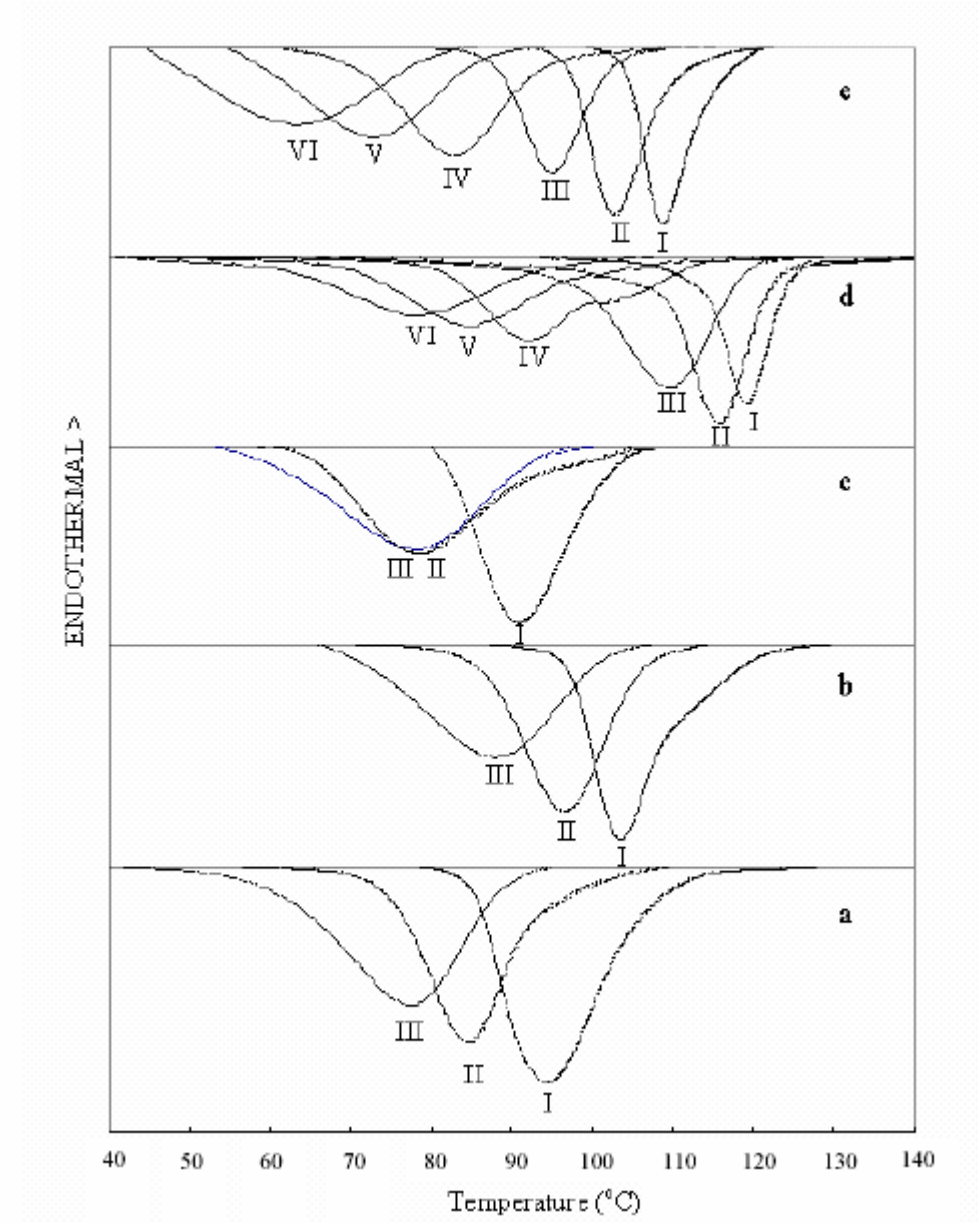

Figure 43. DSC crystallization thermograms for (a) as-synthesized PLLA, (b) PLLA in PCL/PLLLA physical blend, (c) PLLA in as-synthesized PCL-b-PLLA diblock copolymer, (d) IC-coalesced PLLA, and (e) PLLA in IC-coalesced PCL-b-PLLA diblock copolymer. The cooling rates are (I) 5, (II) 10, (III) 20, (IV) 40, (V) 60, and (VI) 80^{o} C/min.

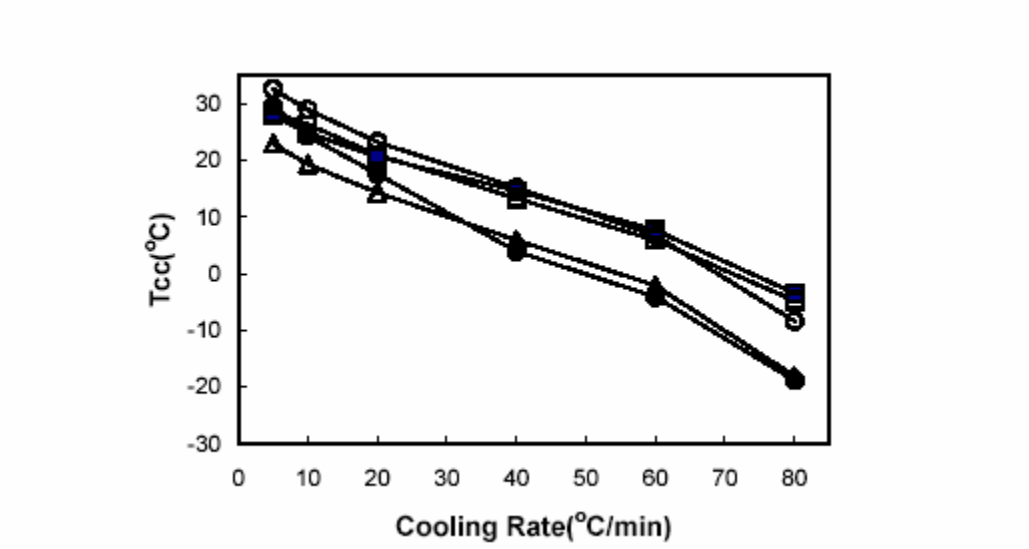

Figure 44. T_{cc} of PCL *vs* cooling rate for (■) as-synthesized PCL, (Δ) PCL/PLLA physical blend, (●) as-synthesized PCL-b-PLLA diblock copolymer, (□) IC coalesced PCL, and (○) IC-coalesced PCL-b-PLLA diblock copolymer.

temperatures. The crystallization temperatures observed on cooling, T_{cc}, for PCL and PLLA in the different samples are presented in Figures 44 and 45 for different cooling rates. In Figure 44 for PCL, almost the same trend was found for the IC-coalesced diblock copolymer and the physical blend of the two homopolymers. The nearly parallel curves for the IC coalesced sample and the physical blend demonstrate that increased cooling rates or shorter crystallization times have the same impact on the chains of crystallizable polymers in the two samples. Moreover, it is found that at the same cooling

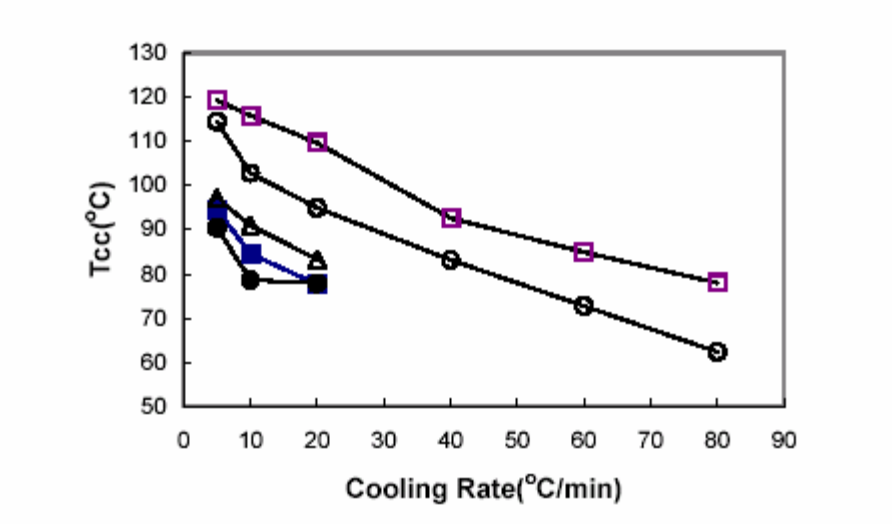

Figure 45. T_{cc} of PLLA *vs* cooling rate for (■) as-synthesized PLLA, (Δ) PCL/PLLA physical blend, (●) as-synthesized PCL-b-PLLA diblock copolymer, (□) IC coalesced PLLA, and (○) IC-coalesced PCL-b-PLLA diblock copolymer.

rate the IC coalesced sample has an overall higher T_{cc} than the physical blend, which further demonstrates that the polymer chains in the IC coalesced sample are more readily incorporated into the crystal lattice, likely because they initially have more extended conformations and are unentangled. However, the as-synthesized, phase-segregated diblock copolymer shows a different change in T_{cc} when the cooling rate is altered. At slow cooling rates, the PCL blocks in the diblock copolymer crystallize at higher temperatures than in the physical blend, while at fast cooling rates, they crystallize at lower temperatures. A similar phenomenon also happens to the PLLA chains as illustrated in Figure 45. Here the change in T_{cc} of as-synthesized PLLA is similar to that of PLLA blocks in the IC-coalesced diblock copolymer, rather than the physical blend of homopolymers or the PLLA blocks in the as-synthesized diblock copolymer. Another exciting result is that, in the primary stages of crystallization, but not at $T < T_g$ where

only very tiny PCL crystals are formed, the PLLA blocks in the IC-coalesced diblock copolymer and IC-coalesced PLLA homopolymer can crystallize even at temperatures near the T_g of PLLA, but they do not crystallize at these low temperatures in the other three samples. Generally, crystallization is expected to take place in the temperature range between T_m and T_g, so we believe the exceptional ability of IC-coalesced polymer chains to crystallize at low temperatures is a consequence of their extended conformations and unentangled morphologies.

Figure 46 shows the dependence on cooling rate of the crystallization enthalpy, ΔH_{cc}. Owing to its flexible nature and polar ester groups, PCL becomes highly crystalline at temperatures above its T_g (~ –50° C). In this study, PCL, unlike PLLA, can crystallize during the whole range of cooling rates, and ΔH_{cc} does not vary too much over this range.

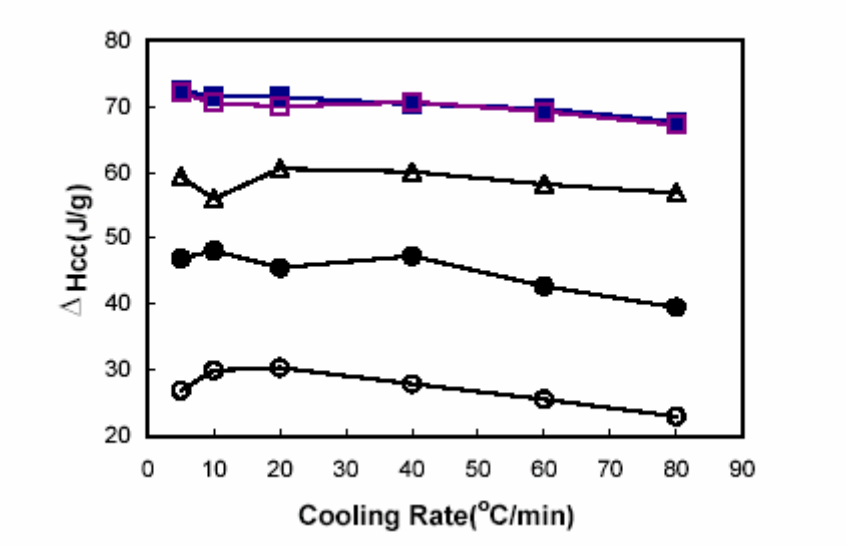

Figure 46. ΔH_{cc} of PCL *vs* cooling rate for (■) as-synthesized PCL, (Δ)PCL/PLLA physical blend, (●) as-synthesized PCL-b-PLLA diblock copolymer, (□) IC coalesced PCL, and (○) IC-coalesced PCL-b-PLLA diblock copolymer.

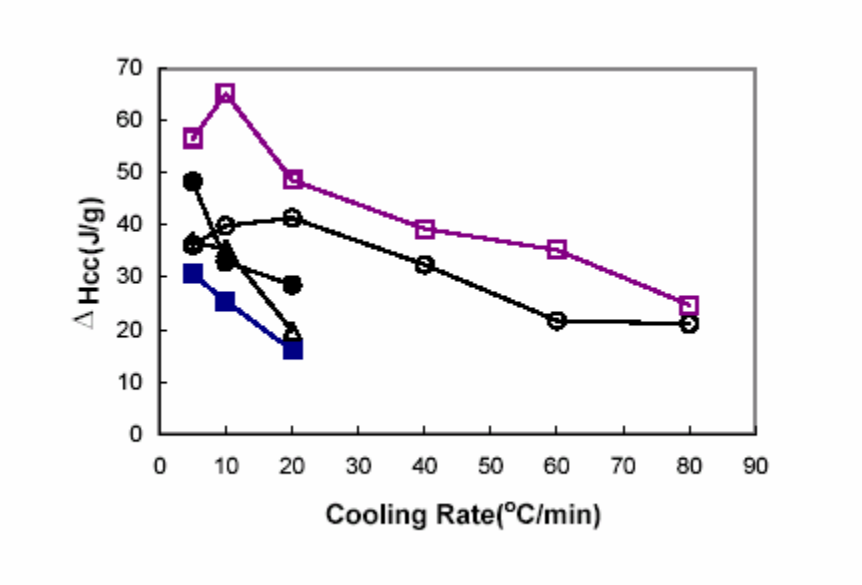

Figure 47. ΔH_{cc} of PLLA *vs* cooling rate for (■) as-synthesized PLLA, (Δ) PCL/PLLA physical blend, (●) as-synthesized PCL-b-PLLA diblock copolymer, (□) IC coalesced PLLA, and (○) IC-coalesced PCL-b-PLLA diblock copolymer.

At each cooling rate, the crystallization enthalpy of PCL in different samples follows the same order : as-synthesized ~ IC-coalesced > physical blend with PLLA > as-synthesized diblock copolymer > IC-coalesced diblock copolymer. (In the two component systems the heats of crystallization have been divided by the mole fraction of PCL to provide ΔH_{cc}'s which are comparable). These results confirm that the IC coalesced diblock copolymer sample has the most amorphous PCL regions. The decrease in ΔH_{cc} for the PCL component in the physical blend and the as-synthesized diblock copolymer, compared to as-synthesized PCL, is caused by the introduction of PLLA chains and this effect is greater in the as-synthesized diblock copolymer, because of the chemical connection between the two kinds of polymer blocks. The variation in ΔH_{cc} for PLLA at

different cooling rates is shown in Figure 47. The largest ΔH_{cc} is observed for the IC-coalesced homopolymer and the lowest for the as-synthesized homopolymer. IC-coalesced PLLA clearly shows an ability to crystallize that is superior to the as-synthesized PLLA. Moreover, the lower the cooling rate, the higher is T_{cc} and the less PLLA crystallizes in the IC-coalesced samples.

In Figures 48 and 49, following the Ozawa treatment, plots of $\ln[-\ln(1-X_{rel})]$ *vs* $\ln(dT/dt)^{-1}$ at several temperatures are shown. Because linear plots were achieved, the validity of applying Ozawa's method to these samples is reinforced. The Avrami

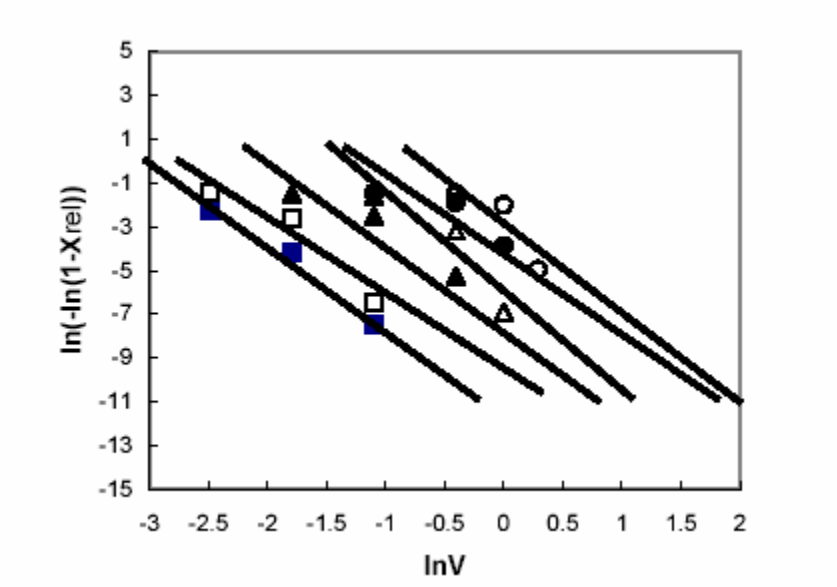

Figure 48. Ozawa plot of $\ln(-\ln(1-X_{rel}))$ versus lnV (V is the cooling rate in the units ^{o}C/s) for the PCL blocks in the IC-coalesced PCL-b-PLLA diblock copolymer at (■) 31.0, (□) 28.9, (▲) 20.8, (Δ)15.7, (●)10.1, and (○) 0.0^{o}C.

exponents for PCL and PLLA crystallized dynamically in non-isothermal cooling scans are listed in Table 10. It is found that the as-synthesized and IC-coalesced

homopolymers, their physical blend, and the individual blocks in the IC-coalesced diblock copolymer samples have an Avrami exponent of ~ 4, while the as-synthesized diblock copolymer has *n* close to 3 for both blocks.

An Avrami exponent of 4 for the two homopolymers in the physical blend results from that the fact that PCL and PLLA are immiscible with each other. Therefore, in a dynamic environment, the two polymers will crystallize without affecting each other. However, a different result occurs in the crystallization of the as-synthesized diblock copolymer. A possible explanation could be that the motion of the two blocks will have an influence on each other's crystallization, such that the crystal of one block might function as a nucleus for the crystallization of the other block, because of the chemical

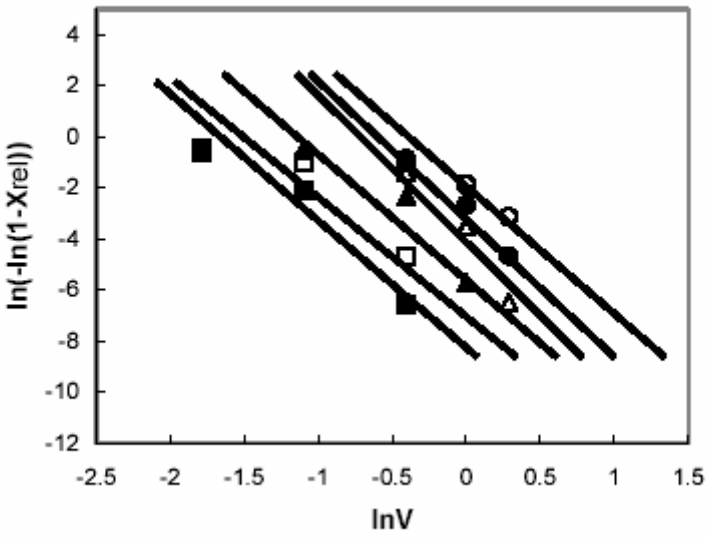

Figure 49. Ozawa plot of $\ln(-\ln(1-X_{rel}))$ versus lnV (V is the cooling rate in the units ^{o}C/s) for the PLLA blocks in the IC-coalesced PCL-b-PLLA diblock copolymer at (■) 95.2, (□) 92.5, (▲) 85.8 , (Δ) 79.7, (●) 75.7, and (○) 69.0^{o} C.

Table 10. The Avrami Index, n, for PCL and PLLA observed in non-isothermal crystallizations

Samples	PCL	PLLA
Pure polymer	4.4	4.2
In PCL and PLLA physical blend	4.4	4.0
In as-synthesized PCL-b-PLLA	3.3	3.2
In IC-coalesced homopolymer	4.4	4.5
In IC-coalesced PCL-b-PLLA	4.5	4.2

bonding between them. In contrast, the IC-coalesced diblock copolymer is more like the pure polymers and their physical blend, rather than the bulk as-synthesized diblock copolymer. The Avrami exponent of 4 for the IC-coalesced diblock copolymer indicates that the two blocks crystallize by a homogeneous process, behaving as if the other block is not present. The reason for this seemingly strange behavior may be that the polymer chains in the IC-coalesced samples are quite extended, with less entanglements, and so very readily and rapidly crystallize neighboring PCL blocks and neighboring PLLA blocks. There simply is not sufficient time for this crystallization to be influenced by the presence of the other chemically distinct block. Another possible reason is that there is much more amorphous material, with more extensive and intimate mixing of the non-crystalline blocks, in the IC-coalesced sample than in the phase-segregated, as-synthesized diblock copolymer, so the potential for mutual nucleation is reduced. By comparing the Avrami exponents of PCL and PLLA, it can be seen that PCL has the higher value in every case except for the IC-coalesced homopolymers.

2.4 Conclusions

Coalescence from their α-CD ICs is so fast that the polymer chains crystallize almost at the same time they are consolidated, without losing the extended conformations required in the α-CD IC channels[156]. Therefore, CD IC formation/coalescence may be an effective way to modify the crystallinity of biomedical polymers. After coalescence, the PCL and PLLA homopolymers show elevated melting temperatures and crystallinities. In the case of their diblock copolymer, phase segregation and consequent block crystallinities are markedly suppressed in the coalesced samples, although the separate crystallization of blocks in the IC-coalesced diblock copolymer do not appear to be influenced by the existence of the other block. Disregarding the possible sub-T_g nucleation by PLLA crystals observed at 0º C, in both the static environment of isothermal crystallization and the dynamic environment of non-isothermal crystallization, analyses show that the PCL and PLLA homopolymers and blocks in the IC-coalesced samples have an Avrami exponent of ~ 4, which is also obtained for the as-synthesized homopolymers, while the as-synthesized diblock copolymer has $n \sim 3$. The two polymer blocks in the IC-coalesced sample show a crystallization process with homogeneous nucleation, while heterogeneous nucleation occurs in the as-synthesized diblock copolymer, and this is a direct consequence of significant differences in their conformations and morphologies. In contrast to the as-synthesized diblock copolymer, the crystallization of blocks in the IC-coalesced diblock sample seems to occur without influence from their covalent connection. Also, because the coalesced polymer chains are much less entangled, they show an overall increased rate of crystallization. These

observations appear consistent with Flory's micellar model of crystallization[157-159], where segments from different polymer chains having similar extended conformations locally organize to provide the crystalline nuclei, rather than the intramolecular chain-folded nucleation of crystal growth. All the results in this study demonstrate that, when coalesced from their cyclodextrin inclusion complexes, both the PCL and PCL homopolymers and the block chains of the PCL-b-PLLA copolymer show crystallization behavior which is clearly distinguishible from that of their as-synthesized samples.

3 Reorganization of the Structures, Morphologies, and Conformations of Engineering Polymers via Coalescence from Polymer-Cyclodextrin Inclusion Complex

3.1 Polyesters

3.1.1 Introduction

Polymers may form non-covalent,crystalline complexes with several small-molecule hosts, such as urea, perhydotriphenylene, and cyclodextrins. In these inclusion complexes (ICs) the guest polymer chains occupy narrow cylindrical channels (D ~ 5-10Å) created by the crystalline host lattice. As a consequence, the included polymer chains are constrained to assume highly extended conformations and are generally segregated from neighboring included polymer chains by the channel walls of the host crystalline lattice. When these polymer-IC crystals are washed with a solvent for the host, but which does not dissolve the guest polymer, the ICs are disrupted, the host is dissolved and removed, and the guest polymer chains are forced to coalesce into a bulk solid. DSC and small-angle X-ray scattering (SAXS) observations[160] of crystallizable polymer samples coalesced from their ICs have often revealed melting temperatures that are elevated from those measured on samples crystallized from their completely disordered solutions and melts, and an absence of discrete reflections from the long spacing between chain-folded lamellae. These observations suggest an extended-chain crystalline morphology for the IC-coalesced polymer samples.

Here initial DSC, TGA, FTIR, and X-ray observations of bulk poly(ethylene terephthalate) (PET) and bisphenol-A polycarbonate (PC) samples obtained by coalescence from their γ-cyclodextrin (CD)-ICs are reported. The coalesced samples were found to evidence structures, morphologies, chain conformations, and presumeably physical properties, which are distinct from those generally observed for their bulk samples.

3.1.2 Experimental

Materials

PET ([η] = 0.59, M_v = 18,000) and PC (M_w = 28,000 and M_n = 17,300) were obtained from Aldrich. γ-CD was obtained from Cerestar, and analytical grade trifluoroacetic acid (TFA), tetrahydrofuran (THF), dimethyl sulfoxide (DMSO), and chloroform (CLF) were obtained from Fisher.

Sample Formation

PET (0.1 g, 0.52 mmol) was dissolved in a combined solvent of 6 mL of TFA and 14 mL of CLF with stirring in a 250-mL boiling flask submerged in an oil bath at approximately 55° C. The PET dissolved within 15 min, and the solution was allowed to stir for approximately 45 min more before an aqueous solution of γ-CD was added to the PET solution dropwise. The aqueous γ-CD solution was created by the dissolution of 2 g of γ-CD in 10 mL of deionized water at room temperature. As the γ-CD solution was

added to the PET solution, a white gel-like foam formed on top of a clear liquid that was thought to be an aqueous phase resting on an organic phase. The combination of solutions was allowed to stir for 1 h in the 250-mL boiling flask submerged in the 55° C oil bath. At the end of this hour, the white foam was still resting on top of the clear liquid as a distinctly separate phase. The white foam was filtered from the liquid by the liquid being pulled through a ceramic frit in a Büchner funnel through a vacuum. The gel-like foam was vacuum-dried at 60° C for 20 h. The dried material was then lightly ground into a coarse powder with a mortar and pestle. Because of its purity, this was the sample primarily investigated here.

PC (0.125 g, 0.48 mmol) was dissolved in 10 mL of THF with stirring at 50° C. Upon the dissolution of PC, the PC/THF solution was slowly added to a solution of γ-CD and DMSO. The γ-CD/DMSO solution was created by the dissolution of 1.886 g (1.5mmol) of γ-CD in 20 mL of DMSO with stirring at 60 ° C. The combination of solutions was heated at 60° C for 3 h with stirring to maintain homogeneity. The temperature of the mixture was then slowly reduced to 20 °C and allowed to stir for about 10 h. The resulting precipitate was filtered out and vacuum-dried for 24 h at 60° C.

IC-coalesced samples were obtained by washing the γ-CD-ICs several times with hot water. The solution cast samples were prepared by dissolving PC in THF and PET in TFA/CLF and then drying the solutions overnight under vacuum at ~ 50^0 C. Intrinsic viscosity measurements not reported here show that the molecular weight of as-received PET is not altered by dissolution in TFA/CLF, which occurred in the formation of PET-γ-CD-IC, from which the coalesced sample was obtained, and in the solution casting of PET.

X-ray Diffraction

The wide angle X-ray diffraction (WAXD) scans of PET and PC samples were carried out with a Seimens type-F X-ray diffractometer. The X-ray source was Ni-filtered Cu K_α radiation (1.54Å), with voltage and current set to 30KV and 20mA. The specimens were mounted on aluminum frames and scanned from 5 to $40^o = 2\theta$ at a rate of ($2\theta = 1.2^o$)/min.

CP-MAS ^{13}C NMR

Solid-state NMR data were collected with a Bruker DSX wide-bore system with a field strength corresponding to a ^1H Larmor frequency of 300.13 MHz. Radio-frequency power levels were 71 kHz for spin-locking and decoupling, corresponding to $\pi/2$ pulse widths of 3.5 s. Data were obtained with MAS speeds of 4-5 kHz on a commercial 7-mm probe. CP contact times were 1ms. Quantitative ^{13}C Bloch decay (single-pulse) experiments employed a 200-s recycle time and a composite pi/2 pulse for background suppression, as described by White et al[161].

Differential Scanning Calorimetric (DSC) Analysis

The thermal scans of as-received and solution-cast polymers and their γ-CD-IC samples, after coalescence by washing with hot water, were performed with a Perkin-Elmer DSC-7 differential scanning calorimeter. The measurements were run in the range of 30-280^o C at heating rates of 10 or 20^o C /min. Cooling rates were as specified.

Thermogravimetric Analysis (TGA)

TGA scans were obtained with a Perkin-Elmer Pyris 1 thermogravimetric analyzer (TGA) on 5-10 mg samples. Samples were placed in open platinum pans which were hung in the heating chamber. The weight percentage of remaining material in the pan was recorded while heating from 25 - 600º C at a heating rate of 20º C/min. Nitrogen was used as the purge gas.

Fourier Transform Infrared Spectroscopy (FTIR)

The FTIR spectral studies of PET and PC samples in the form of KBr pellets were carried out in a Nicolet 510P FTIR spectrometer in the range between 4000 and 400 cm^{-1}, with a resolution of $2cm^{-1}$.

3.1.3 Results and Discussion

X-ray Diffraction

Channel-structure ICs are known to be formed by γ-CD when hosting 1-propanol. The powder diffraction pattern for this model channel structure is provided as a reference in Figure 50. The strong peak at 2 = 7.5° seen in the diffraction pattern for 1-propanol/γ-CD IC has been suggested as an indicator for the channel structure. The diffraction patterns for γ-CD and the TFA/CLF/ γ-CD control are also shown for comparison. Figure 50 also displays the diffraction patterns for PET and its combinations with γ-CD. The diffraction patterns shown in Figure 50 have been normalized so that the magnitude of the most

intense peak in each pattern is equal to the magnitude of the most intense peak in the other six patterns.

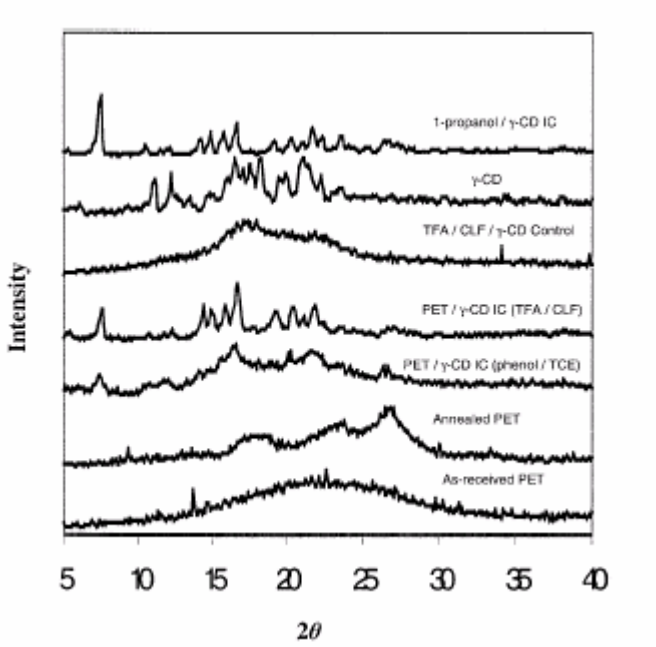

Figure 50. WAXD results for PET samples.

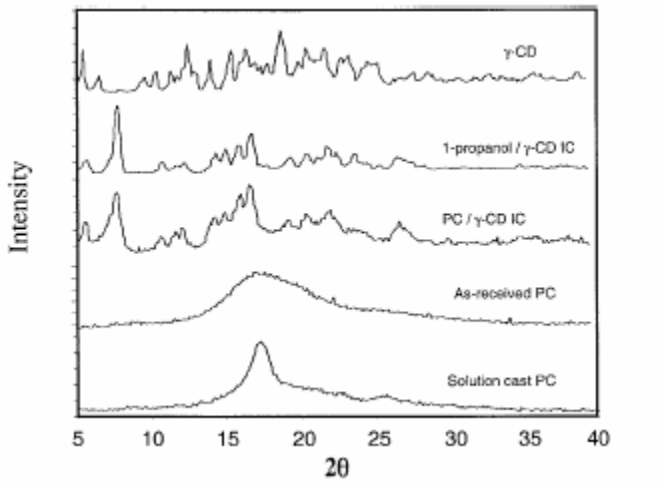

Figure 51. WAXD results for PC samples

The WAXD pattern of PC/ γ-CD-IC is shown in Figure 51, and the diffraction peak at 2θ = 7.8°, which is characteristic of the channel-structure γ-CD-IC, is also clearly

presented. It appears that there was very little free polycarbonate in the PC/ γ-CD-IC sample, because no diffraction peaks characteristic of crystalline PC were found with respect to the as-received, amorphous PC, and solution-cast, semicrystalline PC and because of the close similarity between the diffraction patterns of 1-propanol/-CD-IC and PC/ γ-CD-IC.

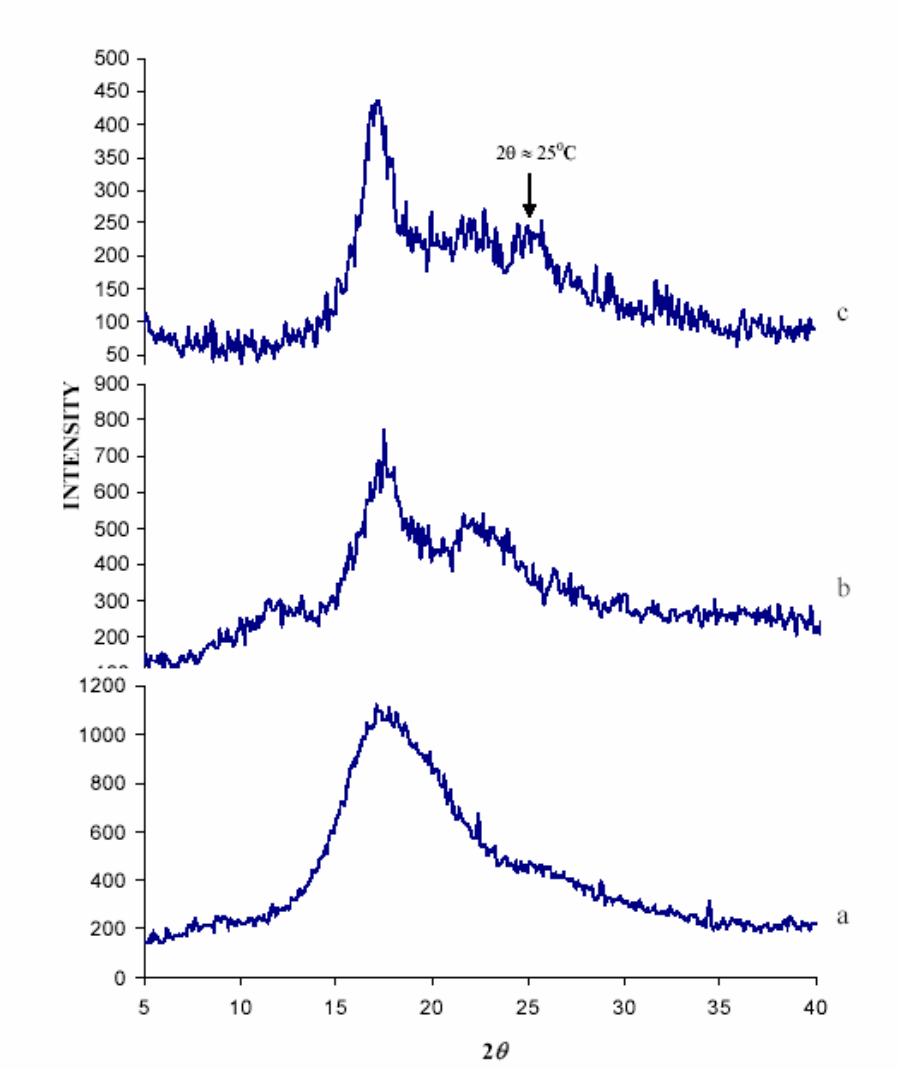

Figure 52. X-ray diffraction of (a) as-received PC, (b) solution-cast PC, and (c) IC-coalesced PC.

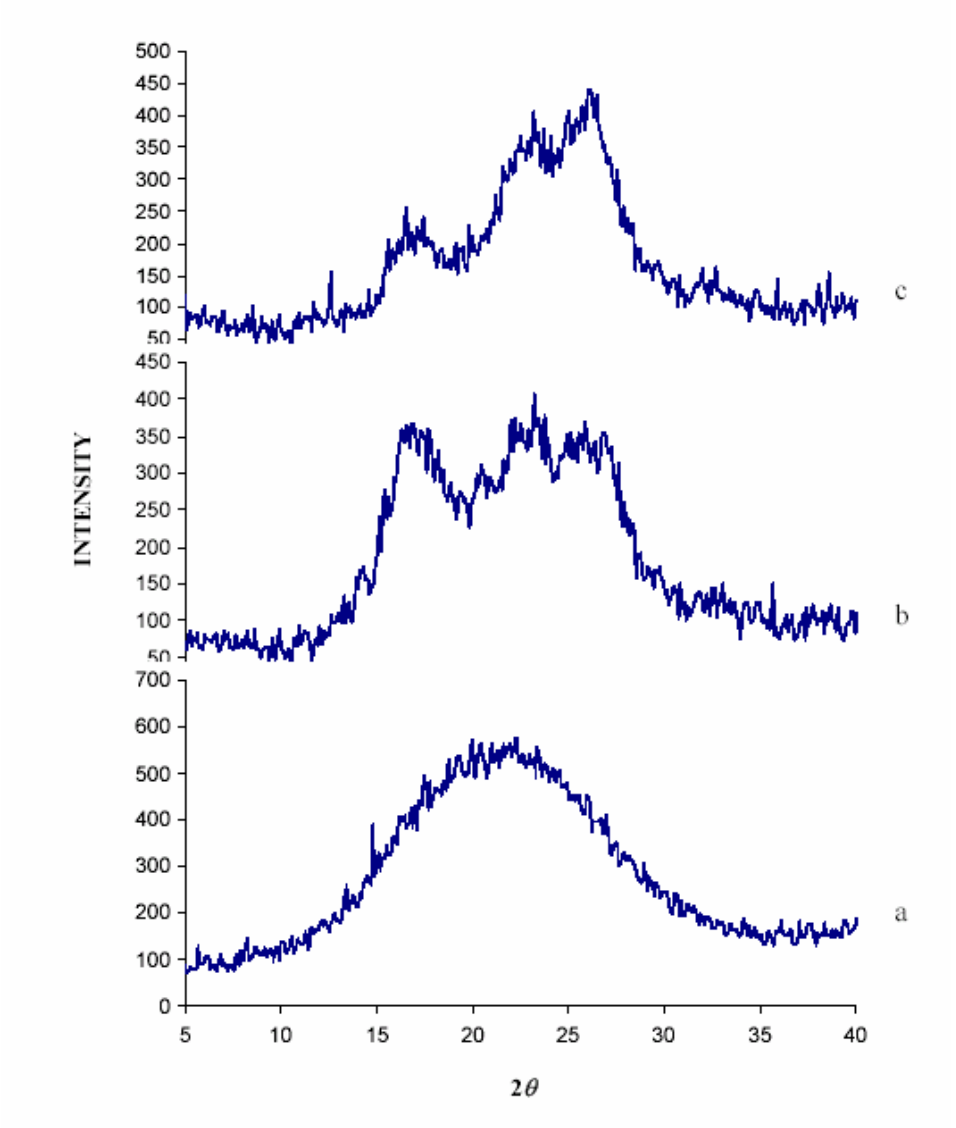

Figure 53. X-ray diffraction of (a) as-received PET, (b) solution-cast PET, and (c) IC-coalesced PET.

The WAXD powder diffractograms recorded for as-received, solution-cast, and coalesced PC and PET samples are presented in Figures 52 and 53, respectively. As-received PC and PET appear to be amorphous, while the solution-cast and coalesced PC

and PET samples are clearly crystalline as seen in the diffractograms of Figures 52 and 53. Solution-cast and coalesced PC samples exhibit very similar diffractograms, with the main diffraction peak at 2θ ~ 18º. A weak peak at 2θ ~ 25º is observed in the diffractogram of coalesced PC, and may be a result of an increase in the ordering along the PC chain axis as retained from its highly extended conformation in the PC-γ-CD-IC channels[161]. Diffraction peaks at 2θ = 16.5, 23.2, and 26.0º, which have been assigned[162] to the (010), ($1\bar{1}0$), and (100) lattice planes, are evident in the diffractograms of solution-cast and coalesced PET in Figure 53. The (100) peak, which is commonly enhanced[163] in oriented samples, such as uniaxially drawn PET fibers and films, is clearly more pronounced in the coalesced sample. It appears that the PET sample coalesced from its γ-CD-IC crystals has crystallized with a higher level of orientational order than the solution-cast sample, likely reflecting the highly ordered environment from which the coalesced PET was crystallized compared with the randomly-coiling environment from which the solution-cast PET sample was crystallized.

CP-MAS ^{13}C NMR

Solid-state ^{13}C NMR spectra of CDs discriminate between free CDs and channel-structure ICs of CDs (free CD is actually a cage structure containing guest water molecules). In the free CDs, several resonances are split, indicating a nonsymmetric conformation of the CDs. However, when channel-structure ICs are formed, less CD resonance splitting is observed, suggesting a more symmetric conformation for the CDs.

Figure 54 (A-C) shows the CP-MAS ^{13}C NMR spectra of cryomilled PET recorded with total sideband suppression, pure γ-CD, and PET/ γ-CD-IC. Figure 54(D) presents

the one-pulse, Bloch decay ^{13}C NMR spectrum of PET/ γ-CD-IC. Figure 54(A) clearly shows the resonances of the carbonyl, nonprotonated, and protonated phenyl ring and methylene carbons at 165, 134 and 130, and 62 ppm, respectively. In Figure 54(C), the intensity of

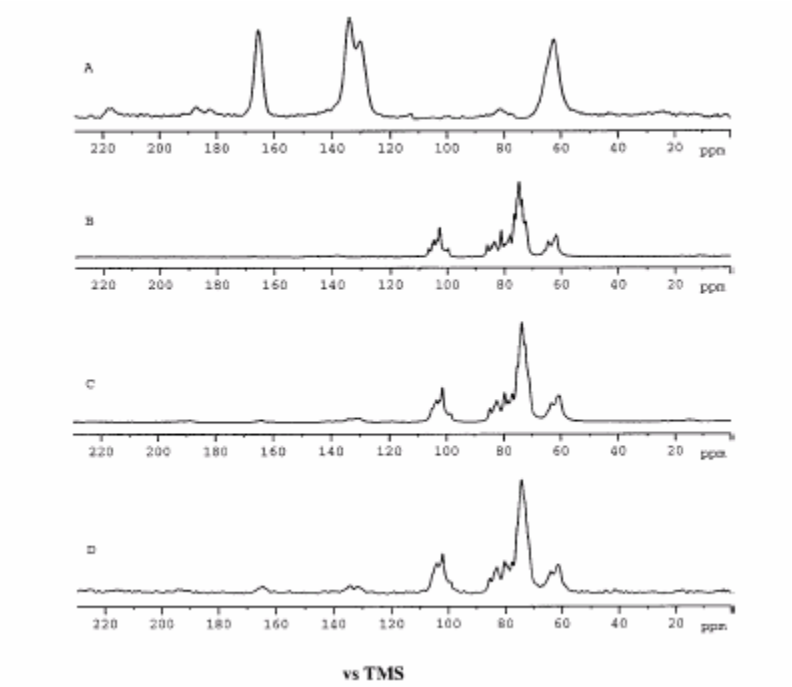

Figure 54. CP-MAS ^{13}C NMR spectra of (A) PET with total sideband suppression, (B) γ-CD, (C)PET/ γ-CD-IC, and (D) PET/ γ-CD-IC with one-pulse Bloch decay.

the PET resonances are quite weak, but the reduced splitting observed for the CD carbon resonances of the CD is noted in comparison with that observed in Figure 54(B) for free CD. This reduction in splitting suggests that in the IC crystals the CDs have adopted a different conformation from that of as-received CDs, thereby confirming the formation of a channel-structure IC with PET. In the one-pulse spectrum of PET/ γ-CD-IC seen in Figure 54(D), the PET resonances are more intense than in the CP spectrum found in

Figure 54(C), because the presumably more mobile PET carbon nuclei do not cross-polarize as efficiently as those of the rigid CD carbons. Remember that the molar stoichiometry expected for PET/ γ-CD-IC is about 2/3 (PET repeat unit/ γ-CD), so, for example, the intensity ratio expected for γ-CD C1 (103 ppm) to PET carbonyl (165 ppm) resonances is (3 × 8 = 24)/(2 × 2 = 4) = 6/1. Because of overlapping with CD resonances, the methylene carbon resonances of PET are not distinguishable in either of the IC spectra.

TGA

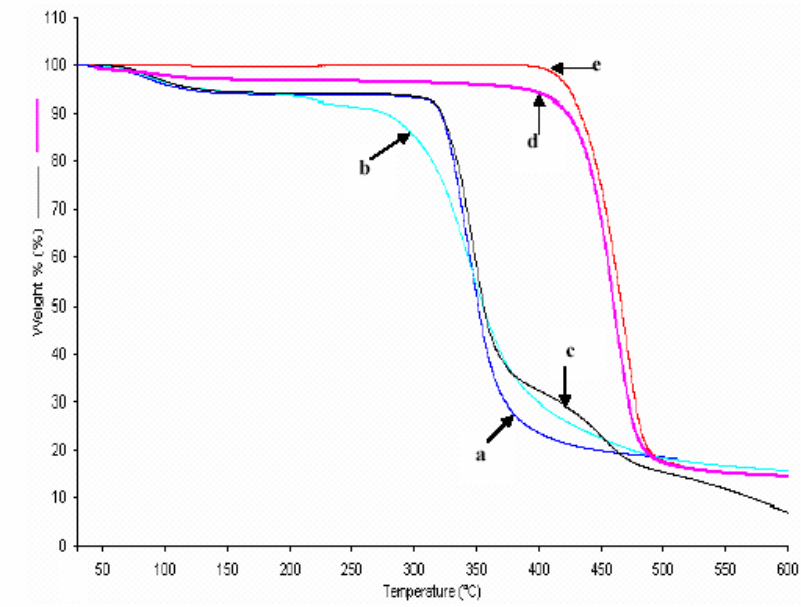

Figure 55. TGA profiles of (a)γ-CD, (b) PET-γ-CD IC, (c) PET and γ-CD physical blend, (d) IC-coalesced PET, and (e) as-received PET.

Figure 55 presents the TGA scans observed for as-received and coalesced PET, for γ-CD, for a physical mixture of PET and γ-CD, and for PET-γ-CD-IC. The TGA scans for

as-received and coalesced PET samples reveal very similar thermal stabilities despite apparent differences in their morphologies, as mentioned above and discussed more fully below. PET begins to decompose at ~408º C, γ-CD decomposition begins at ~310º C, and PET-γ-CD-IC begins to decompose at ~290º C. No evidence of a weight loss in the temperature range of 280-320º C is evident in the TGA scan of coalesced PET, so nearly all the γ-CD was removed during the coalescence process. A similar result is also found in PC samples.

DSC Analysis

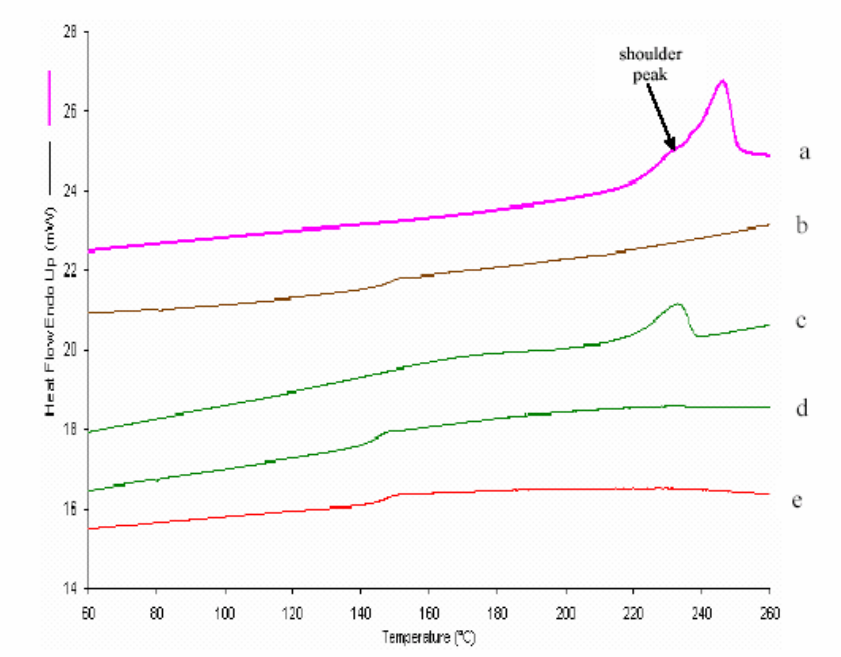

Figure 56. DSC scans of (a) IC-coalesced PC run I , (b) IC-coalesced PC run II, (c) solution-cast PC run I, (d) solution-cast PC run II and (e) as-received PC.

In Figure 56, the DSC scans of as-received, solution-cast, and coalesced PC samples are presented, and they are also summarized in Table 11. As expected, the as-received PC is amorphous with a T_g = 144º C. The PC sample cast from THF shows a melting

Table 11. DSC Results for PC Samples

Sample	Solution-cast PC	IC-coalesced PC
Run I		
Start point of melting (^{0}C)	206.5	207.8
Tm of melting (^{0}C)(peak)	232.9	245.9
ΔH_f of melting (J/g)	33.3	19.8
Run II		
Onset of Tg(^{0}C)*	142.9	145.8

*(Onset of Tg of as-received PC is 144.8)

endotherm at T_m = 233º C on the first scan, but after melting and rapidly cooling, appears totally amorphous in the second DSC scan. The PC sample obtained by hot water coalescence from the PC-γ-CD-IC exhibits a melting endotherm at T_m = 246º C, with a lower temperature shoulder at ~ 232º C. Thus, the process of coalescing PC from its γ-CD-IC has resulted in a crystalline morphology predominantly characterized by crystals that melt some 13º C higher than those cast from THF solution. The coalesced PC sample reverts to normal amorphous PC after melting and rapid cooling, as indicated by its second heating scan. The low temperature (~ 232º C) shoulder appearing on the primary melting endotherm in the first heating of the coalesced PC sample appears to correspond

to the melting endotherm observed in the first heating of the solution-cast sample, with the melting of both PC samples beginning at almost the same temperature. Therefore it may be reasonable to associate the low temperature shoulder of the coalesced sample and the entire melting endotherm of the solution-cast sample with the melting of chain-folded crystalline PC lamellae. Consequently, the primary endotherm observed for the coalesced sample at T_m = 246° C is likely due to the melting of chain-extended PC crystals, though to date no SAXS data has been obtained to confirm the presence of a chain-extended crystalline morphology.

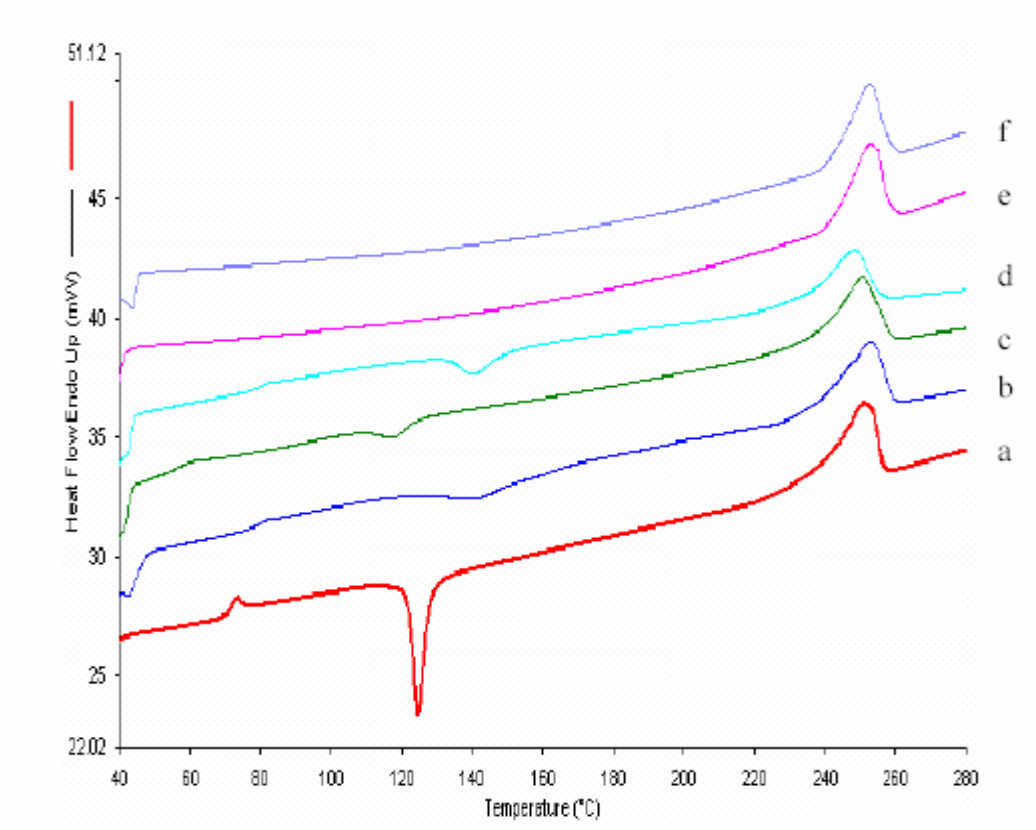

Figure 57. DSC scans of (a) as-received PET run I, (b) as-received PET run II, (c) solution-cast PET run I, (d) solution-cast PET run II, (e) IC-coalesced PET run I, and (f) IC-coalesced PET run II.

Figure 57 presents the DSC heating scans of as-received, solution-cast, and coalesced samples of PET, and a summary of these results can be seen in Table 12. The degree of crystallinity in the original samples, W_c, is obtained from $W_c = \Delta H_{m,obs} / \Delta H_{mO}$, where $\Delta H_{m,obs} = \Delta H_f - \Delta H_c$, ΔH_f is the enthalpy of melting and ΔH_c is the enthalpy of crystallization. ΔH_{mO} = 120 J/g is taken as the enthalpy of melting of 100% crystalline PET[164]. The predominantly amorphous as-received and crystalline solution-cast (TFA/CLF) samples exhibit a glass transition at approximately 50-70º C, a crystallization exotherm at ~120º C, and a melting endotherm at ~ 250º C.

Table 12. Run I and Run II DSC Data for Different PET Samples

Samples		Crystallization			Melting			Difference	
	Tg(^{0}C)	Onset(^{0}C)	Tc(^{0}C)	ΔHc(J/g)	Onset(^{0}C)	Tm(^{0}C)	ΔHf(J/g)	ΔHf-ΔHc(J/g)	Wc(%)
Pure PET run I	70.3	122.0	124.8	27.0	239.9	250.8	44.2	17.2	14.3
Pure PET run II	77.2	125.5	141.2	17.2	241.3	252.8	41.6	24.4	20.3
Cast PET run I	53.8	109.7	117.	5.24	237.2	250.7	43.5	38.3	31.9
Cast PET run II	78.2	133.1	140.50	9.60	234.4	248.2	37.7	28.2	23.5
PET-IC run I	-	-	-	-	237.3	249.7	46.6	46.6	38.9
PET-IC run II	-	-	-	-	241.8	252.9	45.0	45.0	37.5

After rapid cooling from the melt, the second heating scans for both of these PET samples appear similar to their initial heating scans, except the crystallization temperature is significantly higher in the second heating scans. The lower crystallization temperature of the first heat of the as-received PET (pellet form) may be due to oriented chains, resulting from extrusion, acting as nucleation sites for crystallization. The lower crystallization temperature observed in the first heat of the solution-cast PET may be due

to greater chain mobility resulting from plasticization from residual solvent. The reduced T_g seen in the first scan of solution-cast PET is also evidence for plasticization by residual THF/CLF.

The coalesced PET sample only exhibits a T_m at ~ 250º C in the first heating scan, which is consistent with the absence of crystallization that might have been induced by any remaining γ-CD in the sample. In addition, because the melting temperatures of as-received, solution-cast, and coalesced PET samples are nearly identical, coalesced PET likely also crystallizes into a chain-folded morphology. After the first heating and subsequent rapid cooling from the melt, neither a glass transition nor a recrystallization exotherm are observed in the second heating of the coalesced sample.

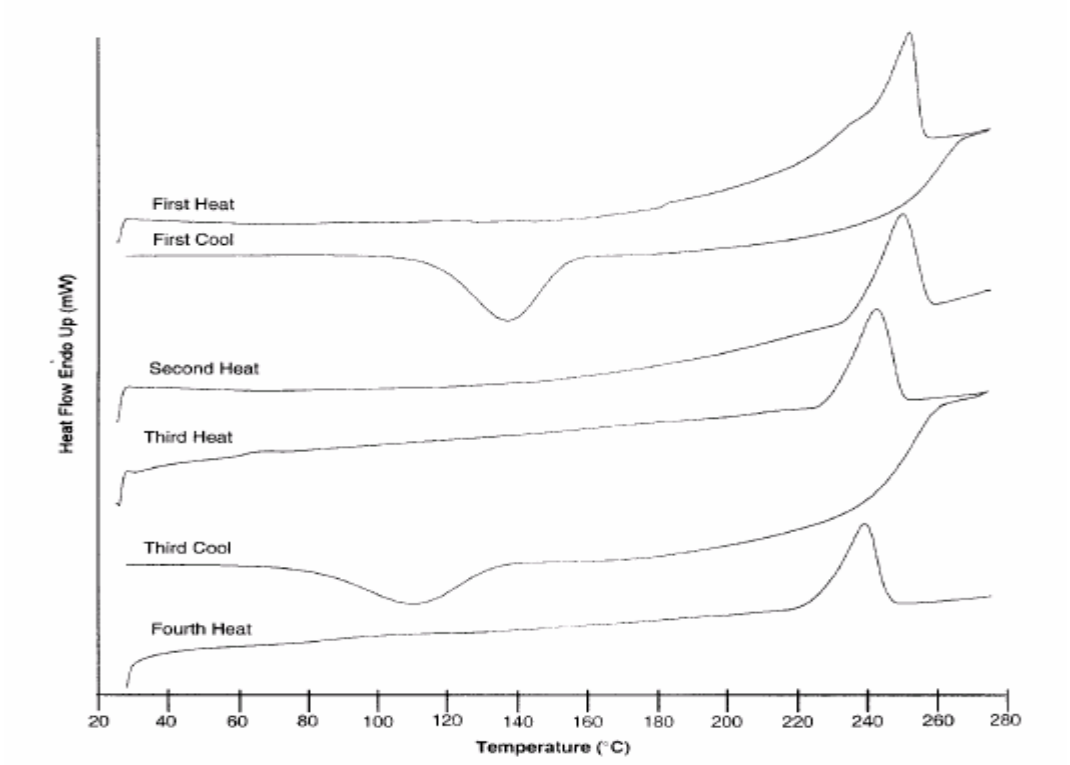

Figure 58. Successive Heating (20º C/min) and Cooling (-200º C/min) of coalesced PET.

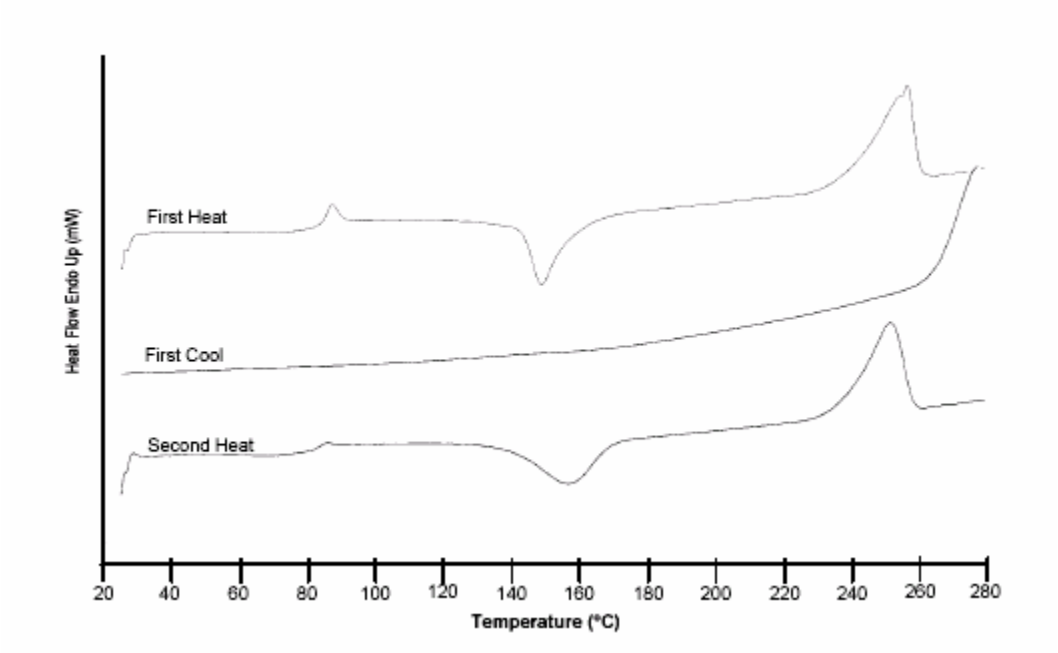

Figure 59. Successive Heating (20º C/min) and Cooling (-200º C/min) of as-received PET

Figure 58 shows four heating and two cooling scans conducted at 20º C/min and -200º C/min, respectively, on the coalesced PET sample. Note that recrystallization exotherms are observed during the two cooling scans, but not during any of the heating scans, even though between the third heat and the third cool the sample was held above T_m for two hours at 275º C. These observations suggest that, immediately following melting, the coalesced PET chains are organized differently than those in the as-received and solution-cast PET melts, because while both of these melts can be quenched to a predominantly amorphous state without crystallization during cooling, as seen in Figure 59 for the as-received PET, the coalesced PET crystallizes substantially during very rapid cooling from the melt. Holding the coalesced sample in the melt at 275º C failed to disrupt the organized structure in the coalesced sample, and so an amorphous melt that is

capable of being quenched was not achieved. Successive heating and cooling of the coalesced sample did produce some changes in the enthalpies and temperatures of crystallization and melting, which will be examined more closely in a future study, but never achieved a typical disordered PET melt that could be quenched into a predominantly amorphous sample.

An obvious possible explanation for this behavior is that chains in the melt of PET coalesced from the host γ-CD-IC channels, wherein the PET chains are both highly extended and segregated, are initially more extended and less entangled than in the melts of as-received or solution-cast PET, because the coalesced PET chains are never allowed to significantly relax, randomly-coil, and entangle during the coalescence process or upon rapid cooling from the melt. To further probe this possible behavior, the coalesced PET was held in the melt at 300º C for various lengths of time before quenching in liquid nitrogen in an effort to determine the time necessary to completely randomly-coil and entangle the PET chains in the coalesced melt. After two hrs above T_m, even at 325º C where slight decomposition (discoloration) of PET takes place, the partially ordered, coalesced PET melt does not become completely amorphous and disordered, with randomly-coiling, interpenetrating PET chains. This conclusion can be drawn because following the rapid quenching of this melt to room temperature, the subsequent heating scan (not presented) shows neither a T_g, nor a T_c, before melting. Judging from the TGA scans seen in Figure 59, heating the coalesced PET sample for 2 hrs at T = 325º C should have removed any remaining γ-CD and/or PET-γ-CD-IC crystals that could have served as nucleating agents for the crystallization of coalesced PET. Thus, the rapid crystallization of the coalesced PET melt appears to be an inherent consequence of the

high extension and improved order of the chains in the non-crystalline regions of the sample prior to melting, as discussed further below.

FTIR Spectra

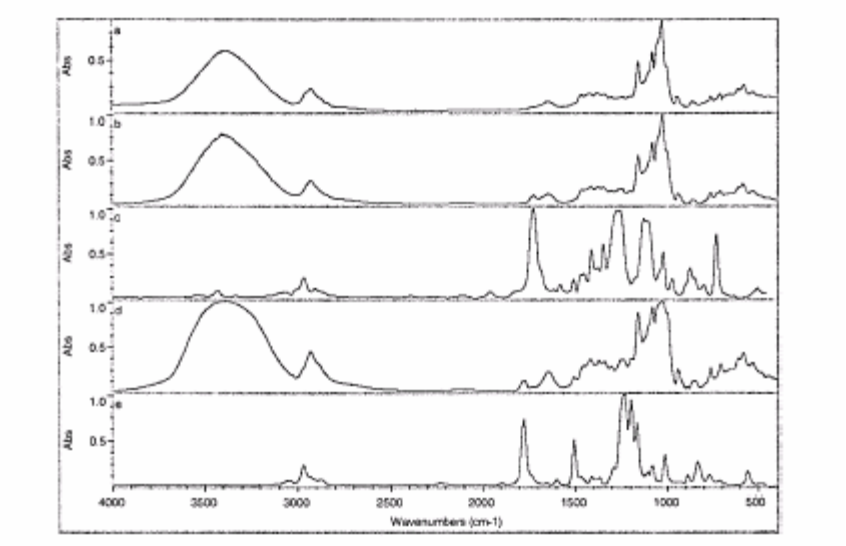

Figure 60. FTIR spectra of (a) γ-CD, (b) PET/ γ-CD-IC, (c) as-received PET, (d) PC/ γ-CD-IC, and (e)as-received PC.

To observe the presence of both host and guests in the ICs, we employed FTIR. The FTIR spectra of pure γ-CD, PET/ γ-CD-IC, as-received PET, PC/ γ-CD-IC, and as-received PC are presented in Figure 60. Here we compare the spectra of the PET and PC guests to those of the ICs. The presence of absorption frequencies characteristic of the guests in the IC spectra confirms IC formation. For γ-CD, the band at 1079 cm^{-1} is contributed by coupled C-C/C-O stretching vibrations, and the band at 1158cm^{-1} is attributed to the antisymmetric stretching vibration of the C-O-C glycosidic bridge. The

pure γ-CD and γ-CD control samples (not shown) display identical spectra, indicating no complexation between γ-CD and the solvent molecules under the environment of polymer-IC fabrication. In contrast, a new band at 1719 cm^{-1}, which is assigned[165] to the carbonyl group of PET, is found in PET/ γ-CD-IC but not in γ-CD. Similarly, the carbonyl band of PC (1770 cm^{-1}) also can be found in the PC/ γ-CD-IC spectrum. However, the carbonyl bands of the two polymers cannot be seen in the γ-CD/solvent control samples.

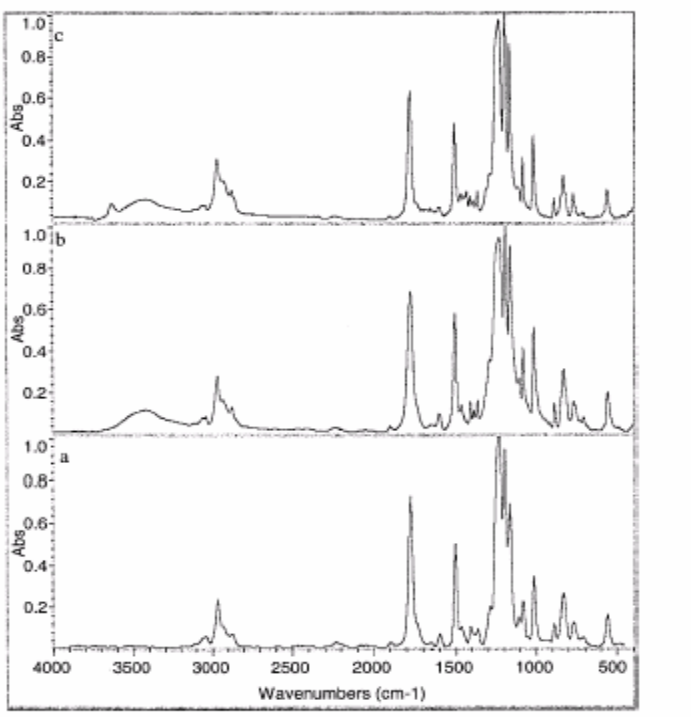

Figure 61. FTIR spectra of (a) as-received, (b) solution-cast, and(c)IC-coalesced PC samples.

The FTIR spectra of the as-received, solution-cast, and γ-CD-IC-coalesced samples of PC and PET are presented in Figures 61 and 62, respectively. Very little difference can be observed between the spectra of the solution-cast and coalesced PC samples. Hence, if

the coalesced PC crystallizes into a predominantly chain-extended morphology, then the distinction between it and the chain-folded crystalline morphology in the solution-cast sample is not manifested by FTIR spectroscopy. Because the FTIR spectra of solution-cast and coalesced PC in Figure 61 are so similar, it is suggested that the non-crystalline regions in both PC samples are also very similar, with randomly-coiling and interpenetrating PC chains. This would explain why, after melting the crystals and rapidly cooling from their melts, both PC samples are completely amorphous and only exhibit a glass transition on subsequent heating.

In contrast to the PC samples, the FTIR spectra of as-received and solution-cast PET samples, though very similar, are clearly distinct from the spectrum of coalesced PET. The most noticeable difference is the much improved resolution observed in the spectrum of PET coalesced from its γ-CD-IC, where nearly every vibrational absorption, except those possibly contributed by residual γ-CD or H_2O above 3200 cm^{-1}, is resolved to the base line. This improved resolution may be a consequence of the already suggested improved order in the non-crystalline regions of the sample; the chains are not nearly as randomly-coiling nor interpenetrating as those in the non-crystalline regions of the as-received and solution-cast samples, and as a consequence do not exhibit a glass transition. The generally broad IR bands observed in polymer samples are undoubtedly due to the large variety of polymer conformations and chain packing environments surrounding each vibrating molecular bond or group. Due to the improved order in the

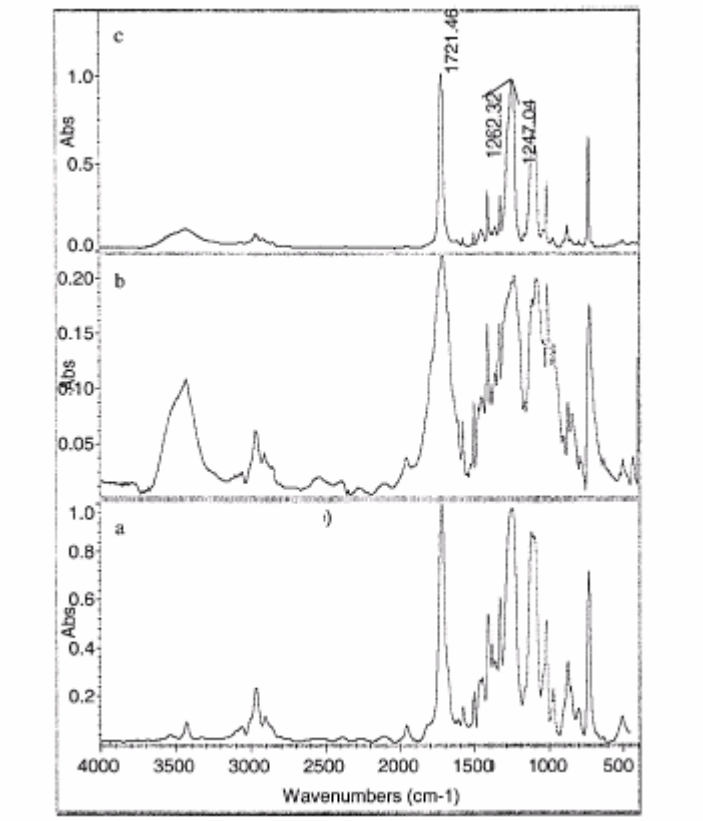

Figure 62. FTIR spectra of (a) as-received PET, (b) solution-cast PET, and (c) IC-coalesced PET samples.

non-crystalline regions of the coalesced PET, vibrating molecular bonds and groups are subjected to smaller variations in their local conformational and packing environments.

For example, a clear doublet band can be seen at 1247 and 1262 cm^{-1} in the coalesced PET spectrum possibly reflecting "crystal or correlation field" splitting generally produced by short-range interchain interactions[166,167] between closely packed molecules in their crystals. Because the X-ray and DSC observations indicate very similar crystal structures for the solution-cast and coalesced PET samples, this vibrational band splitting

may instead be occurring in the non-crystalline regions of the coalesced sample as a consequence of distinct short-range interactions between pairs of PET chains (See the subsequent discussion of highly extended, narrow,non-crystalline conformations containing gauche bonds, which may permit PET chains to be in closer contact than the all-trans chains in their crystals). In fact these vibrations have been associated[168] with the terephthaloyl residues of PET (-OOC-≪o≫-COO-) in the amorphous sample portions[169], with the 1247 cm^{-1} vibration appearing as a shoulder on the 1262 cm^{-1} band. Because these bands appear as a distinct doublet in the coalesced PET spectrum a more homogeneous conformation is suggested for the non-crystalline chains, which are also apparently quite tightly packed with the terephthaloyl residues of neighboring chains in close proximity.

A closer examination of the FTIR spectra of the as-received, solution-cast and coalesced PETs in Figure 62 reveals that the conformations of PET chains in the non-crystalline portions of these samples are quite distinct. In particular we focus on the expanded portions of these spectra between 800 and 1500 cm^{-1} in Figure 63, which include the conformationally-sensitive vibrational bands[170-174]. The CH_2-O stretching vibration at ~971 cm^{-1} has been associated with ethylene glycol units in the trans conformation, with contributions from both crystalline and amorphous regions. On the other hand, the CH_2 wagging mode band at ~1370 cm^{-1} is assigned to the gauche conformation. From a comparison of the intensities of these two bands observed in the PET spectra in Figure 63, it appears that coalesced PET has the smallest content of trans and largest content of gauche conformations for the ethylene glycol fragment, whereas, the solution-cast PET has the largest content of trans and smallest content of gauche

conformations for the ethylene glycol fragment. This is further corroborated by a comparison of the CH_2 bending mode bands at 1473 and 1450 cm^{-1}, which have also been assigned to trans and gauche ethylene glycol conformations, respectively.

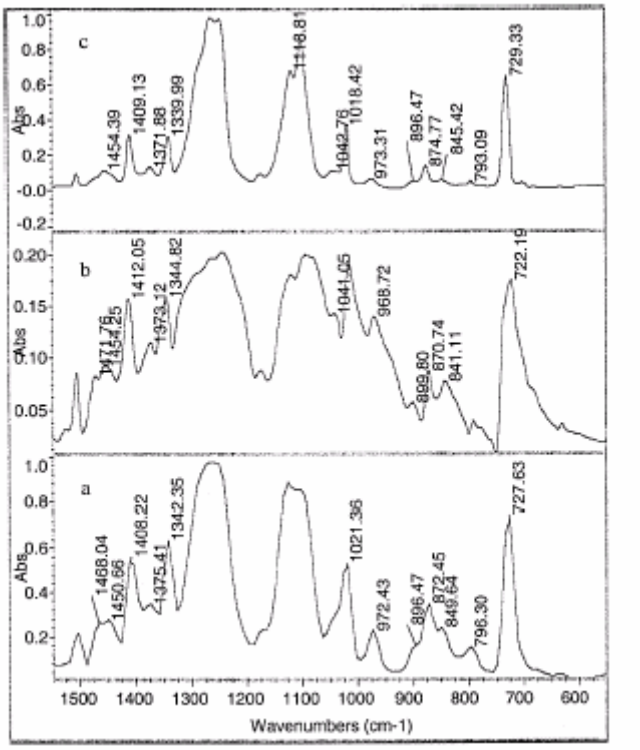

Figure 63. Expanded FTIR spectra of (a) as-received PET, (b) solution-cast PET, and (c) IC-coalesced PET samples.

The CH_2 wagging band observed at 1343 and 1344 cm^{-1} in the as-received and solution-cast PET samples, has been associated[17,18,21] with trans conformations of the ethylene glycol unit. In coalesced and melt-quenched (not presented here) PET samples this vibration is observed at 1339 cm^{-1} and likely reflects the introduction of some gauche character for the $-CH_2-O-$ and $-O-CH_2-$ bonds, which is not possible in PET crystals where the all-trans ethylene glycol conformation is adopted exclusively.

The vibrational bands at ~846 and ~895 cm^{-1}, which have a common base line, have been identified with the rocking modes of CH_2 when the conformations of the ethylene glycol fragments are trans and gauche, respectively. The ratio of absorption intensities at ~846 and ~895 cm^{-1} , A_{846} /A_{895} ~ trans/gauche, is smallest for coalesced PET and largest for solution-cast PET, with the as-received sample having an intermediate value. Thus the content of gauche conformations in the ethylene glycol fragment decreases in the following order: coalesced PET > as-received PET > solution-cast PET.

Finally, these observations lead to a brief discussion which addresses the issue of what portions of the ethylene glycol fragment in PET are assuming trans and gauche conformations. The DSC results summarized in Table 12 demonstrate that the degree of crystallinity in coalesced PET is higher than that observed in the as-received and solution-cast samples. PET chains in the crystal adopt the all trans conformation, so the preponderence of gauche conformations in coalesced PET indicated by FTIR must be occurring in the non-crystalline portions of this sample.

In a previous study concerned with determining those PET conformations that are able to be included as highly extended guests in the narrow channels of their inclusion complexes, it was learned that the kink conformers of the ethylene glycol fragment, where -O-CH_2-, -CH_2-CH_2-, and -CH_2-O- bonds adopt in turn the gauche ±, trans, and gauche ∓ conformations, are nearly as extended as the all trans crystalline conformation [(10.4Å vs 10.75Å)/repeat unit] and have the smallest cross-sections. Thus, of all the extended conformations of PET, the kink conformers occupy the least volume (2/3 of the volume required by the all trans crystalline conformation), an observation that was subsequently confirmed by Auriemma et al.[175] who performed a Monte Carlo analysis of

extended PET oligomer conformations confined inside cylindrical tubes with a diameter =12Å.

Both modeling studies of extended PET conformations concluded that the -CH_2-CH_2- bond must be trans, while the -O-CH_2- and -CH_2-O- bonds can adopt either trans or gauche ± conformations. These extended PET conformations are consistent with the mesomorphic form of PET observed by x-ray diffraction[176] on samples drawn below T_g, where reflections with spacings corresponding to a periodicity of 10.3Å were observed on the meridian. In mesomorphic PET the chains are likely[177] adopting the extended conformations mentioned above and are packed in parallel arrangements which lack rotational (around the chain axis) and translational (along the chain axis) order among the PET chains.

Clearly when included inside the narrow channels (D ~ 8Å) of its γ-CD-IC the PET chains must also be restricted to the extended trans -CH_2-CH_2 - bond conformers. Coalescence of the PET chains from its γ-CD-IC crystals also likely results in extended,all trans -CH_2-CH_2- bond conformers. These may crystallize more rapidly and readily into the all trans crystalline conformation than do completely amorphous, randomly-coiling PET chains found in solution or the melt, because there the -CH_2-CH_2- bond is preponderantly gauche[178,179]. Thus, crystallization of coalesced PET into the all trans conformation proceeds rapidly from preponderantly gauche O-CH_2-, trans -CH_2-CH_2- and gauche -CH_2-O- bond conformers. In contrast, crystallization of solution-cast PET into the all trans conformation proceeds slowly from preponderantly trans -O-CH_2-, gauche -CH_2-CH_2-, and trans -CH_2-O- bond conformers. Therefore, the remaining

uncrystallized chains in these two PET samples are expected to be rich in these same conformations, ie., g±tg∓ and tg±t for coalesced and solution-cast PET, respectively.

As noted above, FTIR has indicated a high concentration of gauche and trans bond conformations, respectively, in the coalesced and solution-cast PET samples. Because the coalesced PET sample is more crystalline than the solution-cast sample of PET, the higher concentration of trans bond conformations in the latter sample cannot be reflecting the conformational character of the $-CH_2-CH_2-$ bond alone, but is instead mainly due to the concentration of trans $-O-CH_2-$ and $-CH_2-O-$ bond conformers, which is higher in the solution-cast PET and lower in the coalesced sample. This is also consistent with expectations of the conformations of PET chains in the non-crystalline portions of these samples. As a consequence, it is proposed here that the conformationally-sensitive vibrational bands observed in PET be reinterpreted to reflect primarily the conformations of $-O-CH_2-$ and $-CH_2-O-$ bonds, and not that of the $-CH_2-CH_2-$ bonds, in the ethylene glycol unit.

Recently Huang et al.[180] interpreted the solid-state ^{13}C-NMR of melt-quenched PET, subsequently annealed above T_g for varying times, in terms of the trans and gauche character of the $-CH_2-CH_2-$ bonds. They assigned the CH_2 resonances observed at 62.0 and 63.7 ppm (versus TMS) to trans and gauche $-CH_2-CH_2-$ bonds, respectively. These assignments were made because the intensity of the resonance at 62.0 ppm increased, while the intensity of the resonance at 63.7 ppm decreased, with increasing annealing times and temperatures. However, though the crystalline content at first increases with annealing, but then levels off, the intensity ratio of the 62.0 ppm:63.7 ppm peaks continues to increase. They suggest that, even though crystallinity ceases to increase

beyond a certain level of annealing, the population of trans -CH_2-CH_2- bonds in the non-crystalline regions of their PET samples continues to increase, thereby further raising the observed 62.0 ppm:63.7 ppm ratio of peak intensities.

Though increasing the temperature above T_g would be expected to increase the population of trans -CH_2-CH_2- bond conformers, it would also be expected to increase the population of gauche -O-CH_2- and-CH_2-O- bond conformers, because in amorphous PET gauche -CH_2-CH_2- and trans -O-CH_2- and -CH_2-O- bonds are preferred. Huang et al.'s suggestion of a three-phase model for PET, ie., crystalline, constrained non-crystalline, and amorphous, which are rich in trans, trans, and gauche -CH_2-CH_2- bond conformers, respectively, might be reasonably expanded to include -O-CH_2- and -CH_2-O- bonds which are trans, mostly gauche, and mostly trans in the three PET phases, respectively. Thus it is suggested here that the PET chains in the constrained non-crystalline phase proposed by Huang et al. for annealed PET samples have conformational similarities with the PET chains in the non-crystalline portions of PET coalesced from its γ-CD-IC crystals.

An alternative interpretation of the annealing-dependent solid-state ^{13}C NMR observations described for PET by Huang et al. may also be suggested. Suppose the resonance frequency of methylene carbons in the ethylene glycol fragment of PET is not sensitive to the conformation of the -CH_2-CH_2- bond, as in fact might be expected[33], because it is rotation about the -O-CH_2 - and -CH_2-O- bonds in the ethylene glycol fragment that determine whether or not the CH_2 carbons are gauche or trans to and therefore are or are not shielded by their γ-substituents, the carbonyl carbons. As a consequence, the CH_2 resonances at 62.0 and 63.7 ppm might be more logically assigned

to gauche and trans -O-CH_2- and -CH_2-O- bond conformations, respectively. As annealing of melt-quenched samples increases the crystallinity, the -O-CH_2- and -CH_2-O- bonds incorporated in the crystals become trans, while those in the non-crystalline sample regions increase their gauche population. If the quantity of -O-CH_2- and -CH_2-O- bonds in the non-crystalline regions that adopt gauche conformations increases faster with annealing than does the quantity of trans -O-CH_2- and -CH_2-O- bonds incorporated in the crystals, then the observation that the 62.0 ppm CH_2 resonance continues to grow at the expense of the 63.7 ppm resonance, even after the degree of crystallinity ceases to increase, is consistent with this alternative interpretation.

3.1.3 Summary and Conclusions

The structures, morphologies, and chain conformations of bulk PC and PET samples coalesced from their γ-CD-ICs were demonstrated to be distinct from those of solution and melt processed samples. Coalesced PC seems to crystallize in a predominantly chain-extended morphology, while PET coalesced from its γ-CD-IC crystallizes in a chain-folded morphology. The non-crystalline portions of the coalesced PC and PET samples also differ. Non-crystalline PC chains appear completely disordered, so upon melting of the chain-extended crystals, the entangled and randomly-coiling PC chains are readily quenched into a completely amorphous sample. PET chains in the non-crystalline portions of the coalesced sample appear more extended and less randomly-coiled and entangled than in a typical PET melt. As a consequence, cooling rapidly immediately after melting results in a rapid recrystallization below T_m. Even after maintaining $T > T_m$ for more than two hours, the coalesced PET sample did not revert to a completely

disordered, entangled, randomly-coiled melt, and so, upon subsequent rapid cooling, could not be quenched to a predominantly amorphous sample.

In light of the conformational characteristics of both randomly-coiling and highly extended PET chains, analysis of the FTIR spectra of as-received, solution-cast, and coalesced PET samples has permitted a reinterpretation of their conformationally-sensitive vibrational bands. In general these vibrational bands are found to be more sensitive to the conformations of the -O-CH_2- and -CH_2-O- bonds, rather than the -CH_2-CH_2- bonds, in the ethylene glycol fragment. When coupled with the recent solid-state ^{13}C-NMR analysis of annealed PET samples reported by Huang et al.[32], a consistent description of the conformations of PET chains in the crystalline, constrained non-crystalline, and amorphous sample portions emerges. PET chains are all trans in the crystal phase, have predominantly gauche -O-CH_2- and -CH_2-O- bonds and trans -CH_2-CH_2- bonds in the constrained non-crystalline phase, and have slightly more trans -O-CH_2- and -CH_2-O- bonds and predominantly gauche -CH_2-CH_2- bonds in the amorphous phase.

The general consensus of this paper is that formation of polymer-CD-ICs, followed by coalescence of their included guest polymers, can produce bulk polymer samples with structures and morphologies where the constituent polymer chains are adopting conformations that are unique and distinct from those achieveable by ordinary melt and solution processing. Presumeably the properties of CD-IC-coalesced polymers will also prove to be unique and hopefully improved, as well. Production of bulk polymer samples fabricated by the formation of and subsequent coalescence from their CD-ICs is presently

being scaled-up in order to begin to examine their physical properties, such as strengths and permeabilities.

3.2 Nylon

3.2.1 Introduction

Nylon polymers consist of polyethylene segments $(CH_2)n$ separated by peptide units (NH-CO) which are packed either parallel or antiparallel in their crystal lattices. These peptide units provide hydrogen bonding between polymer chains, giving nylon some of its unique properties. In contrast to other highly crystalline polymers like polyethylene, nylon polymers can have their degree of crystallinity controlled over a wide range. By changing the crystal structures, one can modify such properties as the melting point, modulus, low temperature impact strength, moisture absorption, and chemical resistance to metal salts and acids[181].

Nylon 6 is a member of the nylon family and is a versatile polymer. Nylon 6 exhibits polymorphic structures that contain two types of stable crystal forms: monoclinic α-form and pseudo-hexagonal (or monoclinic) γ-form, which are very sensitive to the method of preparing samples. The γ-form crystal of nylon 6 can be transformed into the α-form by annealing nylon 6 or drawing.[182,183] The α-form of nylon 6 can also be conversely transformed to the γ-form by treating nylon 6 with iodine.[184] The change in polymorphic structures of nylon 6 results from the spatial rearrangement in the hydrogen bonding between the oxygen in the carbonyl group of one polyamide molecular chain and the hydrogen attached to the nitrogen in the neighboring polyamide molecular chain. The

γ-form nylon 6 crystal is constituted by non-planar polyamide molecules adopting the parallel-chain-arrangement of hydrogen bonding, whereas the polyamide molecules in the monoclinic α-form crystal are planar and packed in the more stable antiparallel-chain-arrangement of hydrogen bonds. The α-form is more stable than the γ-form presumably because of shorter, stronger hydrogen bonds.[185]

In the past, many published works have shown that cyclodextrin (CD) can form molecularly assembled inclusion complexes (ICs) with various high molecular weight polymers.[6-9] In these tubular inclusion complexes, the guest polymer chains occupy narrow cylindrical channels (Diameter ~ 0.5-1.0nm) created by the stacking of cyclodextrins in the crystalline lattice. As a consequence, the included guest polymer chains are constrained to assume highly extended conformations and are generally segregated from neighboring included polymer chains by the channel walls of the host crystalline lattice. When these complex crystals are treated to remove the host, but without damaging or dissolving the guest polymers, they are forced to coalesce into a bulk polymer solid. Our recent work has demonstrated that crystallizable polymer samples coalesced from the cyclodextrin inclusion complexes have often revealed melting temperatures that are elevated from those measured on samples crystallized from their completely disordered solutions and melts, and more perfect crystal forms with extended chain conformation in the crystals. Considering α-form nylon 6 has a more extended chain conformation (longer *C* value, along chain axis, in the crystal lattice) than the γ-form, we anticipate to induce the nylon 6 crystal form changing from γ form to α form by forming and dissociating the nylon 6/α-CD inclusion complex. Meanwhile, the overall crystallinity and hydrogen bonding density are expected to increase by employ

this method since parallel or anti-parallel extended zigzag polymer chains are criteria for nylon crystallization and hydrogen bonding.

3.2.2 Experimental

Sample preparation

To prepare the polymer cyclodextrin inclusion complex, nylon 6 (Aldrich) (0.35g) was dissolved in 3 ml of formic acid (Aldrich, 90%) and then 12 ml of acetic acid (Aldrich) was added to the solution. Eight grams of α-cyclodextrin (Cerestar Co.) were dissolved in 40 ml of dimethyl sulfoxide (Aldrich), which corresponds to more than a two-fold molar excess of α-cyclodextrin. The mixed solutions were stirred on a hot plate for 2 hours at 50^{o} C, and then cooled to room temperature while stirring for another 6 hours. The precipitate was washed with cool water to remove free cyclodextrin and filtered and dried under a heating lamp and in a vacuum oven at 40^{o} C to obtain dry polymer cyclodextrin inclusion complex. To dissociate the inclusion complex, the sample was placed into HCl aqueous solution (pH=1.0) with heating at 80^{o} C. The mixture was stirred for 10 min. and then filtered to remove coalesced polymer. The filtered polymer was washed several times with cool water and then dried in a vacuum oven at room temperature. The physical blend in this study was made by mechanical milling α-cyclodextrin and nylon 6 together (w_{nylon}/w_{CD} = 1:20) into a fine powder.

Measurements

The FTIR spectral studies in the form of KBr pellets were carried out in a Nicolet 510P FTIR spectrometer in the range between 4000 and 400 cm^{-1}, with a resolution of

$2cm^{-1}$. To directly study crystalline related bands, the powder form IC coalesced nylon 6 was also studied by single bound ATR-FTIR (Nicolet 510P) compared with as–received nylon 6. The wide angle X-ray diffraction (WAXD) patterns of samples were obtained with a Seimens type-F X-ray diffractometer. The X-ray source was Ni-filtered Cu K_α radiation (1.54Å), with voltage and current set to 30KV and 20mA. The specimens were mounted on aluminum frames and scanned from 5 to $40^o = 2\theta$ at a rate of ($2\theta = 1.2^o$)/min. Differential Scanning Calorimetric (DSC) Analysis thermal scans were performed with a Perkin-Elmer DSC-7 differential scanning calorimeter. The measurements were run in the range of 30-280^o C at heating and cooling rates of 20^o C /min. The thermal decomposition behaviors of samples were measured with a Perkin-Elmer Pyris 1 thermogravimetric analyzer (TGA) between 40-600° C at a heating rate of 20° C/min. Nitrogen was used as the purge gas. Solid-state ^{13}C NMR data were collected using a Bruker DSX wide-bore system with MAS speeds of 4-5 kHz and a CP contact time of 1ms.

3.2.3 Results and Discussion

Demonstration of inclusion complex formation

In order to observe the presence of both host and guests in the ICs, FTIR was employed. The FTIR spectra of the (a) pure α-CD, (b) as-received nylon 6 and (c) nylon 6/α-CD IC are presented in Figure 64. The presence of absorption frequencies characteristic of the guests in the IC spectra indicates IC formation. For α-CD, the bands at 1026 and 1079 cm^{-1} are contributed by coupled C-C/C-O stretching vibrations, and the band at 1158 cm^{-1} is attributed to the anti-symmetric stretching vibration of the C-O-C

glycosidic bridge. By contrast, a new band at around 1540cm^{-1} which is assigned to the N-H in plane bending deformation of nylon,[186] is found in nylon 6/α-CD IC, but not in α-CD, indicating the formation of nylon 6/α-CD IC. Moreover, this N-H deformation band moves toward to the higher wavenumber. The band shifting verifies that the nylon molecules thread into cyclodextrin channel and are close enough with the host to have some molecular level interaction.

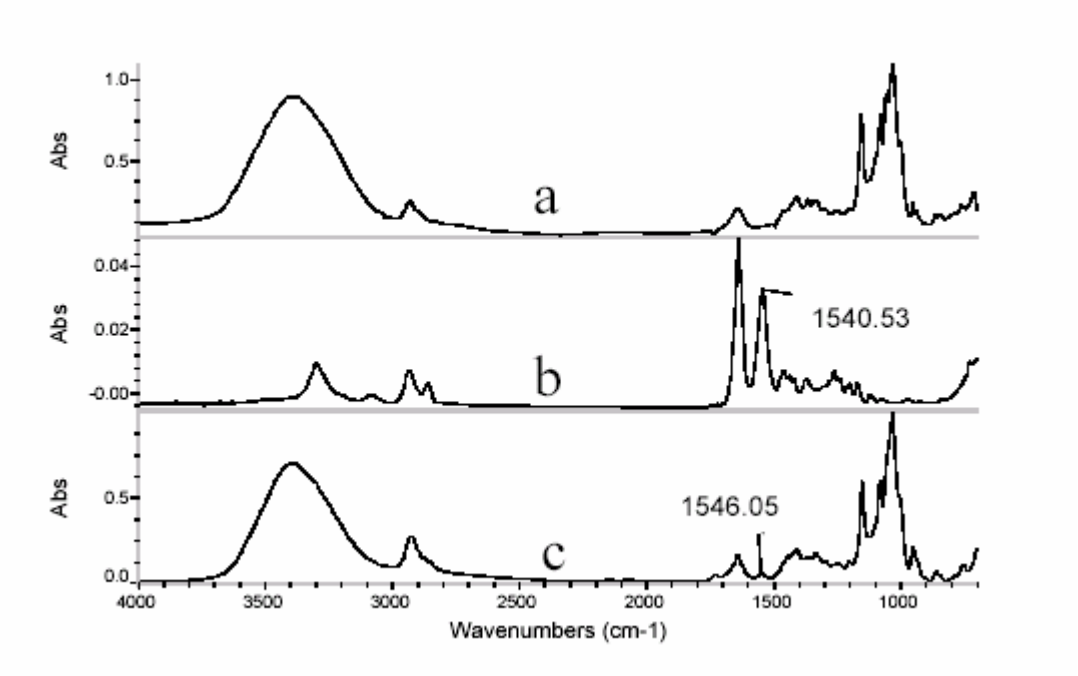

Figure 64. FTIR spectra of (a) α-cyclodextrin, (b)as-received nylon 6, and (c) nylon 6/α-CD inclusion complex

For the α-CD nylon 6 IC, two prominent peaks were observedin its x-ray diffractogram at 20 and 22.6° (2θ), which are well known to be characteristic of α-CD-based IC crystals adopting a channel structure (see Figure 65). This diffraction pattern is

markedly different from semi-crystalline as-received nylon, pure α–CD and their physical blend. The distinct differences between the patterns for inclusion complex and the two starting materials as well as the physical blend are strong evidence that the α–CD is hosting nylon polymer chain in a channel structure inclusion complex.

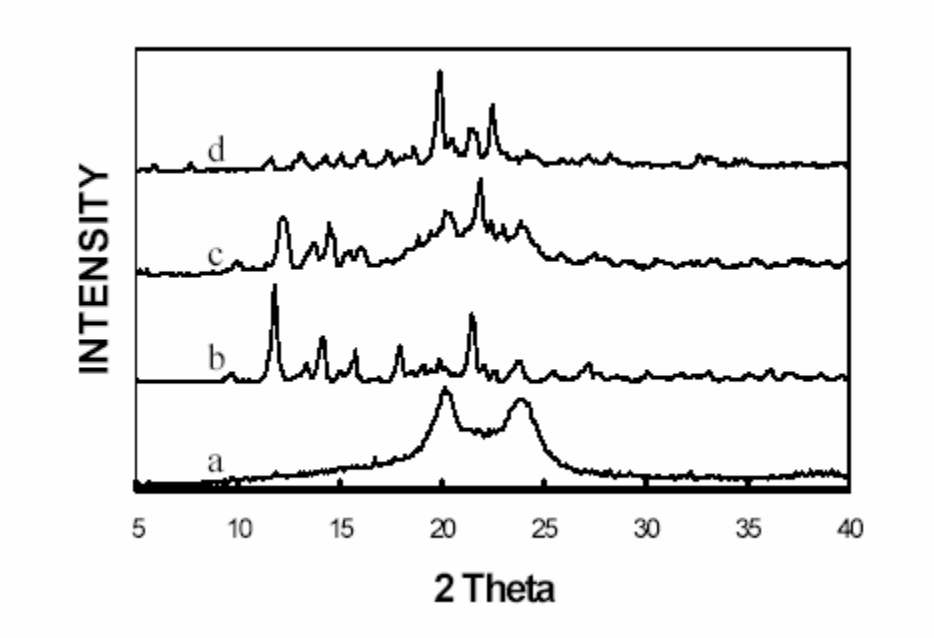

Figure 65. Wide Angle X-ray Diffraction patterns of (a) as-received nylon 6, (b) a-cyclodextrin, (c) α-cyclodextrin/nylon 6 physical blend, and (d) nylon 6/α-CD inclusion complex

The solid-state CP/MAS ^{13}C NMR spectra of as-received nylon 6, α-CD and nylon 6/α-CD IC are shown in Figure 66. The spectrum of α-CD in the uncomplexed state shows strong splitting for all $C_{1\sim6}$ resonances indicating that γ-CD molecules are in a rigid, less symmetric cyclic conformation. On the contrary, for the two ICs prepared here, all ^{13}C resonances of α-CD showed much less splitting. This indicates that α-CD in the

ICs has adopted a different conformation. Similar observations, which are believed to support the formation of ICs between CDs and polymers, have been observed in the solid-state CP/MAS ^{13}C NMR spectra of ICs of various polymers formed with different CDs. When the NMR spectrum of the nylon 6/α-CD IC is examined in the nylon 6 region (see Figure 67), it is found that the methylene carbon connected to the NH group shows a higher CP efficiency than the other nylon 6 methylene carbons, although there is no any change in peak position relative to the as-received nylon 6. This interesting discovery is consistent with that mentioned in our previous FTIR discussion and reveals the molecular level interaction taking place between cyclodextrin and nylon 6 molecules in the inclusion complex.

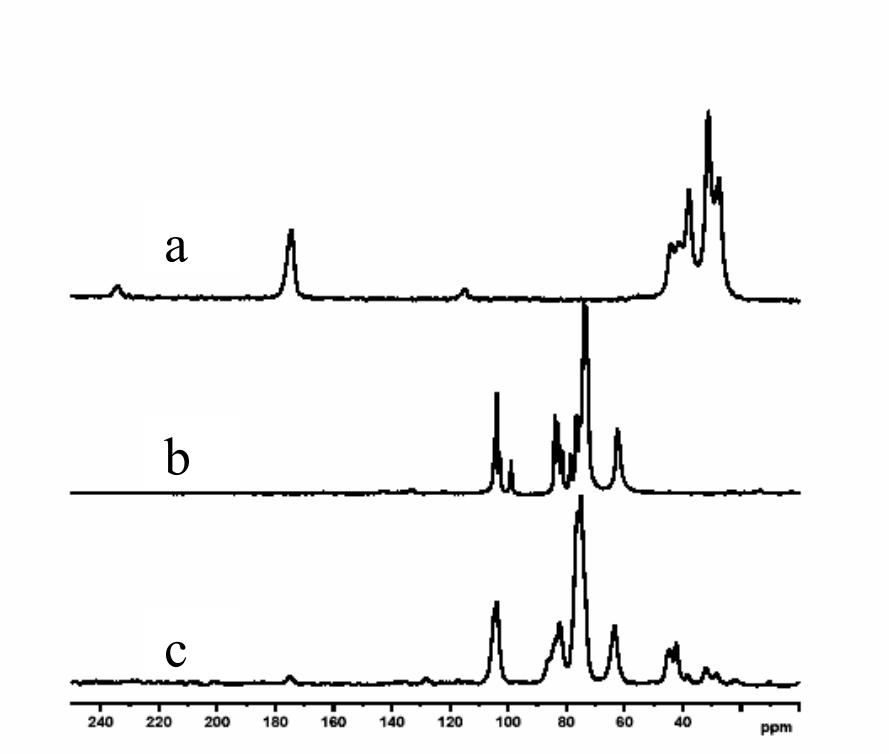

Figure 66. CP-MAS ^{13}C NMR spectra of (a) as-received nylon 6, (b) a-cyclodextrin, (c) nylon 6/α-CD inclusion complex

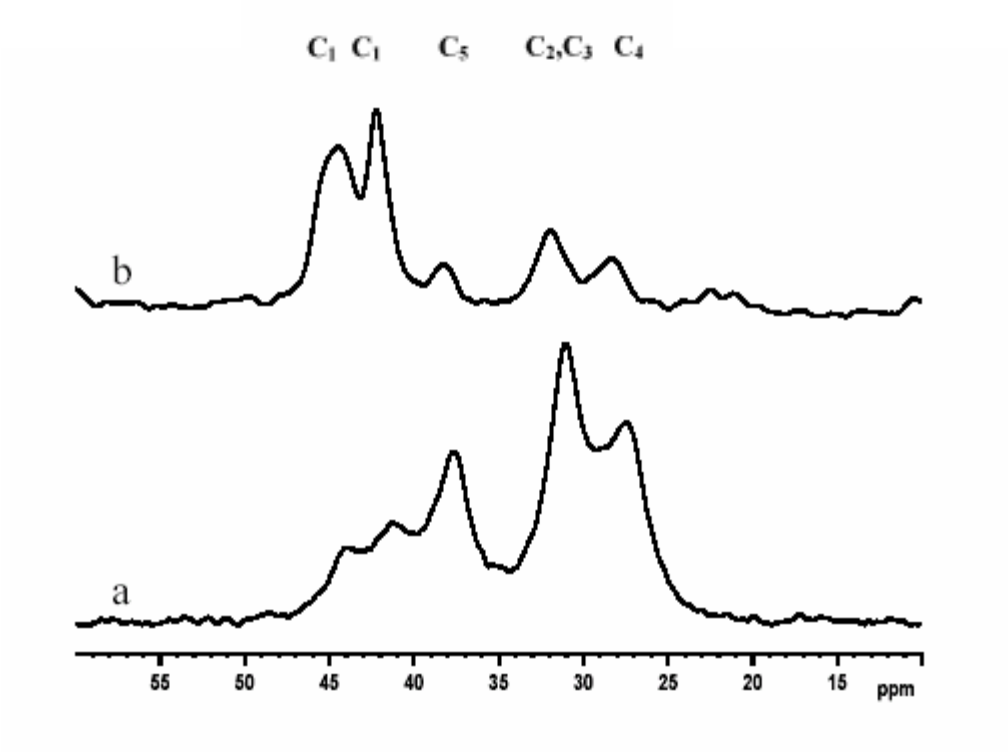

Figure 67. Expended CP-MAS ^{13}C NMR spectra of (a) as-received nylon 6 and (b) nylon 6 in inclusion complex

The DSC heating scan of the nylon 6/α-CD IC is presented in Figure 68. No thermal transitions can be found for the IC sample in the experimental temperature range. However, the physical blend of the same composition shows a melting peak at around 220^{o} C, which is for the thermal fusion of semicrystalline nylon 6. Since cyclodextrin does not have any thermal transition in the range of 25~300^{o} C, the straight DSC line for the IC demonstrates that all the crystallizable nylon 6 chains are covered by cyclic cyclodextrin and isolated in the CD channels.

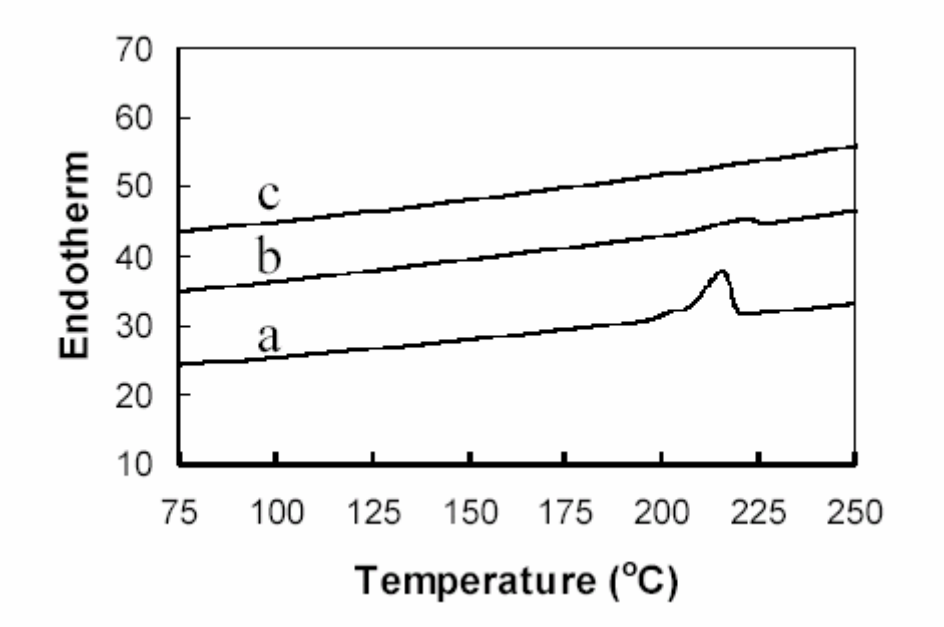

Figure 68. DSC heating scans of (a) as-received nylon 6, (b) α-CD/nylon 6 physical blend (c) nylon 6/α-CD inclusion complex

Manipulation of crystal structures

After removing the cyclodetrin from the polymer inclusion complex, we first examine the chemical composition of our coalesced sample. Figure 69 illustrates the ATR-FTIR spectrum of the coalesced sample comparing to the as-received nylon 6. It is found that the two infrared spectra look almost identical and no bands characteristic of cyclodextrin (1026, 1079 and 1158cm^{-1}) are visible, indicating the nylon 6 polymer chains have been completely extracted out from the cyclodextrin channels. However, it is evident from the bands in the region between 1300 and 800 cm^{-1} that there are clear differences between the crystalline phases of the two nylon 6 samples, since the FTIR band assignments for both α and γ crystal forms of nylon 6 have been reported in the literatures.[187-189] The

bands at 928, 959 and 1200 cm^{-1} were attributed to the α-crystalline phase, whereas the band at 973 cm^{-1} was attributed to

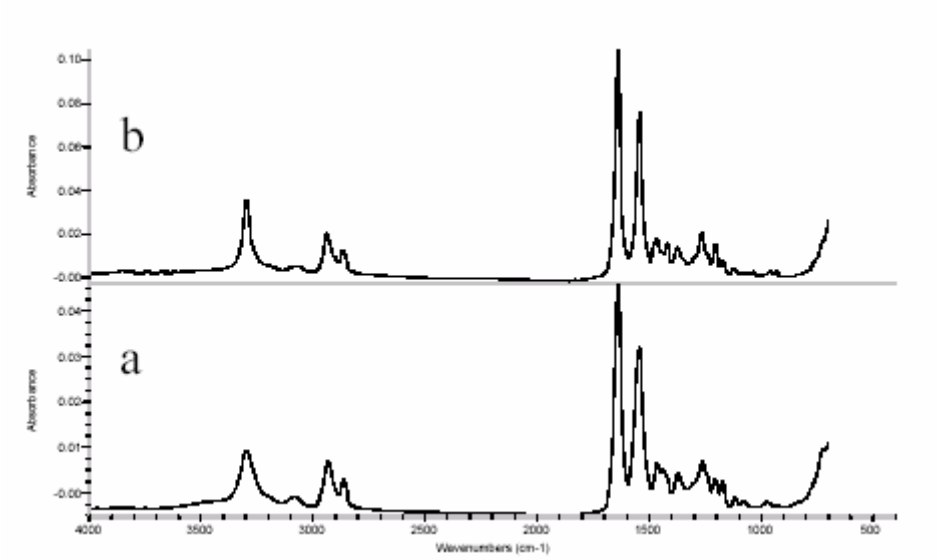

Figure 69. FTIR spectra of (a) as-received nylon 6 and (b) IC coalesced nylon 6

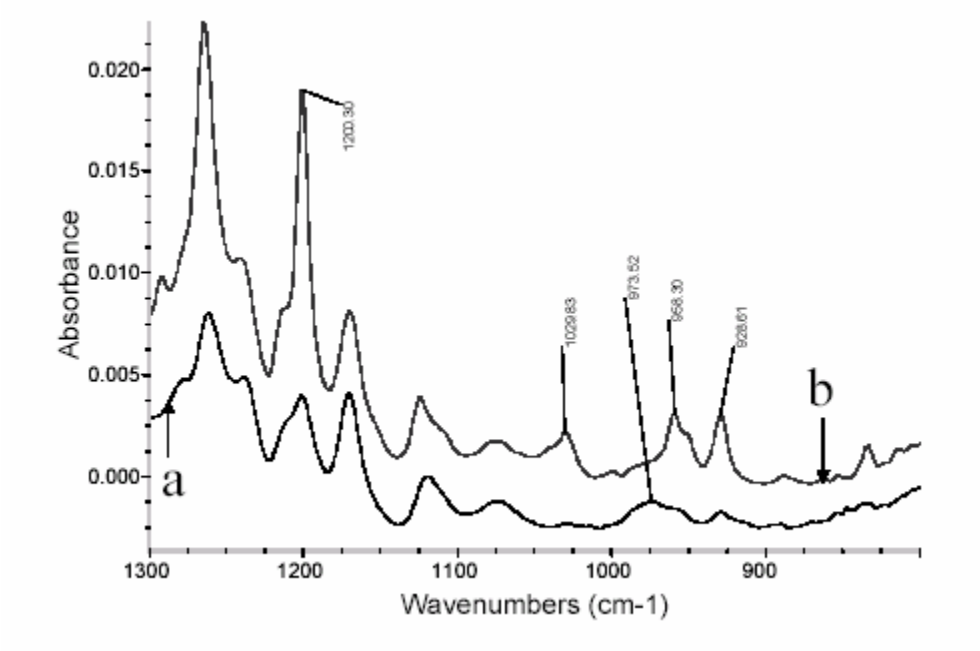

Figure 70. Expanded FTIR spectra of (a) as-received and (b) IC coalesced nylon 6

Table 13. Comparison of hydrogen bonding related FTIR bands between as-received nylon 6 and IC coalesced nylon 6

Sample	Band width at half maximum (cm^{-1})	
	$3297cm^{-1}$	$1637cm^{-1}$
As-received nylon 6	76	33
Nanotube treated nylon 6	36	24

the γ-crystalline phase. In Figure 70, for the as-received nylon 6 chips, there is a strong band at 973 cm^{-1}, showing that these samples contain a considerable amount of the γ-crystal form, with a small amount of the α-crystal form indicated by the weak bands at 928, 959, and 1200 cm^{-1}. In contrast, the FTIR spectrum of nylon 6 coalesced from the cyclodextrin inclusion complex does not show the band at 973 cm^{-1}, but strong bands at 930, 959 and 1200 cm^{-1}, indicating a much higher fraction of α-crystal form. Another exciting result is suggested by the absorption peak at $1030cm^{-1}$. According to FTIR studies of nylon 6 yarns, it is clear that the intensity of this peak increases with increasing draw ratio.[190] In the FTIR spectrum of the inclusion complex coalesced sample, there is a very strong 1030 cm^{-1} peak compared to as-received nylon 6. This may demonstrate that the extended, planar conformation adopted by nylon 6 in the cyclodextrin inclusion complex is substantially retained after coalescence. These peptide units provide hydrogen bonding between polymer chains, giving nylon hydrogen bonding depended crystalline behaviors. The crystalline N-H…O=C hydrogen bond density in nylons can be estimated by measuring the widths of peaks for N-H and O=C stretching at 3297 and 1637 cm^{-1}. The sharper the peaks, the more crystalline the N-H…O=C hydrogen bonds. After

normalizing, the peak widths at half-maximum for the two characteristic bands in the different samples are presented in Table 13. Compared to the as-received sample, the modified nylon 6 has much narrower hydrogen bond related peaks than the as-received nylon 6 sample, showing its higher hydrogen bond density and thus crystallinity.

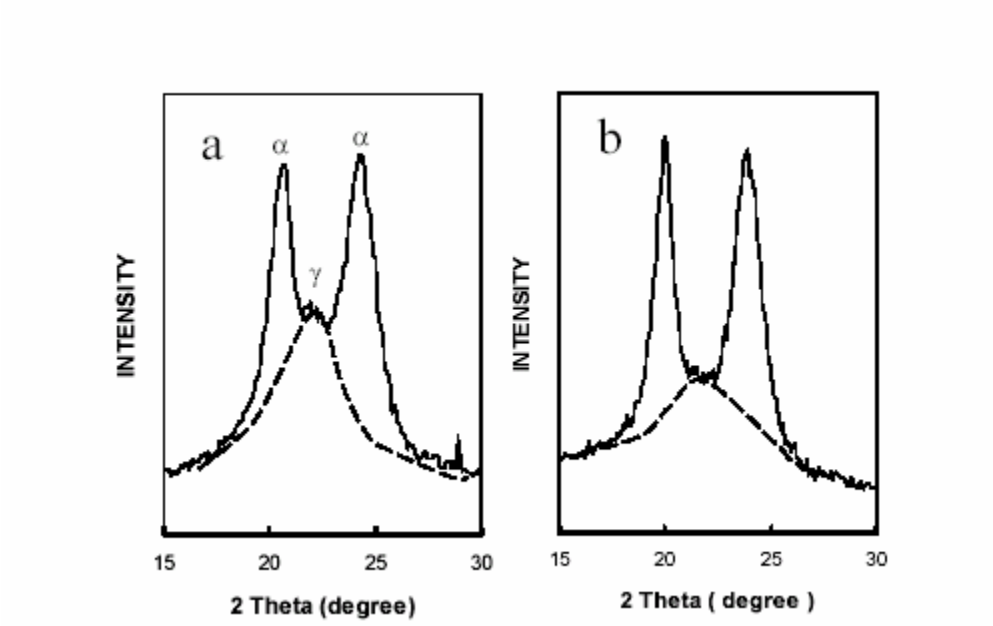

Figure 71. Wide Angle X-ray Diffraction Patterns of (a)as-received nylon 6 (b) IC coalesced nylon 6

Wide-angle X-ray diffraction is often used to determine the total crystallinity and the ratio of α and γ-crystalline phases for nylon 6.[191,192] In the X-ray diffraction patterns of nylon 6, the diffraction peak at $2\theta = 21.8°$ is contributed by the γ-form crystal of nylon and a pair of peaks, $2\theta = 20°,24°$ are distinctive features of the α-form crystal of nylon 6. The single diffraction peak of γ-form nylon 6 is contributed by the {200} plane diffraction and two separated diffraction peaks for α-form come from (200) and (002) planes. Figure 71 shows the WAXD patterns for as-received and coalesced nylon 6. In

the pattern of as received nylon 6, it is apparent that there is a fair amount of γ form crystal, although the peak at 21.8° is overlapped. However, the 21.8° diffraction peak almost disappears in the X-ray pattern of cyclodextrin inclusion complex treated nylon 6. For the treated nylon 6, the two strong diffraction peaks characteristic for the α-form crystal, with much less of the unstable γ-form crystal and amorphous material, can be observed.

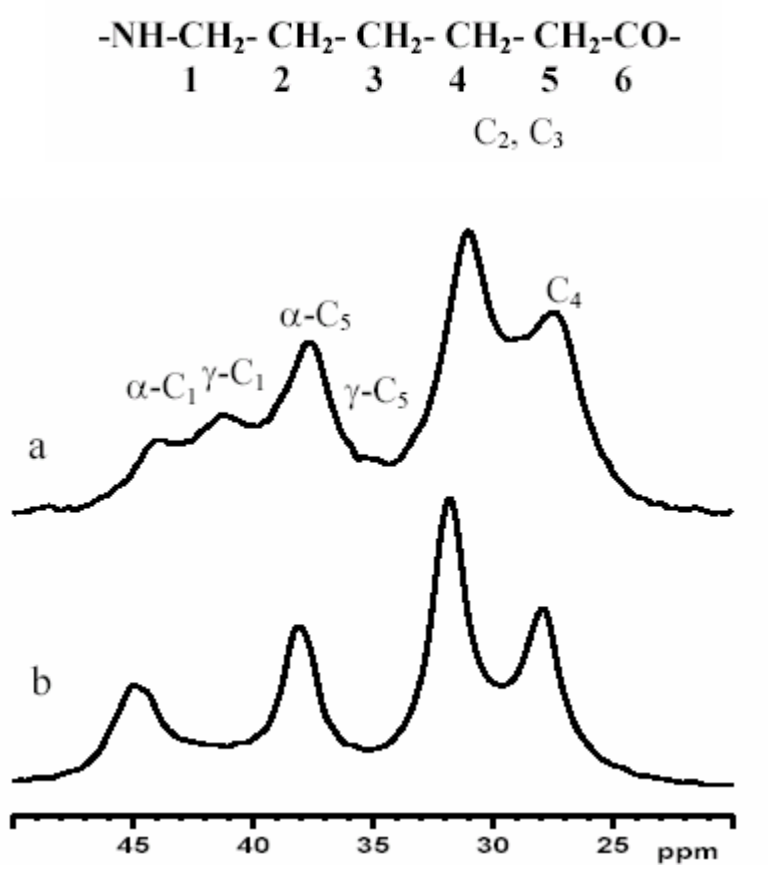

Figure 72. CP-MAS ^{13}C NMR spectra of (a) as-received nylon 6 and (b) IC coalesced nylon 6

Solid-State NMR is one of the more powerful and versatile tools to study polymer structure, morphology and dynamics. The CH_2 ^{13}C resonances of nylon 6 occur in the

range of 15-50 ppm *vs* TMS and overlap strongly. This frequency range includes resonances of the amorphous, γ- and α-crystalline phases. Resonances of the amorphous phase, which are much broader than the crystalline resonances, are not separately visible. However, the narrower line widths of the crystalline fraction cause them to dominate the CP/MAS spectrum, and the lines assigned here are therefore essentially due to the crystalline fraction. Some methylene carbons have chemical shifts which are sensitive to the crystalline modification, and therefore, a distinction between the different crystalline phases is possible.[193,194] The peak at 43.9 ppm is assigned to C1 in the α polymorph and the peak at 41.3 ppm to C1 in the γ form. The CP/MAS ^{13}C NMR spectra of as-received nylon 6 and nylon 6 coalesced from cyclodextrin inclusion complex are given in Figure 72. From this figure, it can be seen that the α form crystal dominates the crystalline region of nylon 6 coalesced from its cyclodextrin inclusion complex.

DSC was carried out to obtain the melting and crystallization behaviors of nylon 6 as-received and coalesced from the inclusion complex, although this method is not an efficient way to distinguish between the two crystal forms of nylon 6. Figure 73 shows the DSC heating and cooling scans and Table 14 lists the melting temperature (T_m), the crystallization temperature observed upon cooling (T_{cc}), and the crystallinity of both nylon 6 samples. Compared to the as-received sample, elevated T_m and an almost doubled crystallinity were found for the sample coalesced from the nylon 6 cyclodextrin inclusion complex. As known, α-form nylon 6 crystals have a higher T_m than γ-form. Therefore, the DSC results, again, reveal that α-form crystals are the dominant component in the coalesced materials. Figure 74 shows the TGA profiles for the coalesced nylon 6 sample. The 30^o C higher thermal degradation temperature of modified

nylon 6 demonstrates the different organization of polymer chains compared with the normal bulk polymer.

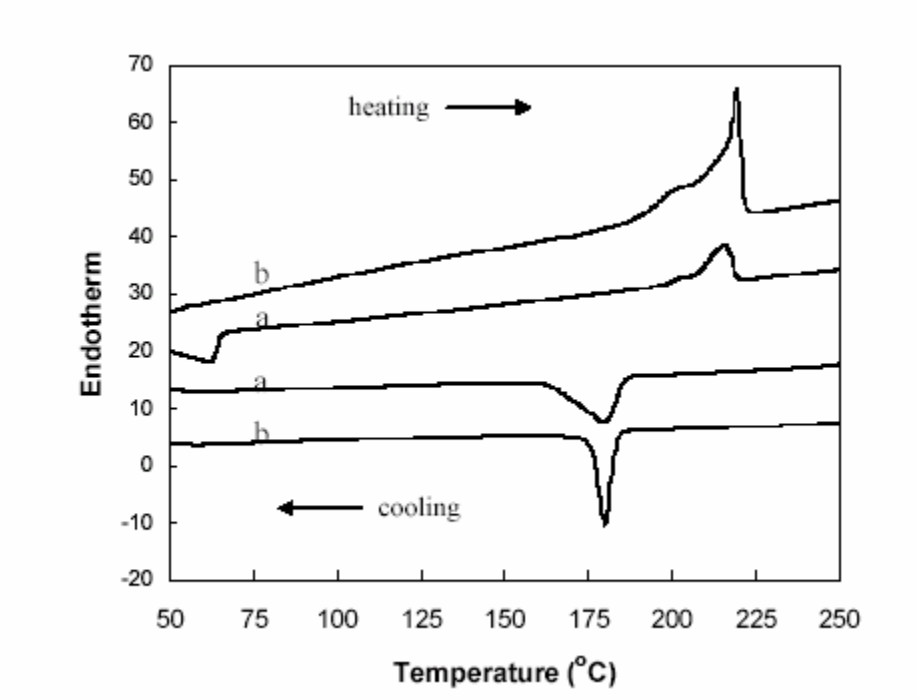

Figure 73. DSC heating and cooling scans of (a) as-received nylon 6 and (b) IC coalesced nylon 6

Table 14. Thermal properties obtained from DSC for as-received nylon 6 and IC coalesced nylon 6

Thermal properties	As received Nylon 6	Coalesced Nylon 6
T_m (^{o}C)	215.6	219.3
ΔH_f (J/g)	55.8	100.4
Crystallinity (%)	29.4	52.9
T_{cc} (^{o}C)	179.9	180.0
ΔH_{cc} (J/g)	60.2	66.2
Temperature range of crystallization(^{o}C)	190.7-156.8	188. 6-161.8

* the ΔH_f of 100% crystalline nylon 6 is taken as 189.8 (J/g)[195]

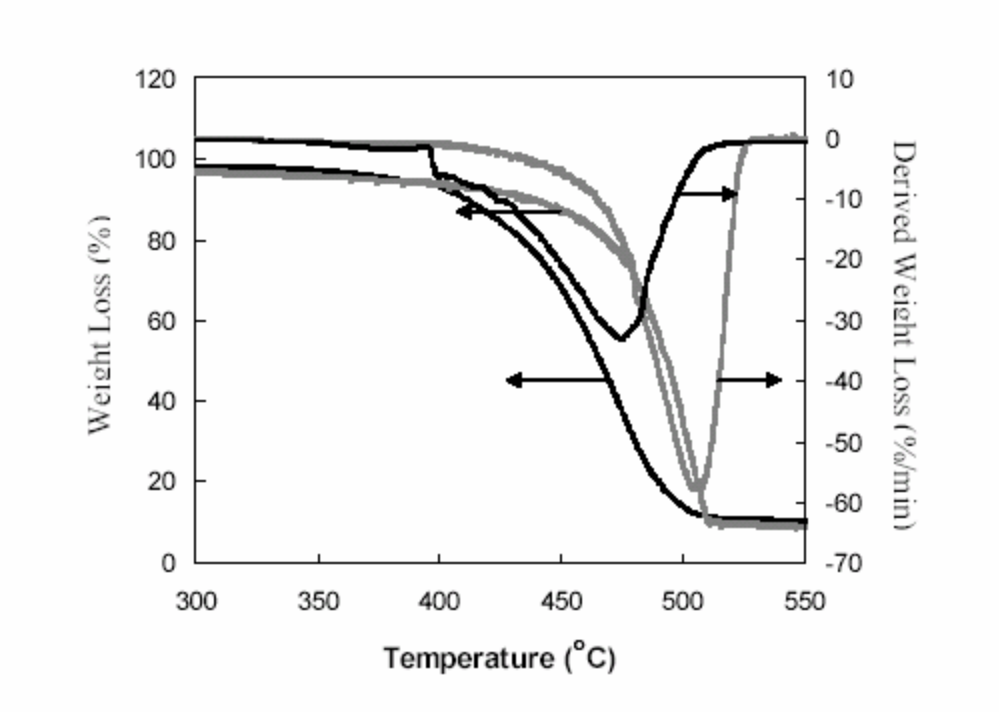

Figure 74. TGA profiles and thermal degradation rate profiles for as-received nylon 6 (solid curve) and IC coalesced nylon 6 (shadow curve)

3.2.4 Conclusions

In summary, threading into and extraction from its α-cyclodextrin inclusion complex is an effective way to both transform nylon 6 from the γ to its α polymorph and to obtain a much higher level of crystallinity. The capability of cyclodextrin inclusion complexes to manipulate the crystal structures of nylons is likely due to the confining channel environment for the included polyamide chains, which requires them to assume highly extended, narrow conformations in order to fit into the stacked cyclodextrin host crystalline channels.

4 Intimate blend of Polymers via Coalescence from Their Common Cyclodextrin Inclusion Complexes

4.1 Blend of polycarbonate and poly (methyl methacrylate)

4.1.1 Introduction

Recently, we reported an attempt to blend polymers by first forming their common inclusion complex (IC) with cyclodextrin (CD) as the host and then coalescing the guest polymers from their CD-IC crystals by washing them with hot water. This procedure was used in the hope of obtaining an intimately mixed, compatible blend of the poly (ε-caprolactone) (PCL)/poly (L-lactic acid) (PLLA) pair, which are normally incompatible. In the PCL/PLLA-α-CD-IC crystals neighboring PCL and PLLA chains residing in the narrow channels provided by the host α-CD lattice are likely in close proximity. When the PCL/PLLA-α-CD-IC crystals are washed with hot water, which does not dissolve either of the guest polymers, the α-CD host is removed and the PCL and PLLA chains coalesce into a blend. Because they are proximal in their common α-CD-IC crystals, we anticipated that the PCL/PLLA blend coalesced from them might be compatible, with an intimate mixing of PCL and PLLA chains.

We observed the coalesced PCL/PLLA blend to no longer evidence crystallinity for the PCL chains, and only a very small fraction (~5%) of the PLLA chains were crystalline. By contrast, when the PCL/PLLA blend is formed by casting from tetrahydrofuran (THF), ~45% of both the PCL and PLLA chains crystallize, and large and small PCL and PLLA spherulites were observed in the photomicrograph of the phase-separated, solution-cast blend. A photomicrograph of the coalesced PCL/PLLA blend, on the other hand, appeared to show an amorphous matrix embedded with a few

small PLLA spherulites. Annealing the PCL/PLLA blend coalesced from their common α-CD-IC crystals for 24 h at 200^{o} C, which exceeds the melting temperatures of both PCL and PLLA, did not appear to alter the as-coalesced, intimate morphology, as evidenced by DSC and microscopic observations. In addition, we have not been able to redissolve the coalesced PCL/PLLA blend, even in THF, which is commonly used to cast their blended films. These intriguing observations have led us to attempt the formation of similar blends with amorphous polymer pairs, such as polycarbonate (PC)/poly (methyl methacrylate) (PMMA) and PC/polystyrene (PS). Here we describe our initial efforts to obtain intimately mixed, compatible blends of the inherently immiscible polymer pairs PC/PMMA and PC/PS by formation of their common γ-CD-ICs, followed by coalescence of the guest polymer pairs from their γ-CD-IC host crystalline lattices.

The miscibility of binary blends of bisphenol A-polycarbonate (PC) with PMMA and their equilibrium phase phenomena have been widely investigated[196-203]. However, the precise phase behavior of the blends remains controversial. A number of papers reported methods to prepare homogeneous blends of the two polymers, but most of the mixtures were found to phase separate after heating to relatively low temperatures (~160^{o} C). These results were explained by the existence of a lower critical solution temperature (LCST) for the system. Cloud point estimates further suggested that the temperature range between the LCST and Tg of PC (~150^{o} C) is too narrow for industrial processing or use. This shortcoming might be surmountable, if specific molecular interactions between the two different polymer chains could be induced. If the two polymers can be well or intimately blended, i.e., at the molecular level, specific interactions between the

polymers might be enhanced and result in stable, intimate PC/PMMA blends which can withstand the heating process.

Since we have found, when inherently immiscible polymers are simultaneously included as guests in the narrow channels of their common inclusion complexes (ICs) formed with host cyclodextrins (CDs) and then these polymer-1/polymer-2-CD-IC crystals are washed with hot water to remove the host CD lattice and coalesce the guest polymers, that an intimately mixed blend of the polymers are obtained, here we extend this procedure to the CD-IC fabrication of PC/PMMA blends.

4.1.2 Experimental Section

Materials

Polycarbonate (PC) of bisphenol A [poly (oxacarbonyloxy-1, 4-phenyleneisopropylidene-1, 4-phenylene) with average molecular weight M_w = 28 800 and M_n = 17 300 was obtained from Aldrich Chemical Co. Inc. Poly (methyl methacrylate) (PMMA) with average molecular weight M_w = 350 000 was also obtained from Aldrich Chemical Co. Inc. γ -Cyclodextrin was purchased from Cerestar Co. Tetrahydrofuran (THF) and dimethyl sulfoxide (DMSO) were analytical grade and obtained from Fisher.

Preparation of Samples

γ-CD was dissolved in DMSO and heated to 60^o C. PC and PMMA with different molar blend ratios (4:1, 1:1, 1:4) were dissolved in THF, and the solutions were heated to 50^o C. The THF solution of PC/PMMA was slowly added to the saturated γ -CD/DMSO solution while stirring and heating. Heating and stirring at 60^o C was continued for 3 h to

keep the combined solution homogeneous. The mixture was slowly cooled to 20^{o} C, and stirring was continued overnight. The resulting precipitate was filtered out and dried in a vacuum oven at 60^{o} C for 24 h.

The physical blends of the two polymers were made by dissolving both polymers in THF and then drying the solutions in a vacuum oven at 60^{o} C for 24 h.

Fourier Transform Infrared Spectroscopy (FTIR)

The FTIR spectral studies of PC, PMMA, γ -CD, PC/PMMA physical blend, PC/PMMA-γ -CD-ICs, and the IC samples after washing with hot water or THF were carried out in a Nicolet 510P FTIR spectrometer in the range between 4000 and 400 cm^{-1}, with a resolution of 2 cm^{-1}.

Differential Scanning Calorimetric (DSC) Analysis

The thermal scans of the individual polymers, polymer blends, and the IC samples before and after coalescence by washing with hot water were performed with a Perkin-Elmer DSC-7 differential scanning calorimeter. The measurements were run in the range of 30-260^{o} C at a heating rate of 10^{o} C /min.

Thermogravimetric Analysis (TGA)

TGA scans of 5-10 mg samples were obtained by using a Perkin-Elmer Pyris 1 thermogravimetric analyzer (TGA). The samples were put into platinum pans, which were hung in the heating furnace. The weight percentage of material remaining in the pan

was recorded while heating from 25 to 800^{o} C at a heating rate of 20^{o} C/min. Nitrogen was used as the purge gas.

X-ray Diffraction

The X-ray diffraction scans of PC, PMMA, γ -CD, and PC/PMMA-γ-CD ICs were carried out with a Seimens type-F X-ray diffractometer. The X-ray source was Ni-filtered Cu K radiation (30 kV, 20 mA). The specimens were mounted on aluminum frames and scanned from 5 to 40^{o} = 2θ at a speed of (2 θ= 1.2^{o})/min.

4.1.3 Results and Discussion

FTIR Analysis

Figure 75 shows the FTIR spectra of (a) PC, (b) PMMA, (c) PC/PMMA physical blend, and (d) PC/PMMA- γ -CD IC coalesced (washed with hot water). The FTIR spectrum of PC is characterized by an intensive C=O band at ~1775 cm^{-1}, a phenyl ring structure band at ~1505 cm^{-1}, and a strong C-O band at 1194 cm^{-1}. The absorption peak at 1386 cm^{-1} is contributed by the terminal phenyl groups in the polymer. In pure PMMA, the characteristic C=O peak occurs at ~1731 cm^{-1} and the peaks at 2950 and 2998 cm^{-1} are contributed by the methyl groups. For γ -CD, the peak at 1079 cm^{-1} is contributed by CH2-OH vibrations and the peak at 1158 cm^{-1} are from the -OHs on the cycle. The C-H

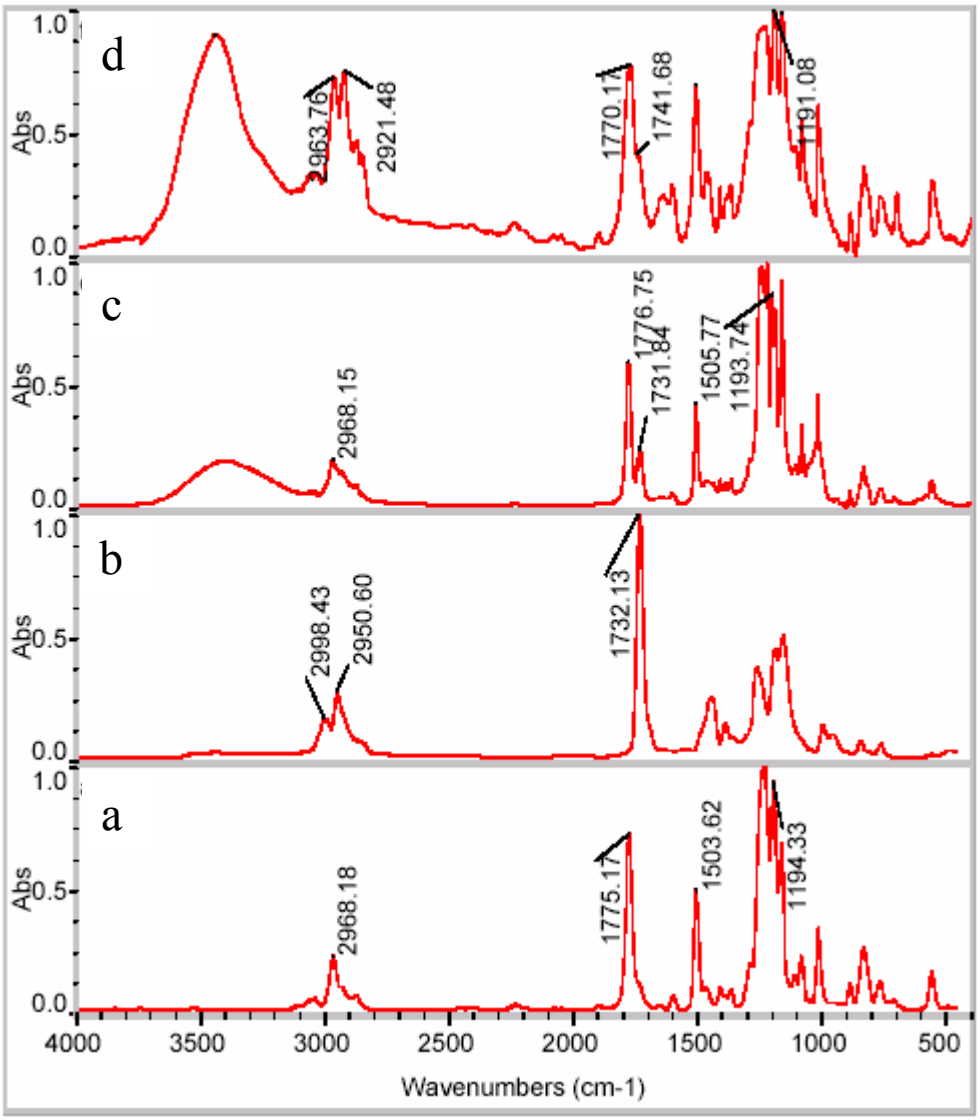

Figure 75. FTIR spectra of (a) PC, (b) PMMA, (c) PC/PMMA physical blend (PC: PMMA = 1:1 molar ratio) and (d) PC/PMMA-γ-CD IC coalesced (washed with hot water, PC: PMMA = 1:1 molar ratio).

bond absorption peak at 2925 cm^{-1} also can been seen for γ -CD in its FTIR spectrum. All of the IR absorption peaks characteristic of PC, PMMA, and γ -CD are found in the

spectrum of PC/PMMA- γ -CD IC in Figure 76b. This means that the experimental sample contains PC, PMMA, and γ -CD. There is very little difference between the FTIR spectrum of the physical blend and the individual FTIR spectra of the pure polymers (see Figure 75a-c). This means that there is no significant interaction between the two components in the physical blend, although some reports[204] suggest that there might be some weak interactions between PC and PMMA.

However, in the spectrum of the PC/PMMA- γ -CD-IC sample coalesced by washing with hot water (Figure 75d) the PMMA C=O absorption peak at 1732 cm^{-1} has shifted to 1741 cm^{-1} and is partly overlapped by the PC C=O, which shifted to 1770 cm^{-1}. Moreover, the peak characteristic for the methyl groups on PMMA also shifted from 2950 to 2921 cm^{-1}. These vibrational shifts may result from interactions occurring between the carbonyl and methyl groups of PMMA with the carbonate groups and phenyl rings of PC [205], which may be facilitated when the chains of the two polymers are close enough, as in the intimately mixed, γ -CD-IC coalesced PC/PMMA blends.

In Figure 76b we observe that both the PC and the PMMA C=O vibrations shift to a single band at 1705 cm^{-1} for the PC/PMMA--CD-IC, which is characteristic of hydrogen-bonded carbonyls[206] and likely results from hydrogen bonds formed with the -OH groups of the γ -CD host. Note that the FTIR spectra of (a) pure γ-CD and (c) PC/PMMA- γ -CD-IC washed with THF in Figure 76 are virtually identical. Apparently, the THF wash completely disrupts the γ-CD-IC crystals and dissolves and removes the included PC/PMMA.

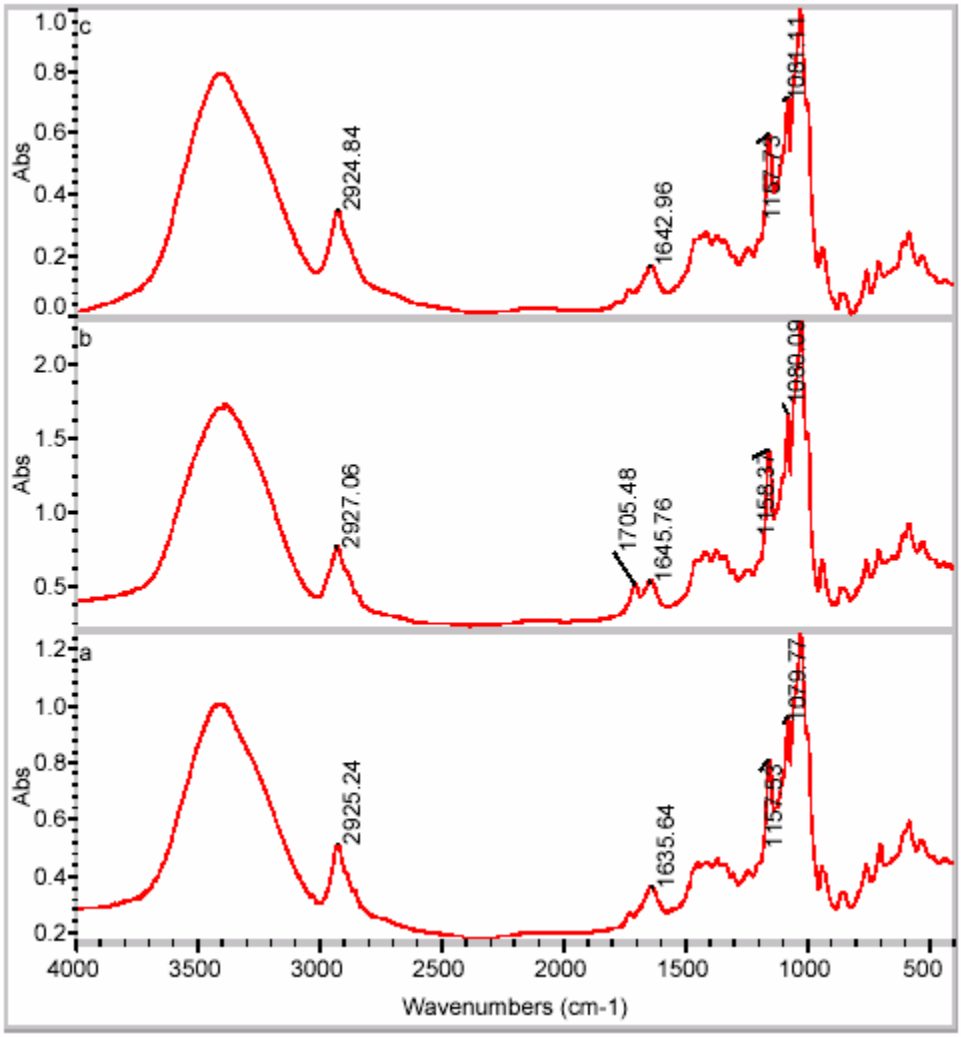

Figure 76. FTIR spectra of (a) γ-CD, (b) 1:1 PC/PMMA-γ-CD IC and (c) 1:1 PC/PMMA-γ-CD IC washed with THF.

Thermal Behaviors

Figure 77 is the DSC thermogram of the solution-cast physical blend of PC/PMMA observed in the second scan after melting of the PC crystals. It indicates that the T_g's of PC and PMMA are unchanged in the physical blend. This means that the two polymers are not miscible when blended in the normal way. For pure γ -CD, there is no thermal

transition in the measured range 30-260^{o} C. In Figure 78, the first DSC scanning results for PC/PMMA blends with different PC/PMMA compositions (molar ratios), which were obtained after washing their common γ -CD-ICs with hot water, are shown. Melting peaks for crystalline PC are clearly observed in Figure 78 (also see the X-ray results below). As we might expect, these PC crystals are not reversibly stable and so disappear after melting and are not re-formed during the second DSC heating. Figure 79 shows the second scans of the washed IC samples. In this figure, we can see that there is only one T_g for each washed IC sample with different blend ratios. These single T_g's decrease with an increase of PMMA content in the coalesced CD-IC blend samples.

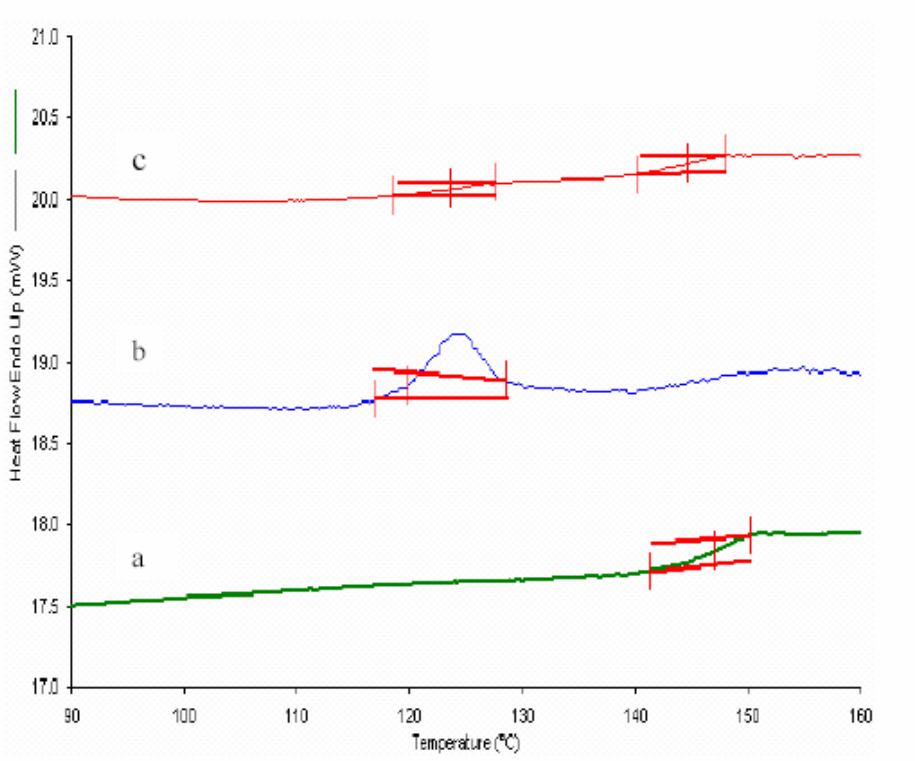

Figure 77. The DSC thermograms of (a) PC, (b) PMMA, and (c) 1:1 PC/PMMA physical blend.

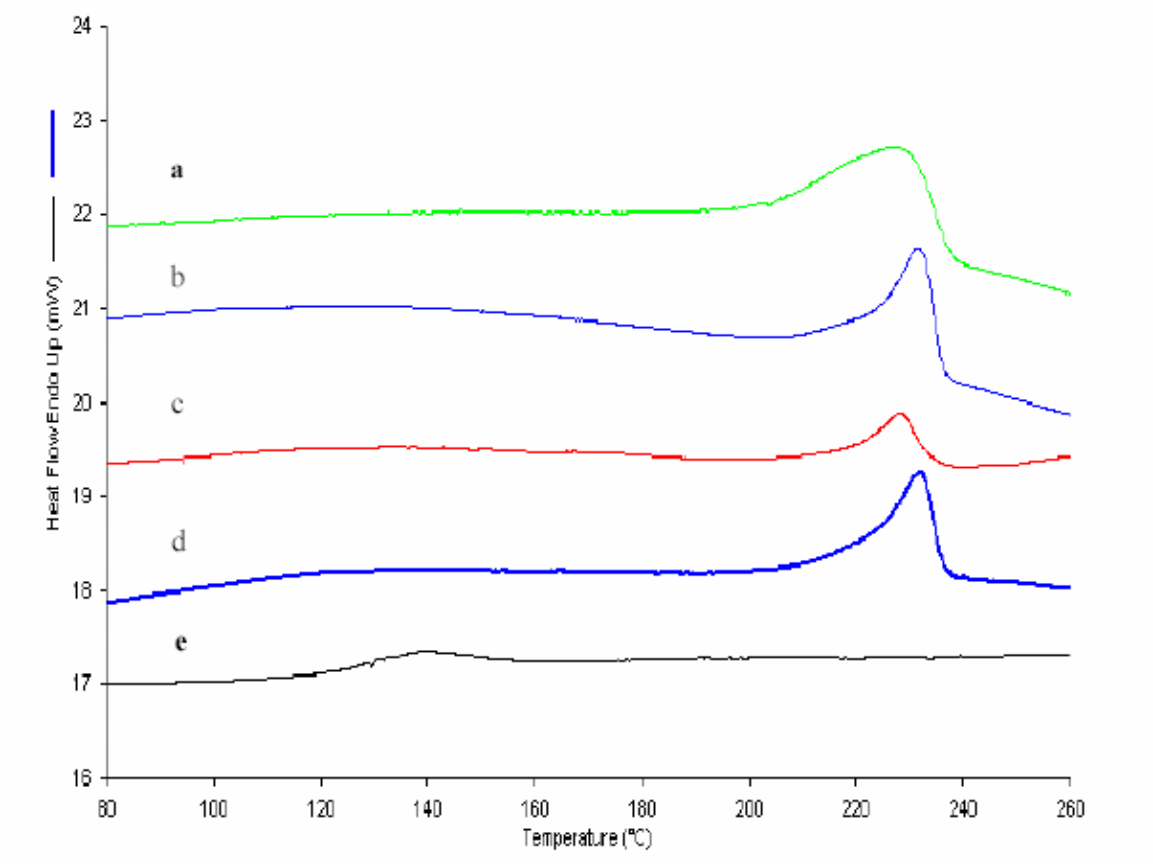

Figure 78. The first DSC scans for the (a) PC-γ-CD IC, (b)PC/PMMA-γ-CD IC (PC: PMMA = 4:1 molar ratio), (c) PC/PMMA-γ-CD IC (PC:PMMA = 1:1 molar ratio), (d) PC/PMMA-γ-CD IC (PC:PMMA = 1:4 molar ratio), and (e)PMMA-γ-CD IC, all after washing with hot water.

This phenomenon is in agreement with the description of miscible polymers by Olabisi et al. The most interesting observation is that for the 1:4 IC blend of PC: PMMA the single T_g of the sample, which is 110^o C, is lower than the T_g of pure PMMA (118^o C). One explanation maybe that the PC chains act as a plastizer in the homogeneous system, because the PC we used has a relatively low molecular weight and correspondingly short

chains. Remember that DSC scans of PC, PMMA, and a solution-cast blend (1:1 mole ratio) (see Figure 77) show that initially pure PC and PMMA are amorphous polymers and only exhibit glass transition temperatures at 145 and 118^{o} C, respectively.

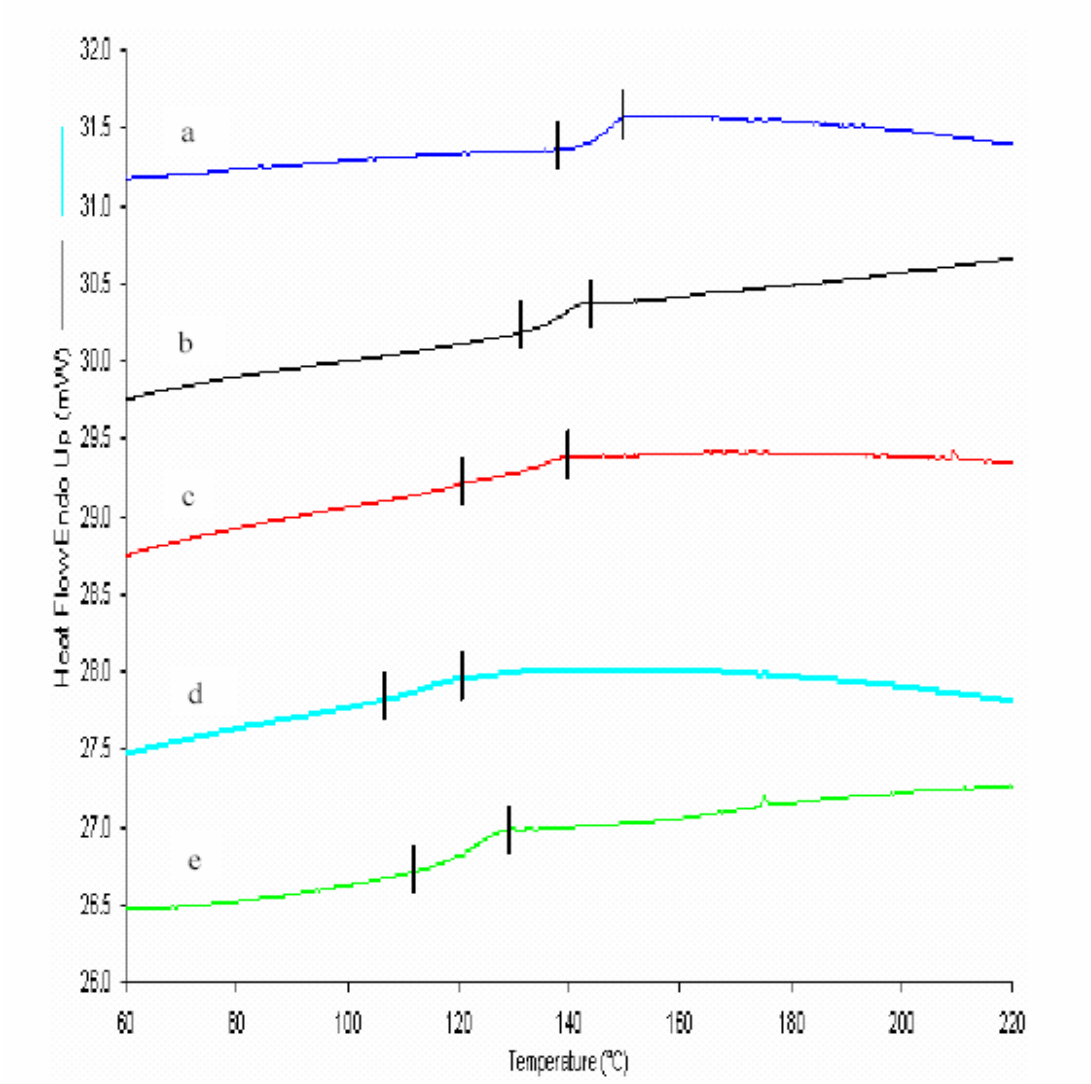

Figure 79. The second heating DSC scans for the (a) PC-γ-CD IC, (b) PC/PMMA-γ-CD IC (PC:PMMA = 4:1 molar ratio), (c) PC/PMMA-γ-CD IC (PC:PMMA = 1:1 molar ratio), (d) PC/PMMA-γ-CD IC (PC:PMMA = 1:4 molar ratio), and (e) PMMA-γ-CD IC, all after washing with hot water.

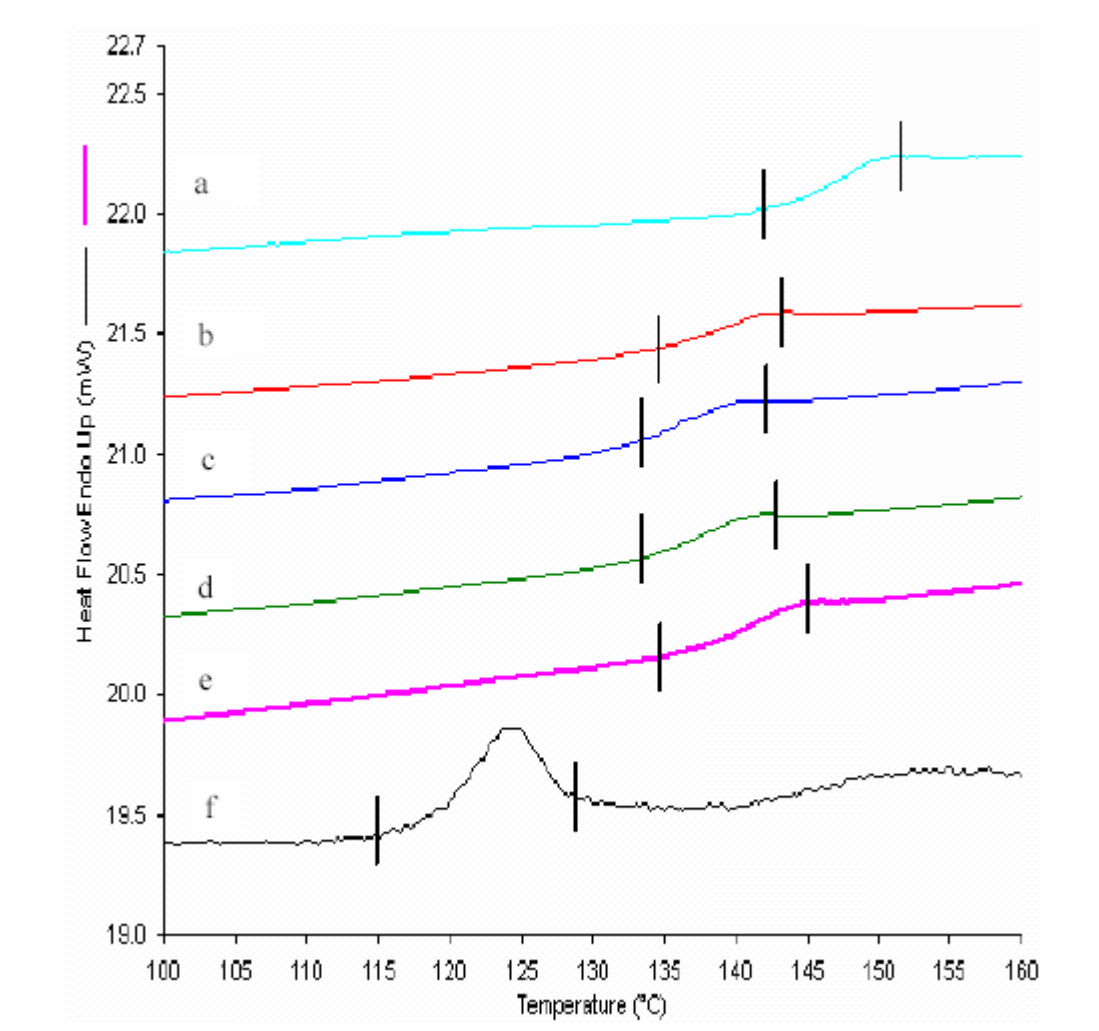

Figure 80. The DSC heating scans of (a) PC, (b) run II of coalesced PC/PMMA-γ-CD IC (PC:PMMA = 4:1 molar ratio), (c) run III of coalesced PC/PMMA-γ-CD IC (PC:PMMA = 4:1 molar ratio), (d) run IV of coalesced PC/PMMA-γ-CD IC (PC:PMMA = 4:1 molar ratio), (e) coalesced PC/PMMA-γ-CD IC (PC:PMMA = 4:1 molar ratio) after annealling for 2hrs at 200º C, and (f) PMMA.

To examine the thermal stability of the intimate blends, repeated heating scans and a scan taken after annealing for 2 h at 200^{o} C were performed on the coalesced PC/PMMA-

γ -CD-IC samples. Figure 80 presents the DSC scans of runs II, III, and IV and the sample annealed at 200 C for 2 h, which were observed for the coalesced PC/PMMA- γ -CD-IC (PC: PMMA = 4:1 molar ratio). As evidenced by the repeated observation of a single T_g between the T_g's of pure PC and PMMA, no phase separation is found to take place after repeatedly heating to 260° C or annealing at 200° C for 2 h.

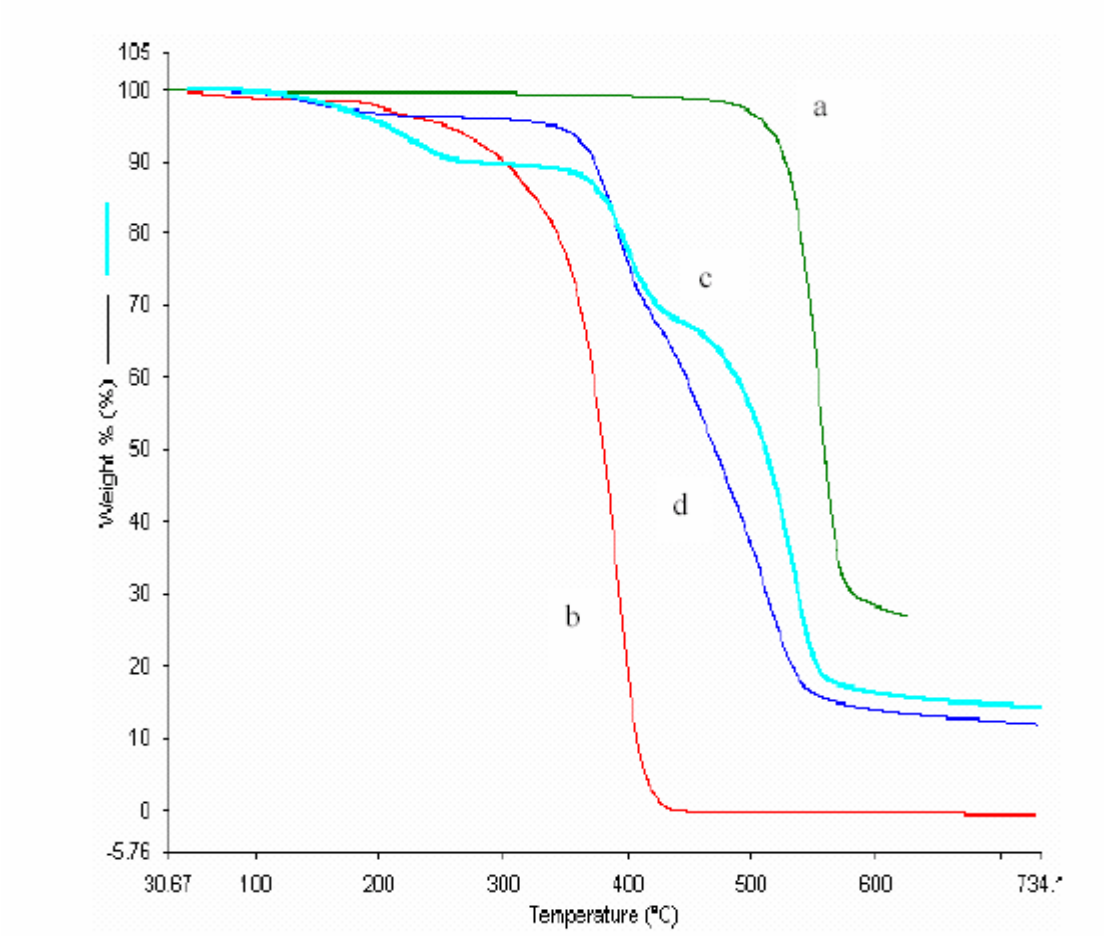

Figure 81. Thermal degradation of (a) PC, (b) PMMA, (c) PC/PMMA physical blend (PC: PMMA = 1:1 molar ratio), and (d) coalesced PC/PMMA-γ-CD-IC (PC:PMMA = 1:1 molar ratio)

Since the CD-IC coalesced blends appear to be homogeneous from both FTIR and DSC observations, the two intimately mixed polymers might be expected to have some effect on each other's decomposition when they are heated to degradation. Figure 81 shows the degradation of a CD-IC coalesced blend compared with the pure polymers and their physical blend. Bisphenol A-polycarbonate exhibits outstanding thermal stability and has a T_d at ~ 510^o C, while PMMA has a lower T_d of 290^o C. Two significant changes in the slopes of the degradation curves can be observed in the physical blend although they are different from the T_d's of the pure polymers. The two transitions disappeared in the CD-IC blended samples, and only a nearly straight line is seen between the decomposition ranges of the two pure polymers. In the blends coalesced from their γ-CD-ICs the two polymers apparently co-degrade together at a molecular level. These results demonstrate that there is likely some interaction between the two polymers and that they form a homogeneous phase.

X-ray Diffraction

The X-ray diffraction patterns of the two polymers, their physical blend, γ -CD, PC/PMMA-γ-CD-ICs, and PC/PMMA- γ -CD-ICs washed with hot water are shown in Figures 82 and 83. As is well known, the peak at 2θ ~ 7.8^o in the wide-angle X-ray scattering is characteristic for the channel structured crystals of γ -cyclodextrin-ICs. This structure is only formed when there are certain guest molecules, such as polymers included. Since both THF and DMSO do not form the channel structure with γ -CD, the two polymers must be the only included guests. The X-ray patterns of PC/PMMA- γ -CD-ICs show no peak for pure PC crystals. This indicates that PC is included in the

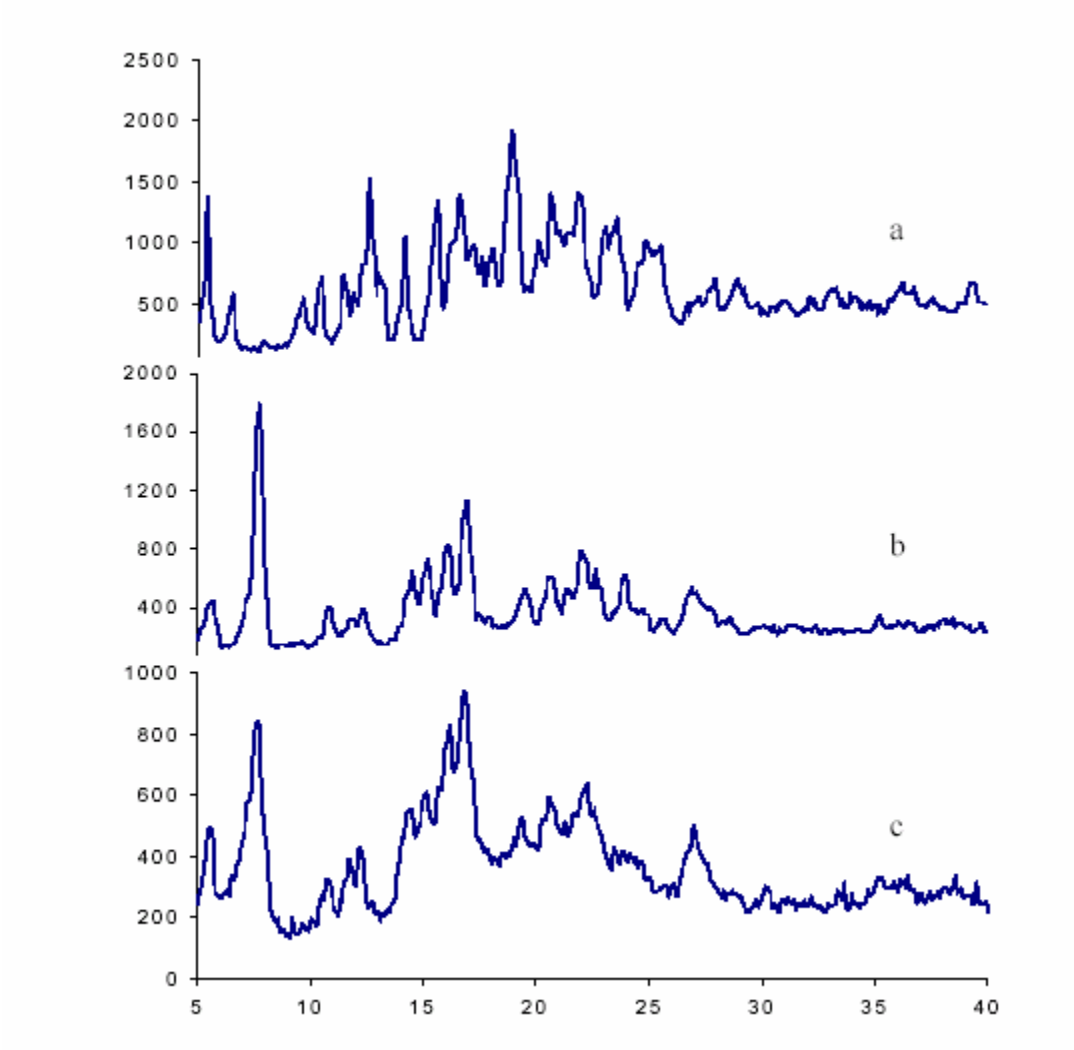

Figure 82. The wide angle X-ray Diffraction of (a) γ-CD (cage structure), (b) 1-propanol-γ-CD-IC (channel structure[15]), and (c) PC/PMMA-γ-CD-IC.

channel structure of γ -CD, with individual isolated chains occupying the channels and so is not able to form macromolecular crystals. However, when the polymer ICs are washed with hot water, the CD that holds the polymers will separate from the guest polymers and the guest polymers will come together again. The process is called "coalescence" and produces the polymer blend. Since there is no difference between the outside surfaces of

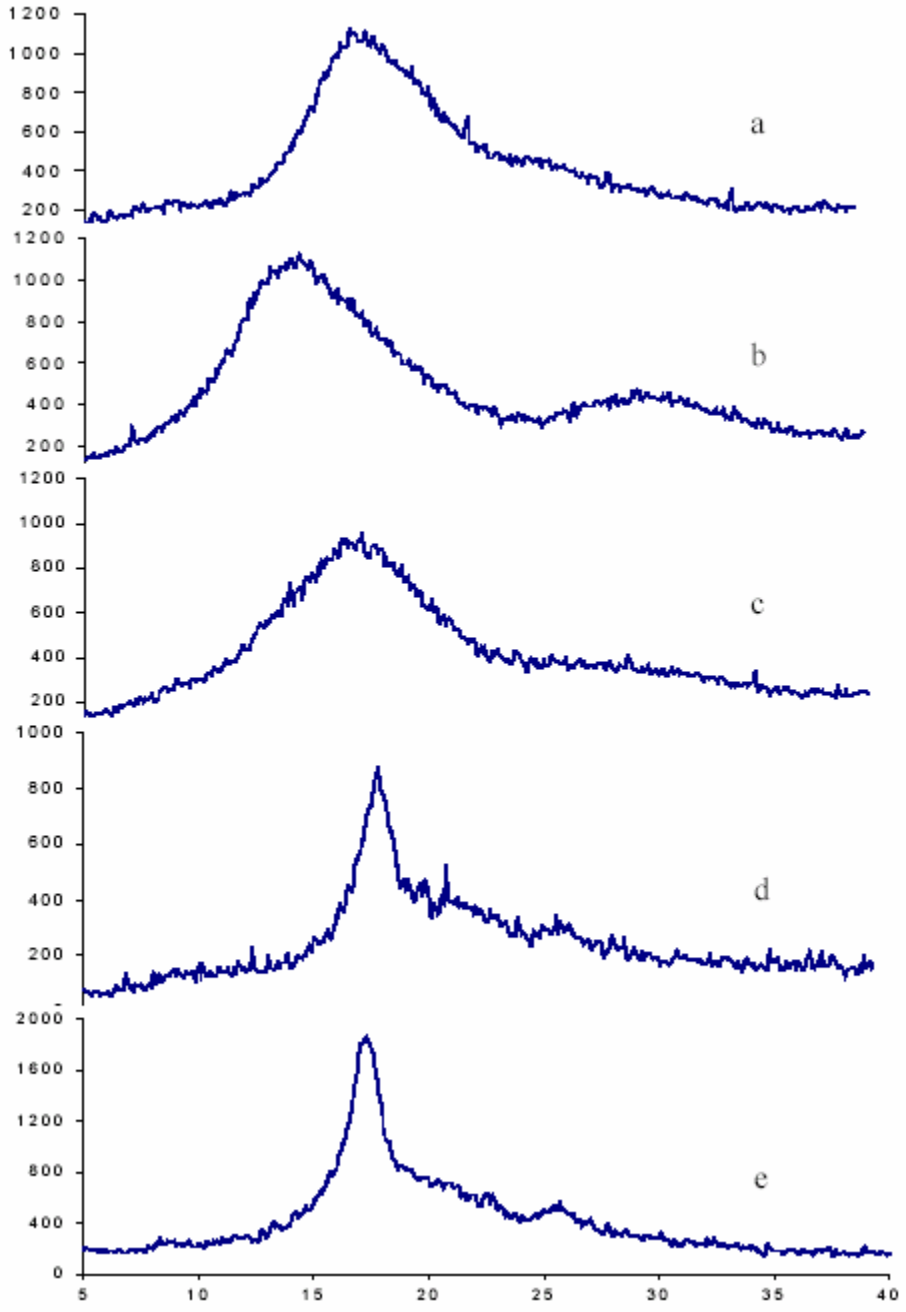

Figure 83. The wide angle X-ray diffraction of (a) PC, (b) PMMA, (c) PC/PMMA physical blend, (d) PC/PMMA-γ-CD-IC coalesced, 1:1 blend, and (e) crystalline PC

the IC crystals, PC-IC, PMMA-IC, or PC/PMMA-IC crystals might be evenly distributed in the sample. Coalescence takes place so rapidly that the polymers have insufficient time to form a separate continuous phase for each polymer component of the blend. Instead, a single phase, miscible polymer blend is obtained in this manner.

Note in Figure 83e the prominent peak at $2\theta = 18^{o}$ attributable to some PC crystals formed during the coalescence of the PC/PMMA blend. When the coalesced blend is heated above the melting temperature of PC, cooled to room temperature, and observed again by X-ray diffraction, the $2\theta = 18^{o}$ peak due to PC crystals disappears, confirming the DSC observations made on the coalesced PC/PMMA blends.

4.4 Conclusions

By simultaneously forming their common inclusion complexes with γ -CD, followed by washing these CD-IC crystals with hot water to coalesce the guest polymers, miscible polycarbonate/poly (methyl methacrylate) blends were obtained. The characteristics of the samples coalesced from their γ -CD-ICs were examined with FTIR, DSC, TGA, and WAXD. WAXD results indicated that PC/PMMA can form a channel structured inclusion complex with γ -CD. PC/PMMA blends coalesced from their common γ -CD-ICs are amorphous and generally exhibit single glass transitions at temperatures (T_g) between the T_g's of pure PC and PMMA. Interestingly, a 1:4 PC: PMMA blend coalesced from its γ -CD-IC is characterized by a T_g lower than that of pure PMMA. In addition, the coalesced PC/PMMA were observed by DSC to be stable to repeated heating and annealing at $T \leq 200^{o}$ C without phase separation. Though not presented here, very

similar results were also obtained from the PC/polystyrene (PS) pair, including a T_g for a PS-rich blend that is below the T_g for pure PS.

The simultaneous,cothermal degradation of PC/PMMA also demonstrated that polymer blends obtained by coalescence from their common γ -CD-ICs are well mixed with intimate contact between the component polymers in the sample. In fact, in the PC/PMMA blends coalesced from their γ -CD-ICs, the C=O stretching bands observed at ~1730 cm^{-1} in pure PMMA and at ~1776 cm^{-1} in pure PC shift to ~1740 and ~1770 cm^{-1}, respectively, where they partially overlap. This serves as a strong indication of specific interactions between the PMMA and PC chains and is a further testament to the intimate mixing of PC and PMMA chains in the blends coalesced from their common γ -CD-IC crystals[207]. More recently solid-state ^{13}C-NMR observed $T_{1\rho}(^1H)$ relaxation measurements (Xingwu Wang, unpublished results) have confirmed the intimate mixing of PC/PMMA and PC/PS chains in their γ-CD IC coalesced blends on a scale ≤ 20 nm.

4.2 Partially Intimate blend of nylon polymers

In this study, we have successfully formed a series of inclusion complexes (ICs) between host α-cyclodextrin (α-CD) and two kinds of guest molecules, nylon 6 and nylon 66. An attempt to achieve an intimate blend between nylon 6 and nylon 66 by forming and dissociating their common α-CD-IC was made. The formation of all inclusion complexes were verified by wide angle x-ray diffraction (WAXD), and FTIR and CP/MAS ^{13}C NMR spectroscopies. Experimental results demonstrate that α-cyclodextrin can only host single nylon polymer chains in the IC channels, either nylon 6 or nylon 66 in their own complexes, and either nylon in neighboring channels of their common IC. The IC coalesced blend of nylon 6 and nylon 66 was obtained after removing cyclodextrin from their common inclusion complex with dimethylsulfoxide. Spectroscopic results illustrate that there is some intimate miscibility existing in the IC coalesced blend, but not in their solution-cast physical blend, though x-ray diffraction patterns show that the crystal structure of the IC coalesced blend appears similar to that of their physical blend. DSC thermal profiles show that nylon 66 first forms crystals during coalescence and the subsequent crystallization of nylon 6 is greatly effected by the nylon 66 crystallites due to the close proximity of the two components in the coalesced blend. CP/MAS ^{13}C NMR observations confirm some mixing of nylon 6 and 66 chains in the vicinity of the crystalline regions of their coalesced blend.

4.2.1 Introduction

Cyclodextrins (CDs) are cyclic oligomers of amylose, which consist of 6, 7, or 8 glucose units, and are named α-, β-, and γ-cyclodextrin. Many researchers have

discovered that CDs may form crystalline inclusion complexes (ICs) with a variety of linear polymeric guests with either hydrophilic or hydrophobic natures.[208-213] Nylon polymers consist of polyethylene segments $(CH_2)_n$ separated by peptide units (NH-CO), which are also present in proteins, giving nylon some of its unique properties and widely used applications. Recently, we have reported the manipulation of nylon 6 crystal structures by forming and coalescing the nylon 6 α-CD inclusion complex.[214] In that work, it was found that threading nylon 6 chains into and extracting them from α-CD is an effective way to both transform nylon 6 from the γ to its α polymorph and to obtain a much higher level of crystallinity. The capability of cyclodextrin inclusion complexation to manipulate the crystal structures of nylons is likely due to the confining channel environment for the included polyamide chains, which requires them to assume highly extended, narrow conformations in order to fit into the stacked cyclodextrin host crystalline channels, as shown in Figure 84.

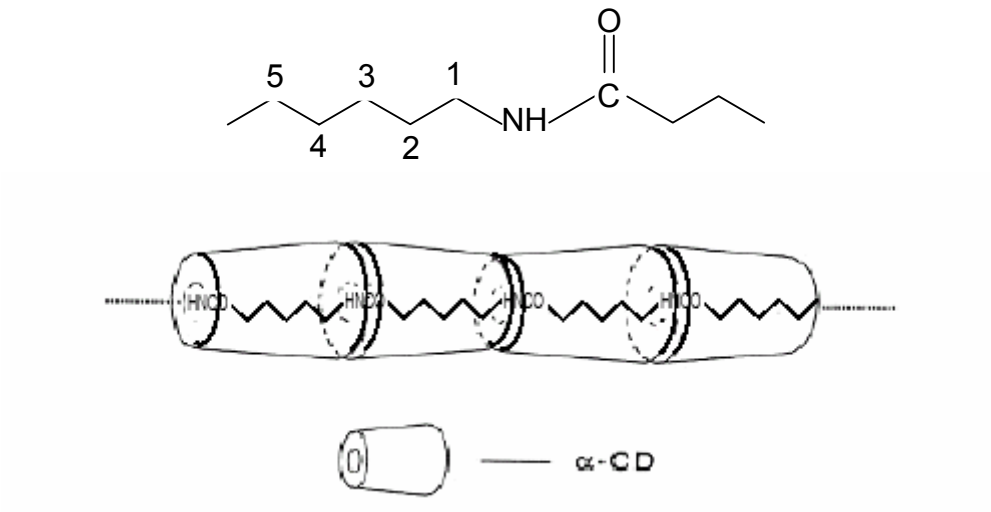

Figure 84. Scheme of the inclusion complex between α-cyclodextrin and nylon polymers.

Two chemically distinct polymers (polymer1/polymer2) can form common inclusion complexes with cyclodextrin. The common IC, containing both polymers, can then be used to obtain intimately compatible blends resulting from the simultaneous coalescence of both guest polymers. An attempt has been made to suppress the phase separation in immiscible polymer blends by first forming their common ICs with CDs and then coalescing the guest polymers from the IC crystals by removing the host with a solvent for cyclodextrin that is a non-solvent for both guest polymers. In this manner, we obtained intimately mixed blends from poly(methyl methacrylate)/polycarbonate (PMMA/PC)[215], atactic poly(*R*,*S*-3-hydroxybutyrate)/poly(ε-caprolactone) (a-PHB/PCL)[105] and PCL/poly(L-lactide) (PCL/PLLA) pairs[103], which are normally incompatible.

In common IC crystals containing chemically distinct polymers, polymer chains randomly reside in the narrow neighboring IC channels provided by the host CD lattice and are thus likely in close proximity. Generally, the phase separation in immiscible blends is composed of nucleation and phase growth stages. If we can mix two kinds of polymers well, such as results in the case of forming/coalescing them from their common IC, the possibility of forming a phase separated nucleus will be decreased. Therefore, phase separation may not take place as easily in the intimately mixed system. Moreover, if in addition the mixing of the two polymers takes place at a temperature lower than their T_gs, which often happens in the coalescence of two polymers from their common IC, the growth of a nucleus to form a separate phase will be frustrated given the absence of polymer chain mobility under this condition.

Nylon 6 and nylon 66 are very important commercial polymers in the nylon family. By blending these two polymers, a remarkable improvement in their inherent mechanical properties can be expected.[216,217] However, the attempt is somewhat frustrated because nylon 6 and nylon 66 are not miscible under normal conditions. In this work, we simultaneously formed the nylon 6/nylon 66 α-cyclodextrin common inclusion complex, and their common IC was coalesced in an attampt to obtain a molecular level, intimate blend between nylon 6 and nylon 66.

4.2.2 Experimental

Sample Preparation

To prepare the individual nylon cyclodextrin inclusion complexes, nylon 6 (Aldrich) (0.18g) or nylon 66 (Aldrich) (0.18g) were dissolved in 3 ml of formic acid (Aldrich, 90%) and then 12 ml of acetic acid (Aldrich) was added to the solution. Eight grams of α-cyclodextrin (Cerestar Co.) were dissolved in 40 ml of dimethylsulfoxide (DMSO) (Aldrich), which corresponds to more than a two-fold molar excess of α-cyclodextrin. The mixed solutions were stirred on a hot plate for 2 hours at 50^{o} C, and then cooled to room temperature while stirring for another 6 hours. The precipitate was washed with cool water to remove free cyclodextrin and filtered and dried under a heating lamp and then in a vacuum oven at 40^{o} C to obtain dry polymer-cyclodextrin-inclusion complex. The preparation of the nylon 6/nylon 66 common IC followed the same procedure used to form the individual nylon ICs, but with 0.09g nylon 6 and 0.09g nylon 66. To dissociate the inclusion complexes, the samples were placed into DMSO and heated at 40^{o} C. The mixture was stirred for 2 hours and then filtered to remove coalesced polymers. The filtered polymers were washed several times with cool water and then dried in a vacuum

oven at room temperature. The physical blend of nylon 6 and nylon 66 in this study was made by dissolving the two nylons (1:1 in weight ratio) in formic acid and then casting a film and drying under vacuum at room temperature.

Sample Characterization

Infrared studies were carried out with a Nicolet 510P FTIR spectrometer in the range between 4000 and 600 cm^{-1}, with a resolution of $2cm^{-1}$. The sample powders were studied by single pass attenuated total reflectance fourier transform infrared spectroscopy (ATR-FTIR). High-resolution solid-state ^{13}C NMR experiments were performed on a Chemagnetics CMC200S spectrometer using cross polarization and magic angle spinning (CP/MAS). The spinning speed ranged from 3 to 4 kHz. The wide angle x-ray diffraction (WAXD) patterns of samples were obtained with a Seimens type-F X-ray diffractometer. The X-ray source was Ni-filtered Cu K_α radiation (1.54Å), with voltage and current set to 30KV and 20mA. The specimens were mounted on stainless steel frames and scanned from 5 to $40^o = 2\theta$ at a rate of ($2\theta = 1.2^o$)/min. Differential scanning calorimetric (DSC) thermal scans were performed with a Perkin-Elmer DSC-7 differential scanning calorimeter. The measurements were run in the range of 30-280^o C at heating and cooling rates of 20^o C /min..

4.2.3 Results and Discussion

When cyclodextrins form inclusion complexes with guest polymer molecules, their crystal form changes from a cage structure, which is its natural, less symmetric state, into a channel structure (See Figure 54), which is more symmetric. Since x-ray diffraction is an efficient means to study crystal forms, this method was used to identify the formation of inclusion complexes. In Figure 85, the as-received α-CD exhibits a major diffraction

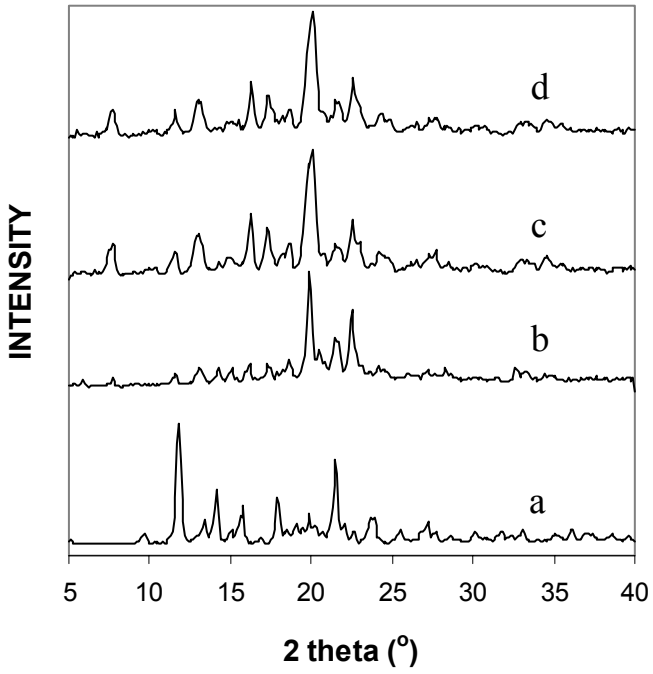

Figure 85. Wide Angle X-ray Diffraction patterns of (a) α-cyclodextrin, (b) nylon 6 α-CD inclusion complex, (c) nylon 66 α-CD inclusion complex, and (d) nylon 6/nylon 66 common α-CD inclusion complex.

peak located at 12° (2θ), characterizing the cage crystal form. However, for all of the nylon-α-CD-ICs, the major peak was observed at 20° (2θ), which is well known to be characteristic of α-CD-IC crystals adopting a channel structure. These diffraction patterns are markedly different from pure α-CD and are strong evidence that the α-CD is hosting nylon polymer chains in channel structure inclusion complexes.

Infrared spectroscopy was employed to observe the presence of both host and guests in the ICs. The FTIR spectra of pure α-CD, as-received nylons and nylon/α-CD-ICs are shown in Figure 86. The presence of absorption frequencies characteristic of the guests in

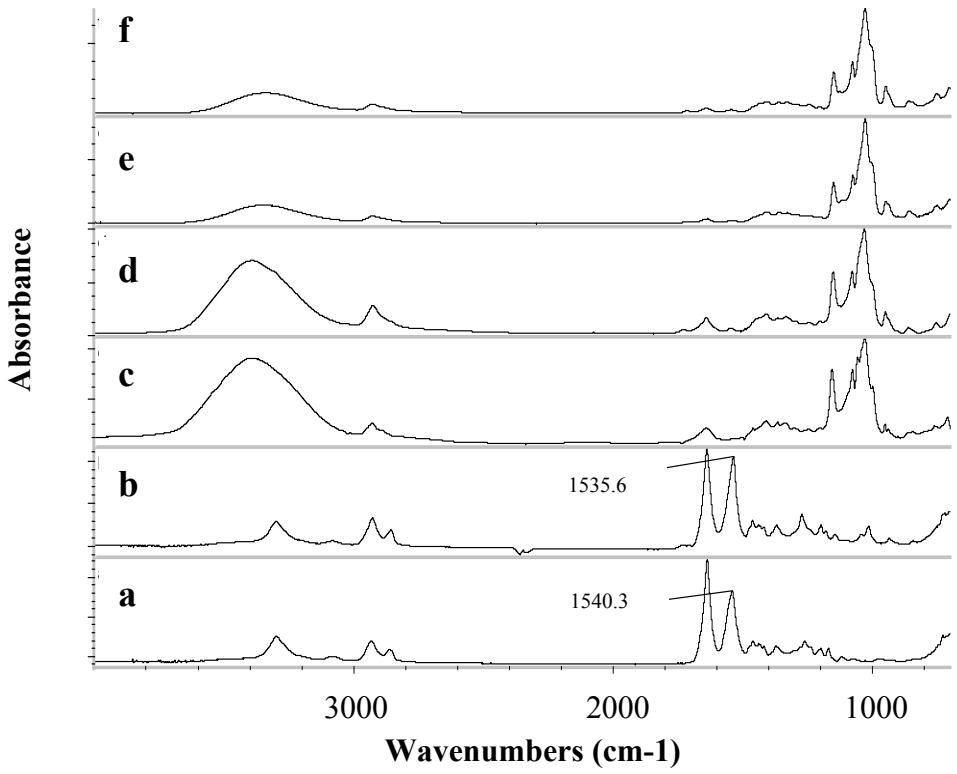

Figure 86. IR spectra of (a) as-received nylon 6, (b) as-received nylon 66, (c) α-cyclodextrin, (d) nylon 6 α-CD inclusion complex, (e) nylon 66 α-CD inclusion complex, and (f) nylon 6/nylon 66 common α-CD inclusion complex.

the IC spectra indicates IC formation. For α-CD, the bands at 1026 and 1079 cm^{-1} are contributed by coupled C-C/C-O stretching vibrations, and the band at 1158 cm^{-1} is

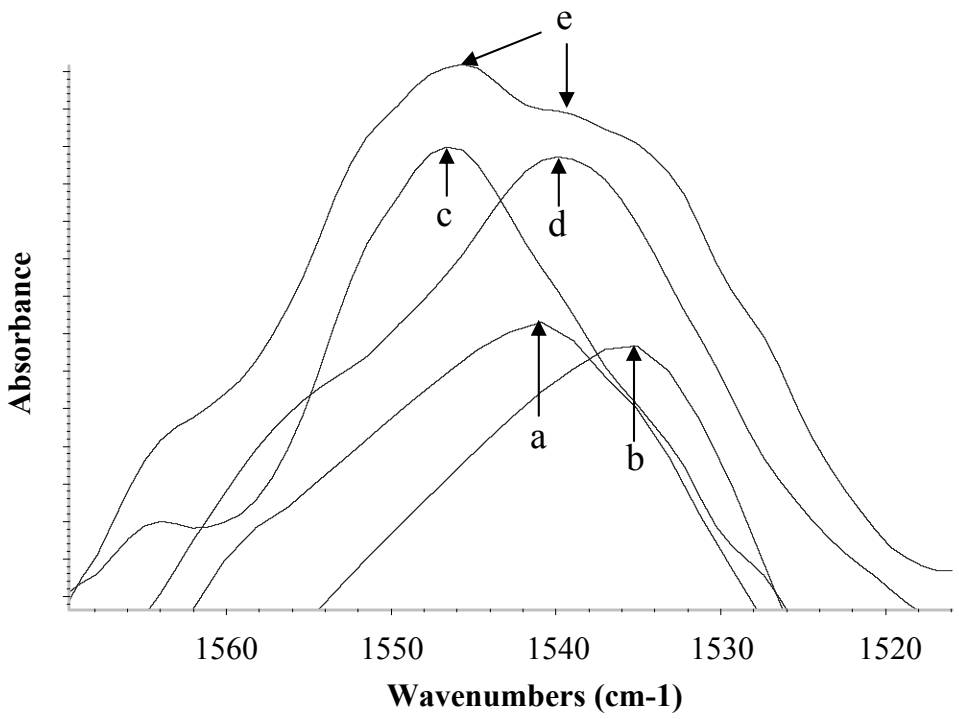

Figure 87. IR spectrum in the N-H band region of (a) as-received nylon 6, (b)as-received nylon 66, (c) nylon 6 α-CD inclusion complex, (d) nylon 66 α-CD inclusion complex, and (e) nylon 6/nylon 66 common α-CD inclusion complex.

attributed to the anti-symmetric stretching vibration of the C-O-C glycosidic bridge. By contrast, a new band at around 1540cm^{-1} which is assigned to the N-H in plane bending deformation of nylons, is found in all nylon-α-CD-ICs, but not in α-CD, indicating the existence of both α-CD and nylon polymers in the ICs. In the expanded view of the N-H

region shown in Figure 87, the characteristic N-H bands in both nylon 6 and nylon 66 move toward higher wavenumber when they are included in the α-CD complex environments. As we mentioned before, this band shifting verifies that the nylon molecules have been threaded into cyclodextrin channels, and the hydrogen bonding of nylons is affected by isolating the nylon chains in the cyclodextrin channels. Because nylon 6 and nylon 66 have different chemical structures, and thus different N-H IR absorbances (1540.3 cm^{-1} for nylon 6 and 1535.6 for nylon 66), in the α-CD inclusion complexes of nylon 6 and nylon 66 their N-H bands also absorb at different wavenumbers.

Interestingly, in the nylon 6 and nylon 66 common IC, the characteristic N-H band is well resolved into two peaks and demonstrates that there are two kinds of complex in the so-called "common IC", formed by either nylon 6 or nylon 66 chains included in the channels of α-CD. According to our calculations, the inner diameter of an α-CD channel is only large enough to host one nylon polymer chain.[218] Therefore, the FTIR results show that single nylon 6 and nylon 66 chains occupy the α-CD channels in their "common IC". Considering that nylon 6 and nylon 66 have such similar chemical structures and both of them are dissolved in the same solvent during the preparation of the common inclusion complex, the common α-CD-IC channels should be randomly occupied by single nylon 6 and nylon 66 chains.

High resolution, solid-State NMR is one of the most powerful and versatile tools to study molecular structure and environment, and thus CP/MAS ^{13}C NMR was used to further our investigation of the common nylon 6/nylon 66-α-CD-IC. When nylon

polymers form ICs with cyclodextrin, it is found[214] that the methylene carbon (C1) directly connected to the N-H group shows a higher nuclear magnetic resonance CP

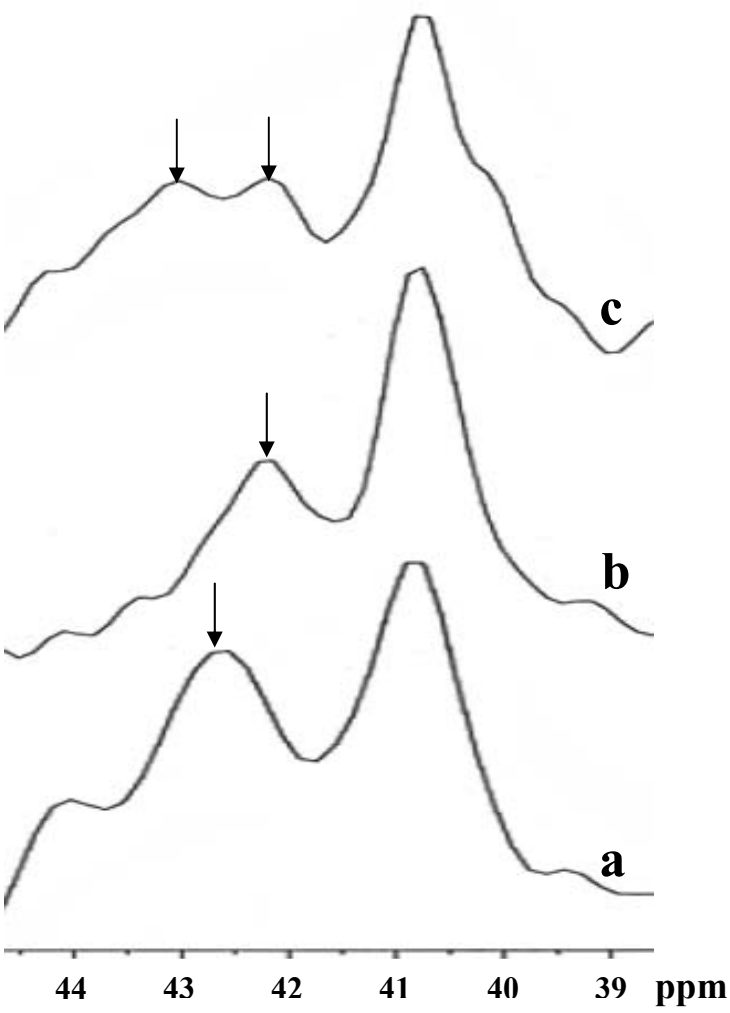

Figure 88. CP-MAS ^{13}C NMR spectra for C1 methylene carbons of (a) nylon 6 α-CD inclusion complex, (b) nylon 66 α-CD inclusion complex, and (c) nylon 6/nylon 66 common α-CD inclusion complex.

efficiency than the other methylene carbons, although without any change in peak position/resonance frequency relative to the as-received nylon. This reveals and is

consistent with the molecular-level interaction taking place between cyclodextin and nylon molecules in the inclusion complex also found by FTIR. Figure 88 presents the NMR spectra observed for nylon 6-α-CD-IC, nylon 66-α-CD-IC, and nylon 6/nylon 66-α-CD-common-IC in the C1 methylene carbon region. It can be see that the C1 carbon in nylon 6-α-CD-IC resonates at a lower frequency (43ppm) than in the nylon 66-α-CD-IC, because of the difference in their chemical structures. As we expected, a superposition of two peaks, instead of one broad peak, is found in the spectra of the common IC, indicated by the arrows in this Figure. This result confirms that α-CD forms an inclusion complex hosting single nylon 6 or nylon 66 chains, but not both side-by-side, in their common IC.

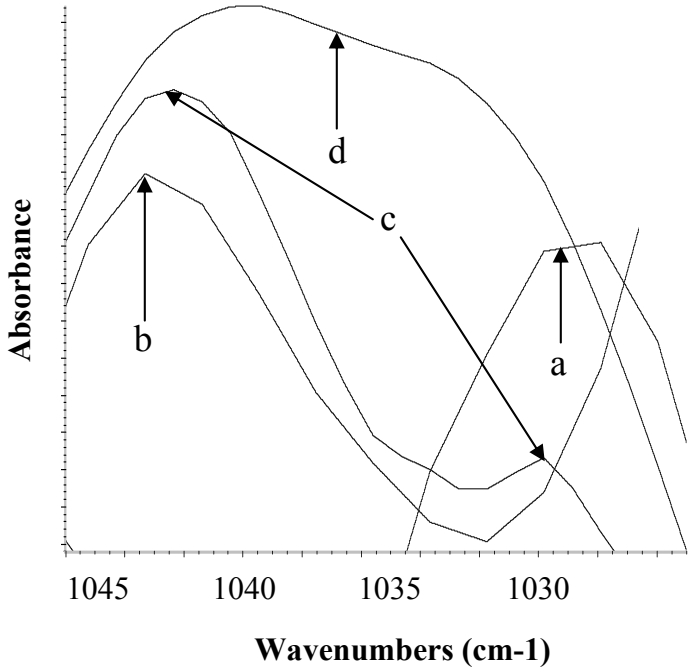

Figure 89. IR spectra in the C-N band region of (a) as-received nylon 6, (b) as-received nylon 66, (c) nylon 6/nylon 66 physical blend, and (d) IC coalesced nylon 6/nylon 66 blend.

After removing cyclodextrin and coalescing the two nylon polymers from their common IC, it was hoped to obtain an intimate blend between nylon 6 and nylon 66. The ATR-FTIR spectra of nylon 6, nylon 66, nylon 6/nylon 66 physical blend, and nylon 6/nylon 66 blend coalesced from their common α-CD IC are shown in Figure 89. The IR band in the range of 1045-1020 cm^{-1} characterizes the C-N stretch in amides. Both nylon 6 and nylon 66 have this absorbance band, which are located at 1028 and 1043 cm^{-1}, respectively. In the IR spectrum of the physical blend of nylon 6 and nylon 66 made by casting from formic acid solution, two separated C-N bands can easily be seen, because of the immiscibility between the two polymers. In contrast, the blend made by coalescing from the common IC of nylon 6 and nylon 66, which is (d) in the figure, only shows one broad band. Since IR absorptions are sensitive to the chemical environment of molecules, the merging of the two nylon C-N bands in the coalesced blend demonstrates that a molecular level intimate blend has been at least partially achieved.

The different chemical structures of nylon 6 and nylon 66 have an influence not only on the IR band frequencies of polar groups, such as C-N, but also on the non-polar groups. The aliphatic regions of the IR spectra of these samples are shown in Figure 90. Typically, in nylon polymers, the IR band around 2880 cm^{-1} is assigned to the C-H symmetric stretch in CH_2 and another band around 2940 cm^{-1} is assigned to the C-H asymmetric stretch in CH_2.[219] Because the two bands in the nylon 6 spectrum are located at higher wavenumber than those in nylon 66, each of these two bands in the physical blend of nylon 6 and nylon 66 can be seen by resolving the two partially overlapped bands, corresponding to the two phase separated components in the blend. However, we can

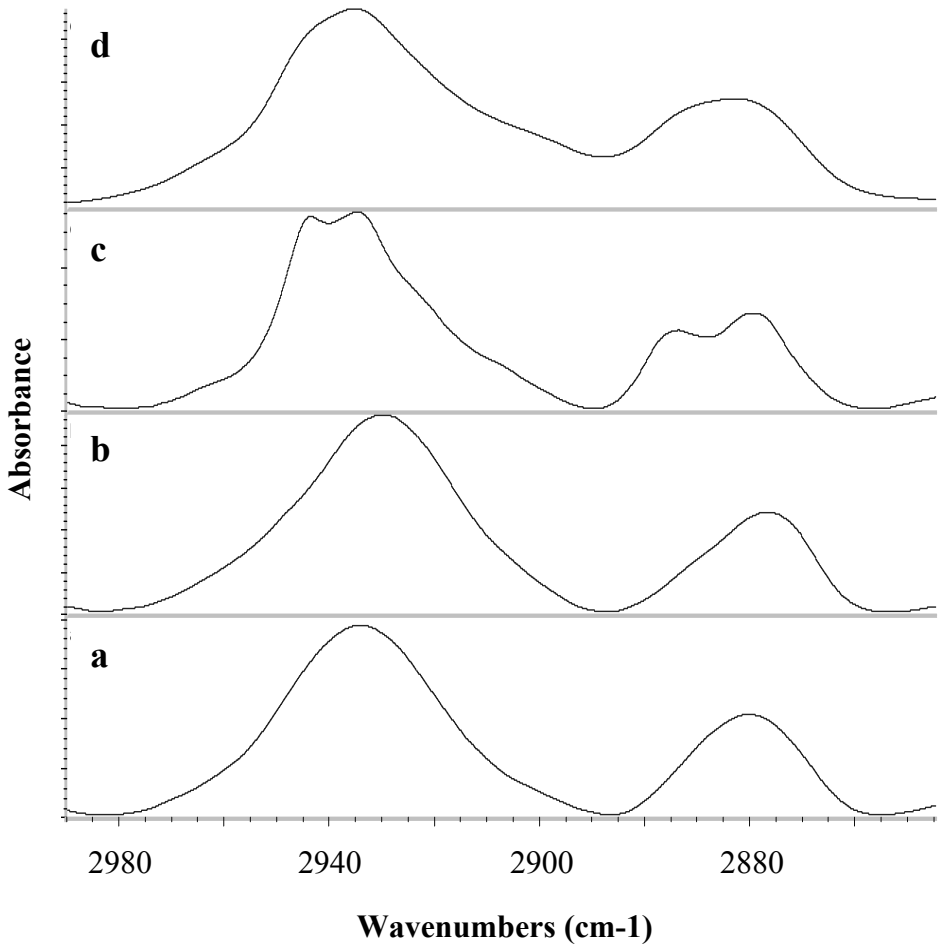

Figure 90. IR spectra in the C-H band region in (a) as-received nylon 6, (b) as-received nylon 66, (c) nylon 6/nylon 66 physical blend, and (d) IC coalesced nylon 6/nylon 66 blend.

only see a single broad band in the coalesced blend for the both C-H symmetric and asymmetric stretching CH_2 bands. This result, again, demonstrates the molecular level miscibility in the nylon 6 and n 66 blend coalesced from the common inclusion complex.

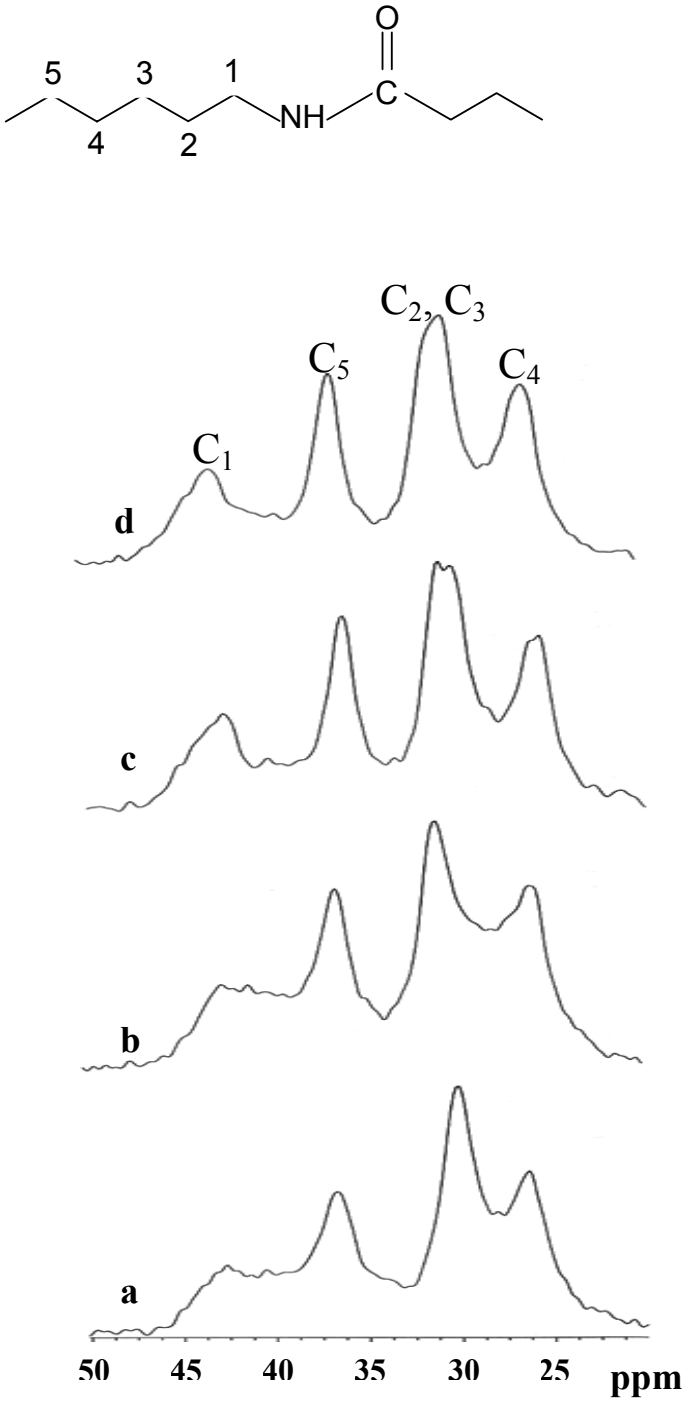

Figure 91. CP-MAS ^{13}C NMR spectra in the meyhlene carbon region of as-received nylon 6, (b) as-received nylon 66, (c) nylon6/ nylon 66 physical blend, and (d) IC coalesced nylon 6/nylon 66 blend.

The CH_2 ^{13}C resonances of nylon occur in the range of 15-50 ppm *vs* TMS and overlap strongly, according to the literature. This frequency range includes resonances of CH_2 carbons in both the amorphous and crystalline phases. Resonances of ^{13}C nuclei in the amorphous phase, which are much broader than the crystalline resonances, are not separately visible. However, the narrower line widths of the crystalline fraction cause them to dominate the CP/MAS spectrum, and the lines assigned here are therefore essentially due to the crystalline fraction. The CP/MAS ^{13}C NMR spectra of nylon 6, nylon 66, and their blends are given in Figure 91. There it can be seen clearly that two NMR peaks are observed for C2,C3 methylene carbons in the physical blend, generated by separated nylon 6 and nylon 66 phases in their immiscible mixture. On the other hand, only one C2,C3 resonance peak is found in the blend generated by coalescing from their common IC, which is consistent with the FTIR spectral analysis. Moreover, the CP/MAS ^{13}C NMR results also demonstrate that the intimate miscibility exists not only in the amorphous regions, but also near the crystalline regions of the coalesced blend.

In Figure 92, WAXD profiles of nylon 6, nylon 66, their physical blend and the blend coalesced from their common IC are presented to investigate their crystal structures. Usually, both nylon 6 and nylon 66 can form α–form crystals, although there is an additional polymorphic modification (γ-form crystals) in nylon 6. The diffraction peaks at $2\theta = 20°,24°$ are distinctive features of the α-form crystals of both nylon 6 and nylon 66, coming from (200) and (002) diffracting planes. Previous work has demonstrated that nylon 6 and nylon 66 in a physical blend crystallize separately and form their individual crystallites, although the x-ray diffraction pattern of the physical blend is very similar to those of the two individual nylons.[220] Unfortunately, given that there are only two

diffraction peaks at about 20 and 24° in the profile of the IC coalesced nylon blend, their miscibility near the crystalline regions, as suggested by the solid-state NMR observations, cannot be corroborated by WAXD.

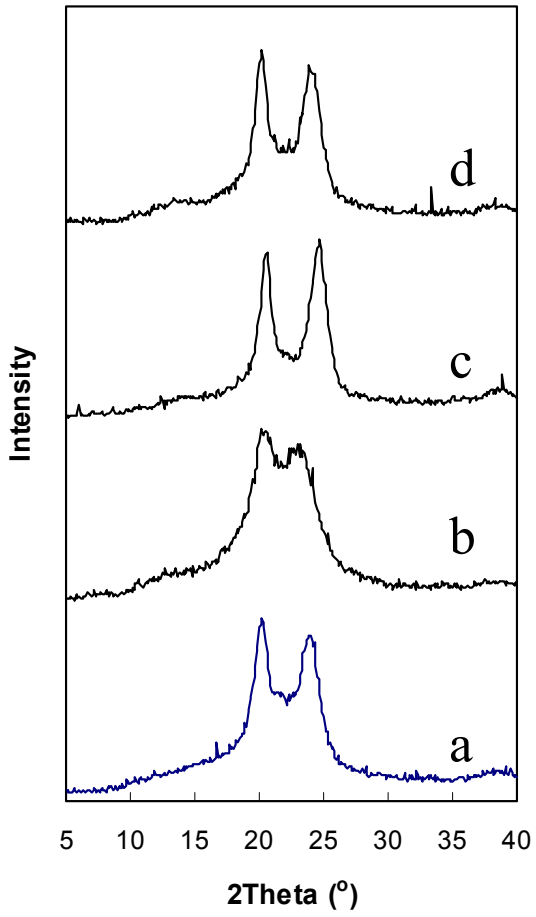

Figure 92. Wide angle x-ray diffraction patterns of (a) as-received nylon 6, (b) as-received nylon 66, (c) nylon 6/nylon 66 physical blend, and (d) IC coalesced nylon 6/nylon 66 blend.

DSC thermal scans of nylon 6, nylon 66, their physical blend and the blend coalesced from their common α-CD-IC were conducted and the results are shown in Figures 93 and

94. In the heating scans seen in Figure 93, two melting peaks are present for both the physical and coalesced blends, coming from nylon 6 (~210^{o} C) and nylon 66 (~260^{o} C), respectively. The melting peaks of nylons in the physical blend have peak shapes similar to those of the neat polymers. In contrast, a sharp melting peak for nylon 66 and a broad melting peak for nylon 6 are observed in the first heating scan for the coalesced blend. We assume that both nylon 6 and nylon 66 can form their own crystallites locally during coalescence, because there are opportunities for the same type of nylon polymer chains to remain side-by-side and form crystals if they were included in neighboring channels of the common α-CD-IC. Due to the apparent superior crystallizablity of nylon 66, this component first forms crystallites after coalescence, and the narrow and sharp melting peak of nylon 66 in the coalesced blend appears similar to that observed previously for coalesced nylon 6 homopolymer, because of the more extended conformations retained from their ICs. However, the subsequent crystallization of nylon 6 is apparently affected by the previously formed crystallites of nylon 66, since the two components are proximal in their coalesced blend. Therefore, a broad melting peak for nylon 6 is observed during the heating scans of the coalesced nylon 6/nylon 66 blend.

In addition, the heat of melting for the nylon 66 crystals in the coalesced blend is significantly larger than observed for as-received nylon 66 (91 J/g *vs* 66 J/g), while the heat of melting for the nylon 6 crystals in the coalesced blend is very similar to that observed for as-received nylon 6 (52 J/g *vs* 56 J/g). So while coalescence increased the nylon 66 crystallinity, the crystallinity of the nylon 6 blend component was not similarly affected. When compared to the increased crystallinity observed for nylon 6 following coalescence from its α-CD-IC, we can suggest that some intimate mixing of nylon 6 and

nylon 66 chains has served to prevent the enhanced crystallinity expected for nylon 6 chains in the blend following coalescence from their common α-CD-IC.

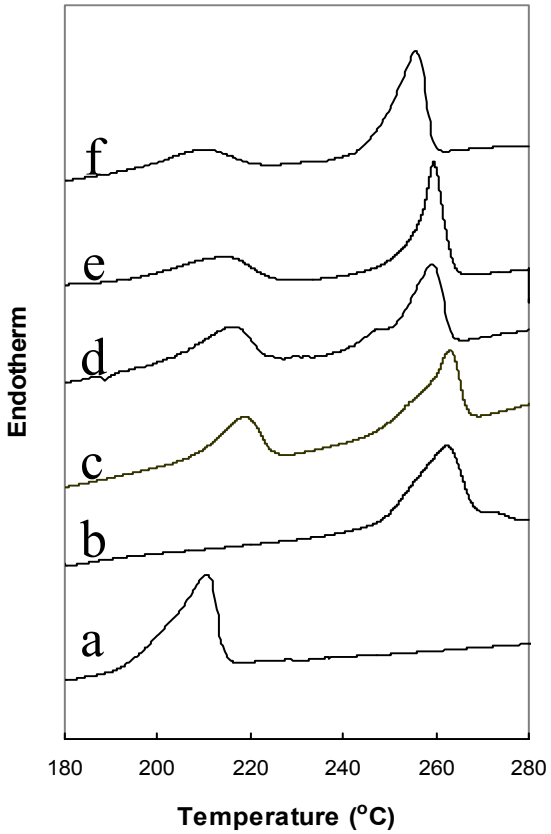

Figure 93. DSC heating scans of (a) as-received nylon 6, (b) as-received nylon 66, (c) nylon 6/nylon 66 physical blend run 1, (d) nylon 6/nylon 66 physical blend run 2, (e) IC coalesced nylon 6/nylon 66 blend run 1, and (f) IC coalesced nylon 6/nylon 66 blend run2.

In the second heating scan, observed after melting the coalesced blend [Figure 93 (f)], the broad melting peak for nylon 6 and the narrow peak for nylon 66 largely remain, indicating thermal stability for the limited miscibility in the coalesced blend. Also the

melting temperatures observed for nylon 6 and nylon 66 crystals in the coalesced blend are lower than those seen in the physical nylon blend, and this may be attributed to the likely smaller size of nylon crystallites in the coalesced blend.

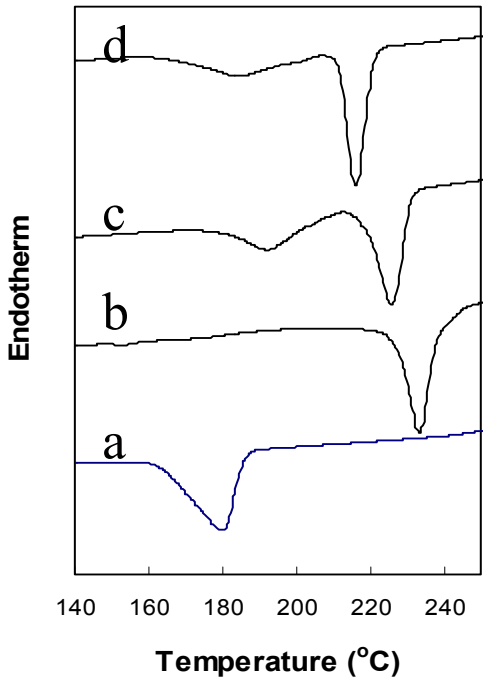

Figure 94. DSC cooling scans observed between first and second heatings of (a) as-received nylon 6, (b) as-received nylon 66, (c) nylon 6/nylon 66 physical blend, and (d) IC coalesced nylon 6/nylon 66 blend.

The DSC cooling scans observed between the first and second heatings are presented in Figure 94. Note that the crystallization of nylon 66 and nylon 6 chains in the coalesced nylon blend occur over narrower and broader temperature ranges, respectively, compared to the physical nylon blend. Nylon 6,66 in both blends crystallize at higher,lower temperatures than the neat nylons, while the crystallization temperatures of both nylons

in the coalesced blend are lower than those observed in the physical blend. This latter observation may be a consequence of the improved miscibility in the coalesced blend, which makes the crystallization of both component nylons more difficult there.

The DSC results further confirm that nylon 6 and nylon 66 chains are more intimately mixed in the coalesced blend than in their physical blend, but without total compatibility as evidenced by the separate melting and recrystallization of nylon 6 and nylon 66 chains. Furthermore, melting of the coalesced nylon blend does not result in phase separation of the initially intimately mixed nylon 6 and nylon 66 chains.

4.2.4 Conclusions

In summary, both nylon 6 and nylon 66 can form inclusion complexes with α-cyclodextrin. Due to the size limit of the α-CD ring, only single nylon chains can be hosted in each channel, and so the common α-CD-IC of nylon 6 and nylon 66 likely contain a random collection of single nylon 6 and nylon 66 chains in neighboring IC channels. By threading nylon 6 and nylon 66 into and then extracting them from a common cyclodextrin complex, a well-mixed, intimate blend of these two polymers can be at least partially achieved in the amorphous regions of the coalesced sample, which is demonstrated by FTIR and NMR observations and analyses. DSC scans reveal that crystallization of nylon 6 and nylon 66 is significantly influenced by the proximity of both nylons in the coalesced blend, again indicating some miscibility, corroborating the FTIR and CP/MAS ^{13}C NMR observations. Furthermore, the intimate miscibility of some nylon 6 and nylon 66 chains in the coalesced blend is not destroyed by melting-induced phase separation.

5 References

1. (a) Schlenk, H., Sand, D. M. *J. Am. Chem. Soc.*, **1961**, *83*, 2313 (b) Szejtli, J, in "Inclusion Compounds" Vol 3. (ed. Atwood, J., Davies, J., MacNicol D.) Academic, London, Chap. 11 (1984) (c) Smith, A.E. *Acta Crystallogr.*, **1952**, *5*, 224 (d) Collombo, A., Allegra, G. *Macromolecules*, **1971**, *4*, 579

2. James, W. J., French, D., Rundle R. E. *Acta Cryst.*, **1959,** *12*, 385

3. Manor, P. C, Saenger W. *Nature,* **1972**, *237*, 392

4. Manor, P. C., Saenger, W. *J. Am. Chem. Soc.*, **1974**, *96*, 3630

5. Saenger, W. *Nature,* **1979**, *279*, 343

6. Lindner, K., Saenger, W. *Acta Crystallogr*, **1982**, *B38*, 203

7. Chacko, K. K., Saenger, W. *J. Am. Chem. Soc*., **1981**, *103*, 1708

8. Lindner, K., Saenger, W. *Angew. Chem., Int. Ed. Engl*., **1978**, *17*, 694

9. Fujiwara, T., Yamazaki, M., Tomizu, Y., Tokuoka, R., Tomita, K., Matsuo, T., Suga, H., Saenger, W. *Nippon Kagaku Kaishi,* **1981**, *181*

10. Steiner, T., Koellner, G. *J. Am. Chem. Soc*., **1994**, *116*, 5122

11. Marini, A., Berbenni, V., Bruni, G., Massarotti, V., Mustarelli, P., Villa, M. *J. Chem. Phys*., **1995**, *103*, 7532

12. Harata, K. *Bull. Chem. Soc. Jpn*., **1987**, *60*, 2763

13. Heyes, S. J., Clayden, N. J., Dobson, C. M. *Carbohydr. Res*., **1992**, *233*, 1

14. Usha, M. G., Wittebort, R. J. *J. Am. Chem. Soc*., **1992**, *114*, 1541

15. Fujiwara, T., Tanaka, N., Kobayashi, S. *Chem. Lett*., **1990**, 739

16. Linert, W., Margel, P., Renz, F. *Chem. Phys*., **1992**, *161*, 327

17. Van Etten, R. L., Sebastian, J. F., Clowes, G. A., Bender, M. L. *J. Am. Chem. Soc*., **1967**, *89*, 3242

18. Uno, B., Kaida, N., Kawakita, T., Kano, K., Kubota, T. *Chem. Pharm. Bull*., **1988**, *36*, 3753

19. Paulson, A., Connors, K. A. In *5th Internat. Sympos. Cyclodextrins*; Duche^ne, Ed.; Editionsde Sante´ Paris, **1990**, p71

20. Cramer, F., Saenger, W., Spatz, H.-Ch. *J. Am. Chem. Soc.,* **1967**, *89*, 14

21. (a) Turro, N. J., Okubo, T., Chung, C. J. *J. Am. Chem. Soc.,* **1982**, *104*, 3953. (b) Cox, G. S., Turro, N. J., Yang, N. C., Chen, M. J. *J. Am. Chem. Soc.,* **1984**, *106*, 422

22. Hamai, S. *J. Phys. Chem*., **1990**, *94*, 2595

23. Ramamurthy, V., Eaton, D. F. *Acc. Chem. Res.,* **1988**, *21*, 300

24. Cox, G. S., Hauptmann, P. J., Turro, N. J. *Photochem. Photobiol*., **1984**, *39*, 597

25. Reichardt, C. *Solvents and Solvent Effects in Organic Chemistry*, 2nd ed.; VCH: Weinheim, **1988**, Chapter 7

26. Heredia, A., Requena, G., Sanchez, F. G. *J. Chem. Soc., Chem. Commun*., **1985**, 1814

27. Kosower, E. M. *An Introduction to Physical Organic Chemistry*; John Wiley: New York, **1968**; Part 2.

28. Street, K. W., Acree, W. E. *Appl. Spectrosc*., **1988**, *42*, 1315

29. Seliskar, C. J., Brand, L. *Science,* **1971**, *171*, 799

30. Kawski, A. *Chimia,* **1974**, *28*, 715

31. Kosower, E. M., Dodiuk, H. *J. Am. Chem. Soc*., **1974**, *96*, 6195

32. DeKorte, A., Langlois, R., Cantor, C. R. *Biopolymers,* **1980**, *19*, 1281

33. Frankewich, R. P., Thimmaiah, K. N., Hinze, W. L. *Anal. Chem*., **1991**, *63*, 2924

34. Al-Hassan, K. A. *Chem. Phys. Lett*., **1994**, *227*, 527

35. Lichtenthaler, F. W., Immel, S. *Liebig's Ann*., **1996**, 27

36. Bender, M.L., Komiyama, M. *Cyclodextrin chemistry* Springer-Verlag, Berlin, **1978**

37. Eaton, P., Vasanthan, N., Shin, I. D., Tonelli, A.E. *Macromolecules,* **1996**,29, 2531

38. Vasanthan, N., Shin, I.D., Tonelli, A.E. *Macromolecules,* **1996**, *29*, 263

39. Maris, T., Henson, M.J., Heyes, S.J., Prout, K. *Chemistry of materials*, **2001,** *13*, 2483

40. Tonelli, A.E. *Macromolecules*, **1991**, *24*, 3069

41. Tonelli, A.E. *Macromolecules,* **1991**, *24*, 1275

42. Saenger, W. *in Inclusion Compounds,* Vol. 2 (Atwood J., Davies J., MacNiclol D. Eds) Academic, London, 1984 chap 8

43. Cramer, F. *Chem. Ber.,* 1951, *84*, 851

44. Clark, J.L., Booth, B.R., Stezowski, J.J. *J. Am. Chem. Soc.,* **2001**, *123*, 9889

45. Penkler, L., Whittaker, D., Glintenkamp, L. WO 97/18245, 1997.

46. Orienti, I., Fini, A., Bertasi, V., Zecchi, V. *Eur J Pharm Biopharm*, **1991**, *37*,110

47. Bettinetti, G., Melani, F., Mura, P., Monnanni, R., Giordano, F. *J Pharm Sci.,* **1991**, *80*,1162

48. Salvadori, P., Uccello-Barretta, G., Balzano, F., Bertucci, C., Chiavacci, C. *Chirality*, **1996**, *8*, 423

49. Ogata, N., Sanui, K., Wada, *J. J Polym Chem.,* **1976**, *14*, 459

50. Maciejewski, M. *J Macromol. Sci. Chem.,* **1976**, *14*, 459

51. Kitano, H., Okubo, T., *J. Chem. Soc. Chem. Commun,* **1990**, 1322

52. Lijima, T., Uemura, T., Tsuzuku, S., Komiyama, J. *J. Polym. Sci. Polym. Phys. Ed.,* **1978**, *16*, 793

53. Harada, A., Li, Kamachi, J. *Carbohydrate Res.,* **1998**, *305*, 127

54. Olson, K., Chen, Y. Y., Baker, G. L. *J. Polym. Sci. Part A: Polym. Chem.* **2001**, *39*, 2731

55. Herrmann, W., Keller, B., Wenz , G. *Macromolecules,* **1997**, *30,* 4966

56. Wenz G, Keller B *Ang. Chem. Int. Ed. Eng.,* **1992**, *31*, 197

57. Topchieva, I.N., Blyumernfel'd, A.L., Klyamkin, A.A., Polyakov, V.A., Kabanov, V.A. *Polymer Sci.,* **1994**, *36*, 221

58. Panova, I.G., Gerasimov, V.I., Grokhovskaya, T.E., Topchieva, I.N. *Doklady Chem.,* **1996**, *347*, 61

59. Panova, I.G., Gerasimov, V.I., Grokhovskaya, T.E., Tashlitskii, V.N., Topchieva, I.N., Kabanov , V.A. *Polymer Sci, Ser, A*, **1997**, *39*, 452

60. Li, J.Y., Yan, D.Y. *Macromolecules*, **2001**, *34*, 1542

61. Mayer, B., Klein, C.T., Topchieva, I.N., Kohler, G. *J. Computer-Aided Molecular Olecular Design*, **1999**, *13*, 373

62. Sandier, A., Brown, W., Mays, H., Amiel, C. *Langmuir,* **2000**, *16*, 1634

63. Popova, E.I., Karpov, I.N., Mikhalev, O.I., Gerasimov, V.I., Topchieva, I.N. *Vysokomolekulyarnye Soedineniya Seriya A & Seriya B*, **1999**,*41*, 1001

64. Amiel, C., Sebille, B. *J. Inclusion Phenomena and Molecular Recognition in Chemistry,* **1996**, *25*, 61

65. Okada, M., Kawaguchi, Y., Okumura, H., Kamachi, M., Harada, A. *J. Polym. Sci. Polym. Chem. Ed.,,* **2000**, *38*, 4839

66. Akira Harada, Toshiyuki Nishiyama, Yoshinori Kawaguchi, Miyuko Okada, and Mikiharu Kamachi *Macromolecules,* **1997**, *30*, 7115

67. Huh, K.M., Ooya, T., Sasaki, S., Yui, N. *Macromolecules*, **2001**,*34*, 2402

68. Jiao, H., Goh, S.H., Valiyaveettil, S. *Macromolecules*, **2001**,*34*, 8138

69. Porbeni, F.E., Edeki, E.M., Shin, I.D., Tonelli, A.E. *Polymer,* **2001**,*42*, 6907

70. Okumura, H., Okada, M., Kawauchi, Y., Harada, A. *Macromolecules,* **2000**,*33*, 4297

71. Yoshida, K., Shimomura, T., Ito, K., Hayakawa, R. *Langmuir*, **1999**,*15*, 910

72. Tonelli, A.E. *Macromolecules,* **1992**,*25*, 3581

73. Pozuelo, J., Mendicuti, F., Mattice, W.L. *Macromolecules*, **1997**,*30*, 3685

74. Pozuelo, J., Madrid, J.M., Mendicuti, F., Mattice, W.L. *Computational and Theoretical Polymer Science,* **1996,** *6*, 125

75. Shuai, X., Porbeni, F.E., Wei, M., Bullions, T., Tonelli, A.E. *Macromolecules,* **2002**

76. Michishita, T., Okada, M., Harada, A. *Macro. Rapid Comm.*, **2001,** *22*, 764

77. Harada, A.; Li, J.; Kamachi, M. *Nature* **1994***, 370*, 126

78. Panova, I. G.; Gerasimov, V. I.; Kalashnikov, F. A.; Topchieva, I. N.; *Polym. Sci. Ser. B* **1998**, *40*, 415

79. Harada, A., Okada, M., Kamachi, M. *Acta Polym.,* **1995**, *46*, 453

80. Harada, A., Okada, M., Kamachi, M. In *proceedings of China-Japan Bilateral Symposium. On Polymer Materials Science,* ed. C. Pan and T. Uryu, P180 Press of University of Science and Technology of China. Hefei. 1995

81. Harada, A., Suzuki, S., Nakamitsu, T., Okada, M., Kamachi, M. *Kobunshi Ronbunshu,* **1995**, *52*, 594

82. Rusa, C.C., Tonelli, A.E. *Macromolecules*, **2000,** *33*, 1813

83. Harada, A., Suzuki, S., Okada, M., Kamachi, M. *Macromolecules*, **1996,** *29*, 5611

84. Harada, A., Li, J., Suzuki, S. *Macromolecules*, **1993,** *26*, 5267

85. Rusa, C.C., Luca, C., Tonelli, A.E. *Macromolecules,* **2001,** *34*, 1318

86. Okumura, Y., Ito, K., Hayakawa, *Phys. Rev. Lett.* **1998,** *80*, 5003

87. Ikeda, E., Okumura, Y., Shimomura, T., Ito, K., Hayakawa, R. *J. Chem. Phys.,* **2000,** *112,* 4321

88. Shimomura, T., Akai, T., Abe, T., Ito, K. *J. Chem. Phys.,* **2002,** *116,* 1753

89. Chatani, Y., Kuwata, S. *Macromolecules,* **1975**,*8*, 12

90. Sivestri, G., Sozzani, P. *in "Comprehensive Polymer Science",* Eastman, G. C., Ledwith, A., Russo, S., Sigwalt, P. Eds., Pergamon Press, Oxford, UK, 1988, Vol. 4, Chap. 18.

91. Sozzani, P., Bovey, F. A., Schilling, F. C. *Macromolecules*, **1989**, *22,*4225

92. Vasanthan, N., Shin, I. D., Tonelli, A. E. *Macromolecules,* **1994**, *27,* 6515

93. Wei, M., Tonelli, A. E. Unpublished results

94. Turska, E., Hurek, J., Zmudzinski, L. *Polymer*, **1979**, *20*, 321

95. Lindner, W. L. *Polymer*, **1973**, *14*, 9

96. Goschel, U. *Polymer*, **1996**, *37*, 4049

97. Gurato, G.; Fichera, A.; Grandi, F. Z.; Zanetti, R.; Canal, P. *Makromol. Chem.* **1974**, *175*, 953.

98. Arimoto, H. *Kobunshi Kagaku* **1962**, *19*, 212.

99. Kinoshita, Y. *Makromol. Chem.* **1959**, *33*, 1.

100. Dasgupta, S., Hammond, W. B., Goddard, W. A. *J. Am. Chem. Soc.* **1996,** *118,* 12291

101. Wei, M., Tonelli, A. E. Unpublished results

102. Olabisi, O., Robeson, L. M., Shaw, M. T. Polymer-polymer miscibility Academic press, New York, 1979.

103. Rusa, C.C., Tonelli, A.E. *Macromolecules,* **2000,** *33*, 5321

104. Bullions, T.A., Edeki, E.M., Porbeni, F.E., Wei, M., Shuai, X., Tonelli, A.E. Unpublished results

105. Shuai, X., Porbeni, F.E., Wei, M., Bullions, T., Tonelli, A.E. *Macromolecules,* **2002,** *35,* 3126

106. Wei, M., Tonelli, A. E. Unpublished results

107. Jenekhe, S. A., Chen, X. L. *Science,* **1999**, *283*, 372

108. Ott, H., Abetz, V., Altsadt, V. *Macromolecules,* **2001**, *34*, 2121

109 Hamley, I. W. *The Physics of Block Copolymers*; Oxford University Press: New York, **1998**

110. Loo, Y. L, Register, R. A., Adamson, D. H., *Macromolecules,* **2000,** *33*, 8361

111. Zhu, L., Cheng, S., Calhoun, B., Ge, Q., Quirk, R., Thomas, E., Hsiao, B., Yeh, F., Lotz, B. *J. Am. Chem. Soc.,* **2000**, *122*, 5957

112. Fujiwara,T., Miyamoto, M., Kimura,Y., Iwata, T., Doi,Y. *Macromolecules* **2001**, *34,* 4043

113. Shuai, X., Porbeni, F.E., Wei, M., Shin, I. D., Tonelli, A.E. *Macromolecules*, **2001**, *34*,7355

114. Shuai, X., Wei, M., Porbeni, F.E., Bullions, T., Tonelli, A.E. *Biomacromolecules*, *3*, 201

115. Shuai, X., Porbeni, F.E., Wei, M., Bullions, T., Tonelli, A.E. *Macromolecules,* **2002,** *35*, 2401

116. Jung, T. A., Schlittler, R. R., Gimzewski, J. K., Tang, H., Joachim, C. *Science,* **1996**, *271*, 181

117. Wada, Y. *Surf. Sci.,* **1997**, *386*, 265

118. Shen, T. C., Wang, C., Abeln, G. C., Tucker, J. R., Lyding, J. W., Avouris, Ph., Walkup, R. E. *Science*, **1995**, *268*, 1590

119. Shigekawa, H., Miyake, K., Sumaoka, J., Harada, A., Komiyama, M. *J. Am. Chem. Soc.*, **2000,** *122*, 5411

120. Gaitano, G.G., Brown, W., Tardajos, G. *J. Phys. Chem. B*, **1997,** *101*, 710

121. Fujita, H., Ooya, T., Yui, N. *Macromolecules*, **1999,** *32*, 2534

122. Huh, K.M., Ooya, T., Lee, W.K., Sasaki, S., Kwon, I.C., Jeong, S.Y., Yui, N. *Macromolecules*, **2001,** *34*, 8657

123. Harada, A. *Accounts Chem. Res.,* **2001,** *34*, 456

124. Castro, R., Cuadrado, I., Alonso, B., Casado, C. M., Moran, M., Kaifer, A. E. *J. Am.Chem. Soc.,* **1997**, *119*, 5760

125. Armspach, D., Ashton, P. R., Moore, C. P., Spencer, N., Stoddart, J. F., Wear, T. J., Williams, D. J. *Angew. Chem., Int. Ed. Engl.,* **1993**, *32*, 854

126. Nakamura K, Nagai M, Kanamoto T, Takahashi Y, Furukawa T *J. Polym. Sci. Polym. Phys. Ed.* **2001**, *39*, 1371

127. Wu, J., Schultz, J.M., Yeh, F.J., Hsiao, B.S., Chu, B. *Macromolecules*, **2000**, *33*, 1765

126. Miller, R. L. *Polymer Handbook*, 3rd ed.; Brandrup, J., Immergut, E. H., Eds.; Wiley Interscience: New York, 1989

127. Dasgupta, S., Hammond, W.B., Goddard, W.A. *J. Am. Chem. Soc.* **1996**, *118,* 12291

128. Hermens, J.J., Deurloo, J.M., Romeijn, S.G., Verhoef, J.C., Merkus, H.M., *Pharm. Res.* **1990**, *7*, 500

129. Loftsson, I., Stefansson, E. *Drug Devel. Ind. Pharm*. **1997**, *23*, 473

130. Tenjarla, S., Puranajoti, P., Kasina, R., Mandal, T., *J. Pharm. Sci.* **1998**, *87*, 425

131. Takahashi, T., Kagami, I., Kitamura, K., Nakanishi, Y., Imasato, Y. *Chem. Pharm. Bull.* **1986**, *34*, 1770

132. Sayani, A.P., Chien, Y.W., *Crit. Rev. Ther. Drug Carrier Syst.* **1996**, *13*, 85

133. Breslow, R., Yang, Z., Ching, R., Trojandt, G., Odobel, F. *J. Am. Chem. Soc.* **1998**, *120*, 3536

134. Georgiadis, M.C., Kostoglou, M, *J. Control. Rel.* **2001**, *77*, 273

135. Ravoo, B. J. *J. Control. Release* **2001**, *72*, 254

136. Sinha, V. R., Kumria, R. *Int. J. Pharm.* **2001**, *224*, 19.

137. Cavalli, R., Peira, E., Caputo, O., Gasco, M. R. *Int. J. Pharm.* **2001**, *182*, 59

138. Hirayama, F., Ogata, T., Yano, H., Arima, H., Udo, K., Takano, M., Uekama, K. *J. Pharm. Sci.* **2000**, *89*, 1486

139. Huang, L., Gerber, M., Taylor, H., Lu, J., Tapaszi, E., Wutkowski, M., Hill, M., Lewis, C., Harvey, A., Herndon, A., Wei, M., Rusa, C. C., Tonelli, A.E. *Macromol. Symp.* **2001**, *176*, 129

14. Huang, L., Taylor, H., Gerber, M., Orndorff, P., Horton, J., Tonelli, A.E. *J. Appl. Polym. Sci.* **1999**, *74*, 937

140. Hill, M., Lu, J., Horton,J., Tonelli, A. E. *J. Appl. Polym. Sci.* **2001**, *82*, 300

141. Martini, L. G., Collett, J. H., Attwood, D. *Drug Dev. Ind. Pharm.* **1999**, *26*, 7

142. Sozzani, P., Bovey, F. A., Schilling, F. C. *Macromolecules*, **1989**, *22,* 4225

143. Vandamme, T. F., Mukendi, J *Int. J. Pharm.* **1996**, *145*, 77

144. Zambaux MF, Bonneaux F, Gref R, Dellacherie E, Vigneron C. *J. Control. Release* **1999**, *60*, 179.

145. Fujiwara, T., Miyamoto, M., Kimura, Y., Sakurai, S. *Polymer* **2001**, *42*, 1515

146. Nelles, G., Weisser, M.; Back, R.; Wohlfart, P.; Wenz, G.; Mittler-Neher, S. *J. Am. Chem. Soc.* **1996**, *118*, 5039-5046

147. Saenger, W. *Angew. Chem. Int. Ed. Engl.* **1980,** *19*, 344

148. Crezcenzi, V.; Manzini, G.; Cazolari, G.; Borri, C. Eur. Polym. J. **1972**, *8*, 449

149. Fischer, E. M.; Sterzel, H. J.; Wegner, G. Colliod Polym. Sci. **1973**, *251*, 980

150. Nishi, T, Wang, T. T. *Macromolecules* **1975**, *8*, 909

151. Avrami, M. *J. Phys. Chem.* **1939,** *7*, 1103

152. Coleman, M.M., Zarian, J., *J. Polym. Sci., Polym. Phys.* **1979,** *17*, 837

153. Goulet, L., Pudhomme, R.E., *J. Polym. Sci., Polym. Phys.* **1990,** *28*, 2329

154. Ozawa, T. *Polymer* **1971**, 12, 150

155. Evans, U.R. *Trans. Faraday. Soc.* **1945**, *41*, 365

156. Howe, C., Sankar, S., Tonelli, A.E. *Polymer* **1993,** *34*, 2674

157. Flory, P. J. *J. Am. Chem. Soc.* **1962**, *84*, 2857

158. Flory, P. J., Yoon, D. Y. *Nature* **1978**, *272,* 226

159. Yoon, D. Y., Flory, P. J. *Faraday Discuss. Chem. Soc.* **1979**, *68*, 288

160. Colombo, A., Allegra, G. *Macromolecules*, **4**, *579*, 1971

161. White, J. L.; Beck, L. W.; Ferguson, D. B.; Haw, J. F. *J. Magn. Reson.* **1992**, *100*, 336

162. Lindner, W. L., *Polymer*, **1973**, *14,* 9

163. Goschel, U. *Polymer*, **1996,** *37,* 4049, 1996

164. Robert, R., *Polymer*, **1969,** 10, 113

165. Daniels, W. W.; Kitson, R. E. *J. Polym. Sci.* **1958**, *33*,161

166. Koenig, J. L. "Spectroscopy of Polymers", Amer. Chem. Soc., Wash., D.C., 1992, Chap.4.

167. Zerbi, G. "Modern Polymer Spectroscopy", Wiley-VCH, 1999, New York, Chap. 3

168. Miyake, A. *J. Polym. Sci.,* **1959**, *38*, 479

169. Esposito, L. D., Koenig, J. L. *J. polym. Sci., Polym. Phys. Ed.,* **1976**, *14,* 1731

170. Ward, I. M. Chem. and Ind. (London), 1102, 1957.

171. Daniels, W. W., Kitson, R. E., *J. Polym. Sci.*, **1958,** *33*, 161

172. Schmidt, P. G., *J. Polym. Sci. Part A,* **1963***, 1,* 1271

173. Lin, S. B., Koenig, J. L., *J. Polym. Sci., Polym. Phys. Ed.,* **1982**, *20*, 2277

174. Ajji, A., Guevremont, J., Cole, K. C., Dumoulin, M. M. *Polymer,* **1996,** *17*, 3707

175. Auriemma, F., Corradini, P., Guerra, G., Vacatello, M., *Macromol. Theory Simul.,* **1995**, *4*, 165

176. Asano, T., Seto, T. *Polym. J.(Tokyo),* **1975,** *5*, 72

177. Auriemma, F., Corradini, P., DeRosa, C., Guerra, G., Petraccone, V., Bianchi, R., DiDino, G., *Macromolecules*, **1992,** 25, 2490

178. Williams, A. D., Flory, P. J., *J. Polym. Sci., A-2,* **1967**, 5, 417

179. Schmidt-Rohr, K., Hu, W., Zumbulyadis, N. *Science*, **1998,** 280, 714

180. Huang, J. M., Chu, P. P., Chang, F.C. *Polymer*, **2000**, *41,* 1741

181. Kohan, M. I. *Nylon Plastics* John Wiley & Sons, New York, 1973

182. Arimoto, H. *Kobunshi Kagaku* **1962**, *19*, 212

183. Kinoshita, Y. *Makromol. Chem.* **1959**, *33*, 1

184. Ito, M.; Mizuochi, K.; Kanamoto, T. *Polymer* **1998**, *39*, 4593

185. Heuvel, H. M.; Huisman, R. *J. Appl. Polym. Sci.* **1981**, *26*, 713

186. Garcia, D; Starkweather, H. W. *J. Polym. Sci. Polym.: Part B: Phys. Ed.* **1985**, *23*, 537

187. Arimoto, H. *J. Polym. Sci.* **1964**, *2*, 2283.

188. Arimoto, H.; Ishibashi, M.; Hirai, M.; Chatani. *J. Polym. Sci. Polym.: Part A: Chem. Ed.* **1965**, *3*, 317.

189. Rotter, G.; Ishida, H. *J. Polym. Sci. Polym.: Part B: Phys. Ed.* **1992**, *30*, 489

190. Vashanthan, N., Salem D. R., *J. Polym. Sci. Polym.: Part B: Phys. Ed.* **2001**, *39*, 536

191. Penel-pierron, L.; Depecker, C.; Seguela, R.; Lefebvre, J. M. *J. Polym. Sci. Polym.: Part B: Phys. Ed.* 2001, *39*, 484

192. Murthy, N. S.; Bray, R. G. *Polymer* **1995**, *36*, 3863

193. Hatfield, G. R.; Glans, J. H.; Hammond, W. B. *Macromolecules* **1990**, *23*, 1654.

194. Schreiber, R., Veeman, W. S. *Macromolecules* **1999,** *32,* 464

195. Brandrup, J., Immergut, E. H., Grulke E. A. *Polymer Handbook* John Wiley & Sons, New York, 1999, (the value used in this paper is obtained by averaging the values listed in the handbook)

196. Ho, J. C., Wei, K. H. *Macromolecules* **2000,** *33,* 5181

197. Kyu, T.; Saldanha, J. M. *J. Polym. Sci., Polym. Lett. Ed.* **1985,** *25*, 741

198. Koo, K.; Inoue, T.; Miyasaka, K. *Polym. Eng. Sci.* **1985**, *27*, 741

199. Chiou, J. S.; Barlow, J. W.; Paul, D. R. *J. Polym. Sci., Polym. Phys. Ed.* **1987**, *25*, 1459

200. Woo, E. W.; Su, C. C. *Polymer* **1996**, *37*, 4111

201. Saldanha, J. M.; Kyu, T. *Macromolecules* **1987**, *20,* 2840

202. Landry, C. J. T.; Henrichs, P. M. *Macromolecules* **1989**, *22,* 2157

203. Debier, D.; Devaus, J.; Legras, R. *J. Polym. Sci., Polym. Phys. Ed.* **1994,** *33*, 407

204. Kyu, T.; Ko, C. C.; Lim, D. S.; Noda, I. *J. Polym. Sci., Polym. Lett. Ed.* **1993**, *31,* 1641

205. Kim, K. C.; Paul, D. R. *Macromolecules* **1992**, *25*, 3097

206. Butzbach, G. D.; Wendorff, J. *Polymer* **1991**, *32,* 1155

207. Coleman, M. M.; Graf, J. F.; Painter, P. C. Specific Interactions and the Miscibility of Polymer Blends; Technomic Publishing: Lancaster, PA, 1991

208. Szejtli, J. *Cyclodextrins and Their Inclusion Complexes* Akademiai Kiado, Budapest, 1982.

209. Harada, A.; Li, J.; Kamachi, M. *Nature* **1993***, 364*, 516.

210. Lu, J.; Mirau, P. A.; Tonelli, A. E. *Macromolecules* **2001**, *34*, 3276.

211. Jiao, H.; Goh, S. H.; Valiyaveettil, S. *Macromolecules*, **2001**, *34*, 8138.

212. Porbeni, F. E.; Edeki, E. M.; Shin, I. D.; Tonelli, A. E. *Polymer* **2001**, *42*, 6907.

213. Wenz, G.; Steinbrunn, M. B.; Landfester, K. *Tetrahedron*, **1997**, *53*, 15575

214. Wei, M; Davis, W; Urban, B; Song, YQ, Porbeni, P. E.; Wang, X.W.; White, J. L.; Balik, C. M.; Rusa, C. C.; Fox, J.; Tonelli, A. E. *Macromolecules*, **2002***, 35*, 8039 (in 3.2).

215. Wei, M.; Tonelli, A.E. *Macromolecules*, **2001**, *34*, 4061.

216. Kitao, T.; Kobayashi, H.; Ikegami, S.; Ohya, S. *J. Polym. Sci. Polym. Chem. Ed.,* **1973**, *11*, 2633.

217. Verma, A.; Deopura, B. L.; Sengupta, A. K. *J. Appl. Polym. Sci.* **1986**, *31*, 747.

218. Tonelli, A. E. *Macromolecules* **1991**, *24*, 1275.

219. Murthy, N. S.; Bray, R. G. *Polymer* **1995**, *36*, 3863.